APPLICATION OF THE "ESCIMO" THEORY

TO TURBULENT DIFFUSION FLAMES

BY

RICHARD LO-TIEN SUN

B.Sc(Eng), M.Sc.

THESIS SUBMITTED FOR THE DEGREE OF

DOCTOR OF PHILOSOPHY

IN THE FACULTY OF ENGINEERING

UNIVERSITY OF LONDON

AND

FOR THE DIPLOMA OF MEMBERSHIP

OF IMPERIAL COLLEGE

Computational Fluid Dynamics Unit,

Imperial College of Science and Technology,

London S.W.7

SEPTEMBER 1982

TO MY PARENTS.

ABSTRACT

The ESCIMO (Engulfment, Stretching, Inter-diffusion and Moving Observer) theory of turbulent combustion is further developed and applied to turbulent diffusion flames. The present theory contains both the demographic (Eulerian) and biographic (Lagrangian) aspects. Major attention is paid in the present work to the development of mathematical formulation and solution procedures for the fold demographic studies.

The distribution of "fold-populations" at each spatial point is described by a set of transport equations which are linked together through the source terms. The source terms in each equation include the effects of fold-ageing, fold-formation and fold re-engulfment, respectively.

Simplifications are made in the biographic analysis in order to reduce the computational task, such as the assumption of a fast, simple chemical reaction system and unity Lewis number. The governing partial differential equation is then solved by the approximate methods, termed the "profile method".

In order to asses the validity of the "ESCIMO" theory, three different sets of experimental data are selected for comparison between the predictions and the measurements. These test cases are:

(1) the diffusion-limited chemical reaction in a turbulent mixing layer;

(2) the hydrogen-air diffusion flame in co-flowing air; and

(3) the natural gas-air free jet diffusion flame.

The quantities calculated by the present theory are classified into various categories presented below:

- the hydrodynamic results which include the mean velocity and the turbulent kinetic energy (obtained from the k-ε model of turbulence);
- the population distribution function of various folds;
- the variation of mean temperature and species concentration across the mixing layer or jet;
- the root-mean-square fluctuation of temperature and species concentration; and
- the probability density function of temperature and species concentration.

Comparisons with the experimental data show that the agreement is fairly good, provided that a suitable choice of input parameters is made. The sensitivity analysis has been performed for both the physical parameters and numerical parameters in order to evaluate their influences on the results. However, there is a need for enlargement of the conceptual content of the "ESCIMO" theory to allow for the role of "Turbulence intermittency".

The direction of this future development is discussed, and suggestions provided.

PREFACE

I joined the Heat Transfer Section of the Mechanical Engineering Department (now the Computational Fluid Dynamics Unit) of the Imperial College of Science and Technology, as a research student, in October 1978. During these past four years, my research activities have been centred on the development of theoretical model for the prediction of two-dimensional turbulent reacting flows. The primary objective of my work has been to establish a more realistic and practical physical model which can be further developed to solve practical combustion problems.

During the first six months of my studies, I followed the M.Sc.courses given by the Heat Transfer Section and worked on the numerical modelling of flows with moving interfaces. The experience obtained during that period was valuable for my later research work. In the next six months, I was working on the application of ESCIMO theory of turbulent combustion to the well-stirred reactor. I was fascinated with the contents and philosophy of the ESCIMO theory and I also realised that a lot of work has to be done in the future. From the second year, I devoted myself to the development of the demographic part of ESCIMO theory in two-dimensional parabolic flows. The first application of this work was the prediction of concentration and its fluctuations in a plane turbulent reacting mixing layer, where the experimental data are available.

The last part of my work was concerned with the calculation of temperature and concentrations in the turbulent jet diffusion flames. It was an exciting and challanging task, especially when the positive results emerged. I have gained more hand-earned knowledge and tasted the academic research life in my final years of study.

ACKNOWLEDGMENTS

I would like to express my gratitude to all those who have helped me during my studies at Imperial College. First and foremost, I am deeply grateful to my supervisors, Professor D.Brian Spalding and Dr.A.S.C.Ma, for their skilful guidance, moral encouragement and financial support. They have taught me not only on the main direction of the research topic, but also instructed me how to overcome the difficulties arising from various aspects. Professor Spalding once told me, "It is the very last detail of the problem which determines either the success or failure". He was right and I am glad that I have learned this experience. The constructive criticism received from Professor Spalding on the technical writings is also very valuable.

Dr.W.M.Pun taught me the basic prediction procedures used in the Heat Transfer Section. He explained all the methods clearly and patiently, I am very grateful. Discussions with Drs.M.A.Noseir and L.T.Tam on the modelling of combustion problems were particularly helpful.

The suggestions given by Dr.Andrzej Przekwas on the development of the demographic part of ESCIMO theory rates special mentioning here. He has shared his time and experience unselfishly with me, even throughout the weekend or in the late evening.

I would like to thank Dr.G.W.Carroll, Dr.A.G.Awn and Dr.Amin Baghdadi for the help on numerical analysis. The

day-to-day exchange of ideas with other post-doctoral fellows, visiting scholars and students has also been most beneficial. These include Dr.Ahmed Abdelmeguid, Mr.W.C.Fan, Mr.S.Parameswaran, Mr.P.A.Shepherd and Mr.S.M.Lo.

Thanks are due to Miss Sue Farmiloe, Mrs.Maggie Dean and Mrs.Frith Oliver for their assistance in administrative matters; Mr.Peter Dale who helped in solving many computing problems. The general help provided by Mr.Bob King is highly appreciated and the friendship between both of us very much enjoyable. I would also like to thank Miss E.M. Archer, Mrs.S.Boot and Miss L.Hamilton for providing very efficient library services.

I am grateful to Miss Janice Lewis and Miss Suzanne Enright for their excellent typing of the thesis, and for their patience and skill in going through every typing detail.

I would like to extend my gratitude to my parents and brothers who offered all possible support and encouragement throughout my studies.

Finally, I wish to thank the Safety in Mines Research Establishment, Health and Safety Executive of Great Britain for providing financial support during my studies.

CONTENTS OF THESIS PAGE NO.

LIST OF FIGURES

LIST OF TABLES PAGE NO.

CHAPTER 1

INTRODUCTION

1.1 The problem considered

There have been extensive theoretical studies in turbulent reacting flows during the last decade. These continuing research activities are inspired by the increasingly urgent requirements of higher combustion efficiency and lower pollutant emissions. A better understanding of the processes involved and a more powerful predictive capability are essential to achieve the purpose.

According to the nature of the combustion problems in many practical devices, the reacting flows can be classified into two limits, namely, the nonpremixed and premixed systems. For the nonpremixed systems, fuel and oxidizer enter the field of interest in two streams, for instance, the primary jet is fuel and the secondary flow is oxidizer. For the premixed systems, the cold, premixed reactants are fed into a single stream and the other stream is composed of hot combustion products. Intermediate cases do exist in reality, e.g., the primary jet is fuel and the secondary stream is a fuel-oxidizer mixture. Up to date, most of the developed theories and methods are confined to the nonpremixed and premixed limits due to the relative simplicity.

Different models have been developed and applied to either the nonpremixed flames (also called as diffusion flames) or the premixed flames, such as those mentioned in the literature by Spalding (1976a), Bilger (1976, 1980)

and Bray (1979,1980). The important phenomena in each type of flames can be fairly predicted with the aid of some assumptions, closures and semi-empirical formulae. However, the majority of theoretical models have been constructed and found successful for one type of flame only.

It is desirable to set up a theoretical framework which is capable of tackling both the turbulent diffusion and premixed flames. The advantage of this kind of theory is that it can be further developed to predict some practical flames, like that in the gas-turbine combustor, which has both diffusion and premixed features.

A general theory of turbulent combustion with the acronym of ESCIMO (Engulfment, Stretching, Coherence, Inter-diffusion and Moving Observer), was proposed by Spalding (1976b,1978b)to meet the need. The theory combined the Eulerian approach (termed the demographic part here) and the Lagrangian approach (termed the biographic part) into one framework. The application of ESCIMO theory to the confined, premixed, baffle-stabilized flame appeared in the work of Noseir (1980), while the other application to the well-stirred reactor (also premixed flames) with complex chemical-kinetics scheme was demonstrated by Tam (1981).

The reacting flows considered in this thesis are of the open, turbulent diffusion types and it is the first test of ESCIMO theory to this kind of flows. The chemical reaction considered herein is fast compared with the rate of turbulent mixing, which is usually classified as diffusion-limited or hydrodynamics-controlled reaction.

1.2 Objectives of the study

The concepts of ESCIMO theory are based on the existence of coherent lumps of fluids, termed the "folds" or "layer-pairs" in the present work and related publications, which travel from one place to the other according to the fluid-dynamics motion. The properties of the flow are determined from the characteristics of different folds coming from various places.

The whereabouts of all folds and the history of each fold are treated in the demographic and biographic parts respectively. The demographic part is more closely related to the hydrodynamic condition than the biographic part. In the previous work of Noseir (1980) and Tam (1981), major attention has been paid to the development of biographic analysis, while the demographic analysis was rather primitive. The results of demographic analysis in the well-stirred reactor can be expressed by the simple exponential function (Tam, 1981), since the properties are uniform in space. On the other hand, Noseir assumed that the time-average profiles of gas properties across the duct are of the top-hat form. This simplification reduces the demographic analysis to a one-dimensional problem, i.e., the population distribution of folds is a function of longitudinal distance only.

The two main objectives of the present study are, consequently:

(1) to set up the mathematical formulation of demographic analysis in actual two-dimensional, turbulent, reacting flows together with the numerical solution procedure; and

(2) to apply the ESCIMO theory to the turbulent free jet-diffusion flames as one further step toward the combustion problems of practical importance.

The results obtained from the present work can be classified into three categories, namely, the turbulent mean properties, the turbulent fluctuation intensities and the probability density functions (pdf) of various scalars.

The presumptions made in ESCIMO theory are mainly based on physical reality, with some simplifications in order to economize the computational task, The influence of various hypothesis and empirical constants on the results have been investigated and demonstrated.

1.3 Practical relevance

The turbulent diffusion flames exist in many industrial processes and natural fires, which can be divided into the following groups:

(1) Gas turbine combustors: the fuel is injected into the primary combustion zone through the injector and the air enters from the front of the combustor or from large holes in the combustor liner. The fuel and air are injected separately, mix and, subsequently, react. However, in the secondary combustion zone and dilution zone of the combustor, more air is added through the film cooling slots, indicating that the combustion changes from the diffusion type to the premixed one.

(2) Industrial furnaces: the fuel jet and air flow are supplied separately to the confined combustion chamber.

(3) Compression-ignition (diesel) engine: much of the combustion occurs at a rate controlled by the mixing of fuel spray and air.

(4) Rocket exhaust plumes: the exhaust gases from the rocket nozzle usually contain some amount of oxidisable material and secondary flame may occur when the gases mix with the surrounding air. The secondary combustion is responsible for the emission of light, intensified heat radiation, etc. in the trail of the rockets and missiles.

(5) Fires: the large scale forest fires, building fires, and the flaring waste gases are mostly mixing-controlled diffusion flames.

Usually, the higher combustion efficiency in the engineering equipments is accompanied by lower emission of soot agglomerates (smoke) and pollutants such as carbon monoxide and nitric oxide, since less amount of fuel is wasted. The detailed chemistry of soot and pollutant formation is very complex and depends on the detail thermal and hydrodynamic conditions of the flows considered. Therefore, a reliable and powerful model in the prediction of flame properties is the prerequisite for the solution of our energy and environmental problems.

1.4 Previous work

It happens in many practical cases that the kinetics of the overall chemical reaction are relatively fast compared with the rate of turbulent mixing. The equilibrium concentrations of final products is then assumed to prevail everywhere in a diffusion flame (Spalding,1970a; Bilger,1976;

Libby and Williams, 1981). The additional assumption of equal mass diffusivity are also often made and justified, so that the concentration of fuel, oxidant and product are uniquely related to the mixture fraction which is a conserved scalar. The value of enthalpy can also be determined by the mixture fraction if the enthalpies of fuel and oxidant streams are uniform. Therefore, all the thermodynamic properties of the mixture are functions of mixture fraction only. This conserved scalar approach substantially simplifies the analysis of the problem, since the difficulties in modelling the turbulent mean reaction rate are largely obviated.

The turbulence fluctuation in the flames is taken into account by presuming a probability density function (pdf) for the fluctuating mixture fraction so that the mean concentrations and temperature can be evaluated. The work of Kent and Bilger (1973), Lockwood and Naguib (1975), Jones and Whitelaw (1978) and Kolbe and Kollman (1980) all follow this line. The shape of pdf is assumed as a "clipped Gaussian" or of beta function distribution. The common practice in these approaches is to obtain the mean mixture fraction and its variance (the fluctuation) from the modelled transport equation. The variance was obtained by solving the "g-equation" proposed by Spalding (1971a) or other equation with some modification.

The predictions obtained from the presumed pdf approach compared favourably with the experimental data on time mean quantities, although some discrepancies do exist. It has been demonstrated by Kent and Bilger (1976) that the predictions on mean composition and temperature do not seem very sensitive

to the variations in the pdf profiles. The limitation of this approach is that a sufficiently realistic pdf has to be specified in advance and the task becomes more difficult when the combustion process can not be properly described by a single-step reaction (Spalding, 1979a).

Another approach, proposed by O'Brien (1971), Dopazo (1975), Pope (1976) and Janicka et al (1978), is to construct the transport equation of pdf from the conservation laws. But the molecular diffusion and turbulent transport terms are unclosed and have to be modelled in all such pdf equations for reactive flow systems. The major advantage of the pdf method for reactive flows is the closed-form treatment of the species production rate, which makes it attractive especially for combustion problems. But the number of independent variables increases substantially and the numerical methods become more sophisticated and time consuming, especially when the chemistry is complex.

Following the line of using a deterministic approach to the specification of a scalar pdf in a single reaction progress variable, proposed by Bray and Moss (1977), Libby et al (1979), Roberts and Moss (1981) has demonstrated a "wrinkled flame" interpretation of the open turbulent diffusion flame. It is argued in the wrinkled flame model that a laminar flamelet profile is the microscopic element in a turbulent ensemble. The pdf of any conserved scalar is related to the instantaneous flame profile through the flame sheet model, where the two parameters in the instantaneous flame profile are determined from the measured mean temperature and temperature fluctuation. The measured probability density

function of temperature, in the open turbulent methane diffusion flame, has been reproduced from this wrinkled flame model. Roberts and Moss (1981) claimed that this model is simpler and more economical in the descriptions of scalar pdfs than the multi-dimensional joint pdfs.

When the finite-rate chemistry is present in the flow, or the flame is a partially premixed one, the transport equation of one reacting species (usually is the fuel) has to be solved in addition to the mixture fraction. The production rate (or consumption rate) of the species appears in the source term of the balance equation and must be modelled. This approach is often termed the two-variable approach or two-variable formalism (Lockwood and Naguib, 1975; Lockwood, 1977; Janicka and Kollman, 1979; Bilger, 1980). The second variable is a kind of progress variable such as reactedness or other combined variables.

The closure of the production term for the second variable has been treated in various ways. Some authors simply use a mean kinetic rate based on the mean concentrations and mean temperature only. This is unsatisfactory because the effects of fluctuations and mixing are disregarded in the calculation of the reaction rates. Borghi (1974) and Hutchinson et al. (1978) employed an expansion procedure to include the effects of temperature and concentration fluctuations on the reaction rates, but the correlation terms have to be obtained by second-order closure of their balance equations. The closure problem seems to overshadow the advantage gaining from the use of conserved scalar (i.e. the first variable).

Spalding (1971b) proposed the "eddy break up" model to combine the effects of turbulent mixing and chemical kinetics. Hence, the reaction rate is a function of the local turbulence Reynolds number, the turbulent kinetic energy and its dissipation rate, the concentration fluctuation and the kinetic rate of reaction. Many similar expressions have appeared in the literature (Lockwood, 1977; Bray and Moss, 1977) and some degree of success was achieved, such as the work of Mason and Spalding (1973), Stephenson (1972) and Serag-Eldin (1977). However, this approach is semi-empirical and some uncertainties do exist.

Alternatively, Janicka and Kollmann (1979) employed the joint pdf of two variables to tackle the chemical reaction term. Several constraints imposed by the moments and the bounds of the variables can be placed on the pdf. The second-order moments are obtainable from the modelled balance equations and the chemical production terms from the joint pdf. Plausible results have been obtained for the concentrations of major species and nitric oxide.

Bilger (1979) proposed the "perturbation approach" to handle the source term of the second variable. The term "perturbation" here means the departure from the equilibrium or fast chemistry solution. A new term which represents the production rate of out-of-equilibrium material (by the fine scale turbulent mixing) arose in the equation. The treatment of this microscale mixing source term has been demonstrated by the author. In the mean time, the mean production rate was found to be better conditioned, in terms

of the departure from equilibrium, than the usual approach so that a lower-order closure is sufficient.

All the approaches described in the preceding paragraphs include the concept of conserved scalar. There exist some problems in which it is impossible or inappropriate to define and utilize the conserved scalar. These problems usually fall into one of the classes presented below;
(1) when the turbulence Reynolds number is low and differential diffusion (in the molecular diffusion level) effects are important; or
(2) the composition and enthalpy in the fuel stream and oxidant stream are not uniform and constant; or
(3) the complex chemical reactions are far from the equilibrium conditions so that little advantage can be gained from the two-variable approach.

Some authors has already suggested that it is necessary to attempt direct closure of the chemical production term by either the moment closure or the pdf closure methods. The typical examples appeared in the work of Borghi (1974), Donaldson and Hilst (1972), Bonniot et al. (1978), Donaldson (1974). However, these methods have been developed for problems of relatively simple chemistry and equal molecular diffusivity so far. The demonstration of this approach to the more difficult problems remains to be done.

Another approach based on the detailed computations of each hypothetical element in the turbulent reaction zone has been illustrated by the earlier work of Mao and Toor (1970). They treated the flows as composed of multi-layered

sandwich, which contains either oxidant-rich layer or fuel-rich layer. The phenomena occurring in the sandwich is supposed to be unsteady and laminar, so that the full multicomponent diffusion effects and complex free radical chemical mechanism can be incorporated in the model. The effect of shear or stretching strain was, however, not considered in the early version given by Mao and Toor (1970), i.e., the model is purely diffusional. They were able to predict the experimental data of Vassilatos and Toor (1965) in the plug flow reactor over a wide range of Damköhler number and stoichiometry parameter, if the thickness of layer is properly prescribed.This model bears some resemblance in the conceptual framework to the ESCIMO theory to be presented in the present thesis.

1.5 Layout of the thesis

The remainder of the thesis is presented in eight chapters. The physical model of the ESCIMO theory will be provided in the next chapter.

The mathematical analysis of the theory is presented in Chapters 3, 4 and 5. Chapter 3 contains the mathematical formulation of the hydrodynamic computations and demographic part. The partial differential equations are two-dimensional steady and parabolic which can be solved by the marching method (in the space direction). Chapter 4 provides the mathematical framwork of the biographic part in ESCIMO theory. The equations which describe the behaviour of each fold are one-dimensional, unsteady with the laminar diffusion coefficients. An approximate method, called as "profile method" is adopted to obtain a closed form solution. Chapter 5

describes how the results obtained from the demographic and biographic parts can be linked together to yield the various turbulence properties in the flow systems of interest.

The first test case in the present work, namely, the diffusion-limited chemical reaction in the turbulent mixing layer, is demonstrated in Chapter 6. The influence of various assumptions and parameters is also discussed.

Chapter 7 is devoted to the application of ESCIMO theory to the turbulent jet diffusion flames, including the hydrogen-air diffusion flame and methane-air diffusion flame. The results are compared with the measurements from Kent and Bilger (1973), Lenze and Günther (1975), Lenz and Günther (1980).

Chapter 8 presents the sensitivity analysis for the turbulent diffusion flames, It includes the influence of fold formation rate, the fold composition at birth, the initial fold size and stretching rate on the prediction of flame properties. The influence of different grid sizes is also investigated and demonstrated in this chapter.

Finally, the main achievements of the present work and some proposals for further development of the theory are stated in Chapter 9.

CHAPTER 2

THE PHYSICAL MODEL OF THE ESCIMO THEORY

2.1 Introduction

In this chapter the various components of the ESCIMO theory from both the demographic (Eulerian) and the biographic (Lagrangian) aspects will be described; the presentation will be based on the physical phenomena first and then followed by simple mathematical formulation only. The detailed partial differential equations are depicted in the next two chapters.

The turbulence model for the time-average flow field is first presented as the starting base, followed by the description of the creation of the folds (or eddies) and the coalescence of the old folds into the new ones. The stretching effect of the folds due to the shear strain and the transport of different folds by the mean turbulent flow will be explained afterwards.

The definition of the age in the fold-history and the relevant quantities are then provided in the subsequent sections of this chapter. Finally, the molecular diffusion which occurs inside each fold and its interaction with the main flow field will be discussed.

2.2 The time average flow

Two types of similar flow field are considered in the present work, namely the turbulent plane mixing layer and the turbulent axisymmetric round jet. Both of them belong to the two-dimensional parabolic flows, thus simplifying the flow

field solution so that more efforts can be spent on the development of the ESCIMO model itself. The physical laws which govern these flows include the conservation of mass, momentum and scalar properties and the universal gas law. These laws have been written in mathematical forms and simplified according to the boundary layer assumptions, such as by Schlichting (1979), Kays (1969) and Spalding (1971a)

However, there is a need in modelling the turbulence quantities for the determination of turbulent fluxes which appear in the momentum conservation equation. In order to obtain reasonable accuracy on one-hand and the computational practicability on the other, the widely used two-equation model of turbulence given by Harlow and Nakayama (1968) and Launder and Spalding (1973) is employed here in this work.

In two-equation k-ε model, it is supposed that the turbulence is characterised by two quantities, namely:

k - kinetic energy of turbulence; and

ε - dissipation rate of turbulent kinetic energy.

The "eddy viscosity" or "turbulent viscosity" used in the momentum equation is then calculated from the values of k and ε with the aid of an empirical constant. The turbulence length scale is also related to k and ε instead of being assigned a specific value such as in the Prandtl's mixing length theory. The full mathematical presentation of the hydrodynamics calculation will appear in the next chapter.

2.3 Fold formation and re-engulfment

The earlier experimental work of Brown and Roshko (1974) on non-reacting plane turbulent mixing layer with free streams of different densities has provided considerable evidence on the existence of "large scale coherent structure". The rolling up of the interface (vortex sheet) between two streams to form "layer pairs" or "folds" was revealed by the high speed photography.

The recent work of Ganji and Sawyer (1980) in the turbulent premixed step-combustor also reported the similar coherent structure. There are a number of "layer-pairs" or "sandwiches" in the mixing region and they are randomly distributed at any instantaneous moment. The fresh reactants are continuously entrained or enfolded with the products to form new eddies. From the high-speed Schlieren film record of the flame presented by Ganji and Sawyer (1980), it can be observed that the eddy ahead is being pushed downstream, and the following eddy moves up. At the same time, they rotate around each other and finally become a single entity (at least optically). This phenomenon can be termed the "re-engulfment process".

In the framework of the ESCIMO theory, the formation rate of "folds" or "eddies" is determined by the entrainment rate which is obtained from the hydrodynamics calculation. However, the distribution of the formation rate across the shear layer or the jet at fixed downstream location has to be postulated. There is no experimental evidence reported up to date concerning this problem, hence different hypothesis will be employed and tested in the present work to demonstrate its influence.

The distribution can be assumed to be proportional to the local mean velocity gradient; to the local mean velocity; or to the normalized stream function.

After the fold is created inside the mixing region, it is carried downstream by the mean flow field and will finally be swallowed by another fold to form a new and larger fold. Ganji and Sawyer reported a relationship, which obeys the experimental law approximately, between the percentage of survived eddies and the surviving distance. Therefore, a distribution of the percentage (or population) of various folds formed at different upstream locations is expected at any downstream position. The folds can be identified according to their birthplaces and hence be classified into different groups.

Re-engulfment and formation rates are directly linked, conditional upon their difference being equal to the entrainment rate from the mass conservation law. Should a new fold contain equal amounts of fresh and old material, the quotient of re-engulfment to formation rates would be 0.5. Generally speaking, this quotient is a function of position across a shear layer or jet. Thus, the function can be expressed as:

$$\dot{R}_R = (1-Mo)\dot{R}_F \qquad , (2.3\text{-}1)$$

where $\dot{R}_R$ and $\dot{R}_F$ represent the re-engulfment rate and formation rate respectively, Mo is the mass fraction of the fresh fluid in the newly formed fold ($0<Mo<1$).

The re-engulfment rate of each group of folds is therefore calculated from the total re-engulfment rate (Eqn.2.3-1) multiplied by the population distribution obtained from the demographic analysis.

2.4 Fold Stretching

Winant and Browand (1974) observed the deformation of vortices during their pairing process in turbulent boundary layers. The vortices become elongated in the flow direction while they roll around each other which indicates strains imposed by the stream velocities.

Spalding (1976b) has attributed two factors to the rate of distortion of layers, namely the mean motion of the fluid and the random turbulence eddying movements. The random turbulence motion is very complex and not yet well understood. Hence, only the rate of distortion brought about by the mean turbulent flow is considered in the present work and it is hoped that the main effects of stretching are adequately included, at least for the present.

If the average thickness of the fold is defined as Z, the stretching rate (or the reduction rate of a certain scale) is related to the rate of strain through the following expression:

$$\frac{dZ}{dt} = -\left| \frac{\partial u}{\partial y} + \frac{\partial v}{\partial x} \right| Z \qquad , (2.4\text{-}1)$$

where t is time, u and v represent the mean velocity in the x and y direction respectively. Eqn.(2.4-1) is further reduced according to the boundary layer assumption

as:

$$\frac{dZ}{dt} = - \left| \frac{\partial u}{\partial y} \right| Z \qquad , (2.4\text{-}2)$$

in the present computation.

2.5 Fold Transport

The basic transport mechanism of the folds is the mean convective flow motion, although the local vorticity can induce the turn-over of the folds. The trajectories of the eddies in the free shear layer has been first studied by Brown and Roshko (1974) and followed by Ganji and Sawyer (1980). It has been reported in their later work that the trajectories are nearly parellel to each other, indicating that the vortices nearly move with the same convective velocity in space.

In the case of a free jet where the maximum velocity decays in the downstream direction, the trajectories of the eddies are supposed to be somewhat different from those of free shear layer where the boundary velocities are constant. It is assumed in the present work that the folds move with the local mean velocity along the path of constant mixture fraction, the mixture fraction being defined as:

$$f \equiv \frac{\phi - \phi_e}{\phi_e - \phi_\infty} \qquad , (2.5\text{-}1)$$

where

$$\phi \equiv s^* m_{fu} - m_{ox} \qquad , (2.5\text{-}2)$$

and m_{fu} and m_{ox} are the mass fractions of fuel and oxidant

and s is the stoichiometric oxydant required to burn 1kg of fuel. ϕ_e and ϕ_∞ are the values of ϕ at the fuel pipe exit and the surrounding air.

The present assumption on the fold trajectories implies that the elemental composition of each fold remains constant during its life time (before it is re-engulfed by other fold to form a new one). This hypothesis is consistent with the coherent assumption that each individual fold does not communicate with the others within its life span (Spalding, 1979b).

2.6 Fold age and the quantities correlated with it.

The fold which is formed at a particular point in the flow field will take a finite time to travel to another place (before it is re-engulfed). Spalding (1976b) suggested the use of an "age" dimension to describe the fold-history. The definition of "age" employed in the ESCIMO theory is the time elapsed since fold formation. Thus, it is related to the convective velocity and the distance from the birth place along the fold path.

The mathematical relation between the age and the relevant quantities is now written as:

$$A \equiv \int_{c^{x_b}}^{x} \frac{dx}{u} \qquad , (2.6\text{-}1)$$

where A is the age of the fold and x_b is the x-value at the birth place. c is the trajectory of the fold.

Folds which have survived through various periods of time can be characterised by their ages. Samples taken

at a particular point in a flow field over a significant time interval should be able to exhibit folds having various ages owing to the turbulent fluctuation. Consequently a population distribution curve based on age can be constructed.

The task in the demographic part of the ESCIMO theory is to obtain the population distribution of folds in the flow domain. The mathematical framework and computational technique share some similar feature with the computation of particle-size distribution in coal combustion (Gibson and Morgan, 1970; Richter and Quack, 1975) and in droplet combustion (Elgobashi, Pratt, Spalding and Srivatsa, 1976). The detail analysis is to be described in the next chapter.

2.7 Phenomena occuring within the fold

While the creation and transport of the large scale coherent structures, such as folds, are dominated by the turbulent mixing processes, the interaction between the interface of fresh reactant and the product inside each fold is a molecular one. The molecular diffusion, heat conduction and chemical reaction which take place in direction normal to the interface are subject to the laminar law and hence the laminar exchange coefficient can be employed in the computation.

The properties of the fresh component (reactant) of the fold are those which belong to the undisturbed irrotational fluid outside the shear layers or jets. On the other hand, the properties of the re-engulfed

component of the fold are determined by the mean turbulent values and the fluctuation values inside the mixing region.

The inter-diffusional and chemical-reaction processes within the fluid element are influenced by the stretching effect from the mean turbulent motion such that the distances over which the reactants must travel become steadily smaller. The interaction between turbulence and combustion is embodied in this aspect of the ESCIMO theory.

Since the moving observer concept is adopted in the biographic analysis, the equations describing the heat and mass transfer inside the fold can be reduced to more tractable partial differential equations without the non-linear convection terms. Extensive reports on this formulation can be found in the related work by Noseir (1980) and Tam (1981).

2.8 Closure

A summary of the main points in the physical model of the ESCIMO theory are listed below.

(1) The turbulent flow field has to be solved by considering the time-averaged equation of motion. The turbulence quantities are determined by the two-equation model, namely the kinetic energy of turbulence and its dissipation rate.

(2) The eddies, or folds, are created inside the mixing region and they are composed of the fresh irrotational fliud and the fluid element already

existing in the mixing region. The rate of formation is determined by the entrainment process.

(3) The folds are being continuously subject to the shear strain caused by the turbulence motion. Only the effect of mean turbulent motion is considered in the current work.

(4) The main mechanism of the fold transport is the mean convective motion.

(5) There exists a distribution of folds which have survived through various periods of time since formation at any point in the flow domain due to the turbulent mixing.

(6) The process which takes place at the interface between the fresh and the re-engulfed part of each fold is dominated by the molecular diffusion.

(7) The mean turbulent properties at any location can be obtained from the corresponding quantities of each fold multiplied by the population distribution function there.

The mathematical formulation and the solution procedure will be set up and described in the next chapters.

CHAPTER 3

THE MATHEMATICAL ANALYSIS: DEMOGRAPHIC ASPECTS

3.1 Introduction

The governing equations of the mean velocity, turbulence quantities and the mixture fraction will be supplied in this chapter firstly, because all the results obtained herein serve as the necessary input to the ESCIMO theory.

Secondly, the transport equations which describe the population distribution of various folds will be provided. The equations will then be transformed into a non-dimensional form in order to promote the convenience of solution procedure. The boundary conditions of these equations are also discussed.

The transformed partial differential equations of folds population distribution are then written in the finite difference form which lead to a set of algebraic equations. These algebraic equations are solved by tridiogonal matrix algorithm (TDMA, see Smith (1974)). The age space is discretised into a finite number of intervals for the sake of practical calculation.

Finally, the solution procedure of the finite difference equations will be presented in detail and the upwind difference scheme is employed in both the space coordinate and the age coordinate to procure physically realistic results.

3.2 The Hydrodynamic Calculation

3.2.1 The Basic Equations in Polar Coordinate

The conservation laws of mass and momentum are applied to axisymmetrical, isobaric free boundary layers. The transport equations for the axially-directed momemtum and for the mixture fraction, given by Spalding (1971a) are listed below.

$$\rho u \frac{\partial u}{\partial x} + \rho v \frac{\partial u}{\partial r} = \frac{1}{r} \frac{\partial}{\partial r} (r \mu_t \frac{\partial u}{\partial r}) + (\rho_\infty - \rho) g \quad ,(3.2\text{-}1)$$

and

$$\rho u \frac{\partial \bar{f}}{\partial x} + \rho v \frac{\partial \bar{f}}{\partial r} = \frac{1}{r} \frac{\partial}{\partial r} (r \frac{\mu_t}{\sigma_f} \frac{\partial \bar{f}}{\partial r}) \quad ,(3.2\text{-}2)$$

where u and v are, respectively, the time-averaged axially and radially-directed velocities of the jet flow; x and r are the axial and radial coordinates; $\bar{f}$ is the time-averaged mixture fraction (defined in Eqn2.5-1), ρ is the density of the mixture and ρ_∞ is its value in the surroundings; g is the gravitational acceleration assumed to be aligned with the axis of symmetry, μ_t is the "turbulent viscosity", and σ_f is the turbulent Prandtl/Schmidt number.

The pressure gradient term does not exist in Eqn. (3.2-1) because the flow considered is free jet (or free shear layer). The turbulent Lewis numbers for all species have been assumed to be unity so that Eqn(3.2-2) contains no source term on the right hand side. It implies that the turbulent diffusion coefficients of all species are equal to each other.

The equations for the turbulent kinetic energy and the dissipation rate of turbulent kinetic energy given by Launder and Spalding (1973) are presented below:

$$\rho u \frac{\partial k}{\partial x} + \rho v \frac{\partial k}{\partial r} = \frac{1}{r} \frac{\partial}{\partial r} \left(r \frac{\mu_t}{\sigma_k} \frac{\partial k}{\partial r} \right) + G_k - \rho \varepsilon \quad , \quad (3.2\text{-}3)$$

and

$$\rho u \frac{\partial \varepsilon}{\partial x} + \rho v \frac{\partial \varepsilon}{\partial r} = \frac{1}{r} \frac{\partial}{\partial r} \left(r \frac{\mu_t}{\sigma_\varepsilon} \frac{\partial \varepsilon}{\partial \theta} \right) + \frac{\varepsilon}{k} (C_1 G_k - C_2 \rho \varepsilon), \quad (3.2\text{-}4)$$

where C_1 and C_2 are empirical constants.

G_k is the rate of generation of turbulence energy which is given by the following expression:

$$G_k = \mu_t \left(\frac{\partial u}{\partial r} \right)^2 \quad , \quad (3.2\text{-}5)$$

The turbulent viscosity is calculated in the k-ε model by the relation

$$\mu_t = C_\mu \rho \frac{k^2}{\varepsilon} \quad ; \quad (3.2\text{-}6)$$

where C_μ is an empirical constant.

The combination of the laminar viscosity and the turbulent viscosity is termed the "effective viscosity":

$$\mu_e = \mu_\ell + \mu_t \quad . \quad (3.2\text{-}7)$$

The values of C_1, C_2, C_μ and σ_k, σ_ε used here are the same as those given by Launder and Spalding (1973), namely:

$$C_1 = 1.43, \quad C_2 = 1.92, \quad C_\mu = 0.09$$

$$\sigma_k = 1.0, \quad \sigma_\varepsilon = 1.3$$

3.2.2 The Transformation of the Equations to the x∿ω coordinates

In the actual solution procedure, the numerical scheme of Patankar-Spalding (1967) embodied in the GENMIX computer

$$\omega = \int_0^y r\rho u dy \;/\; \int_0^{y_E} r\rho u dy \qquad , (3.2\text{-}11)$$

and

$$\int_0^y r dy = (\psi_E - \psi_I) \int_0^\omega (\rho u)^{-1} d\omega \qquad . (3.2\text{-}12)$$

The standard mathematical technique is now employed to transform Eqn.(3.2-8) into the $x \sim \omega$ coordinate system.

The task is to express $(\frac{\partial \phi}{\partial x})_\psi$ in terms of $(\frac{\partial \phi}{\partial x})_\omega$ and $(\frac{\partial \phi}{\partial \omega})_x$; and $(\frac{\partial \phi}{\partial \psi})_x$ in terms of $(\frac{\partial \phi}{\partial x})_\omega$ and $(\frac{\partial \phi}{\partial \omega})_x$ respectively.

From the differentiation rule, the following results are obtained:

$$(\frac{\partial \phi}{\partial x})_\psi = (\frac{\partial \phi}{\partial x})_\omega + (\frac{\partial \phi}{\partial \omega})_x (\frac{\partial \omega}{\partial x})_\psi \qquad , (3.2\text{-}13)$$

and

$$(\frac{\partial \omega}{\partial x})_\psi = \frac{1}{\psi_E - \psi_I} \{\frac{d\psi_I}{dx} + \omega \frac{d(\psi_E - \psi_I)}{dx}\} \qquad , (3.2\text{-}14)$$

since $d\psi = 0$ at fixed ψ.

Hence

$$(\frac{\partial \phi}{\partial x})_\psi = (\frac{\partial \phi}{\partial x})_\omega - \frac{1}{(\psi_E - \psi_I)} \{\frac{d\psi_I}{dx} + \omega \frac{d(\psi_E - \psi_I)}{dx}\} (\frac{\partial \phi}{\partial \omega})_x$$

. (3.2-15)

Equation (3.2-13) is now rewritten in the compact form as:

$$(\frac{\partial \phi}{\partial x})_\psi = (\frac{\partial \phi}{\partial x})_\omega + (a + b\omega)(\frac{\partial \phi}{\partial \omega})_x$$

program is employed. The partial differential equations for u, f, k, ε etc are first derived in the "Von Mises" coordinate system, x∿ψ. They are expressed in the general form given below (Spalding (1978a)).

$$\frac{\partial \phi}{\partial x} = \frac{\partial}{\partial \psi} \left(r^2 \rho u \Gamma_{\phi,eff} \frac{\partial \phi}{\partial \psi} \right) + \frac{1}{\rho u} S_\phi \quad , (3.2\text{-}8)$$

where ϕ stands for any of the quantities u, f, k, ε etc and S_ϕ stands for the corresponding source term, $\Gamma_{\phi,eff}$ is the "effective exchange coefficient" for the variable ϕ and ψ is the stream function given by:

$$\psi \equiv \int_0^y r\rho u dy \quad . (3.2\text{-}9)$$

For the sake of economy of computer storage in the numerical calculation, Eqn.(3.2-8) is then transformed into the x∿ω coordinate system; here the coordinate ω is defined by:

$$\omega \equiv (\psi - \psi_I)/(\psi_E - \psi_I) \quad , (3.2\text{-}10)$$

where ψ_E and ψ_I stand for respectively, the value of ψ at the external and internal boundary of the calculation domain. The values of ψ_E and ψ_I are chosen in such a way that the whole of the interesting region is covered within the I and E boundaries and therefore ω takes values between 0 and 1. Note that ψ_E and ψ_I are functions of x and are calculated during the course of computation.

From the definition of ψ and ω, given by Eqns.(3.2-9) and (3.2-10), the following relations can be achieved:

Here a and b are defined by:

$$a \equiv \frac{-1}{(\psi_E-\psi_I)} \frac{d\psi_I}{dx} \quad , (3.2\text{-}16)$$

$$b \equiv \frac{-1}{(\psi_E-\psi_I)} \frac{d}{dx} (\psi_E-\psi_I) \quad . (3.2\text{-}17)$$

Similarly, for the definition of ω;

$$\left(\frac{\partial\phi}{\partial\psi}\right)_x = \left(\frac{\partial\phi}{\partial\omega}\right)_x \left(\frac{\partial\omega}{\partial\psi}\right)_x$$

$$= \frac{1}{(\psi_E-\psi_I)} \left(\frac{\partial\phi}{\partial\omega}\right)_x \quad . (3.2\text{-}18)$$

Since $(\psi_E-\psi_I)$ is a constant at fixed x, the following relation is readily established:

$$\left[\frac{\partial\phi}{\partial\psi} \{r^2\rho u\Gamma_{\phi,eff}\left(\frac{\partial\phi}{\partial\psi}\right)_x\}\right]_x \equiv \left[\frac{\partial\phi}{\partial\omega} \{c\left(\frac{\partial\phi}{\partial\omega}\right)_x\}\right]_x \quad , (3.2\text{-}19)$$

in which c is defined by:

$$c \equiv \frac{r^2\rho u\Gamma_{\phi,eff}}{(\psi_E-\psi_I)^2} \quad . (3.2\text{-}20)$$

Thus the resulting transformed form of Eqn.(3.2-8) in the $x\sim\omega$ coordinate system is:

$$\frac{\partial\phi}{\partial x} + (a+b\omega)\frac{\partial\phi}{\partial\omega} = \frac{\partial}{\partial\omega} (c\frac{\partial\phi}{\partial\omega}) + d \quad .(3.2\text{-}21)$$

(i) (ii) (iii) (iv)

Term (i) in Eqn.(3.2-21) represents the longitudinal convection of variable ϕ, term (ii) stands for the lateral

convection. Term (iii) stands for the cross-stream diffusion and term (iv) is the "source" of the entity.

It should be mentioned here that the quantities a and b are respectively, the rate of inflow to the boundary layer through the I boundary and the sums of the rates of outflow from the boundary layer through both the I and E boundaries, Hence:

$$a = r_I \dot{m}_I''' / (\psi_E - \psi_I) \quad , \quad (3.2\text{-}22)$$

$$b = (r_E \dot{m}_E''' - r_I \dot{m}_I''') / (\psi_E - \psi_I) \quad , \quad (3.2\text{-}23)$$

where the mass fluxes $\dot{m}_E'''$ and $\dot{m}_I'''$ are mass flow rates per unit area across grid boundaries, as shown in Fig.3.2-1.

The values of a and b are calculated as those in the standard GENMIX program, hence only the brief description will be given below:

• When there is a symmetry axis or symmetry plane in the flow, this will be used as one boundary of the domain of integration and the relevant $\dot{m}'''$ must be equal to zero.

• When the boundary of calculation domain expands to cover the boundary layer, the mass transfer rate is chosen so that material flows into the boundary layer at such a rate that conditions just within the layer differ from those in the undisturbed stream by a small specified amount. This device is applicable to the boundary of shear layers, jets, etc.

• When the integration domain is bounded by the impermeable wall, the mass transfer rate is equal to zero;

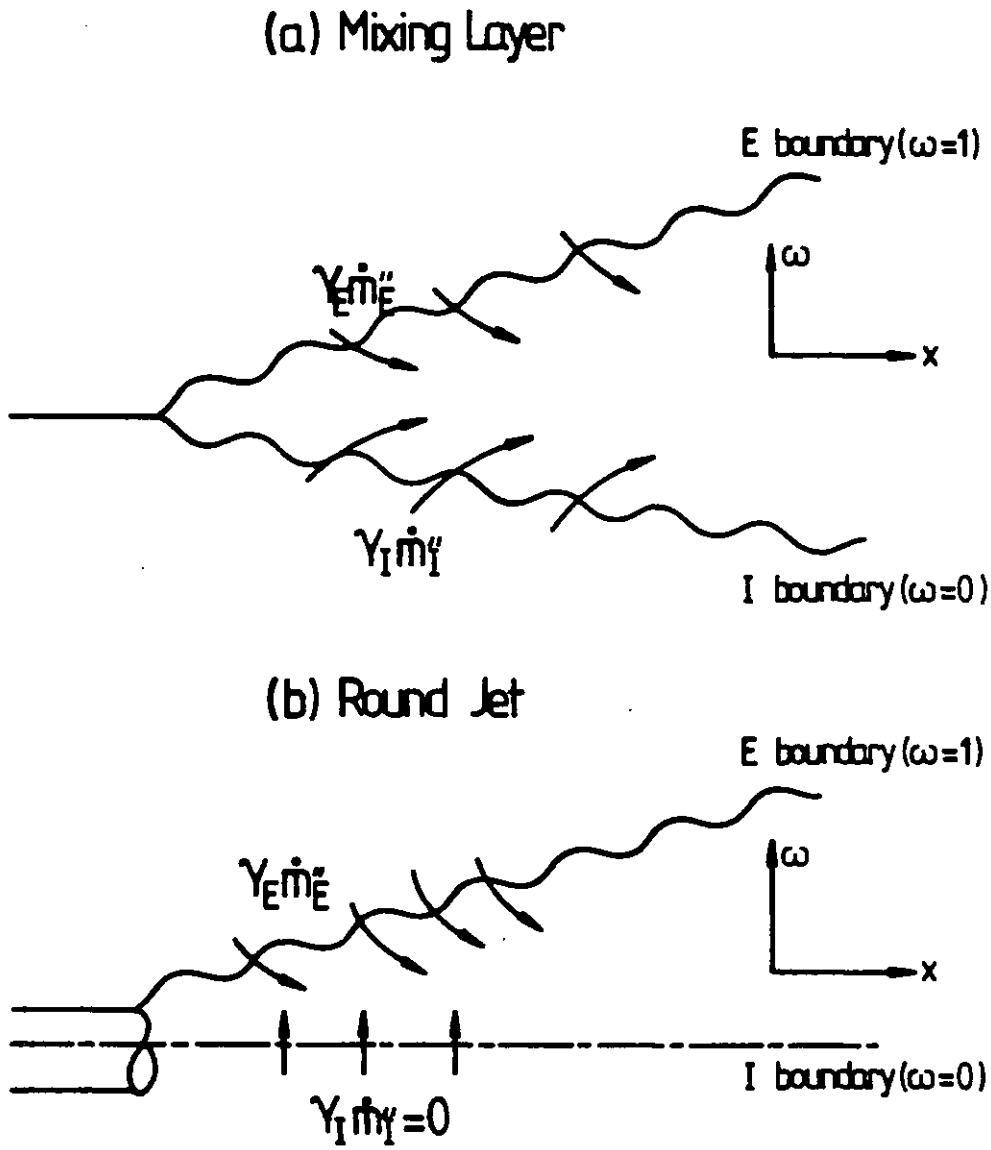

Fig.3.2-1 Boundaries of the computation domain

otherwise it should be equal to the mass transfer rate prevailing in the actual problem.

The source terms, d, for the equation of u, f, k and ε have been established in the previous work of Launder and Spalding (1974), Spalding (1978a). They are now listed in Table 3-2:

Variable	Source term, d
u	$\frac{1}{\rho u}(\rho_\infty-\rho)g$
f	0
k	$\frac{1}{\rho u}(G_k-\rho\varepsilon)$
ε	$\frac{1}{\rho u}\frac{\varepsilon}{k}(C_1G_k - C_2\rho\varepsilon)$

Table 3-2 Source terms for the relevant equation in the general form.

3.3 The Basic Differential Equations for the Fold Population.

At a certain location in a flow region, the population of folds there has different ages and is defined in the present theory as the propability of finding particular folds per unit age. Thus, the population P is a conserved property and has the dimension of $(age)^{-1}$ and obeys the following relation:

$$\int_0^\infty P dA = 1 \qquad .(3.3\text{-}1)$$

The task in the demographic analysis is to solve the conservation equation for P of the kind described in the preceding section, viz:

$$\frac{\partial P}{\partial x} + (a+b\omega)\frac{\partial P}{\partial \omega} = \frac{\partial}{\partial \omega}(c\frac{\partial P}{\partial \omega}) + dp \qquad ,(3.3\text{-}2)$$

The source term dp includes the "simple-aging", fold formation and fold re-engulfment rates. It is presumed here that the simple aging part is $-\partial P/\partial A$; this signifies that the folds can only become older and that the value of P at one value of A is influenced by the shape of the population-distribution function itself. The relation between the formation rate and re-engulfment rate has already been described in Sec.2.3.

The creation of a new fold is always accompanied by the death of an existing fold as a kind of "reincarnation" under present conceptual framework, since all the fluid in the mixing region is fold material. The source term in Eqn.(3.3-2) is therefore given by

$$dp = \left[-\rho\frac{\partial P}{\partial A} + \rho\dot{R}_F\delta(A) - \rho\dot{R}_R P - \rho Mo\dot{R}_F P \right] /\rho u \qquad ,(3.3\text{-}3)$$

$$= \left[-\frac{\partial P}{\partial A} + \dot{R}_F\delta(A) - \dot{R}_F P \right] /u \qquad ,(3.3\text{-}4)$$

where $\delta(A)$ is the Dirac delta function defined as :

$$\delta(A) = \lim_{\Delta A \to 0} \begin{cases} \frac{1}{\Delta A} & \text{for } 0<A<\Delta A \\ 0 & \text{for } A>\Delta A \end{cases} \qquad ,(3.3\text{-}5)$$

with the property of $\int_0^\infty \delta(A)dA = 1$ (the portion of $A<0$ is not considered here because of the non-negativity of age).

The second term on the right hand side of Eqn.(3.3-3) represents the generation of new folds at A=0 only (it needs to be approximated by a small interval in the finite difference formulation). The third and fourth terms denote, respectively, the consumption of fold material required for the re-engulfed and fresh part of newly formed folds. Note that the value of Mo does not appear explicitly in the final expression of Eqn(3.3-4).

3.4 Transformed Differential Equation of Fold Population

From the definition of age in Eqn.(2.6-1) it can be observed that the maximum age in question increases with the longitudinal distance x. Hence, it will be necessary to employ a large number of sub-intervals in the age-coordinate in order to obtain reasonably accurate results in the downstream region of the flame jet.

A non-dimensional age $\bar{A}$, is now introduced to economize the computational procedure and to cover the age-interval of important interest, viz:

$$\bar{A} \equiv AF\{x\} \qquad ,(3.4\text{-}1)$$

where $F\{x\}$ indicates that F is a function of x only.

The characteristics of non-dimensional age, $\bar{A}$, are similar to those of non-dimensional strean function, ω, in the Patankar-Spalding procedure. The function F is chosen in such a way that the whole of the interesting region in the age-dimension is included and $\bar{A}$ takes the value between 0 and 1. This device is justified because the population of the very old folds (in the boundary layer type flow at least) must be negligibly small. Thus, a moderate number of sub-division in the $\bar{A}$-coordinate is sufficient to yield acceptable accuracy.

The standard mathematical technique is now employed to transform Eqn.(3.3-2) from the x, ω, A coordinate system into the X, W, $\tilde{A}$ one with the following definition:

$$X \equiv x \quad ; (3.4\text{-}2)$$

$$W \equiv \omega \quad ; (3.4\text{-}3)$$

$$\tilde{A} \equiv AF\{x\} \quad . (3.4\text{-}4)$$

It can be shown from the chain rule of differentiation that

$$\frac{\partial P}{\partial x} = \frac{\partial P}{\partial X}\frac{\partial X}{\partial x} + \frac{\partial P}{\partial W}\frac{\partial W}{\partial x} + \frac{\partial P}{\partial \tilde{A}}\frac{\partial \tilde{A}}{\partial x} \quad , (3.4\text{-}5)$$

$$\frac{\partial P}{\partial \omega} = \frac{\partial P}{\partial X}\frac{\partial X}{\partial \omega} + \frac{\partial P}{\partial W}\frac{\partial W}{\partial \omega} + \frac{\partial P}{\partial \tilde{A}}\frac{\partial \tilde{A}}{\partial \omega} \quad , (3.4\text{-}6)$$

$$\frac{\partial P}{\partial A} = \frac{\partial P}{\partial X}\frac{\partial X}{\partial A} + \frac{\partial P}{\partial W}\frac{\partial W}{\partial A} + \frac{\partial P}{\partial \tilde{A}}\frac{\partial \tilde{A}}{\partial A} \quad . (3.4\text{-}7)$$

From the definitions in Eqns.(3.4-2) to (3.4-4), the following relations are valid:

$$\frac{\partial X}{\partial x} = 1 \ , \quad \frac{\partial W}{\partial \omega} = 1 \ , \quad \frac{\partial \tilde{A}}{\partial A} = F \quad , (3.4\text{-}8)$$

$$\frac{\partial \tilde{A}}{\partial x} = \frac{\partial \tilde{A}}{\partial X} = A\frac{\partial F}{\partial X} = \frac{\tilde{A}}{F}\frac{\partial F}{\partial X} \quad , (3.4\text{-}9)$$

$$\frac{\partial W}{\partial x} = \frac{\partial W}{\partial X} = 0 \quad , (3.4\text{-}10)$$

$$\frac{\partial \tilde{A}}{\partial \omega} = \frac{\partial \tilde{A}}{\partial W} = 0 \quad , (3.4\text{-}11)$$

$$\frac{\partial X}{\partial \omega} = \frac{\partial X}{\partial W} = 0 \qquad , (3.4\text{-}12)$$

$$\frac{\partial X}{\partial A} = \frac{\partial x}{\partial A} = 0 \qquad . (3.4\text{-}13)$$

Hence:

$$\frac{\partial P}{\partial x} = \frac{\partial P}{\partial X} + \frac{\partial P}{\partial \tilde{A}} \frac{\tilde{A}}{F} \frac{\partial F}{\partial X} \qquad , (3.4\text{-}14)$$

$$\frac{\partial P}{\partial \omega} = \frac{\partial P}{\partial W} \qquad , (3.4\text{-}15)$$

$$\frac{\partial P}{\partial A} = \frac{\partial P}{\partial \tilde{A}} F \qquad . (3.4\text{-}16)$$

Equation (3.3-2) written in X, W, $\tilde{A}$ coordinate system is now given by:

$$\frac{\partial P}{\partial X} + (a+bW) \frac{\partial P}{\partial W} = \frac{\partial}{\partial W}(c\frac{\partial P}{\partial W}) - (\frac{\tilde{A}}{F} \frac{\partial F}{\partial X} + \frac{F}{u}) \frac{\partial P}{\partial \tilde{A}}$$

$$+\left[\dot{R}_F F \delta(\tilde{A}) - \dot{R}_F P \right] /u \qquad , (3.4\text{-}17)$$

since $\tilde{A} = 0$ when $A = 0$.

The second transformation to the dependent variable, P, is now introduced to satisfy the requirement of:

$$\int P dA = \int \tilde{P} d\tilde{A} \qquad , (3.4\text{-}18)$$

i.e., the area under the $\tilde{P} \sim \tilde{A}$ curve will be equal to that of the $P \sim A$ curve. Noted that $\tilde{P}$ and $\tilde{A}$ are both dimensionless.

because F and u are not functions of $\tilde{A}$. From now on the variables X and W can be restored to the original forms of x and ω, since they are identical to each other.

3.5 Discretisation of Age-Interval

The new feature of the $\tilde{P}$-equation is that an additional coordinate (or dimension), $\tilde{A}$, has been introduced. It is essential to divide the age-coordinate into a number of sub-intervals in the numerical solution procedure, as for x and ω coordinates. The problem is analogous to the particle-size distribution in coal combustion and droplet size distribution in droplet combustion and hence similar technique of discretisation is employed here.

The $\tilde{P}$-equation is now represented by a set of equations, each one represents the probability, $\tilde{P}_j$, of finding the folds which belong to a finite age-interval, $\Delta\tilde{A}_j(\equiv\tilde{A}_{j+1}-\tilde{A}_j)$. Each equation is then coupled with the other through the source terms, viz:

$$\frac{\partial\tilde{P}_1}{\partial x}+(a+b\omega)\frac{\partial\tilde{P}_1}{\partial\omega}=\frac{\partial}{\partial\omega}\left(c\frac{\partial\tilde{P}_1}{\partial\omega}\right)-\frac{\partial}{\partial\tilde{A}}\left[\left(\frac{F}{u}+\frac{\tilde{A}}{F}\frac{dF}{dx}\right)\tilde{P}\right]_{12}+\frac{1}{u}\left[\frac{\dot{R}_F}{\Delta\tilde{A}_1}-\dot{R}_F\tilde{P}_1\right], \quad ,(3.5\text{-}1)$$

$$\frac{\partial\tilde{P}_2}{\partial x}+(a+b\omega)\frac{\partial\tilde{P}_2}{\partial\omega}=\frac{\partial}{\partial\omega}\left(c\frac{\partial\tilde{P}_2}{\partial\omega}\right)-\frac{\partial}{\partial\tilde{A}}\left[\left(\frac{F}{u}+\frac{\tilde{A}}{F}\frac{dF}{dx}\right)\tilde{P}\right]_{23}+\frac{1}{u}\left[-\dot{R}_F\tilde{P}_2\right], \quad ,(3.5\text{-}2)$$

$$\vdots$$

$$\frac{\partial\tilde{P}_j}{\partial x}+(a+b\omega)\frac{\partial\tilde{P}_j}{\partial\omega}=\frac{\partial}{\partial\omega}\left(c\frac{\partial\tilde{P}_j}{\partial\omega}\right)-\frac{\partial}{\partial\tilde{A}}\left[\left(\frac{F}{u}+\frac{\tilde{A}}{F}\frac{dF}{dx}\right)\tilde{P}\right]_{j,j+1}+\frac{1}{u}\left[-\dot{R}_F\tilde{P}_j\right], \quad ,(3.5\text{-}3)$$

Thus, P is now expressed as:

$$P = \tilde{P}\frac{d\tilde{A}}{dA}$$

$$= \tilde{P}F\{x\} \qquad . \quad (3.4\text{-}19)$$

Hence:

$$\frac{\partial P}{\partial X} = F\frac{\partial \tilde{P}}{\partial X} + \tilde{P}\frac{\partial F}{\partial X} \qquad , \quad (3.4\text{-}20)$$

$$\frac{\partial P}{\partial \tilde{A}} = F\frac{\partial \tilde{P}}{\partial \tilde{A}} + \tilde{P}\frac{\partial F}{\partial \tilde{A}}$$

$$= F\frac{\partial \tilde{P}}{\partial \tilde{A}} \quad \text{(since F does not depend on } \tilde{A}\text{)} \qquad , \quad (3.4\text{-}21)$$

$$\frac{\partial P}{\partial W} = F\frac{\partial \tilde{P}}{\partial W} + \tilde{P}\frac{\partial F}{\partial W}$$

$$= F\frac{\partial \tilde{P}}{\partial W} \qquad . \quad (3.4\text{-}22)$$

Equation (3.4-17) is now transformed into the following form with the aid of Eqns.(3.4-20) to (3.4-22):

$$\left(F\frac{\partial \tilde{P}}{\partial X} + \tilde{P}\frac{\partial F}{\partial X}\right) + (a+bW)F\frac{\partial \tilde{P}}{\partial W} = \frac{\partial}{\partial W}\left(cF\frac{\partial \tilde{P}}{\partial W}\right) - \left(\frac{\tilde{A}}{F}\frac{\partial F}{\partial X} + \frac{F}{u}\right)F\frac{\partial \tilde{P}}{\partial \tilde{A}}$$

$$+\left[\dot{R}_F F\delta(\tilde{A}) - \dot{R}_F \tilde{P}F\right]/u \qquad . \quad (3.4\text{-}23)$$

Equation (3.4-23) is rearranged after algebraic manipulation to yield the following form:

$$\frac{\partial \tilde{P}}{\partial X} + (a+bW)\frac{\partial \tilde{P}}{\partial W} = \frac{\partial}{\partial W}\left(c\frac{\partial \tilde{P}}{\partial W}\right) - \frac{\partial}{\partial \tilde{A}}\left[\left(\frac{F}{u} + \frac{\tilde{A}}{F}\frac{\partial F}{\partial X}\right)\tilde{P}\right]$$

$$+\left[\dot{R}_F\delta(\tilde{A}) - \dot{R}_F\tilde{P}\right]/u \qquad , \quad (3.4\text{-}24)$$

where the $\frac{\dot{R}_F}{\Delta\tilde{A}_1}$ term in Eqn.(3.5-1) is the finite difference approximation of $\dot{R}_F\delta(\tilde{A})$ for the generation of folds; the quantity $\frac{\partial}{\partial\tilde{A}}\left[(\frac{F}{u}+\frac{\tilde{A}}{F}\frac{\partial F}{\partial x})\tilde{P}\right]_{j,j+1}$ includes the $\tilde{P}_{j-1}$, $\tilde{P}_j$ and $\tilde{P}_{j+1}$ terms which will be discussed in Sec.3.7.

3.6 Boundary Conditions and Initial Conditions

The zero gradient boundary conditions have been employed at the jet (and mixing layer as well) edge and the jet axis for $\tilde{P}$ for all age sizes. This is easy to understand if one regards the folds as being formed by "injection" into the inside of the jet (or mixing layer) of material "shot" from outside; they do not arrive by molecular diffusion. Thus,

$$\frac{\partial\tilde{P}}{\partial\omega} = 0 \qquad \text{at } \omega = 0 \text{ and } \omega = 1 \qquad .(3.6\text{-}1)$$

It is assumed in the present work that only the newly formed folds exist at the nozzle exit plane (or the initial cross section of the mixing layer). Hence,

$$\begin{aligned} \tilde{P} &= 0 \qquad \text{for } \tilde{A}>\tilde{A}_2 \text{ at } x=0 \\ \tilde{P} &= \frac{1}{\Delta\tilde{A}_1} \qquad \text{for } 0\leq\tilde{A}\leq\tilde{A}_2 \text{ at } x=0 \end{aligned} \qquad ,(3.6\text{-}2)$$

where $\Delta\tilde{A}_1 = \tilde{A}_2-\tilde{A}_1 = \tilde{A}_2$ $(\tilde{A}_1=0)$.

The influence of the initial conditions will gradually die out as the marching procedure in x-direction proceeds.

3.7 Finite Difference Approximation of the Differential Equation

The finite difference equations for u, f, k, ε are the same as those employed by the GENMIX computer program, while

the finite difference form for $\tilde{P}$-equations are new only in the expression of source terms. The full contents of the equations will be provided below for the sake of completeness.

The general Eqn.(3.3-2) is first integrated over the control volume defined between $\omega_{i+\frac{1}{2}}$, $\omega_{i-\frac{1}{2}}$, X_u and X_D, as shown in Fig.3.7-1.

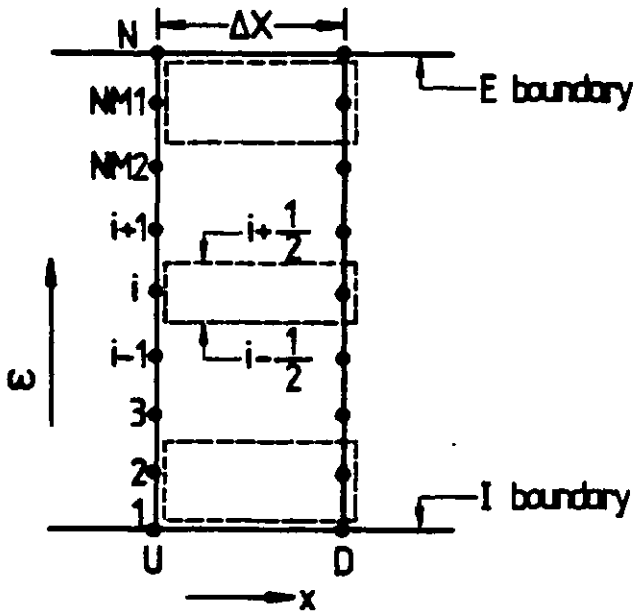

Fig.3.7-1 $x\sim\omega$ grid and control volumes used for the derivation of the finite-difference equations

The values of $\omega_{i+\frac{1}{2}}$ and $\omega_{i-\frac{1}{2}}$ are defined by:

$$\omega_{i-\frac{1}{2}} = \tfrac{1}{2}\,(\omega_{i-1}+\omega_i)$$

$$\omega_{i+\frac{1}{2}} = \tfrac{1}{2}\,(\omega_i+\omega_{i+1}) \qquad \text{for } i \neq 2 \text{ or NM1} \quad , \quad (3.7\text{-}1)$$

and

$$\omega_{i-\frac{1}{2}} = 0 \qquad \text{for } i = 2 \qquad , \quad (3.7\text{-}2)$$

$$\omega_{i+\frac{1}{2}} = 1 \qquad \text{for } i = NM1 \qquad . \quad (3.7\text{-}3)$$

The integrated form of Eqn.(3.3-2) combined with the fully implicit scheme is given by:

$$(1/\Delta x) \int_{i-\frac{1}{2}}^{i+\frac{1}{2}} (\phi_D - \phi_u) d\omega - b \left[\int_{i-\frac{1}{2}}^{i+\frac{1}{2}} \phi d\omega \right]_D$$

$$+ \left[\{(a+b\omega)\phi\}_{i+\frac{1}{2}} - \{(a+b\omega)\phi\}_{i-\frac{1}{2}} \right]_D$$

$$= \left[\left(c\frac{\partial\phi}{\partial\omega}\right)_{i+\frac{1}{2}} - \left(c\frac{\partial\phi}{\partial\omega}\right)_{i-\frac{1}{2}} \right]_D + \left[\int_{i-\frac{1}{2}}^{i+\frac{1}{2}} d \cdot d\omega \right]_D \qquad . \quad (3.7\text{-}4)$$

It can be seen that the only upstream value of ϕ appeared in the first term of Eqn.(3.7-4), while all other ϕ-values are taken from the downstream station. The finite difference expression of Eqn.(3.7-4) takes the following form:

$$\frac{1}{\Delta x} \left[\frac{(\psi_E - \psi_I)_D}{(\psi_E - \psi_I)_u} \phi_{i,D} - \phi_{i,u} \right] (\omega_{i+\frac{1}{2}} - \omega_{i-\frac{1}{2}})$$

$$+ \frac{1}{2(\psi_E - \psi_I)_u} \{\dot{m}'_{i+\frac{1}{2}} (\phi_i + \phi_{i+1})_D - \dot{m}'_{i-\frac{1}{2}} (\phi_i + \phi_{i-1})_D\}$$

$$= \frac{1}{(\psi_E - \psi_I)_u} \{Q_{i+\frac{1}{2}} (\phi_{i+1} - \phi_i)_D - Q_{i-\frac{1}{2}} (\phi_i - \phi_{i-1})_D\}$$

$$+ d_{i,D} (\omega_{i+\frac{1}{2}} - \omega_{i-\frac{1}{2}}) \qquad , \quad (3.7\text{-}5)$$

wherein $\dot{m}'_i \equiv (1-\omega_i)(r\dot{m}')_I + \omega_i(r\dot{m}')_E$, (3.7-6)

$$Q_{i+\frac{1}{2}} \equiv (r\Gamma_{\phi,eff})_{i+\frac{1}{2}}/(y_{i+1}-y_i)_u \quad , (3.7\text{-}7)$$

and $$Q_{i-\frac{1}{2}} \equiv (r\Gamma_{\phi,eff})_{i-\frac{1}{2}}/(y_i-y_{i-1})_u \quad , (3.7\text{-}8)$$

$$d_{i,D}(\omega_{i+\frac{1}{2}}-\omega_{i-\frac{1}{2}}) \equiv S_i + S'_i\phi_{i,D} \quad . (3.7\text{-}9)$$

Eqn.(3.7-4) can be written in the more compact form given by:

$$\zeta_i\phi_{i,D} = \alpha_i\phi_{i+1,D} + \beta_i\phi_{i-1,D} + \gamma_i \quad , (3.7\text{-}10)$$

where

$$\alpha_i \equiv \max\left[0, (Q-\tfrac{1}{2}\dot{m}')_{i+\frac{1}{2}}, -\dot{m}'_{i+\frac{1}{2}}\right] \quad , (3.7\text{-}11)$$

$$\beta_i \equiv \max\left[0, (Q+\tfrac{1}{2}\dot{m}')_{i-\frac{1}{2}}, \dot{m}'_{i-\frac{1}{2}}\right] \quad , (3.7\text{-}12)$$

$$\gamma_i \equiv \phi_{i,u}(\psi_E-\psi_I)_u(\omega_{i+\frac{1}{2}}-\omega_{i-\frac{1}{2}})/\Delta X + S_i \quad , (3.7\text{-}13)$$

$$\zeta_i \equiv \alpha_i+\beta_i+(\psi_E-\psi_I)_u(\omega_{i+\frac{1}{2}}-\omega_{i-\frac{1}{2}})/\Delta X - S'_i \quad . (3.7\text{-}14)$$

The upwind difference scheme is adopted in Eqns.(3.7-11) and (3.7-12) to ensure physically realistic results for the case of high lateral convection. A similar technique has to be employed in the finite difference form of the source terms for $\tilde{P}_j$-equations, so that negative values of $\tilde{P}_j$ will be prevented. The reason is given below.

The folds can only become older in the real age-space and will not be influenced by folds having larger age, but this statement is not always true when the non-dimensional age is used due to the moving grid effect. On the present

transformed coordinates, it is the sign of the term $(\frac{F}{u} + \frac{\tilde{A}}{F}\frac{\partial F}{\partial x})$, multiplying $\frac{\partial \tilde{P}}{\partial \tilde{A}}$ in Eqn.(3.5-1), which determines whether the high-$\tilde{A}$ or low-$\tilde{A}$ value is to be regarded as crossing the $\tilde{A}$-interval boundaries. A better understanding can be achieved with the aid of the figure presented below:

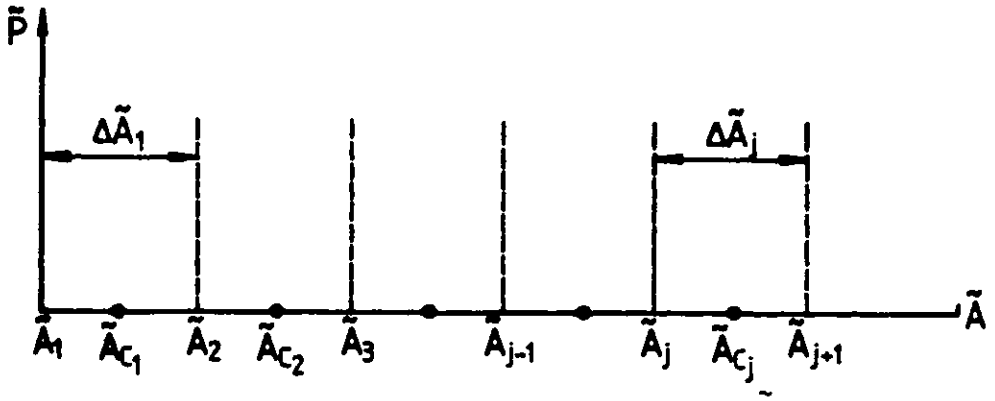

Fig.3.7-2 Grid nodes and intervals of $\tilde{A}$ used in the finite difference form

The values of $\tilde{P}_j$ are stored in the centres of the intervals and the simple ageing term appropriate to the age interval $\Delta\tilde{A}_j$ is:

$$-\frac{\partial}{\partial\tilde{A}}\left[(\frac{F}{u}+\frac{\tilde{A}}{F}\frac{\partial F}{\partial x})\tilde{P}\right]_{j,j+1} = -\frac{1}{\Delta\tilde{A}_j}\left[(\frac{F}{u}+\frac{\tilde{A}_{j+1}}{F}\frac{\partial F}{\partial x})\tilde{P}_{j+}\right.$$

$$\left. -(\frac{F}{u}+\frac{\tilde{A}_j}{F}\frac{\partial F}{\partial x})\tilde{P}_{j-}\right] \quad , \quad (3.7\text{-}15)$$

where $\tilde{P}_{j+}$ and $\tilde{P}_{j-}$ are determined by the upwind difference as:

$$\tilde{P}_{j+} = \tilde{P}_j \quad \text{when } \left(\frac{F}{u} + \frac{\tilde{A}_{j+1}}{F}\frac{\partial F}{\partial x}\right) \geq 0 \quad , \text{(3.7-16)}$$

$$\tilde{P}_{j+} = \tilde{P}_{j+1} \quad \text{when } \left(\frac{F}{u} + \frac{\tilde{A}_{j+1}}{F}\frac{\partial F}{\partial x}\right) < 0 \quad , \text{(3.7-17)}$$

and

$$\tilde{P}_{j-} = \tilde{P}_{j-1} \quad \text{when } \left(\frac{F}{u} + \frac{\tilde{A}_j}{F}\frac{\partial F}{\partial x}\right) \geq 0 \quad , \text{(3.7-18)}$$

$$\tilde{P}_{j-} = \tilde{P}_j \quad \text{when } \left(\frac{F}{u} + \frac{\tilde{A}_j}{F}\frac{\partial F}{\partial x}\right) < 0 \quad , \text{(3.7-19)}$$

where

$$\Delta\tilde{A}_j \equiv \tilde{A}_{j+1} - \tilde{A}_j \text{ and } \tilde{A}_{c_j} = 0.5(\tilde{A}_j + \tilde{A}_{j+1}) \quad . \text{(3.7-20)}$$

Finally, the expression for the total (positive and negative) source term of $\tilde{P}_j$ - equation is:

$$S_1 = -\frac{1}{\Delta\tilde{A}_1}\left[\left(\frac{F}{u} + \frac{\tilde{A}_2}{F}\frac{\partial F}{\partial x}\right)\tilde{P}_{1+}\right] + \frac{1}{u}\left[\frac{\dot{R}_F}{\Delta\tilde{A}_1} - \dot{R}_F\tilde{P}_1\right] . \text{(3.7-21)}$$

and

$$S_j = -\frac{1}{\Delta\tilde{A}_j}\left[\left(\frac{F}{u} + \frac{\tilde{A}_{j+1}}{F}\frac{\partial F}{\partial x}\right)\tilde{P}_{j+} - \left(\frac{F}{u} + \frac{\tilde{A}_j}{F}\frac{\partial F}{\partial x}\right)\tilde{P}_{j-}\right]$$

$$+ \frac{1}{u}\left[-\dot{R}_F\tilde{P}_j\right] \text{ for } j \neq 1. \quad . \text{(3.7-22)}$$

3.8 Solution Procedure

The order of variables solved in the demographic part of the current work are u, f, k, ε, $\tilde{P}_1$, $\tilde{P}_2$, $\tilde{P}_3$, ..., $\tilde{P}_j$, ..., $\tilde{P}_{NA}$, where NA is the number of subdivisions in the $\tilde{A}$-coordinate. The tridiagonal matrix algorithm (TDMA) has been employed in solving Eqn.(3.7-10) and the marching procedure in longitudinal direction is also the same as that embodied in GENMIX program. The enthalpy, temperature and species concentration are calculated

from the combined biographic and demographic analysis in a different manner to be described in the next chapters.

What remains to be emphasised here is that the iteration procedure has been introduced in the calculation of $\tilde{P}_j$, because the values of $\tilde{P}_{j+1}$ are unknown when we are solving for $\tilde{P}_j$. Hence, the value of $\tilde{P}_{j+1}$ in the corresponding upstream position is taken as the initial guess and the iteration loop is given by:

$$(\tilde{P}_1, \tilde{P}_2, \ldots, \tilde{P}_{j-1}, \tilde{P}_j \tilde{P}_{j+1}, \ldots, \tilde{P}_{NA})$$

$$\rightarrow (\tilde{P}_1, \tilde{P}_2, \ldots, \tilde{P}_{j-1}, \tilde{P}_j, \tilde{P}_{j+1}, \ldots, \tilde{P}_{NA})'$$

$$\rightarrow (\tilde{P}_1, \tilde{P}_2, \ldots, \tilde{P}_{j-1}, \tilde{P}_j, \tilde{P}_{j+1}, \ldots, \tilde{P}_{NA})'' \text{ etc}$$

where the single dash and double dash stand for the values obtained after the first and second iteration respectively.

According to the experience obtained during the computation, only four or five iterations are sufficient to achieve the convergent solution because the $\tilde{P}_j$ values do not change drastically in one marching step.

3.9 Closure

The partial differential equations, finite difference equations and the solution procedure of the demographic analysis have been presented in this chapter. The formulation is partly new and partly old; the new part refers to those related to the population distribution function and the old part stands for the integration domain and solution algorithm for other hydrodynamics variables.

In the next chapter, the mathematical analysis of the biographic aspects will be provided and the accuracy of the results assessed.

CHAPTER 4

THE MATHEMATICAL ANALYSIS: BIOGRAPHIC ASPECTS

4.1 Introduction

The Lagrangian (moving observer) approach of the biographic part of the ESCIMO theory has been reported by the earlier work of Noseir (1980) and Tam (1981) for the premixed flames in simple hydrodynamic flows. The purpose of the present chapter is to describe how the biographic calculation can be performed for the turbulent jet diffusion flames with a rather moderate computing cost.

The basic partial differential equation for the fast chemistry diffusion-controlled reaction will be presented first and followed by the description about the fold characteristics at the birth place, because these properties will serve as the initial conditions to the equation.

An approximate method, termed the "profile method", is then introduced to obtain the closed form solution of biographic equation. The computer time is considerably reduced when compared with the corresponding one used in the "time marching method".

The presentation of the profile method is followed by the description of solution procedure to demonstrate where and how the biographic analysis is performed during the course of complete computation. Finally, the accuracy of the profile method will be discussed and attempt has been made to compare the results with those obtained from the more accurate time marching method.

4.2 The Basic Partial Differential Equation

The general transport equation for any conserved property, ϕ, such as mass, momentum and enthalpy, in the fixed coordinate system takes the following form in Spalding (1978b):

$$\frac{\partial \rho\phi}{\partial t} + \mathrm{div}(\rho\vec{u}\phi) = \mathrm{div}(\mathcal{D}_\phi \mathrm{grad}\phi) + S_\phi \quad , \quad (4.2\text{-}1)$$

where $\vec{u}$ is the velocity vector, $\mathcal{D}_\phi$ is the diffusion coefficient for the quantity ϕ, ρ is the density.

The second term in the left-hand side of Eqn.(4.2-1) disappears when the moving observer approach is adopted, i.e., the coordinate system is moving at the same velocity with the fluid element. Hence, Eqn.(4.2-1) is simplified to:

$$\frac{\partial \rho\phi}{\partial t} = \mathrm{div}(\mathcal{D}_\phi \mathrm{grad}\phi) + S_\phi \quad . \quad (4.2\text{-}2)$$

Therefore the nonlinear convection term has been dropped out and the mathematical task becomes easier; this is one of the major advantage in the Lagrangian approach.

The diffusion coefficient, $\mathcal{D}_\phi$, is a laminar one in the biographic analysis (the "small scale mixing" is treated as the laminar process) and hence no modelling is required in its evaluation.

It has been shown by many authors, such as Hawthorne et al. (1949) and Bilger (1980), that the mixture fraction f for a fast chemical reaction process (when the diffusion coefficients are equal) is an important and useful Zeldovich function. The enthalpy and mass fraction of species are uniquely determined by f and hence the other thermodynamics

variables can also be related to f.

Another advantage in using f as the main dependent variable is that Eqn.(4.2-2) contains no source term in the present case, this means that no chemical-kinetic knowledge is needed for the solution of this problem.

If the average density is employed in the calculation, the governing equation for f is now expressed as:

$$\rho \frac{\partial f}{\partial t} = \mathrm{div}(\mathcal{D}_f \mathrm{grad}\, f) \qquad , (4.2\text{-}3)$$

The chemical reaction and diffusion processes inside the fold are assumed to take place in the direction normal to the interface between the fresh and old layer. Thus, Eqn. (4.2-3) reduces to a one-dimensional, unsteady type differential equation given by:

$$\rho \frac{\partial f}{\partial t} = \frac{\partial}{\partial z} \left(\mathcal{D}_f \frac{\partial f}{\partial z}\right) \qquad , (4.2\text{-}4)$$

where z is the distance normal to the interface inside the fold, In reality, the processes should be described by two (or even three)-dimensional equations, but the computing cost will be significantly enlarged without gaining a clear advantage as mentioned by Spalding (1979b).

If the further assumption of uniform diffusion coefficient in the fold is made, Eqn.(4.2-4) takes the simpler form:

$$\frac{\partial f}{\partial t} = - \frac{\mathcal{D}_f}{\rho Z^2} \frac{\partial^2 f}{\partial \eta^2} \qquad , (4.2\text{-}5)$$

where Z is the thickness of the fold and η is z/Z.

From now on the independent variable, t, will be replaced by the "age" of the fold, A. However, the fold

thickness, Z, varies with age as a consequence of the stretching effect and the relation between them is supposed to be:

$$\frac{1}{Z}\frac{dZ}{dA} = -R \quad , \quad (4.2\text{-}6)$$

so that:

$$Z = Z_o \exp(-RA) \quad , \quad (4.2\text{-}7)$$

where Z_o is the fold thickness at birth (at A=0). Eqn.(4.2-7) implies that the fold size diminishes and the "average" stretching rate, R, is taken.

When Eqn.(4.2-5) is combined with Eqn.(4.2-7), a compact form is achieved after some mathematical manipulation:

$$\frac{\partial f}{\partial A^*} = C\frac{\partial^2 f}{\partial \eta^2} \quad , \quad (4.2\text{-}8)$$

where A* is a kind of non-dimensional age and C is a non-dimensional constant; they are defined by:

$$A^* \equiv \exp(2RA)-1 \quad , \quad (4.2\text{-}9)$$

$$C \equiv \mathscr{D}_f/(2\rho R Z_o^2) \quad . \quad (4.2\text{-}10)$$

The value of 1 in Eqn.(4.2-9) has been chosen in such a way that A* = 0 when A = 0.

4.3 The Fold Characteristics at Birth

The initial conditions of Eqn.(4.2-8) are the values of f in the fresh and old part of the fold at birth place. In the mean time, the fold size at birth and the local

stretching rate are needed in the evaluation of the constant C. Therefore, the necessary information will be provided below.

4.3.1 The Fold Size at Birth

It is assumed in the present work that the fold size at the birth place is proportional to the local length scale of turbulence, viz:

$$Z_0 = C_Z k^{3/2}/\varepsilon \quad , \qquad (4.3\text{-}1)$$

where C_Z is the proportionality constant. Various values of C_Z have been investigated and it has been recognized that the value of 0·328 yields reasonable agreement with experimental data of Batt (1977), Kent and Bilger (1973), Lenz and Günther (1980). The value of 0.328 is actually obtained from the k-ε model.

The present assumption implies that the fold size is proportional to local jet width (about 1/20 in the round jet) or local shear layer width (about 1/16 in the shear layer). Hence, the size of folds created in the downstream region of the flow is larger than the counter part in upstream points.

4.3.2 Fold Composition at Birth

The fresh part of the fold is always supposed here to be the irrotational fluid, while the old (re-engulfed) part of the fold has the properties derived from those of the local mean values. The situation in the mixing layer and jet are slightly different and hence will be discussed separately:

The Mixing Layer Case

In the case of the mixing layer, both of the free streams

are irrotational fluid and capable of forming the new fold. Two kinds of new folds are represented in the graphs:

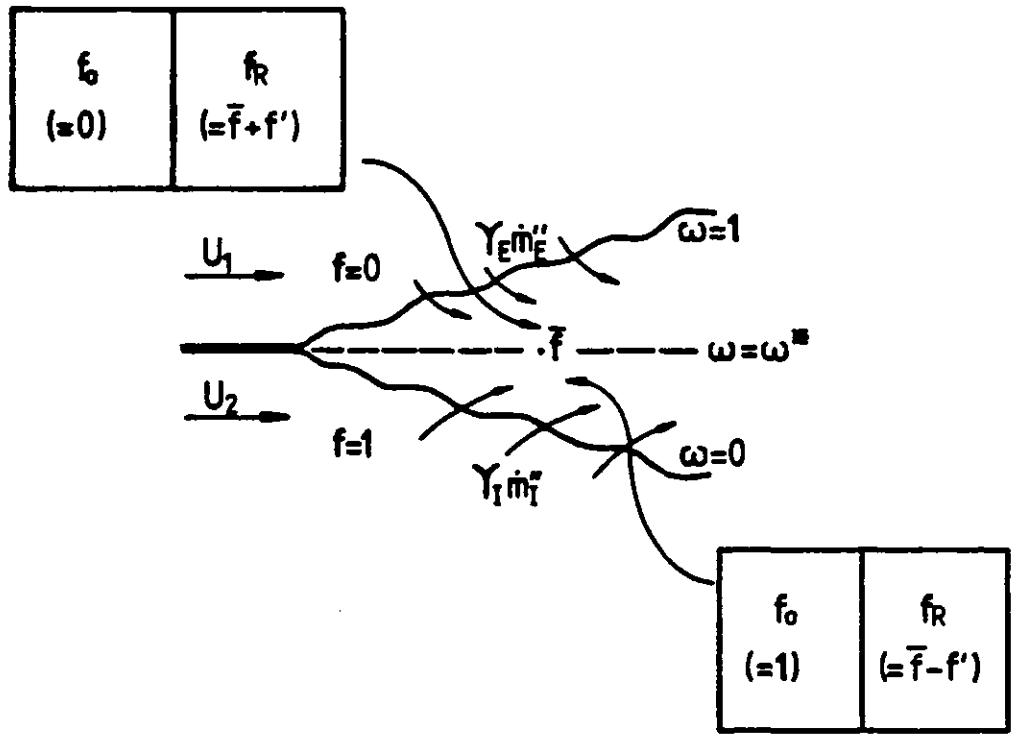

Fig.4.3-1 Composition of folds at birth in the mixing layer

The value of f′ is calculated in accordance with:

$$f' = C_F \ell \left| \frac{\partial \bar{f}}{\partial y} \right| \qquad , (4.3\text{-}2)$$

where C_F is the proportionally constant, ℓ is the local length scale of turbulence. The symbol f_0 and f_R stand for the mixture fraction of the fresh part and re-engulfed part repectively. The value of ω* is given by:

$$\omega^* = \frac{r_I \dot{m}''_I}{r_I \dot{m}''_I - r_E \dot{m}''_E} \qquad , (4.3\text{-}3)$$

so that:

$$f_0 = 1 \qquad f_R = \bar{f} - f' \qquad \text{when } 0 \leq \omega \leq \omega^* \quad , \quad (4.3\text{-}4)$$

and

$$f_0 = 0 \qquad f_R = \bar{f} + f' \qquad \text{when } \omega^* < \omega \leq 1 \quad . \quad (4.3\text{-}5)$$

The Round Jet Case

In the case of the round jet, the irrotational fluid is the surrounding air only ($f_0 = 0$) and hence only one kind of fold exists, viz:

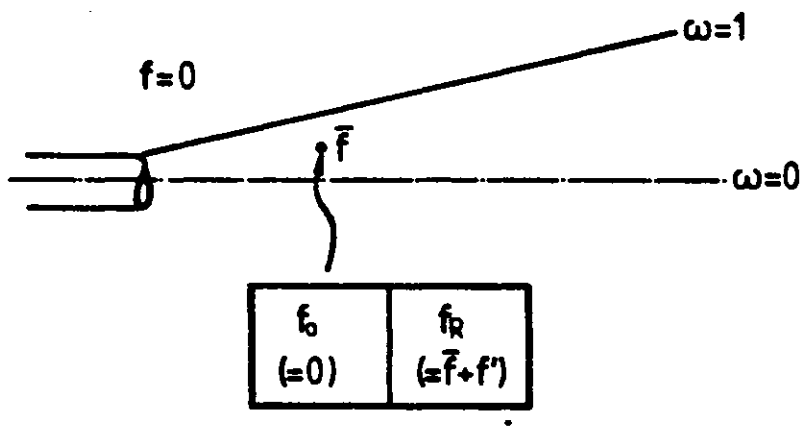

Fig.4.3-2 Composition of folds at birth in the round jet

The composition is now given by:

$$f_0 = 0 \qquad f_R = \bar{f} + f' \qquad \text{when } 0 \leq \omega \leq 1 \quad . \quad (4.3\text{-}6)$$

The Mass Fraction of Fresh Mass in the Fold

The mass fraction of the fresh part, characterised by f_0, in the newly formed fold is determined in such a way that the average f-value in the fold is equal to the local mean value, $\bar{f}$. Hence,

$$f_0 M_0 + f_R(1-M_0) = \bar{f} \quad , \quad (4.3\text{-}7)$$

or

$$M_0 = \frac{f_R - \bar{f}}{f_R - f_0} \quad . \quad (4.3\text{-}8)$$

The M_0 values may vary between 0 an 1 at different places in the calculation domain. It will be shown in the later chapters that the M_0 value is larger near the outer region of the flow, this implies that more irrotational fluid exists in the fold.

4.3.3 The Stretching Rate of the Fold

The stretching rate varies with the path of the fold and hence it is not constant during the lifetime of the fold. However, the "average" stretching rate is employed in Eqn. (4.2-10) to simplify the computational task.

The arithmetic mean between the stretching rate at the birth place and that at the point of combined computation (demographic and biographic analysis) is taken in the present work. The expression takes the form as:

$$R = C_S \left[0.5\left(\left|\frac{\partial u}{\partial y}\right|_b + \left|\frac{\partial u}{\partial y}\right|_\ell \right) \right] \quad , \quad (4.3\text{-}9)$$

where C_S is the stretching rate constant. The subscripts b and ℓ refer to the birth place and the point where the combined analysis is performed. Various values of C_S (from 0.1 to 2.0) have been investigated in the present work.

4.4 The Relation Between Mixture Fraction and Other Variables

The chemical reaction is represented by the single-step, irreversible, global reaction scheme. The intermediate species and radicals are being neglected to allow more attention to be paid on the development of demographic analysis. The previous work of Tam (1981) has already demonstrated that the complex chemical kinetics scheme can be handled in the biographic part of ESCIMO theory.

The chemical reaction rate is assumed to be fast and the laminar exchange coefficients of all species and heat transfer are also assumed to be equal. therefore the relation between the mixture fraction and other variables can be represented by the graph below:

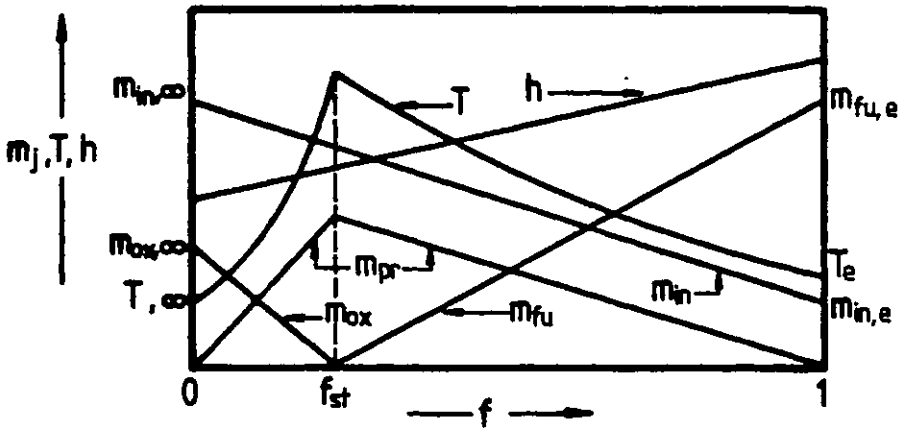

Fig.4.4-1 Sketch of dependencies of various flow properties on mixture fraction

The mathematical formulae are listed below:

$$m_{fu} = 0,\ m_{ox} = m_{ox,\infty}\left(\frac{f_{st}-f}{f_{st}}\right) \text{ when } 0 \leq f \leq f_{st} \quad , (4.4\text{-}1)$$

$$m_{fu} = m_{fu,e}\left(\frac{f-f_{st}}{1-f_{st}}\right),\ m_{ox} = 0 \text{ when } f_{st} < f \leq 1 \quad , (4.4\text{-}2)$$

$$m_{in} = m_{in,e} + (m_{in,e} - m_{in,\infty}) \text{ when } 0 \leq f \leq 1 \quad , (4.4\text{-}3)$$

$$m_{pr} = 1 - m_{fu} - m_{ox} - m_{in} \quad , (4.4\text{-}4)$$

$$h = h_e f + h_\infty (1-f) \quad , (4.4\text{-}5)$$

$$T = (h - m_{fu}H_{fu})/C_{P,mix} \quad , (4.4\text{-}6)$$

$$\rho = W_{mix}p/R_uT \quad , (4.4\text{-}7)$$

wherein:

f_{st} stands for the mixture fraction of the stoichiometric mixture,

m_{in} represents the mass fraction of inert species,

m_{pr} is the mass fraction of product,

h is the enthalpy of the mixture,

T is the temperature of the mixture,

H_{fu} is the heat of combustion of fuel,

p is the pressure of the mixture,

R_u is the universal gas constant,

W_{mix} is the molecular weight of the mixture,

C_p is the specific heat of the mixture.

The subscript e and ∞ denote, respectively, the values at the jet exit and the surrounding air stream.

The specific heat of mixture, $C_{p,mix}$ is calculated in accordance with:

$$C_{p,mix} = \sum_j m_j C_{p_j}(T) \quad , \quad (4.4\text{-}8)$$

where m_j is the mass fraction of the j-th species and C_{p_j} is the corresponding specific heat. The temperature dependent function of C_{p_j} is taken from the third order polynomial of Perry and Chilton (1973):

$$C_{p_j} = K_1 + K_2 T + K_3 T^{-2} \quad , \quad (4.4\text{-}9)$$

where K_1, K_2 and K_3 are constants given in Table 4.4-1.

Species	K_1	K_2	K_3
H_2	13849.62	1.6945	0
O_2	1081.3	0.0337	-0.2454×10^8
N_2	1021.3	0.1346	-0.0179×10^8
CO_2	1005.83	0.1998	-0.196×10^8
H_2O	1698.06	0.572	0
CH_4	1478.53	2.994	-0.12×10^8

Table 4.4-1 The specific constants for various species (the SI unit of $J/^0K\,Kg$ is adopted)

4.5 The Profile Method

Equation (4.2-8) belongs to the category of second order, linear, parabolic partial differential equation. This type of equation often appears in the unsteady heat conduction problem and has been solved in various ways, such as Fourier series expansion, the time marching method and the profile

method. The profile method has enjoyed its simplicity and rather satisfactory accuracy in the boundary-layer theory recorded by Von Karman (1921) and Pohlhausen (1921). It has also been applied to flame problems by Marble and Adamson (1954).

The major feature of the profile method is that the solution of the governing equation is assumed to obey a certain type of function, while the parameters are determined by the integral form of the governing equation together with the initial and boundary conditions. Usually, the linear profile, sinusoidal profile and other polynomial profiles are the popular choice. The sinusoidal profile has been employed in the current work for the sake of simplicity. Thus, the solution of Eqn.(4.2-8) has the form given by:

$$f = \xi_1\{A^*\} \sin\left[\xi_2\{A^*\} + \xi_3\{A^*\}\eta \right] \quad , \quad (4.5\text{-}1)$$

where $\xi_1\{A^*\}$, $\xi_2\{A^*\}$ and $\xi_3\{A^*\}$ are functions of A^* which represent the amplitude and wavelength of the profile.

The variation of the amplitude and wavelength are governed by the integral form of Eqn.(4.2-8), namely:

$$\int_0^1 \frac{\partial f}{\partial A^*}\, d\eta = \int_0^1 C\frac{\partial^2 f}{\partial \eta^2}\, d\eta \quad , \quad (4.5\text{-}2)$$

and

$$\int_0^{\eta_D} \frac{\partial f}{\partial A^*}\, d\eta = \int_0^{\eta_D} C\frac{\partial^2 f}{\partial \eta^2}\, d\eta \quad , \quad (4.5\text{-}3)$$

where η_D is the η-value which separates the fresh part and re-engulfed part at fold-formation time.

The boundaries of the fold are assumed to be plane

symmetric and hence the zero-gradient boundary conditions are employed:

$$\frac{\partial f}{\partial \eta} = 0 \qquad \text{at } \eta = 0 \text{ and } \eta = 1 \qquad . \quad (4.5\text{-}4)$$

Generally speaking, the value of η_D is not equal to 0.5 (because the M_0-value is not equal to 0.5) and the evolution of the sinusoidal profile with age is divided into three stages (as shown in Fig. 4.5-1), namely:

(1) In the first stage, the curve spreads from the initial position toward the boundaries of the fold until one of them is reached. The amplitude is constant and equal to $\frac{1}{2}|f_R - f_0|$.

(2) During the second stage, the curve further spreads until it covers the whole distance across the fold. The amplitude also diminishes during the course.

(3) In the third stage, only the amplitude of the curve decreases as age increases.

The resulting formulae representing the f-distribution in each stage are obtained by inserting Eqn.(4.5-1) into Eqns(4.5-2) and (4.5-3) with the aid of Eqn.(4.5-4) and the auxiliary information listed above. Subsequently, a set of coupled ordinary differential equations which describe the variation of amplitude and wavelength of the profile are constructed. These equations can be solved by the standard mathematical technique and the results are given below:

(I) In the first stage ($A^* \leq A^*_1$):

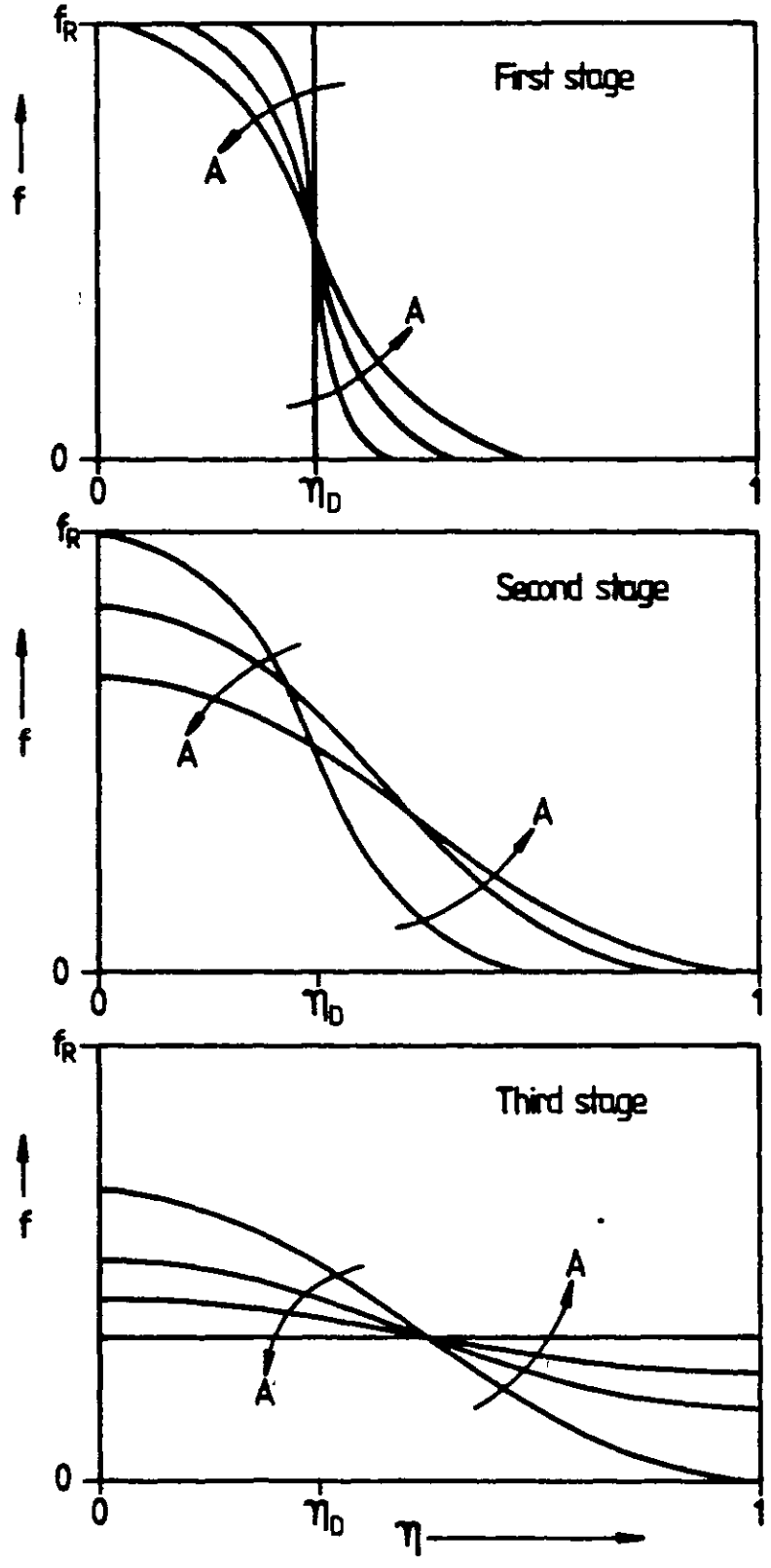

Fig.4.5-1 Evolution of the f-profile inside a fold at various stages

$$f = f_1 \qquad \text{for } 0 \le \eta \le \eta_D - \delta$$

$$f = f_3 + f_4 \sin\left[\frac{\pi}{2}\left(\frac{\eta_D - \eta}{\delta}\right)\right] \qquad \text{for } \eta_D - \delta < \eta \le \eta_D + \delta \quad , \quad (4.5\text{-}5)$$

$$f = f_2 \qquad \text{for } \eta_D + \delta < \eta \le 1$$

wherein:

$$f_1 = \max(f_R, f_0) \quad , \quad (4.5\text{-}6)$$

$$f_2 = \min(f_R, f_0) \quad , \quad (4.5\text{-}7)$$

$$f_3 = \tfrac{1}{2}|f_R + f_0| \quad , \quad (4.5\text{-}8)$$

$$f_4 = \tfrac{1}{2}|f_R - f_0| \quad , \quad (4.5\text{-}9)$$

$$\delta = \left[C\pi A^* f_4 / (f_3 - \frac{2}{\pi} f_4)\right]^{\frac{1}{2}} \quad , \quad (4.5\text{-}10)$$

$$A_1^* = (f_3 - \frac{2}{\pi} f_4 - f_2)\delta_1^2 / C f_4 \pi \quad , \quad (4.5\text{-}11)$$

$$\delta_1 = \min(\eta_D, 1 - \eta_D) \quad . \quad (4.5\text{-}12)$$

(II) In the second stage ($A_1^* < A^* \le A_2^*$)

If $\eta_D < 0.5$ the following relation holds:

$$f = f_5 + f_6 \sin\left[\frac{\pi}{2}\left(1 + \frac{\eta}{\delta_2}\right)\right] \qquad \text{for } 0 \le \eta \le 2\delta_2$$

$$f = f_2 \qquad \text{for } 2\delta_2 < \eta \le 1 \quad , \quad (4.5\text{-}13)$$

wherein:

$$f_5 = f_1 - f_6 \quad , \quad (4.5\text{-}14)$$

$$f_6 = f_4 \cdot \frac{\delta_1}{\delta_2} \quad , \quad (4.5\text{-}15)$$

$$\delta_2 = (C\pi A^* + \delta_1^2)^{\frac{1}{2}} \quad , (4.5\text{-}16)$$

$$A_2^* = A_1^* + (\tfrac{1}{4}-\delta_1^2)/C\pi \quad , (4.5\text{-}17)$$

If $\eta_D \geq 0.5$, the relation is:

$$f = f_1 \qquad \text{for } 0 \leq \eta \leq 1-2\delta_2$$
$$f = f_7 + f_6 \sin\left[\frac{\pi}{2}\left(1+\frac{\eta}{\delta_2}\right)\right] \qquad \text{for } 1-2\delta_2 < \eta \leq 1 \quad , (4.5\text{-}18)$$

where

$$f_7 = f_1 - f_6 \quad . (4.5\text{-}19)$$

(III) In the third stage ($A^* > A_2^*$):

$$f = f_8 + f_9 \sin\left[\pi(\tfrac{1}{2} - \eta)\right] \qquad \text{for } 0 \leq \eta \leq 1 \quad , (4.5\text{-}20)$$

where

$$f_8 = f_1\eta_D + f_2(1-\eta_D) \quad , (4.5\text{-}21)$$

$$f_9 = f_1\delta_1 \exp\left[-C\pi^2(A^*-A_2^*)\right] \quad . (4.5\text{-}22)$$

4.6. The Solution Procedure

The biographic analysis described in this chapter is performed after the demographic analysis at each grid node in the computational domain. The folds are supposed to be formed in each grid-cell and the characteristics at birth are stored in the computer storage from the first step of calculation (i.e. the marching in the longitudinal direction is adopted). This information has been stored outside the central core memory of the computer system, i.e., in the disc or the tape, so that the computer program can be accomodated

even in the smaller machine such as Perkin-Elmer 3220.

The values of A* of different folds are calculated from Eqns.(3.4-1) and (4.2-9) as:

$$A^*_{C_j} = \exp(2R\tilde{A}_{C_j}/F)-1 \quad , \quad (4.6\text{-}1)$$

where $A^*_{C_j}$ is the A*-value of folds which belong to the j-th group at the mid-point of the age interval.

The f~η distribution of each group of folds are then determined with the aid of the profile method, followed by the calculation of temperature and species concentration through Eqns.(4.4-1) to (4.4-6). The sinusoidal profile has been divided into 20 intervals and hence all the required quantities are obtained at those discrete points. The fold-average properties, $\tilde{\phi}$, are computed numerically in accordance with:

$$\tilde{\phi}\{A^*\} = \int_0^1 \phi\ \{A^*,\eta\}d\eta$$

$$\simeq \sum_j \phi\ \{A^*,\eta_j\}\Delta\eta_j \quad . \quad (4.6\text{-}2)$$

4.7 The Accuracy of the Profile Method

The accuracy of the profile method, compared with the known exact solutions, has been investigated in the work of Spalding (1958) on the constant-enthalpy flames. The governing equation of the temperature across the flame is similar to that of Eqn.(4.2-8), except that a non-linear source term exists.

The temperature gradient and the speed of steady flame propagation obtained from linear profile, sinusoidal profile

and parabolic profile have been compared with the exact solutions. It has been pointed out that the accuracy is normally better than 20% and can achieve excellent agreement (2%) with the exact solutions in some cases. Of course, the accuracy of profile method varies from problem to problem and can not be predicted in advance.

The more accurate time marching method has been employed to solve Eqn.(4.2-8) in the hydrogen-air jet diffusion flame, by Fan (1982), to assess the reliability of profile method. The difference in the results obtained from the two methods is of the order of 1% only. Therefore, the errors caused by the profile assumption are negligible in the present problem.

Since the computer time is increased by a factor of three when the profile method is replaced by the marching method, it is probable that the former method will still be useful in the future work to reduce the computational task.

4.8 Closure

The mathematical analysis of biographic aspects has been presented in this chapter for the simple chemical reaction system. The more realistic, multi-step chemical reaction scheme can be incorporated in the future development of ESCIMO theory without formidable difficulties. Of course, an efficient computer program which combines the numerical solution procedure of the present work and that of Tam (1981) is needed.

Some presumptions about the size and the composition of folds at birth have been made to initiate the computation.

The influence of various parameters has been investigated for the reacting mixing layer and jet diffusion flames and will be presented in Chapters 6 and 8.

The profile method is able to produce satisfactory results in the present problem, according to the comparison with the more accurate time marching method.

The more interesting results of turbulent reacting flows are obtained from the coupling of the demographic and biographic analysis, such as the mean turbulent quantities and the fluctuation quantities; the coupling procedure will be described in the next chapter.

CHAPTER 5

THE COMBINED MATHEMATICAL ANALYSIS

5.1 Introduction

The purpose of this chapter is to demonstrate how the demographic analysis and the biographic analysis are linked together to yield the useful information in turbulent combustion.

The average birth places of all kinds of folds arriving at a particular point have to be located first, this will be described in Sec.5.2. Then, the fold-average properties will be multiplied by the population distribution function, $\tilde{P}$, to obtain the population-average quantities (i.e., the turbulent time average quantities); the description is provided in Sec. 5.3.

The root mean square fluctuation of temperature and species concentration are of great importance in the turbulent reacting flows; the calculation of these quantities will be presented in Sec.5.4.

The detail information of turbulence can be seen only from the probability density functions of various quantities and they can be predicted by the ESCIMO theory; the computational process is to be demonstrated in Sec.5.5. Finally, a short summary will be provided in Sec.5.6.

5.2 The Tracing of the Folds

It has been mentioned in Sec.2.5 that the fold trajectories are supposed to follow the constant mixture fraction line, and that all folds move downstream with the mean convective

velocity. The birth place of the folds which arrive at a particular point can therefore always be located at the upstream position, since the flow considered here is a parabolic one.

A simple function of $F\{x\}$, which appears in Eqn.(3.4-1), is chosen in the calculation of the mixing layer and jet diffusion flame, namely:

$$F\{x\} \equiv \frac{U_{min}}{x} \qquad \text{for reacting mixing layer,} \quad (5.2\text{-}1)$$

$$F\{x\} \equiv \frac{U_{ref}}{x} \qquad \text{for jet diffusion flame} \quad , \quad (5.2\text{-}2)$$

where U_{min} is the velocity of lower-speed stream and U_{ref} is a chosen reference velocity. U_{min} is a constant, but U_{ref} can be a constant or a function of distance x (see Chapter 7).

The physical meaning of $F\{x\}$ can be regarded as a kind of scaling factor, or the reciprocal of the maximum reference age. Thus, the maximum reference age defined in Eqns.(5.2-1) and (5.2-2) are x/U_{min} and x/U_{ref} respectively and the maximum distance from the birth place of any fold to the point in question is smaller than or equal to x.

The following procedure has been adopted in this work to locate the birth place of each kind of folds, viz:
(1) calculate the longitudinal distance which the folds of age, $\tilde{A}_{c_j}$, have travelled through, in accordance with:

$$x_{F_j} = x_D(1 - \tilde{A}_{c_j}) \qquad , \quad (5.2\text{-}3)$$

where x_{F_j} is the average journey length of folds belonging to the j-th age-interval. The effect of the curvature of

constant mixture fraction line on x_{Fj} is neglected here.
(2) Usually the value of x_{Fj} lies between two consecutive marching steps at which the information about fold characteristics at birth are stored in the computer memory. The larger of the two (in the x-value), say x_R, is chosen as the representative step to be searched in the cross-stream direction. The birth place of the folds which survive at $x = x_D$ with $\tilde{A} = \tilde{A}_{cj}$ and $f = \bar{f}$ is supposed to stand at $x = x_R$.
(3) The ω value of the birth place, ω_b, is determined by:

$$\omega_b = \omega_i + \frac{f_i - \bar{f}}{f_i - f_{i+1}} (\omega_{i+1} - \omega_i) \qquad , (5.2\text{-}4)$$

where $f_i \geq \bar{f} \geq f_{i+1}$ and f_i, f_{i+1} represent the stored f-values at $\omega = \omega_i$ and $\omega = \omega_{i+1}$ respectively. Eqn.(5.2-4) implies a linear interpolation procedure to obtain the required fold characteristics at ω_b from information stored at ω_i and ω_{i+1}. The figure provided below serves as the supplementary explanation to the searching process of the birth place:

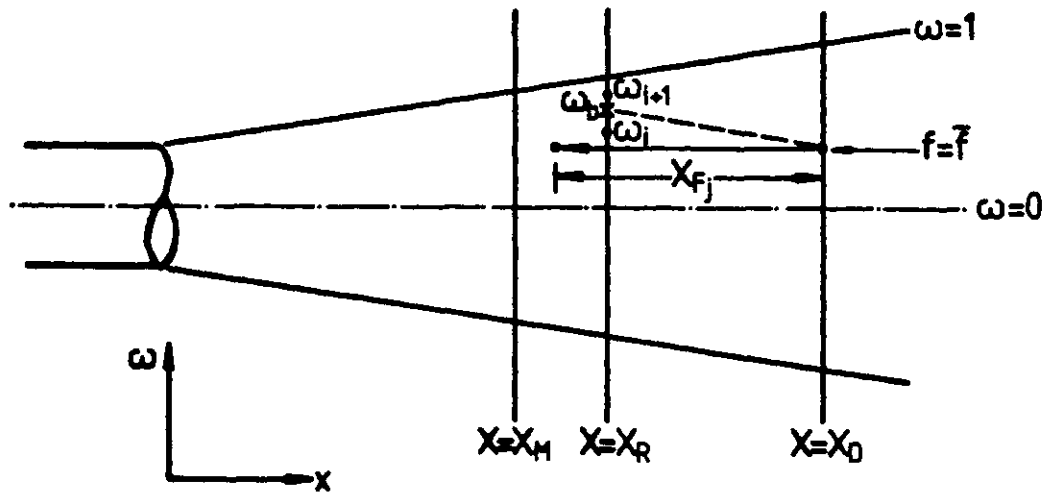

Fig.5.2-1 Tracing of folds in the jet

5.3 The Population Average Properties

Once the birth places of various folds have been spotted and all relevant information obtained from the interpolation procedure described in the preceding section, the biographic calculation can be performed via the profile method and the fold-average values computed with the aid of Eqn.(4.6-2).

The local time average value of any property, $\bar{\phi}$, is deduced from the fold-average values of all folds multiplied by the population distribution function in ESCIMO theory and termed the "population-average property". The expression is given below:

$$\bar{\phi} = \int_0^{\infty} \tilde{\phi}\{\tilde{A}\}\tilde{P}d\tilde{A}$$

$$= \int_0^1 \tilde{\phi}\{\tilde{A}\}\tilde{P}d\tilde{A} \quad , \quad (5.3\text{-}1)$$

$$\approx \sum_{j=1}^{NA} \tilde{\phi}\{\tilde{A}_{c_j}\}\tilde{P}_j\Delta\tilde{A}_j \quad . \quad (5.3\text{-}2)$$

It can be observed that the population distribution function, $\tilde{P}$, in Eqn.(5.3-1) serves as a kind of weighting function during the course of computation. Therefore the variation of properties in each group of folds will make a certain contribution to the local population-average values. The shape of the $\tilde{P}$~$\tilde{A}$ curve is the most important factor which determines the $\bar{\phi}$-value, while the quantitative difference in $\tilde{P}$'s values (under the same shape) has less critical influence.

The local average density, $\bar{\rho}$, is also calculated from Eqn.(5.3-2) in which the fold-average density is obtained by

the biographic analysis. The hydrodynamics results are affected by the chemical reaction mainly through the density variation.

5.4 The Root Mean Square Fluctuation Quantities

The turbulence intensity of each variable in the turbulent flow is usually represented by the "root mean square" fluctuation quantity and defined by:

$$\sqrt{\overline{(\phi')^2}} = \sqrt{\overline{(\phi-\bar{\phi})^2}} \quad , \quad (5.4\text{-}1)$$

where the over bar stands for the local time-average value.

In the framework of ESCIMO theory, the root mean square fluctuation is calculated from the difference between the ϕ-profile inside each fold and its population-average quantity, viz:

$$\begin{aligned}
\overline{(\phi')^2} &= \int_0^1 \{ \int_0^1 \left[\phi\{\tilde{A},\eta\} - \bar{\phi} \right]^2 d\eta \} \tilde{P} d\tilde{A} \\
&= \int_0^1 \{ \int_0^1 \phi^2 d\eta \} \tilde{P} d\tilde{A} - 2 \int_0^1 \{ \int_0^1 \phi \cdot \bar{\phi} d\eta \} \tilde{P} d\tilde{A} + \bar{\phi}^2 \\
&= \int_0^1 \tilde{\phi}^2 \tilde{P} d\tilde{A} - 2\bar{\phi} \int_0^1 \tilde{\phi} \tilde{P} d\tilde{A} + \bar{\phi}^2 \\
&= \overline{\phi^2} - (\bar{\phi})^2 \quad . \quad (5.4\text{-}2)
\end{aligned}$$

The younger folds have a larger contribution in the fluctuation level, since the degree of non-uniformity is more pronounced in those folds. Lower stretching rate can also result in higher fluctuation value, since the layer thickness, hence the distance for diffusive material to

travel, will not be reduced rapidly and a larger difference in properties remains in the fold. Therefore it is expected that the influence of population distribution function and stretching can be examined more thoroughly by the distribution of root mean square fluctuation quantities.

5.5 The Probability Density Functions

The value of any property, ϕ, fluctuates within a particular range in the turbulent flows, say between ϕ_{max} and ϕ_{min}. If someone is taking the instantaneous sampling at a fixed point, he will recognise that the time portion occupied by various ϕ-values are normally different and hence there exists a probability in finding the signal (which represents the magnitude of ϕ) prevailing at the interval between ϕ and $\phi + \delta\phi$. The shape of the probability density functions is of great interest to the researchers in turbulent reacting flows, since it reveals the detail structure of turbulence.

In the present approach of ESCIMO theory, there are two kinds of probability density functions which have to be distingushed, namely:

(1) The probability density function in a fold (fold-pdf) and

(2) The population-average probability density function at a point in the fluid region.

The latter is equivalent to those employed in other models of turbulent combustion. The methods of computation for them are to be presented below.

5.5.1 The definitions of pfd in ESCIMO approach

(a) The fold probability density function $\tilde{P}_{\phi}$

It has been explained in the biographic analysis that the properties across each fold are non-uniform and can be represented by a certain profile. The probability density function of the fold, $\tilde{P}_\phi \delta\phi$, is defined as the mass fraction of material having the property which lies between ϕ and $\phi + \delta\phi$. Hence, at any particular age, the $\tilde{P}_\phi$ distribution is computed in accordance with:

$$\tilde{P}_\phi\{\phi, \tilde{A}\} = \frac{\sum_{\phi}^{\phi+\delta\phi} \frac{d\eta}{\int_0^Z d\eta}}{\delta\phi} \qquad . \quad (5.5\text{-}1)$$

The summation in Eqn.(5.5-1) refers to all possible portion of fold, $d\eta$, which have the property between ϕ and $\phi + \delta\phi$.

(b) <u>The population-average probability density function $\bar{P}_\phi$</u>

Once the fold pdf has been obtained for all folds belong to different age-group, the population-average pdf, $\bar{P}_\phi$, is computed from the following expression:

$$\bar{P}_\phi\{\phi\} = \int_0^1 \tilde{P}_\phi\{\phi, \tilde{A}\} \tilde{P} d\tilde{A} \qquad . \quad (5.5\text{-}2)$$

The argument that the $\bar{P}_\phi$ in Eqn.(5.5-2) has the same physical meaning as those used by Borghi (1979), Kennedy and Kent (1981), Ballantyne and Bray (1976) can be proved from the derivation provided below:

The fold-average value of ϕ, $\tilde{\phi}$, is given by

$$\tilde{\phi}\{\tilde{A}\} = \int_0^1 \phi d\eta$$

$$= \int_{\phi min}^{\phi max} \phi \, \tilde{P}_\phi\{\phi, \tilde{A}\} d\phi \qquad , (5.5\text{-}3)$$

and the time-average value of ϕ, $\bar{\phi}$, by

$$\bar{\phi} = \int_0^1 \tilde{\phi}\{\tilde{A}\}\tilde{P}d\tilde{A}$$

$$= \int_0^1 \left[\int_{\phi_{min}}^{\phi_{max}} \phi \tilde{P}_\phi\{\phi, \tilde{A}\} d\phi \right] \tilde{P}d\tilde{A}$$

$$= \int_{\phi_{min}}^{\phi_{max}} \phi \left[\int_0^1 \tilde{P}_\phi\{\phi, \tilde{A}\}\tilde{P}d\tilde{A} \right] d\phi$$

$$= \int_{\phi_{min}}^{\phi_{max}} \phi \bar{P}_\phi\{\phi\} d\phi \qquad , (5.5\text{-}4)$$

where Eqn.(5.5-4) is the conventional form adopted by the other approaches in turbulent reacting flows.

5.5.2 The Computational Procedure

The detail numerical computation of fold pdf and population average pdf is now described as follows:

(i) Search for the maximum and minimum ϕ-values from the biographic analysis in a kind of fold. Then divide the whole domain (from ϕ_{min} to ϕ_{max}) into a number of uniform intervals, each of which takes the value of:

$$\delta\phi = (\phi_{max} - \phi_{min})/N_\phi \qquad , (5.5\text{-}5)$$

where N_ϕ is the total number of fraction intervals (N_ϕ = 10 is the typical value chosen in the computation).

(ii) The values of ϕ-profile across the fold are calculated at each discrete point (20 points in the present work).

Identify all these ϕ-values with their appropriate $\delta\phi$-intervals defined in step (i): - If a pair of consecutive ϕ-values, say ϕ_{j-1} and ϕ_j, lie within the i-th ϕ-interval, $\delta\phi_i$, assign the mass fraction in $\Delta\eta_j$, occupied by the $\Delta\phi_j$ $(\equiv\phi_j-\phi_{j-1})$, to the "fold-pdf domain" of $\delta\phi_i$, $\tilde{P}_\phi$, with the aid of Eqn.(5.5-1). The process is illustrated in Fig.5.5-1. Linear interpolation is employed if $\Delta\phi_j$ ranges across the $\delta\phi_i$ and $\delta\phi_{i+1}$ interval.

(iii) Repeat steps (i) and (ii) for all kinds of folds and determine a suitable set of maximum and minimum values of ϕ, say $\bar{\phi}_{max}$, and $\bar{\phi}_{min}$ for the whole population of folds. Of course, the following relation should be satisfied:

$$\bar{\phi}_{max} \geq \max(\phi_{max,1}, \phi_{max,2}, \ldots, \phi_{max,NA}) \quad , (5.5\text{-}6)$$

$$\bar{\phi}_{min} \leq \min(\phi_{min,1}, \phi_{min,2}, \ldots, \phi_{min,NA}) \quad , (5.5\text{-}7)$$

where

$\phi_{max,i}$ is the value of ϕ_{max} for the folds belonging to the $(\Delta\tilde{A}_i)$ interval,

$\phi_{min,i}$ is the value of ϕ_{min} for the folds belonging to $(\Delta\tilde{A}_i)$ interval.

The domain defined by $\bar{\phi}_{max}$ and $\bar{\phi}_{min}$ here is called the "population domain of ϕ", in contrast to the "fold domain of ϕ" mentioned in step (ii). The reason for using two different domains is to increase the accuracy of fold-pdf. The population domain of ϕ, is again divided into a number of uniform intervals, given by:

$$\delta\bar{\phi} = (\bar{\phi}_{max} - \bar{\phi}_{min})/Np \quad , (5.5\text{-}8)$$

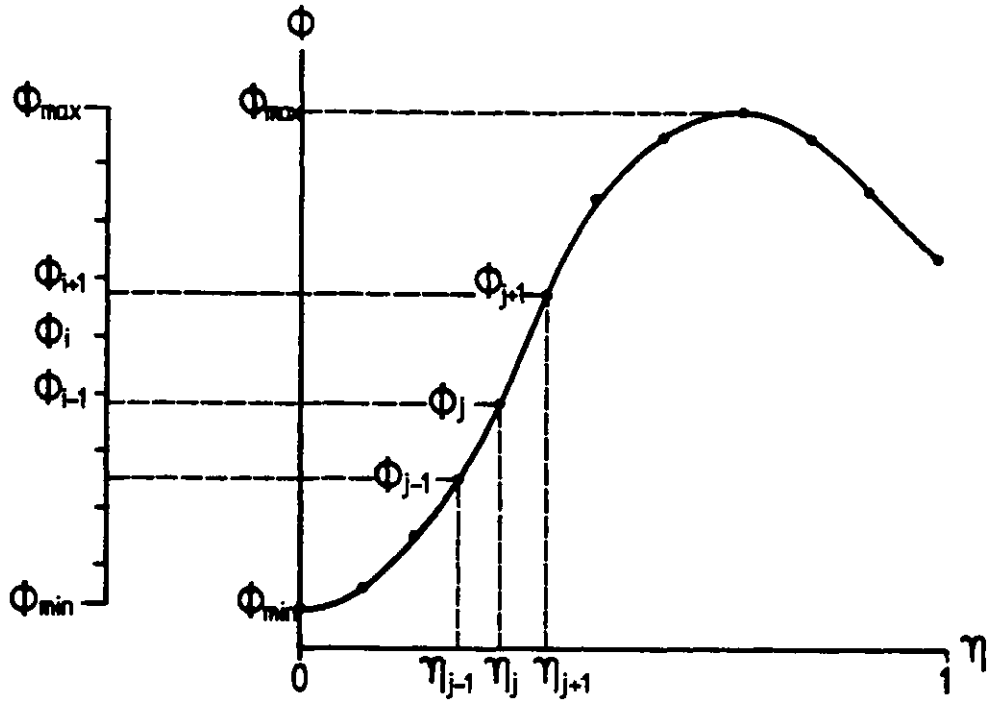

Fig.5.5-1 Calculation of fold-pdf

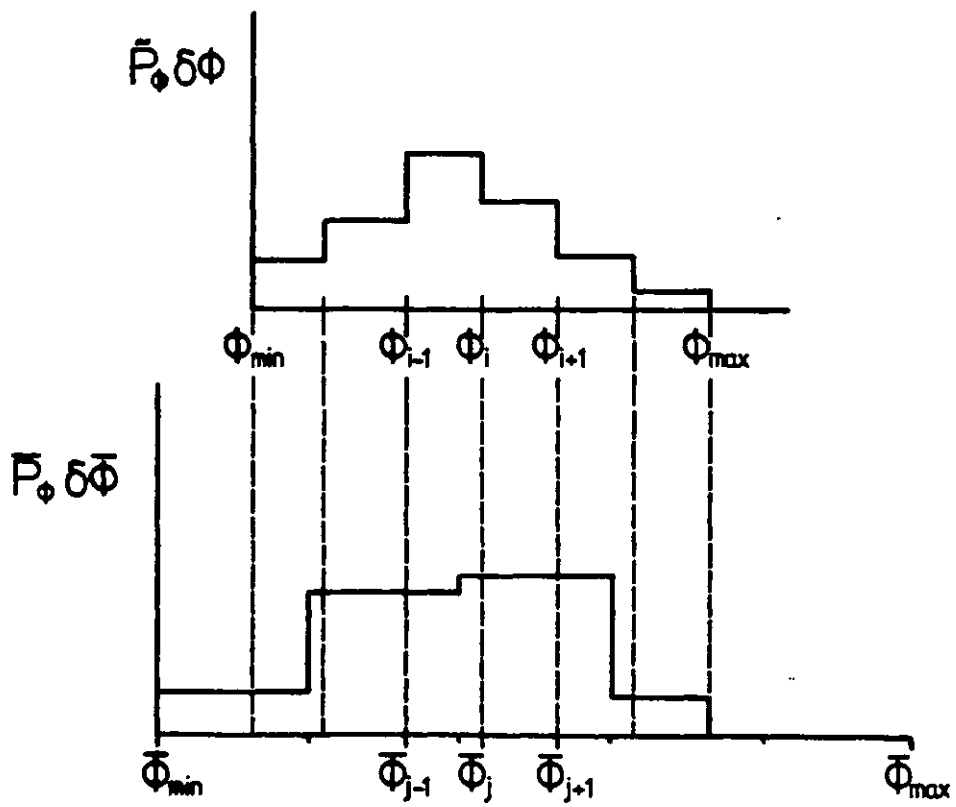

Fig.5.5-2 Redistribution of fold-pdf to the population domain of ϕ

where N_p is the total number of fraction intervals (N_p=10 is the typical value used in the computation).

(iv) Redistribute the fold-pdf, $\tilde{P}_\phi$, obtained in step (ii) to the population domain given by Eqn.(5.5-8), as follows: Identify all the ϕ-values with their appropriate $\delta\bar{\phi}$-intervals defined in Eqn.(5.5-8): - If a pair of consecutive ϕ-values, say ϕ_{i-1} and ϕ_i ($\delta\phi_i = \phi_i - \phi_{i-1}$), lie within the j-th $\bar{\phi}$-interval, $\delta\bar{\phi}_j$, assign the corresponding $\tilde{P}_\phi\delta\phi$ value to the "population-averaged pdf" of $\bar{P}_\phi\delta\bar{\phi}$. Linear interpolation is also adopted if the values inside $\delta\phi_i$ ranges across $\delta\bar{\phi}_j$ and $\delta\bar{\phi}_{j+1}$. The process is further illustrated in Fig.5.5-2.

(v) Multiply the redistributed values of $\tilde{P}_\phi\delta\phi$ by the population distribution function $\tilde{P}$ for all folds to give the population average pdf:

$$\bar{P} = \frac{\int_0^1 (\tilde{P}_\phi\delta\phi)\tilde{P}d\tilde{A}}{\delta\bar{\phi}} \qquad . \quad (5.5\text{-}9)$$

Another reason for redistribution of fold pdf to the population domain in step (iv) is that a common domain is essential for the relation in Eqn.(5.5-9) to be valid.

5.6 Closure

The coupling procedure of the demographic and biographic analysis has been developed and described in the present chapter. Some presumptions about the trajectories of the folds have been made in order to simplify the calculations, but the essential features of fold motion have been considered.

The detail structure of turbulence, such as the

probability density functions of various properites, can be predicted by the ESCIMO theory as well as the turbulent mean quantities and the root mean square fluctuation level.

The theory has been applied to the two-dimensional turbulent reacting mixing layer and turbulent jet diffusion flames and the results will be presented in the next two chapters.

CHAPTER 6

THE TURBULENT REACTING MIXING LAYER

6.1 Introduction

In the earlier works of Noseir (1980) and Tam (1981), the simplified demographic analysis was incorporated with the more advanced biographic analysis. The results of the demographic computation is either presumed to be of the "top-hat" profile (uniform in the cross-stream direction) or expressed in an analytical form. Therefore, the complete set of transport equations for the population distribution has neither been formulated nor solved in their work.

The purpose of the present work is to set up the mathematical framework for the calculation of population distribution function in two-dimensional boundary layer flow problems, to allow for the variation in the cross-stream direction as well as the longitudinal one.

The plane mixing layer is the first flow process to be investigated, because of the simple fixed boundary conditions and entrainment rate involved therein. Also, the self-similarity prevails in the fully developed region of the mixing layer. Very few experimental results on the turbulent reacting mixing layers are available in the present literature and those obtained by Batt (1977) have been regarded as reliable and typical. Thus, the flow configuration of Batt's experiment has been chosen in the prediction and will be described in Sec.6.2.

The numerical input of the computation will be listed

in Sec.6.3, followed by the results obtained from the demographic analysis in Sec.6.4. The results obtained from the combined analysis will be presented in Sec.6.5 and the influence of various physical parameters demonstrated in Sec.6.6. The effects of numerical grid size have also been investigated and will be illustrated in Sec.6.7. The discussion of the results is to appear in Sec.6.8, followed by a closure in Sec.6.9.

6.2 Description of the flow configuration

The test case considered is a two-dimensional turbulent shear layer in which the mixing of both a passive and a chemically reacting streams occurred. The velocities of two streams are 23ft/s and 2ft/s respectively. The high speed stream is composed of low temperature air (252°K) seeded with dilute concentrations of N_2O_4, while the low speed stream consists of hot and clear air (310°K).

A schematic diagram of the shear layer and a list of test conditions are shown in Fig.6.2-1:

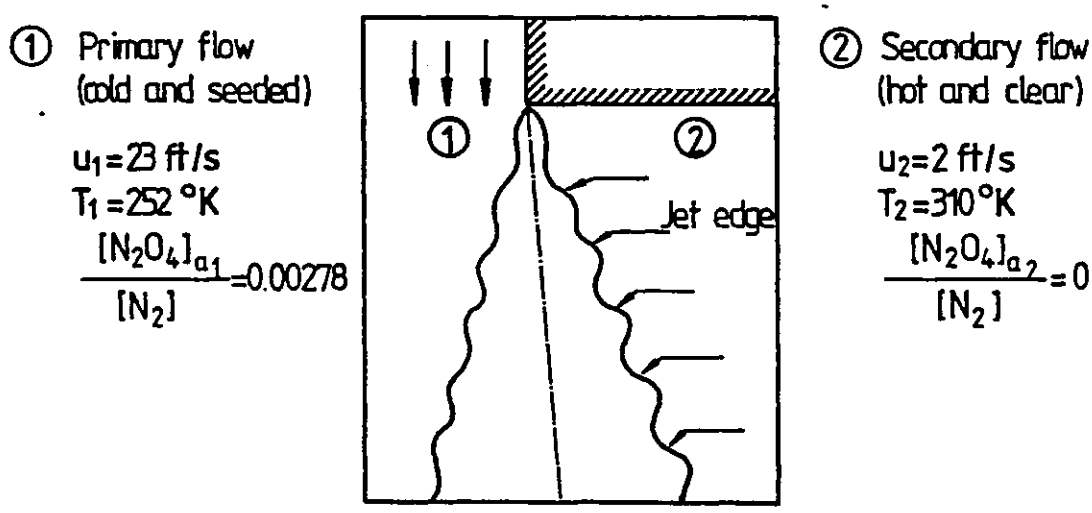

Fig.6.2-1 Test configuration of reacting shear layer

Batt (1977) has mentioned that the flow is directed vertically downwards through the 5ft long test section in order to minimize the buoyancy effects accompanying the imposed thermal gradients.

The chemical process is a kind of first order dissociation-recombination reaction denoted by:

$$N_2 + N_2O_4 \rightleftharpoons 2NO_2 + N_2 \qquad . \quad (6.2\text{-}1)$$

The recombination-rate constants have been measured extensively and successfully by Wegener (1959) in a supersonic nozzle flow.

It should also be noted that a unique feature of the tetroxide dissociation is that if the temperature is varied from -20°C to room temperature the degree of dissociation changes from 0·3 to 0·96.

The heat released from the chemical reaction is negligible in the present flow process since the concentration of N_2O_4 is lower than 0·5% (by volume).

6.3 Computational Notes

6.3.1 The Grid Systems

The expanding grid of GENMIX code is employed in the present prediction with 20 cross-stream grid nodes (N = 20). The intervals of ω (from 0 to 1) are distributed in accordance with the expression given below:

$$\omega_i = \left(\frac{i-1}{N-1}\right)^{0.5} \qquad i=1,2,3,\ldots,N \qquad . \quad (6.3\text{-}1)$$

Therefore, the grids are more densely distributed near the external boundary where the velocity is lower.

The total number of marching steps to reach the

downstream distance of x = 1·52m (5ft) is equal to 300 in the typical computation. The initial width of the mixing layer is 0·001m. The forward marching step size is controlled by the following formulae as in GENMIX program:

$$\Delta x = \min\left[\Delta x_1, \Delta x_2, \Delta x_3, \Delta x_4, \Delta x_5\right] \quad , (6.3\text{-}2)$$

where

$$\Delta x_1 = \lambda_1 y_{N-2} \quad , (6.3\text{-}3)$$

$$\Delta x_2 = \frac{\Delta x_1 \cdot (\psi_E - \psi_I)}{0{\cdot}5(r_1 + r_N)\mu_1} \quad , (6.3\text{-}4)$$

$$\Delta x_3 = \lambda_2 \Delta x_{last} \quad , (6.3\text{-}5)$$

$$\Delta x_4 = \frac{\lambda_3 \cdot (\psi_E - \psi_I)}{(r_I \dot{m}''_I - r_E \dot{m}''_E)} \quad , (6.3\text{-}6)$$

$$\Delta x_5 = \Delta x_{max} \quad , (6.3\text{-}7)$$

and

$\lambda_1 = 1$

$\lambda_2 = 5$

$\lambda_3 = 0{\cdot}01$

y_{N-2} is the value of y at the N-2th grid node

μ_1 is the viscosity at the 1st grid node

r_1 is the radius of 1st grid node (=1 for plane flow)

r_N is the radius of Nth grid node (=1 for plane flow)

Δx_{last} is the value of Δx in the previous step

$\Delta x_{max} = 5$

The total number of age-intervals, NA, is equal to 10 and they are uniformly distributed, viz:

$$\tilde{A}_j = \frac{j-1}{NA} \qquad j = 1,2,3,\ldots,NA+1 \qquad , (6.3\text{-}8)$$

The total number of sub-divisions inside the profile of fold-biography calculation, NP, is equal to 10 in the current calculation.

6.3.2 The chemical reaction rate constants

The local chemical equilibrium condition has been assumed to prevail in the test conditions considered herein, based on the equilibrium conclusion which has been reached in the work of Batt (1977). It has been observed that the magnitude of the measured eddy decay time of turbulence (30ms) is large compared with the typical chemistry times ($\leq$1ms).

The chemical equilibrium constant is taken from the measured data of Wegener (1959):

$$k_D \left[N_2O_4\right]\left[N_2\right] = k_R \left[NO_2\right]^2 \left[N_2\right] \qquad , (6.3\text{-}9)$$

and

$$K_C = k_D/k_R = \frac{1}{82T} \exp(20{\cdot}72 - \frac{6747}{T}) \qquad , (6.3\text{-}10)$$

where

k_D is the forward dissociation rate constant ,

k_R is the recombination rate constant ,

K_C is the equilibrium constant ,

$\left[N_2O_4\right]$ is the mole fraction of N_2O_4 species ,

$\left[NO_2\right]$ is the mole fraction of NO_2 species ,

$\left[N_2\right]$ is the mole fraction of N_2 species ,

The production rate for the total oxide mass fraction is zero, under the present reaction scheme, i.e.

$$\dot{m} = \dot{m}_{N_2O_4} + \dot{m}_{NO_2} = 0 \quad , \quad (6.3\text{-}11)$$

where $\dot{m}$ stands for the production rate (mass fraction per unit time). The relation between the total mass fraction of oxide and the mole fractions of oxide is given by:

$$m = m_{N_2O_4} + m_{NO_2}$$

$$= \left[N_2O_4\right] W_{N_2O_4} + \left[NO_2\right] W_{NO_2} \quad , \quad (6.3\text{-}12)$$

where $W_{N_2O_4}$ and W_{NO_2} are the molecular weight of N_2O_4 and NO_2 species respectively. Thus, the value of m obeys the species conservation equation of the boundary layer form:

$$\frac{\partial m}{\partial x} + (a+b\omega)\frac{\partial m}{\partial \omega} = \frac{\partial}{\partial \omega}\left(c\frac{\partial m}{\partial \omega}\right) \quad , \quad (6.3\text{-}13)$$

with the boundary conditions:

$$m = m_1 \qquad \text{at } \omega = 0 \quad , \quad (6.3\text{-}14)$$

$$m = 0 \qquad \text{at } \omega = 1 \quad . \quad (6.3\text{-}15)$$

The next expression can be established by dividing the both sides of Eqn.(6.3-12) by $W_{N_2O_4}$:

$$\left[N_2O_4\right]_a = \left[N_2O_4\right] + \tfrac{1}{2}\left[NO_2\right] \quad , \quad (6.3\text{-}16)$$

where $\left[N_2O_4\right]_a \equiv m/W_{N_2O_4}$ and called as the "available" mole fraction of N_2O_4 for the reaction. Obviously, the relation between $\left[N_2O_4\right]_a$ and m is:

$$\frac{[N_2O_4]_a}{[N_2O_4]_{a_1}} = \frac{m}{m_1} \quad , \quad (6.3\text{-}17)$$

or

$$[N_2O_4]_a = [N_2O_4]_{a_1} \frac{m}{m_1} \quad , \quad (6.3\text{-}18)$$

where the $[N_2O_4]_{a_1}$ is the value of $[N_2O_4]_a$ in the primary flow.

The local equilibrium mole fraction of NO_2 is obtained by inserting Eqn.(6.3-16) into Eqn.(6.3-10), viz:

$$\frac{[NO_2]}{[N_2]} = \frac{K_c}{4} \{(1+16[N_2O_4]_{a_1} \frac{m}{m_1} \frac{1}{K_c})^{\frac{1}{2}} - 1\} \quad . \quad (6.3\text{-}19)$$

The quantity, m/m_1, varies from 0 to 1 across the mixing layer (according to Eqns.(6.3-13) to (6.3-15)) and can be treated as the mixture fraction in the present case. The value of m/m_1 will be solved at every ω-node in the prediction with the turbulent diffusion coefficient obtained from the turbulent viscocity and uniform Schmidt number (the turbulent Schmidt number measured by Batt is equal to 0·5). The value of m/m_1 will be given the symbol f in this chapter and all argument about f in Chapter 4 applies to m/m_1 from now on, i.e.:

$$f \equiv \frac{m}{m_1} \quad , \quad (6.3\text{-}20)$$

for the present chemical reaction process.

6.3.3 <u>The computations performed</u>

Several computations have been performed, with different combinations of input empirical constants, in order to investigate the influence of each presumption on the results.

All computations are characterised as indicated in Table 6.3 and the entry under "Mode" indicates the presumption used about the distribution of fold-formation rate. The number of "Mode" refers to:

Mode (i) - proportional to the local mean velocity gradient,

Mode (ii) - proportional to the local mean velocity,

Mode (iii) - proportional to the normalized stream function.

Same notation applies to the calculation in the next two chapters.

Table 6.3: Characterisations of computer runs

Run No.	C_Z	C_F	C_S	Mode	NA
1	0.164	2	1	(i)	10
2	0.164	2	1	(ii)	10
3	0.164	2	1	(iii)	10
4	0.328	2	1	(i)	10
5	0.164	3	1	(i)	10
6	0.164	2	0.3	(i)	10
7	0.328	2	0.5	(i)	10

6.4 Results of demographic analysis

6.4.1. The population distribution versus age at a fixed position

The population distribution with respect to age will be presented in this subsection, for three different runs, i.e., Run No.1 to Run No.3. All 3 runs have some conditions

except the assumption on fold-formation rate. Firstly, results obtained from Run No.1 are shown in Fig.6.4-1, at three different positions across the mixing layer. The abscissa is the non-dimensional age, $\tilde{A}$, while the ordinate represents the non-dimensional population of folds having a particular age. The three curves in the figure refer to the population distribution prevailing at position near the high speed edge (η_T = -1.5), the centre (η_T = -0.4) and the low speed edge (η_T = 1.5) of the mixing layer respectively. The mixing-layer similarity parameter η_T stands for the width of the mixing layer and is defined by the following realtion:

$$\eta_T \equiv \frac{12(y-y_{0.5})}{x-x_0} \qquad , (6.4\text{-}1)$$

where $y_{0.5}$ is the value of y in which $\bar{T}$ is equal to 0.5 (T_1+ T_2), x_0 is the effective origin of the mixing layer. The value of x_0 is taken from Batt's measurements (=3in) in the present computation.

It can be observed from Fig.6.4-1 that the $\tilde{P}$~$\tilde{A}$ curve has the steepest slope in the centre of the mixing layer, where the fold formation rate reaches its maximum value according to the presumptions made here. The curve has a similar shape of exponential decay near the low speed edge, but with a less steep gradient. The distribution near the high speed boundary is however somewhat different, the curve being almost flat for $0 \leq \tilde{A} \leq 0.15$ and followed by a sudden drop to the range of $0.2 \leq \tilde{A} \leq 0.35$.

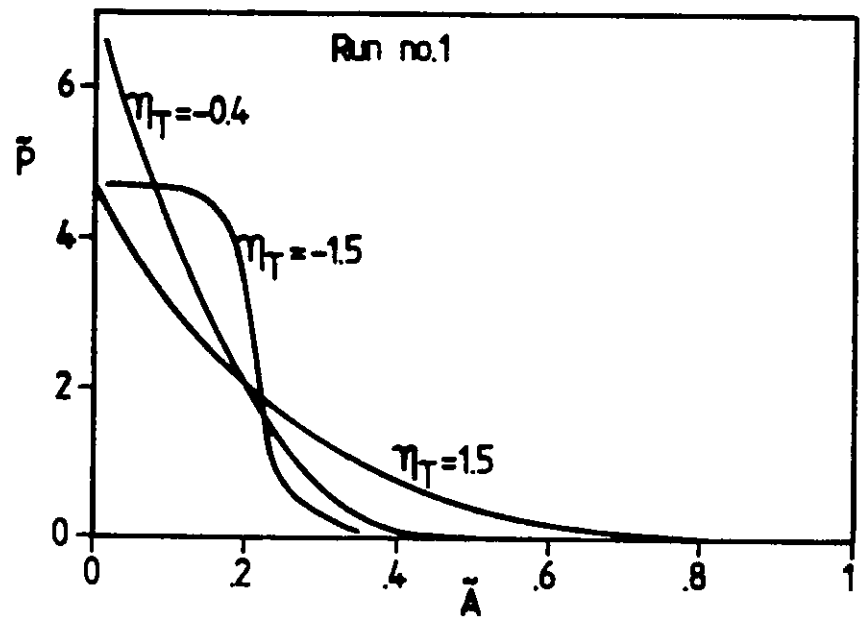

Fig.6.4-1 Population distribution function with respect to age

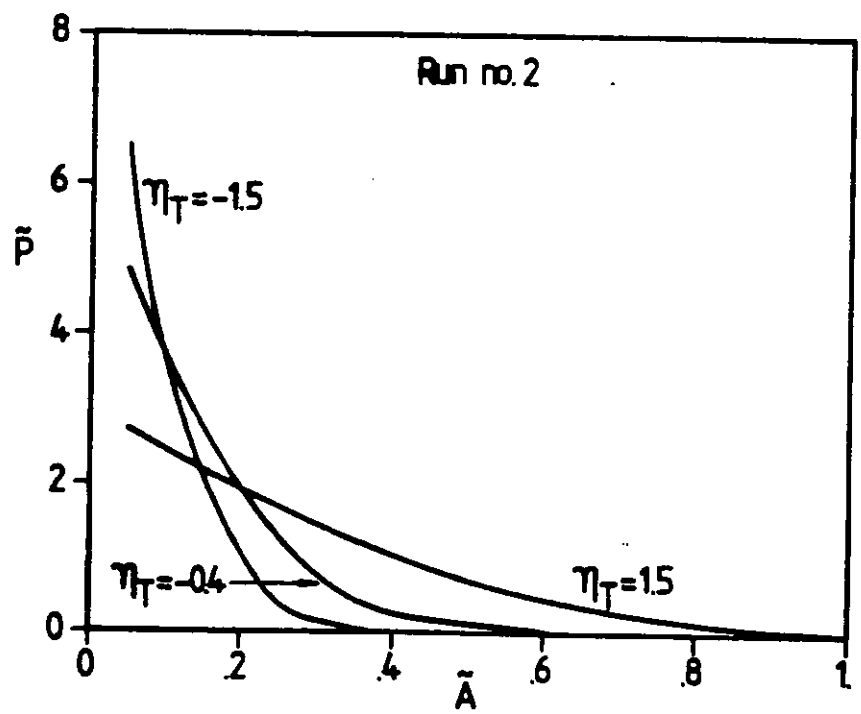

Fig.6.4-2 Population distribution function with respect to age

The overall feature of the population distribution is that the youngest folds are the most popular ones in the present case. The population of very old folds (say, $\tilde{A}>0.6$) is negligible, signifying that most folds are born in near up-stream locations.

Secondly, the results from Run No.2 are demonstrated in Fig.6.4-2 in which the distribution of fold formation rate is assumed to be proportional to local mean velocity. The three curves correspond to the same positions as in Fig.6.4-1. Inspection of the figure reveals that all curves belong to the type of exponential decay and the curve near the high speed edge has the largest slope where the fold formation rate is the highest. The population distribution near the low speed stream is more uniform here, with significant amount of old folds (e.g. $\tilde{A}>0.6$) in existence.

Finally, the results from Run No.3 are provided in Fig.6.4-3. The distribution of fold formation rate is supposed to be proportional to the "local entrainment rate", $(r\dot{m}'')_{\ell}$, defined by

$$(r\dot{m}'')_{\ell} \equiv (1-\omega)r_I\dot{m}_I'' + \omega r_E\dot{m}_E'' \qquad . (6.4\text{-}2)$$

It can be seen that the fastest diminution of population with respect to age again happens near the high speed edge of the mixing layer where the entrainment rate is at its peak. The population distribution at the low speed side is now even more uniform than that obtained

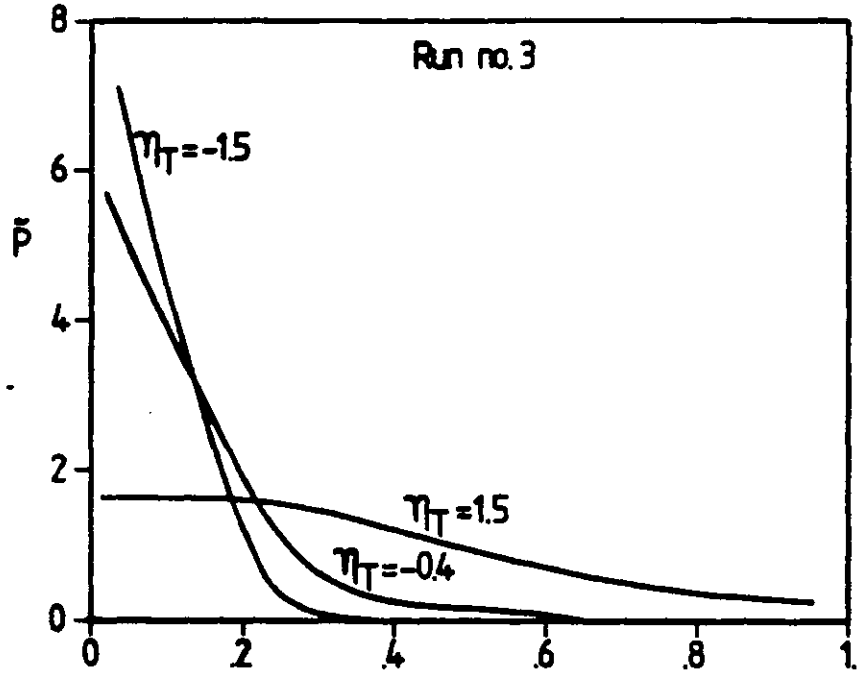

Fig.6.4-3 Population distribution function with respect to age

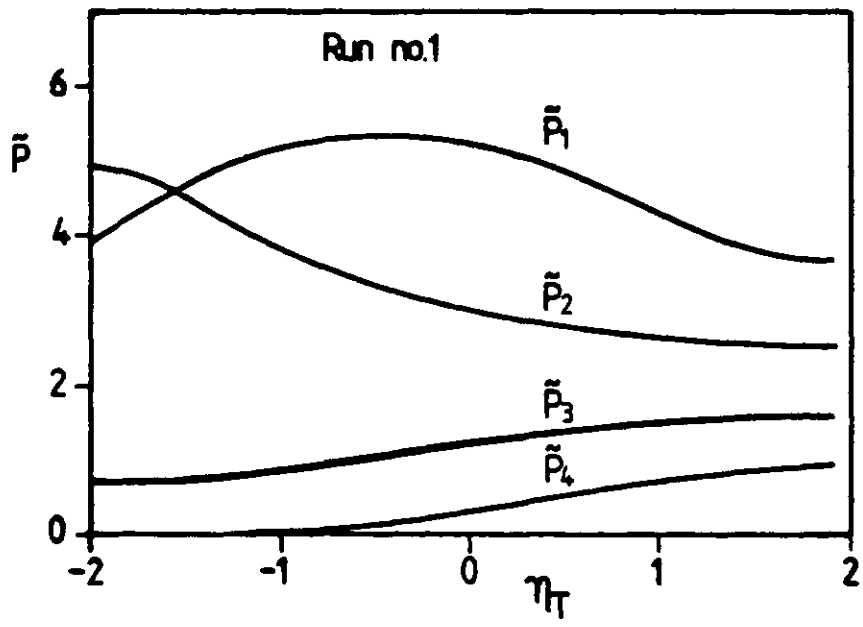

Fig.6.4-4 Radial variation of population of folds belonging to a particular age interval

from Run No.2, and there remains a finite amount of the oldest folds which are born in the far upstream region of the mixing layer and have undergone lower re-engulfment rate.

6.4.2 The population distribution across the mixing layer at fixed age

Further illustration for the spatial variation of the population distribution is supplied by the diagram of $\tilde{P}_j$ (at fixed $\tilde{A}_j$) versus η_T through Figs.6.4-4 to 6.4-6. The results presented in these figures are obtained in the self-similar region (at x = 0.47m).

In Fig.6.4-4, the results obtained from Run No.1 are presented and each curve stands for the population of folds belonging to a particular age-interval. Only four lines are shown here, since the magnitude of other groups outside the range are much smaller. The population of the youngest folds, $\tilde{P}_1$ has the peak value at $\eta_T \simeq -0.4$ where the velocity gradient and the fold formation rate attain the maxima. The $\tilde{P}_2$ distribution behaves as a monotonic decreasing function with respect to η_T, while the population of older folds $\tilde{P}_3$ and $\tilde{P}_4$ reflect the opposite tendency.

The corresponding results from Run No.2 are plotted in Fig.6.4-5. The curve representing $\tilde{P}_1$ now has its highest value at the high speed edge of the mixing layer where the fold formation is large under the present presumption. The $\tilde{P}_2$ distribution is fairly uniform in

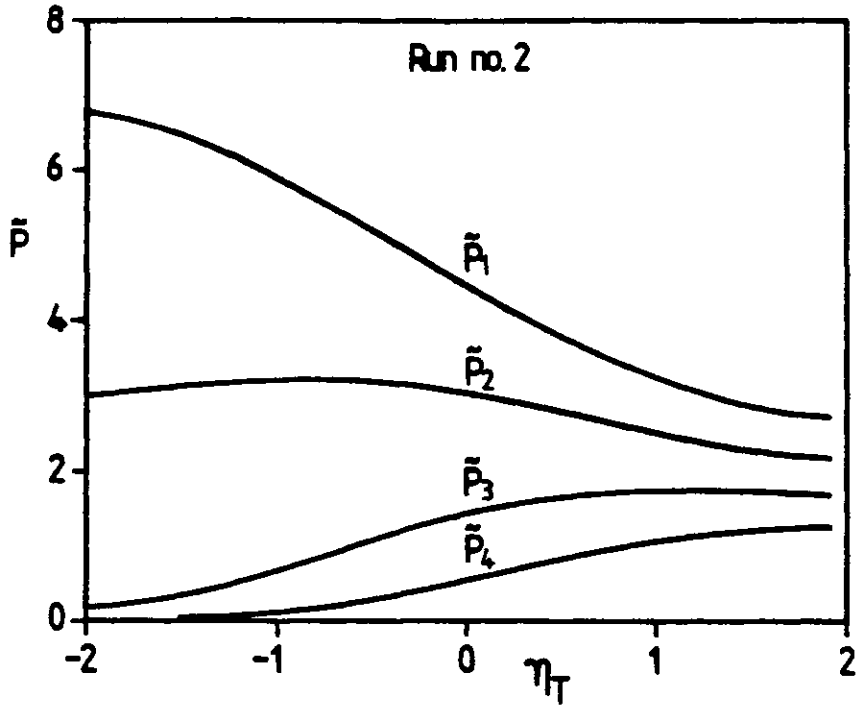

Fig.6.4-5 Radial variation of population of folds belonging to a particular age-interval

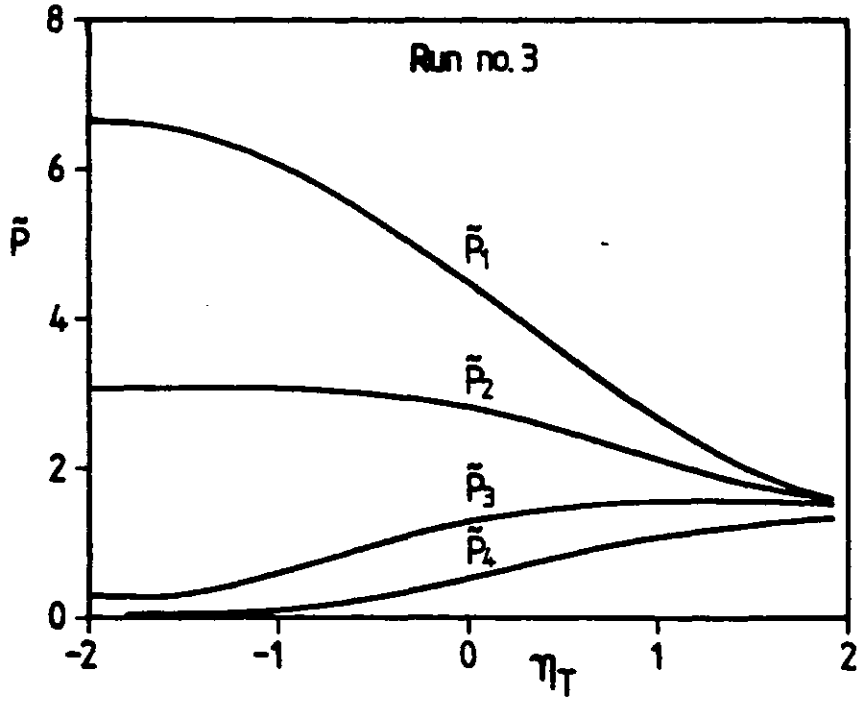

Fig.6.4-6 Radial variation of population of folds belonging to a particular age-interval

the region between $-2 \leq \eta_T \leq -0.4$ and then decreases smoothly towards the low speed boundary. The shapes of $\tilde{P}_3$ and $\tilde{P}_4$ distribution are similar to those in Fig.6.4-4.

Finally, the results produced by Run No.3 are again provided in Fig.6.4-6. All curves have actually the same qualitative characteristics as their counterparts in the previous diagram, except that the difference between each curve diminishes quickly as η_T approaches the value in low speed stream.

6.4.3 The average age of the folds versus position

Another interesting quantity in the demographic analysis is the average age of the folds defined by:

$$\tilde{A}_{ave} \equiv \int_0^1 \tilde{A}\tilde{P}d\tilde{A} \qquad . \quad (6.4\text{-}3)$$

The variation of the average age across the mixing layer are plotted in Fig.6.4-7 for Run Nos.1 to 3. In the case of Run No.1, the minimum value occurs at $\eta_T \tilde{=} -0.8$, while it happens at $\eta_T \tilde{=} -2.0$ for other cases. The average age in the centre of the layer ($-0.2 \leq \eta_T \leq 0.2$) is not larger than 0.2 for all cases, signifying that most of the folds are created within the distance of $0.2X_D$ from the point in question. However, the difference between the average age calculated from three cases is remarkably large in the region near the low speed stream. For instance, the $\tilde{A}_{ave}$ at $\eta_T = 1.6$,

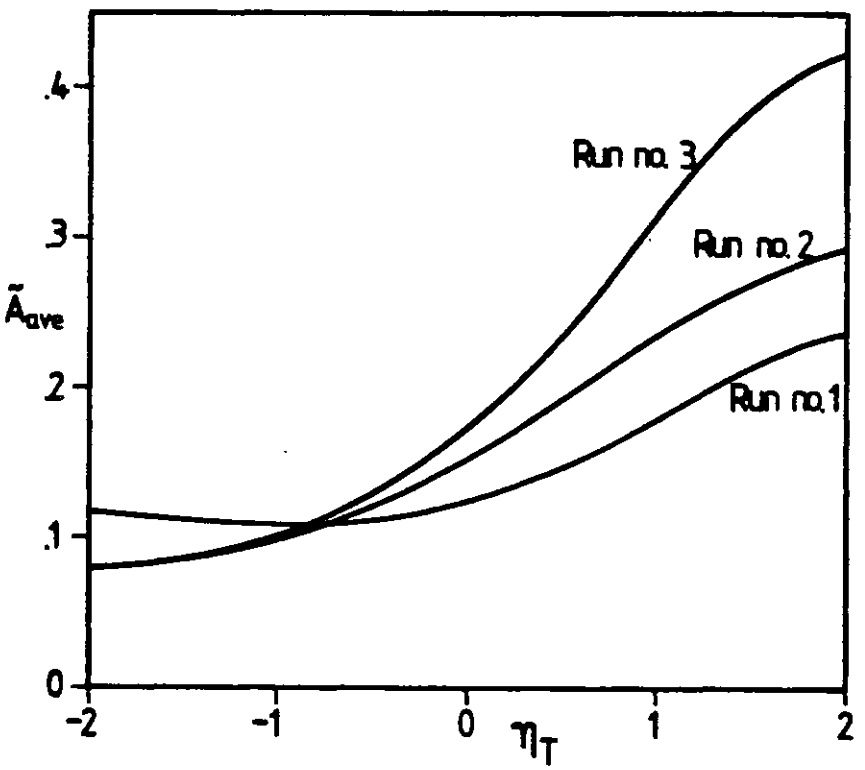

Fig.6.4-7 Average age across the mixing layer

varies from 0.25 to 0.4 under different hypothesis regarding the distribution of fold formation rate.

6.5 Results of the combined analysis

6.5.1 The mean temperature profile

The normalized mean temperature profile across the mixing layer for Run No.1 (at x = 0.47m) is plotted in Fig.6.5-1 together with the measurements from Batt (1977). It should be noted that the mean temperature is calculated from the solution of enthalpy equation which did not contain the heat release effect in the present chemical reaction scheme. Therefore, the contribution of ESCIMO theory does not appear in the mean temperature.

The quantitative agreement between the predictive results and the measured data is satisfactory as revealed by the graph, this implies that the turbulent diffusion coefficient is adequately determined by the turbulent model employed. The mean temperature is important in the calculation of NO_2 concentration since the chemical equilibrium constant is temperature dependent.

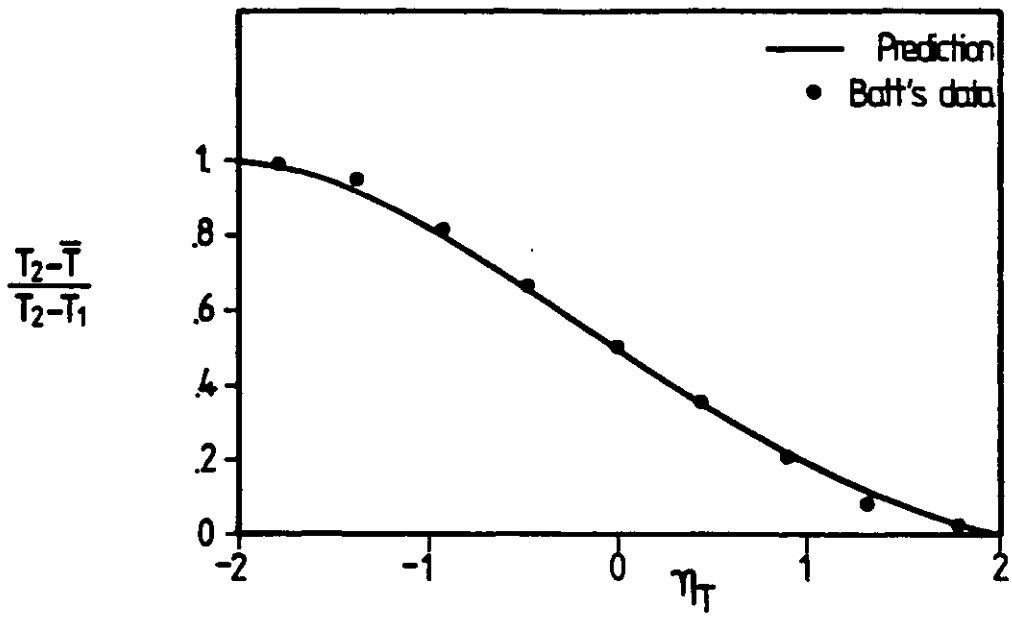

Fig.6.5-1 Radial profile of mean normalized temperature at x=0.47; Run no.1

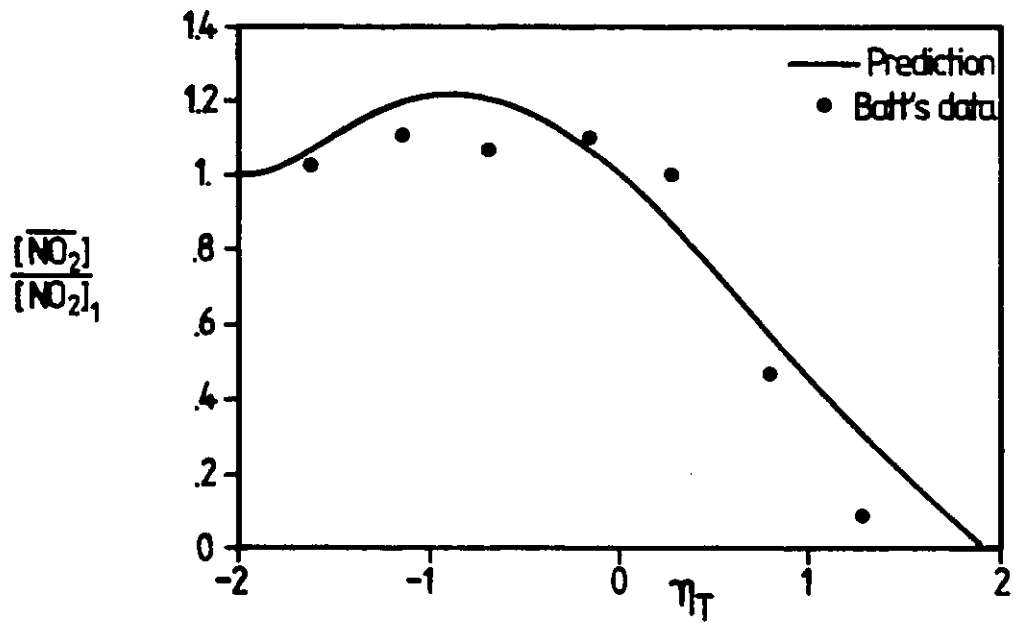

Fig.6.5-2 Radial profile of mean normalized concentration of NO_2 at x=0.47; Run no.1

6.5.2 The mean concentration profile of nitrogen dioxide

The normalized mean NO_2 concentration profile across the mixing layer for Run No. 1 is plotted in Fig.6.5-2. The experimental results from Batt (1977) are also shown in the figure (by the solid symbols). Now that the mean concentration is calculated from the full ESCIMO approach described earlier.

The prediction exhibits a hump near $\eta_T=-1$, where the normalized concentration of NO_2 is equal to 1·2. However, there appears a slight double hump when the measured data points are connected with a smooth curve. No explanation about the existance of this double hump has been provided in Batt's paper, but the author did mention that the concentration measurement accuracy in this case is roughly ±10% of the core-flow concentration levels. The maximum measured value of NO_2 is equal to 1·1, while the NO_2 concentration calculated from the mean temperature and local equilibrium condition (excluding the concentration fluctuation effect) could reach 1.3. Thus, the non-uniformity of properties (in each fold) accounted by ESCIMO theory has reduced the peak level of NO_2 by 10 per cent.

The level of NO_2 concentration decays slightly faster according to Batt's data than the present prediction, in the region where $\eta_T>0·5$.

6.5.3 The root-mean-square fluctuation of temperature

The variation of root mean square fluctuation on temperature for Run No.1, across the mixing layer is presented in Fig.6.5-3. The predictions show a maximum fluctuation of

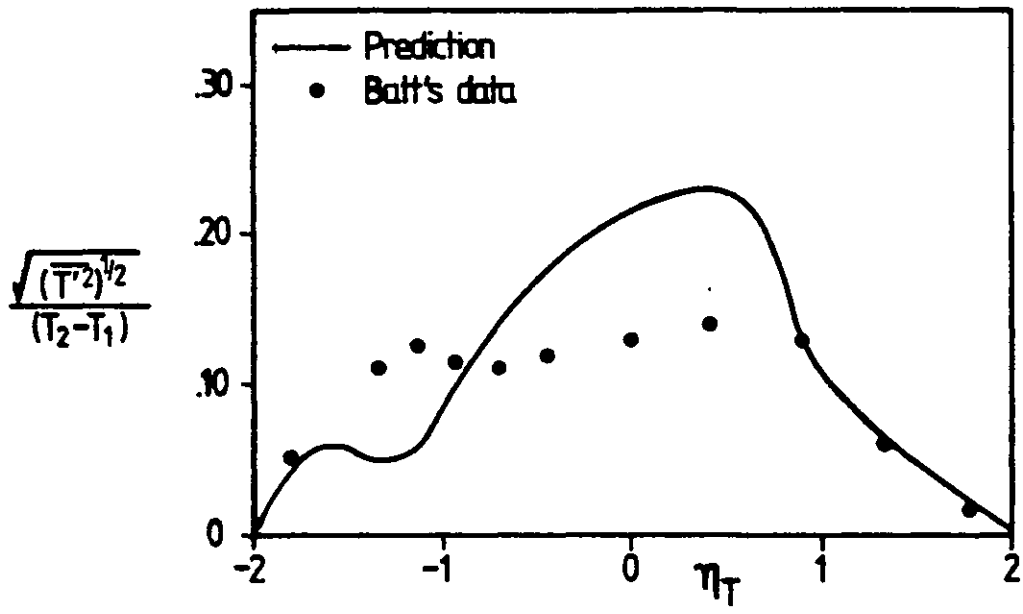

Fig.6.5-3 Radial profile of temperature fluctuation intensities; Run no.1

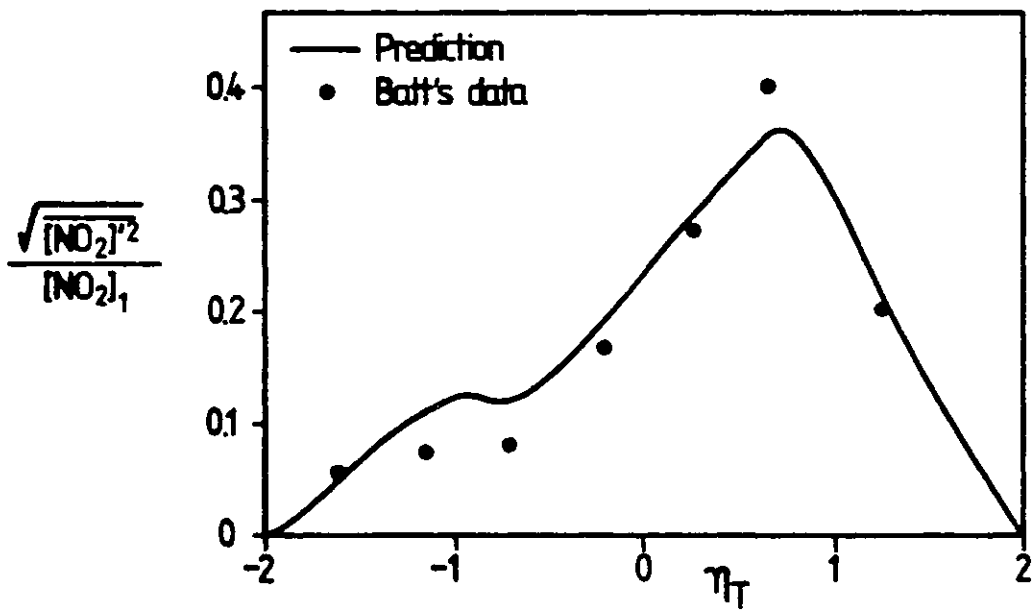

Fig.6.5-4 Radial profile of NO_2 concentration fluctuation intensities; Run no.1

0•23 at $\eta_T \simeq 0•5$, followed by a sharp decrease until the magnitude is smaller than 0•1. The experimental data, however, reveal a slight double hump with a rather flat plateau in the central part of the mixing layer. The maximum measured value is around 0•14 and is lower than the present prediction.

Brown and Roshko (1974) have performed the experiments on turbulent shear layers with density gradients and Fiedler (1974,1975) has studied the temperature field within a plane mixing layer. They have found out that instantaneous density (temperature) fluctuations were often equivalent to the density (temperature) difference between the two external streams. Fiedler (1975) has also measured the maximum fluctuating temperature intensities which are as large as 0.20, considerably larger than the corresponding results for the Batt (1977) study.

6.5.4 The root mean square fluctuation of species concentration

The fluctuation intensities of NO_2 across the mixing layer, obtained from Run No.1, are plotted in Fig.6.5-4. The predicted results exhibit a small hump ($\simeq$0•11) near $\eta_T = -1•0$, with the maximum fluctuation intensity equal to 0•36 and located at $\eta_T = 0•7$.

The experimental data share the similar characteristics with the predictions, though some quantitative discrepancy still exist. The maximum measured fluctuation intensity is equal to 0•4 which is about 10% higher than the calculated one, while the results in the region of $-1•5 \leq \eta_T \leq -0•5$ are slightly overpredicted.

The prediction of concentration fluctuation is one of the main contributions made by ESCIMO theory, since the effect of local unmixedness has been taken into account for the eddies (or folds) coming from various places.

6.5.5 The probability density function of temperature

The temperature probability distributions at different locations across the shear layer, under the conditions of Run No.1, are now shown in Fig.6.5-5. The distributions have been represented by the step functions profile in order to indicate the intervals without causing any confusion.

The predictions reveal a one-sided pdf near the mixing layer boundaries (at $\theta = 0{\cdot}82$ and $\theta = 0{\cdot}22$) where the mean temperatures are close to the free stream conditions. The distributions broaden as the locations are further from the boundaries, e.g. at $\theta = 0{\cdot}74$, $0{\cdot}64$, $0{\cdot}56$ and $0{\cdot}32$. In the central part of the layer, e.g., at $\theta = 0{\cdot}56$ and $0{\cdot}44$, the pdf mainly consists of three portions, namely those correspond to the free stream value, the mean value and the value of re-engulfed part in the newly formed folds.

The measured probability distributions from Batt (1977) are also indicated in the figure (by broken lines). It can be observed that the pdf are nearly Gaussian over a broad domain (approximately the mid-50% of the shear layer), which has not been fully portrayed by the present computations.

6.6 The influence of various assumptions

6.6.1 The influence of fold formation rate

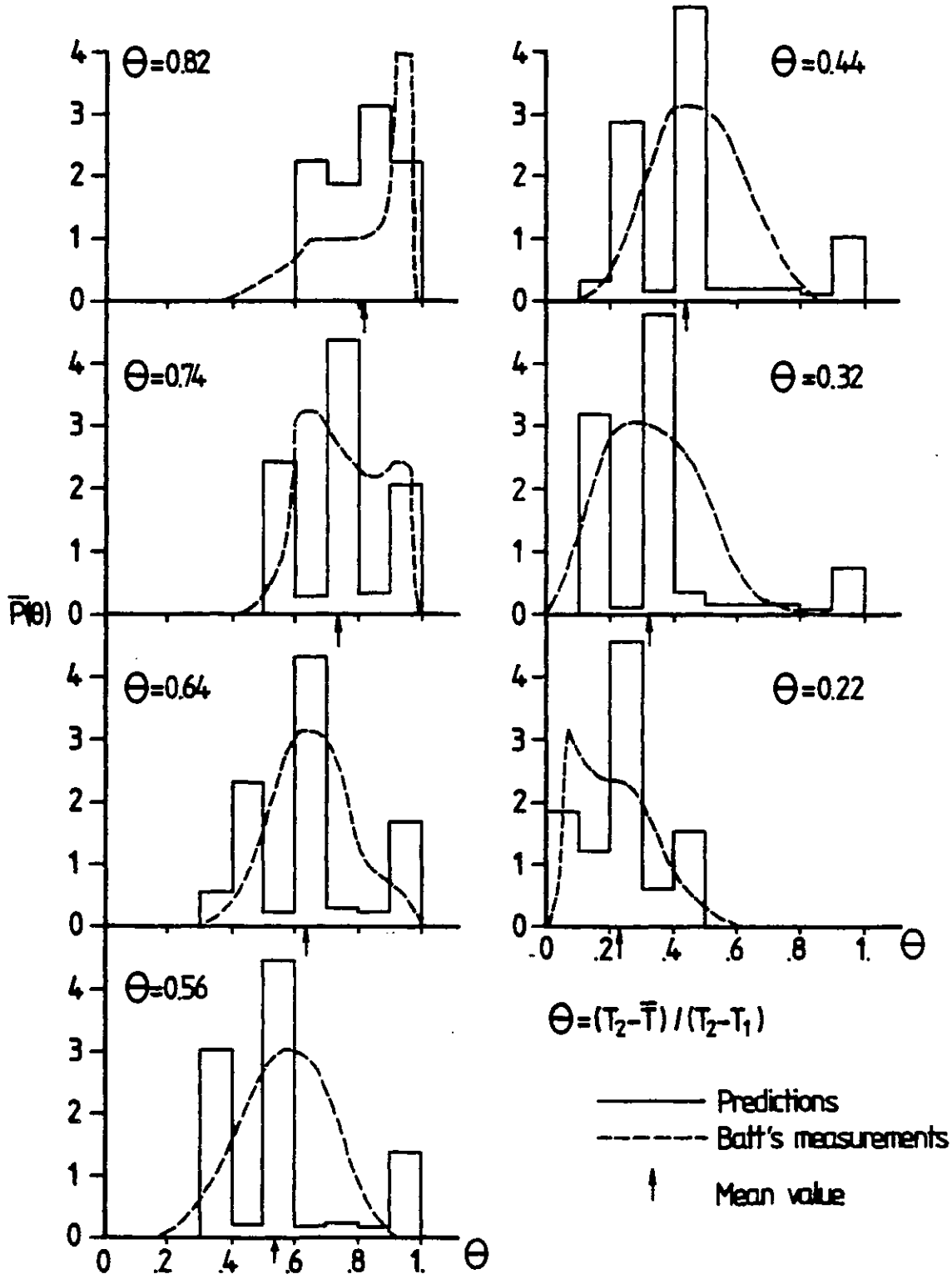

Fig.6.5-5 Temperature Probability Distributions at Different Locations Across the Shear Layer

Various hypothetical distributions about the fold formation rate have been adopted in the current study and hence it is important to assess their influences on the results. Firstly, the influence of different distributions on the mean NO_2 concentration profile are presented in a tabulated form listed below, since the difference between each set is too small to be distinguished on the graph.

Location across the mixing layer, η_T	Normalised mean NO_2 concentration obtained from each mode no.		
	Mode (i)	Mode (ii)	Mode (iii)
-2.00	1.00	1.00	1.00
-1.50	1.10	1.10	1.10
-1.07	1.21	1.20	1.20
-0.674	1.21	1.22	1.21
-0.300	1.13	1.15	1.15
0.104	0.947	0.989	0.988
0.508	0.712	0.756	0.764
0.889	0.575	0.582	0.586
1.17	0.398	0.400	0.403
1.57	0.178	0.179	0.179

Table 6.6-1: The influence of distribution of fold formation rate on NO_2 concentration

The maximum difference between each set of results occurs around $\eta_T = 0.508$, where the relative difference reaches 7%. However, the relative difference is very small in most part of the mixing layer and lower than 2%.

On the other hand, the influence of fold formation rate on the concentration fluctuation intensities of NO_2 is more significant and can be presented in graphic form as Fig.6.6-1. The results obtained from three runs are almost identical in the region of $-2 \leq \eta \leq 0$, especially those correspond to Run No.2 and Run No.3 (hence the results of Run No.3 are not shown in this part). The discrepancies become more apparent when $\eta_T > 0.3$ and the maximum fluctuation intensity varies from 0.36 in the Run No.1 to 0.29 in Run No.3. The predicted locations of the peak value are slightly shifted towards the low speed side of the mixing layer when compared with the data of Batt (1977).

6.6.2 The influence of fold size

The results produced by Run No.1 and Run No.4 are compared in the table 6.6-2.

It should be noted that the fold size at birth is taken as the length scale of turbulence in Run no.1, while it is equal to twice as the length scale in Run no.4. The influence of fold size on the mean NO_2 concentration is significant only in the central part of the mixing layer. Thus, the assumption about the fold size within present range is not crucial to the mean concentrations.

The influence is more visable for the fluctuation intensities of NO_2 as shown in Fig.6.6-2. The maximum

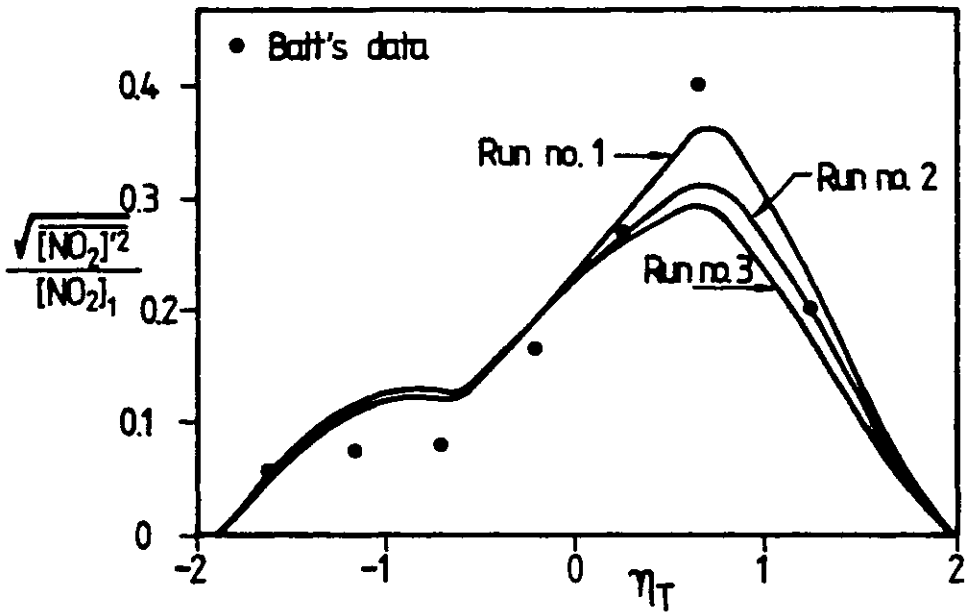

Fig.6.6-1 Influence of distribution of fold formation rate on the concentration fluctuation intensity

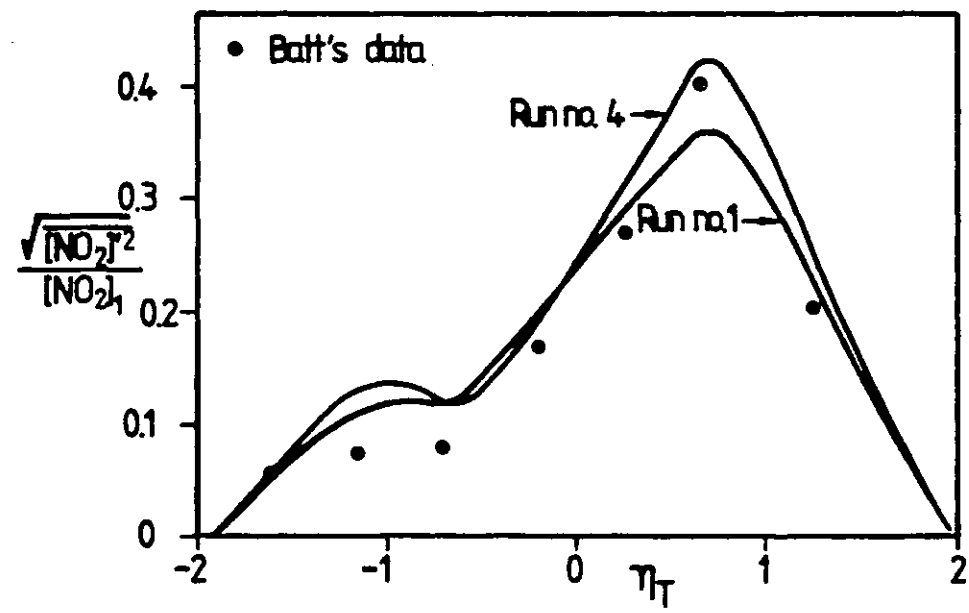

Fig.6.6-2 Influence of fold size on the concentration fluctuation intensity

Location across the mixing layer, η_T	Mean NO_2 concentration	
	Run No.1 C_Z =0.164	Run No.4 C_Z =0.328
-2.00	1.00	1.00
-1.50	1.10	1.09
-1.07	1.21	1.20
-0.674	1.21	1.18
-0.300	1.13	1.10
0.104	0.947	0.907
0.508	0.712	0.669
0.889	0.575	0.565
1.17	0.398	0.397
1.57	0.178	0.180

Table 6.6-2 Influence of fold size on NO_2 concentration

predicted value is equal to 0.42 in Run No.4, compared with the value of 0.36 in Run No.1. The results obtained from Run No.4 are generally larger than the measured data, indicating that larger fold size will yield higher fluctuation intensities.

6.6.3 The influence of fold composition

The results of mean NO_2 concentration from Run No.1 and Run No.5 are given in the following table:

Location across the mixing layer, η_T	Mean NO_2 concentration	
	Run No.1 C_F=2.0	Run No.5 C_F=3.0
-2.00	1.00	1.00
-1.50	1.10	1.10
-1.07	1.21	1.21
-0.674	1.21	1.20
-0.300	1.13	1.07
0.104	0.947	0.884
0.508	0.712	0.663
0.889	0.575	0.574
1.17	0.398	0.398
1.57	0.178	0.179

Table 6.6-3 Influence of fold composition on NO_2 concentration

Again, the discrepancies are apparent only in the mid-region of the mixing layer, where the relative difference between each set is around 7% (e.g. at η_T=0.104). The peak

value is almost identical under both cases.

The fluctuation intensities calculated from Run No.1 and Run No.5 are now plotted in Fig.6.6-3. Considerable increase in the fluctuation intensities are observed for $-0.5<\eta_T<0.6$ and the peak value computed from Run No.5 is equal to 0.43 (the measured value is 0.40). The percentage difference in two runs can reach 40% (atη_T=0) and hence the parameter C_F is an important factor in determining the fluctuation level. The location of the peak was also shifted from $\eta_T\approx0.8$ to $\eta_T\approx0.40$ when C_F changes from 2.0 to 3.0.

6.6.4 The influence of the stretching rate

The mean NO_2 concentration computed from Run No.1 and Run No.6 are provided in the following table:

Location across the mixing layer, η_T	Mean NO_2 concentration	
	Run No.1 C_S=1.0	Run No.6 C_S=0.3
-2.00	1.00	1.00
-1.50	1.10	1.09
-1.07	1.21	1.19
-0.674	1.21	1.14
-0.300	1.13	1.03
0.104	0.947	0.840
0.508	0.712	0.621
0.889	0.575	0.558
1.17	0.398	0.391
1.57	0.178	0.177

Table 6.6-4 Influence of stretching rate on NO_2 concentration

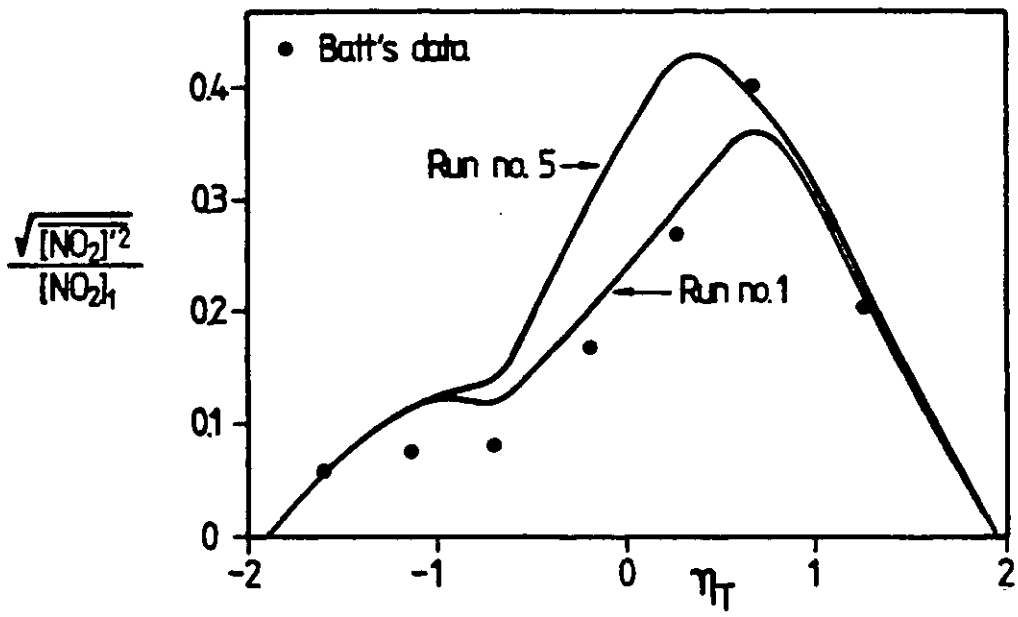

Fig.6.6-3 Influence of fold composition on the concentration fluctuation intensities

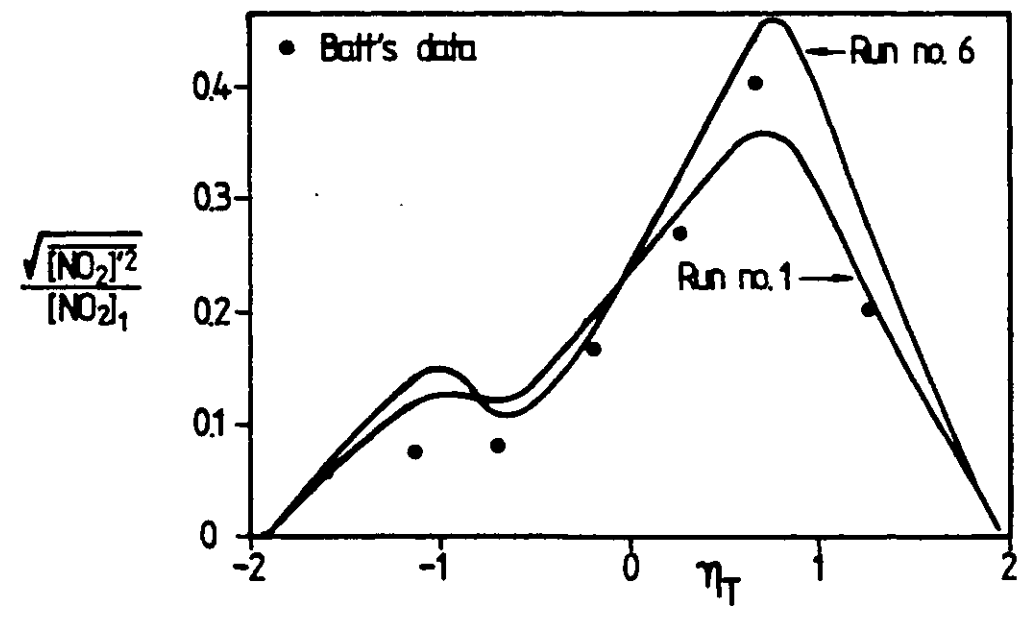

Fig.6.6-4 Influence of stretching rate on the concentration fluctuation intensity

Inspection of Table 6.6-4 reveals that the maximum difference between the results computed from two runs is now around 11%. The peak value is lower in Run No.6 and equal to 1.19.

More evident influence has been realised in the concentration fluctuation intensities as in the other cases, this is now presented in Fig.6.6-4. The secondary hump (at $\eta_T \tilde{=} -1.1$) is magnified in the case of low stretching rate and the maximum fluctuation increases up to 0.46 now. The predictions are in good quantitative agreement with the measurements over the range of $-0.5 \leq \eta_T \leq 0.6$ in Run No.6. However, the fluctuation level is overpredicted in the near high speed area ($-1.4 \leq \eta_T \leq -0.8$) for both runs.

Further investigation about the influence of stretching effect have been carried out in the comparison between Run No.4 and Run No.7, where the fold size at birth is twice as large as those in the other runs. The results are presented in Figs.6.6-5 and 6.6-6.

It can be observed , in Fig.6.6-5, that the mean NO_2 concentration is lower as the stretching rate decreases. The results obtained from Run No.7 show better aggrement with the experimental data in the outer regions of the mixing layer (i.e. for $-1.5 \leq \eta_T \leq -0.5$ and $0.5 \leq \eta_T \leq 1.5$), but larger deviation occurs in the central part of the layer ($-0.5 \leq \eta_T \leq 0.5$).

On the other hand, inspection of Fig.6.6-6 reveals

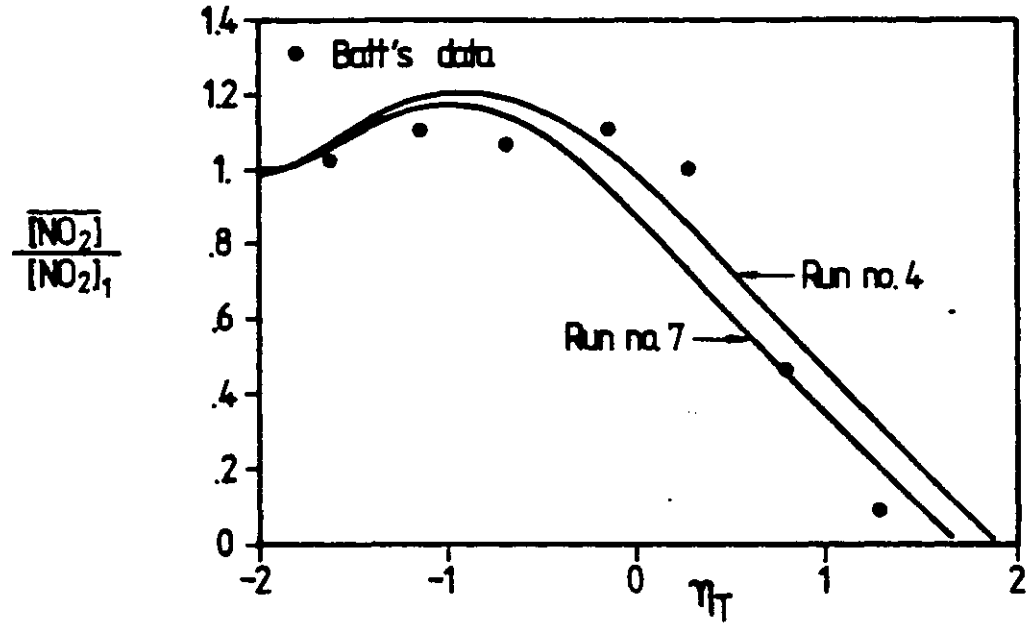

Fig.6.6-5 Influence of stretching rate on the mean concentration

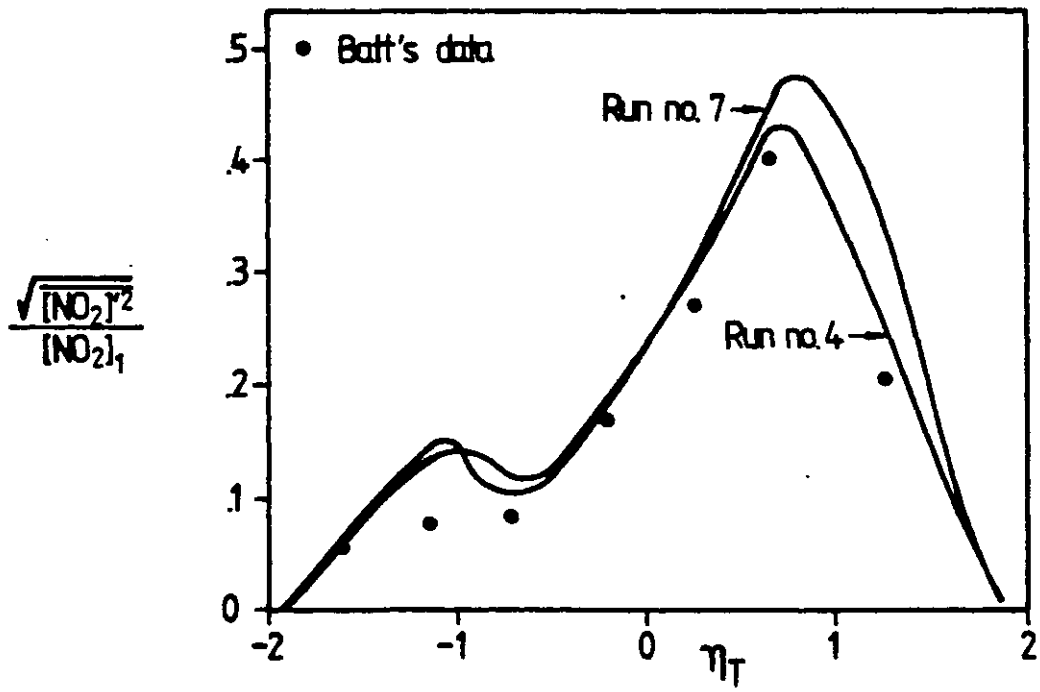

Fig.6.6-6 Influence of stretching rate on the concentration fluctuation intensity

that the fluctuation level calculated from Run No.7 is generally higher and the peak level attains the value of 0.47. The secondary hump is also more significant when the stretching is moderate.

6.7 The influence of grid size

6.7.1 The influence of forward marching step size

It has been observed that the step size of forward marching is controlled by the factor, λ_3, in Eqn.(6.3-6) under present computational conditions. Hence, three different values of λ_3 have been employed to investigate the influence of step size, Δx, on the results and the comparison is presented in Table 6.7-1. The RMS values of NO_2 concentration are chosen for the comparison, since they are more sensitive to step size than the mean NO_2 concentration. All physical constants are the same as those employed in Run No.1.

The results from three different λ_3 values are close to each other, signifying that the influence of marching step size is a minor one for the problem considered. The value of λ_3=0.02 actually yields the grid independent results.

Location across the mixing layer, η_T	RMS of NO_2 concentration fluctuation		
	λ_3=0.04	λ_3=0.02	λ_3=0.01
-2.00	0	0	0
-1.50	0.0686	0.0700	0.0706
-1.07	0.117	0.120	0.121
-0.674	0.123	0.124	0.124
-0.300	0.181	0.182	0.182
0.104	0.262	0.261	0.260
0.508	0.315	0.313	0.313
0.889	0.333	0.337	0.340
1.17	0.244	0.249	0.252
1.57	0.113	0.115	0.116

Table 6.7-1 Influence of forward marching step size on NO_2 concentration fluctuation

Location across the mixing layer, η_T	RMS of NO_2 concentration fluctuation		
	N = 20	N = 40	N = 60
-2.00	0.0	0.0	0.0
-1.50	0.0414	0.0700	0.0792
-1.07	0.126	0.120	0.118
-0.674	0.121	0.124	0.126
-0.300	0.213	0.182	0.185
0.104	0.317	0.261	0.260
0.508	0.388	0.313	0.312
0.889	0.364	0.337	0.330
1.17	0.264	0.249	0.245
1.57	0.102	0.115	0.121

Table 6.7-2 Influence of cross stream grid no. on NO_2 concentration fluctuation

6.7-2 The influence of numbers of grid

The RMS fluctuations of NO_2 concentration computed from three different cross-stream grid numbers, N, are listed in Table 6.7-2. The discrepancies between the results from N=20 and N=40 are significant, i.e., the maximum relative difference at η_T=0·508 is of the order of 20%. However, the calculated values from N=60 are only slightly different from those of N=40. Thus, 40 grids across the mixing layer can actually achieve the grid-independent results.

6.7-3 The influence of subdivisions in age-coordinate

The age-coordinate and its subdivisions are the newly introduced grid system in the current work and hence it is important to assess their influences on the results. Three values of NA have been employed in the computations and the RMS values of NO_2 fluctuation are provided in Table 6.7-3.

The difference between the results from NA=5 and NA=10 are small over most part of the mixing layer, while they are more negligible in the cases of NA=10 and NA=15. Therefore it can be concluded that 10 age intervals are sufficient to produce the grid independent results. It should be noted here that all other numerical and physical constants are the same as those appear in Run No.1.

6.8 Discussion of the results

The population distribution of folds

The major significance of the results obtained from the demographic analysis (in Sec.6.4) is that the cross-stream variation has been calculated from the transport equations.

Location across the mixing layer, η_T	RMS of NO_2 concentration fluctuation		
	NA = 5*	NA = 10	NA = 15
-2.00	0.0	0.0	0.0
-1.50	0.0595	0.0700	0.0705
-1.07	0.113	0.120	0.120
-0.674	0.124	0.124	0.124
-0.300	0.182	0.182	0.182
0.104	0.261	0.261	0.261
0.508	0.313	0.313	0.313
0.889	0.329	0.337	0.337
1.17	0.231	0.249	0.249
1.57	0.103	0.115	0.115

Table 6.7-3 Influence of age-intervals on NO_2 concentration fluctuation

* The distribution of age-interval in this case is:

0., 0.1, 0.3, 0.5, 0.7, 1

The location-dependence of the population distribution, as indicated in Figs.6.4-1 to 6.4-3, is significant in the mixing layer. The basic factors which contribute to the cross-stream variation are the turbulent diffusion effect and the distribution of fold formation rate.

The turbulent diffusion effect is determined by the turbulent viscosity and turbulent Schmidt number which are taken from the existing turbulence model as the necessary input to ESCIMO theory. No special attention has been paid to the development of the turbulence model itself, since it does not belong to the scope of current study.

On the other hand, the hypothesis about the distribution of fold formation rate is a new and unique feature of present approach. According to the knowledge of the author, there are no direct experimental measurements to verify the hypothesis. Therefore, only the influence on the mean properties and RMS quantities can be tested.

Nevertheless, there is a common trend from the average age described in Fig.6.4-7 where the $\tilde{A}_{ave}$ is always larger on the slower-moving side of the layer for all three runs. The explanation of this variation lies on the velocity distribution across the mixing layer, since higher velocity results in the shorter time (and hence smaller age) for a fold born in the upstream position to travel to downstream region.

The mean NO_2 concentration profile

It has been pointed out that the quantitative agreement between the present predictions and the measurements are reasonably good in Fig.6.5-2. However, some degree of

discrepancies do exist near the hump of the concentration profile and the probable explanations will be given below.

Apart from the uncertainties in experimental measurements declared by Batt (1977), the effects of non-equilibrium chemistry and turbulence intermittency factor may cause the diviation of predictions from measured values.

Alber and Batt (1975) has estimated six time scales regarding the chemical reaction and fluid mechanical processes, namely, the time scale associated with:

(1) chemical dissociation ($\tau_{chem} \simeq 0{\cdot}00016$sec),

(2) chemical recombination ($\tau_{chem} \simeq 0{\cdot}00016$sec),

(3) turbulent dissipation ($\tau \simeq 0{\cdot}0007$sec),

(4) turbulent convection ($\tau \simeq 0{\cdot}01$sec),

(5) turbulent diffusion ($\tau \simeq 0{\cdot}05$sec),

(6) laminar diffusion ($\tau \simeq 400$sec),

The chemical reaction rate is so rapid that only the turbulent dissipation time scale associated with the smallest scale eddies is of the same order as τ_{chem}. Hence, the non-equilibrium phenomena (i.e. finite rate chemistry) may only appear in the finest scale of turbulence structure.

Batt (1977) has studied the effect of finite rate chemistry and the interaction between chemical kinetics and turbulence intensities by including the second-order correction to the effective rate expression. It was recognised that the result changed by -5% approximately.

The turbulence intermittency factor, defined as the time portion when the flow exhibits the turbulent characteristics, has not been accounted in the present model. According to

the experimental data of Sunyach and Mathieu (1969), Batt (1977), the intermittency factor varies from zero near both edges of the mixing layer to unity in the mid-region. Strictly speaking, the results calculated from ESCIMO theory refer to the fully turbulent part only and hence should be weighted by the intermittency factor. Consequently, the contribution of the irrotational potential flow will be more dominant near the boundaries of the mixing layer and the results will be given by:

$$\overline{\overline{[NO_2]}} = (1-I)\,[NO_2]_p + I \cdot \overline{[NO_2]} \quad , \quad (6.8\text{-}1)$$

where $\overline{\overline{[NO_2]}}$ is the mean concentration of NO_2 including the intermittency factor, I is the intermittency factor, $[NO_2]_p$ is the concentration of NO_2 in the potential flow and $\overline{[NO_2]}$ is the mean concentration obtained from the ESCIMO theory excluding the intermittency effect. Therefore, it is expected that the results calculated from Eqn.(6.8-1) will be somewhat different from the present ones.

The fluctuation intensities of NO_2 concentration

There are more influential factors in the determination of fluctuation intensities of NO_2 concentration than the mean quantities described above. The various parameters employed in ESCIMO theory play the significant role on the quantitative comparison with experimental data.

The following remarks can be made from the sensitivity analysis performed in Sec.6.6:

• The fluctuation intensities at a fixed position increase when the population of youngest folds become more prominent. This is reflected in the results of Fig.6.6-1 where the population of youngest folds is highest for Run No.1 near $\eta_T \approx 0 \cdot 8$. The reason is that the profile in each fold is evened out by molecular diffusion and fold stretching as the fold gets aging.

• The fluctuation intensities magnify as the fold size at birth increases, because the distance which the diffusion process must travel is longer.

• The fluctuation level heightens as the properties of the re-engulfed part in the newly formed fold are further different from the local mean values (in the case of larger C_F value), since the initial profile in the fold is steeper and it remains so if other parameters are the same.

• Slower stretching rate yields larger fluctuations over most part of the mixing layer, except in the region between $-0 \cdot 8 \leq \eta_T \leq 0$ where the mean concentration is high. The reason is that the thickness of the fold does not reduce so rapidly and the non-uniformity of the properties within each fold can last longer. Since the relation between the temperature and NO_2 concentration is non-linear and not a monotonic one, it is possible that the fluctuation intensity of concentration is lower even when the temperature fluctuation is high under the low stretching condition.

Therefore, satisfactory agreement with the experimental data can be realised if a set of optimised parameters is employed in the computation.

The temperature fluctuation intensities

The maximum fluctuation intensities have been overpredicted by the order of 60%, as shown in Fig.6.5-3. This is in remarkable contrast with the fluctuation intensities of NO_2 concentration (from Run No.1) which are underpredicted by 10% only.

Batt (1977) suggested that the relative low fluctuation level was caused by random motion or three-dimensionality effects in the experiment and less influenced by large-scale two-dimensional coherent structures which has been observed in other shear-layer investigations.

The probability density function of temperature

The predicted pdf near both sides of the mixing layer show similar trend with the measured ones, i.e., they all behave as skewed one-sided pdf. But in the fully turbulent zone of the mixing layer where the intermittency factor is of the order of unity, the experimental results are almost Gaussian and cover the whole temperature domain. Unfortunately, the calculated pdf do not fulfill this requirement.

The careful review of the presumption regarding the fold composition at birth provides the answer to the discrepancy between measured and predicted pdf. The newly formed folds are composed of two parts having different properties (the fresh part and the re-engulfed part) and hence the pdf of these folds mainly consist of two blocks. The population average pdf is significantly influenced by the

pdf of younger folds because of their high proportion. Therefore, the shape of population average pdf contains three amjor portions which correspond to the fresh stream value, the population-average value and the value associated with the re-engulfed part in new born folds.

6.9 Closure

The application of ESCIMO theory to the turbulent reacting plane mixing layer has been described in this chapter. The population distribution of folds have been presented in two-dimensional flows for the first time and the influence of various hypotheses about the distribution of fold formation rate tested.

The mean turbulent properties, the RMS fluctuation intensities and the probability density functions have been calculated and compared with the experimental data of Alber & Batt (1975) and Batt (1977). The sensitivity analysis about various presumptions made in the present theory have been carried out. The grid independence test was also performed to assess the influence of all grid sizes.

The quantitative agreement between measured and predicted results is acceptable on the overall basis, although some discrepancies happen in the fluctuation intensities of temperature and the pdf related to it.

In order to further evaluate the applicability and the credibility of ESCIMO theory, it is essential to perform more test cases and compared with other experimental work. Therefore, the application of ESCIMO theory to the turbulent hydrogen-air diffusion flame and the turbulent

methane-air diffusion flame will be presented in the next chapter.

CHAPTER 7

THE TURBULENT JET DIFFUSION FLAMES

7.1 Introduction

The application of the ESCIMO theory to the turbulent round jet diffusion flames which have more practical importance is presented in this chapter. The chapter is mainly divided into two parts, the first part is associated with the hydrogen-air diffusion flame (Sections 7.1-7.5) and the second part with the methane-air diffusion flame (Sections 7.6-7.9).

In each part of the presentation, the results of the hydrodynamic calculations (from the k-ε model of turbulence), the population distribution of folds, the turbulent mean quantities, the RMS fluctuation intensities and the probability density functions of scalar and species concentration will be provided and compared with the experimental data available. The measurements obtained from Kent and Bilger (1973) in H_2-air flame and Lenz and Günther (1980) in methane-air flame have been chosen for the comparison, since the results are more comprehensive and regarded as reliable ones.

All the numerical factors and physical presumptions have been kept unchanged for both cases in order to assess the generality of those constants in the current work. The influence of different parameters on the predictions will be discussed separately in the next chapter. Therefore, all results produced in this chapter are based on a single set of constants.

7.2 The turbulent hydrogen-air diffusion flame

The experimental work of Kent and Bilger (1973) was carried out for turbulent diffusion flames of a horizontal round jet of hydrogen issued in a co-flowing stream of air. The jet diameter at the exit plane was 7.62mm and the cross-section of wind tunnel was 305 by 305mm. The tunnel cross-section is large enough so that the wall effects can be neglected and the pressure gradient is almost equal to zero. It was also mentioned by Kent and Bilger (1973) that the buoyancy effects were negligible.

The measurements were made at jet to external stream-velocity ratios of 2, 5, 8 and 10 to 1. The particular set of data from velocity ratio of 10 to 1 has been selected here for the comparison, because they are more extensively presented in the literature. The jet velocity at jet exit-plane is equal to 151m/s and the free-stream velocity is 15.1m/s.

The temperature measurements were made with a Pt-Rh (5% and 20%) thermocouple, coated with a special noncatalyic coating developed by Kent (1970). The samples of different species were withdrawn from the flow iso-kinetically with the aid of a hot-water-cooled probe. The samples were analyzed on-line using a lithium chloride hygrometer for water vapour, a katharometer for hydrogen, and a paramagnetic analyzer for oxygen. The radiation corrections have also been performed.

7.3 The computational aspects

The grid system

Twenty-grid nodes across the jet are employed in the

x-ω coordinate system, i.e.,N=20. The distribution of ω-intervals is given by the following expression:

$$\omega_i = \left(\frac{i-1}{N-1}\right)^2 \qquad i=1,2,\ldots,N \qquad . \quad (7.3\text{-}1)$$

The ω grid-nodes are more densely distributed near the jet axis where the temperature is high and hence the density is lower. The actual distance (y-interval) between each grid node is then nearly uniform.

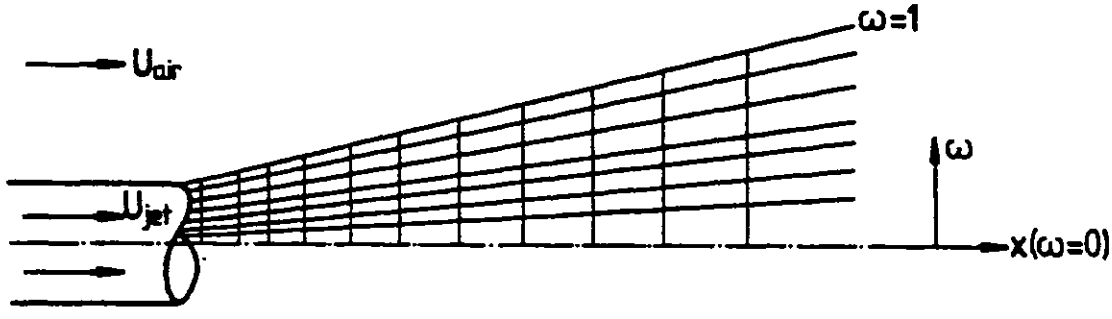

Fig.7.3-1 Grid system

The size of forward marching (in x-direction) step, ΔX, is calculated according to Eqns.(6.3-2) to (6.3-7) with the same numerical factors.

The number of intervals in the age-coordinate, NA, is again equal to 10. The distribution of these intervals is given by:

0, 0.05, 0.1, 0.15, 0.2, 0.3, 0.4, 0.5, 0.65, 0.8, 1.

The transformation function F(X) in Eqn.(5.2-2) is chosen as:

$$F(X) \equiv \frac{U_{air}}{X} \qquad , \quad (7.3\text{-}2)$$

where U_{air} is the velocity of co-flowing air and does not vary with x.

The computer time and storage required

The central processor unit time (CPU time) required for the calculation in this case is 360 seconds in the CDC 6600 machine. Hence, the computation time for each grid point in each marching step is approximately equal to 0.033sec.

The central core memory required is equal to 30 K words, while the additional information of the fold characteristics are stored in the magnetic tape.

The thermodynamics properties

The specific heat of each species and mixture are calculated according to the Eqns.(4.4-7) and (4.4-8). The heat of combustion of hydrogen is taken as 1.208×10^8 J/Kg from the standard thermodynamics handbook.

Both turbulent Prandtl and Schmidt number is assumed to be equal to 0.9 in the computations and hence the turbulent Lewis number is taken as unity.

The laminar diffusion coefficients of all species and heat transfer have been assumed to be equal in the fold biography analysis. It has been recognised that the molecular diffusivity of hydrogen is two or three times faster than the other species because of its small molecular weight. Therefore a definite amount of error will be introduced from the assumption of unity laminar Lewis number.

The error in the above mentioned assumption was tolerated, because the uncertainties in the fold size at birth and the

stretching rate are of the same order of the error introduced by the hypothesis of equal diffusivities. In the mean time, the simple chemical reaction scheme, described in Sec.4.4, will not be valid if the differential diffusion effect is considered and hence additional transport equations will have to be solved for each fold. The considerable expansion of computing time was not favoured at the present stage of development, since the influence of other presumptions will have to be tested first.

7.4 Presentation of results

7.4.1 The hydrodynamic results

The results of hydrodynamic calculation form the basis for the further combustion computation and hence it is desirable to check the turbulence model at the first place.

The axial distribution of jet centre-line velocity is plotted in Fig.7.4-1 together with the experimental data from Kent and Bilger (1973). The quantitative agreement between the predicted and measured values are satisfactory, signifying that the k-ε model of turbulence is capable of producing correct results about the global turbulent diffusion effects for this flow case.

The turbulence levels on the centre line of the jet are plotted in Fig.7.4-2. The predictions are obtained from the turbulent kinetic energy based on the assumption of isotropic turbulence, while the data points stand for the measurements of radial velocity turbulence intensity, $\sqrt{\overline{v'^2}}$, on the centre-line of the flame. Therefore, only a qualitative comparison can be expected for this case.

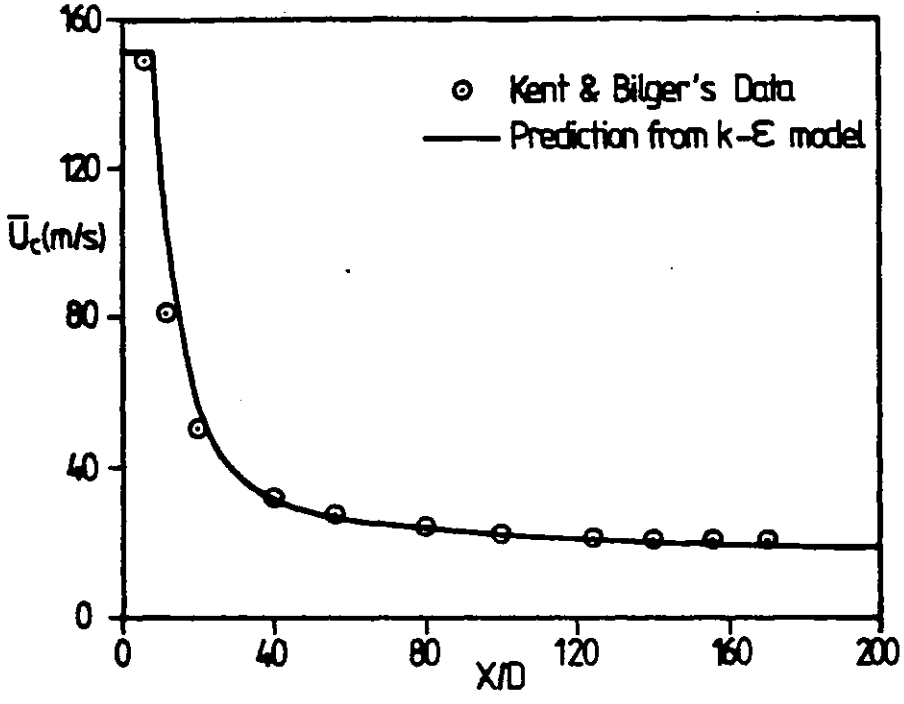

Fig.7.4-1 Variation of axial-velocity in hydrogen-air flame

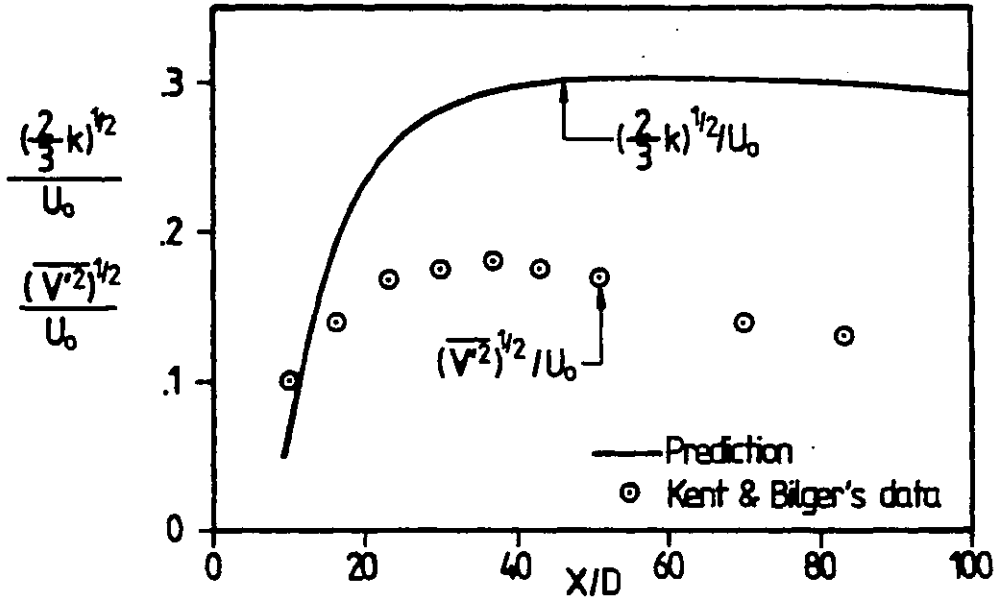

Fig.7.4-2 Variation of axial turbulence-intensities in hydrogen-air flame

7.4.2 The population distribution of folds

The results to be presented in this chapter are obtained from the assumption that the fold formation rate across the jet is proportional to the gradient of local mean axial velocity. Firstly, the population distribution with respect to age, at three different downstream locations, will be presented in Figs.7.4-3 to 7.4-5 respectively.

In Fig.7.4-3, the three curves represent the $\tilde{P}$~$\tilde{A}$ distribution at three radial positions for X/D=40. The folds having age between 0.1 and 0.15 are the most popular near the jet axis (i.e., r/D=0.27), in which the fold formation rate is minimum. On the other hand, the youngest folds are more dominant in the mid-region (r/D=2.10) and the outer region (r/D=4.04) of the jet. It should be noted that the highest population of the newly formed folds appear at r/D=2.10 where the fold formation rate reaches its climax (the velocity gradient is large there).

Similar results at X/D=80 are shown in Fig.7.4-4, where the slope of each curve is now more moderate. Eventually, inspection of Fig.7.4-5 reveals that the population distributions become rather uniform at the further downstream region of X/D=120, where the velocity gradient diminishes and the fold formation rate also follows suit.

Secondly, the radial variation of the population of folds belonging to a particular age-interval are demonstrated through Figs.7.4-6 to 7.4-8. In Fig.7.4-6, the population of four kinds of folds, at X/D=40, are plotted against the radial distance. The population of the youngest folds, $\tilde{P}_1$,

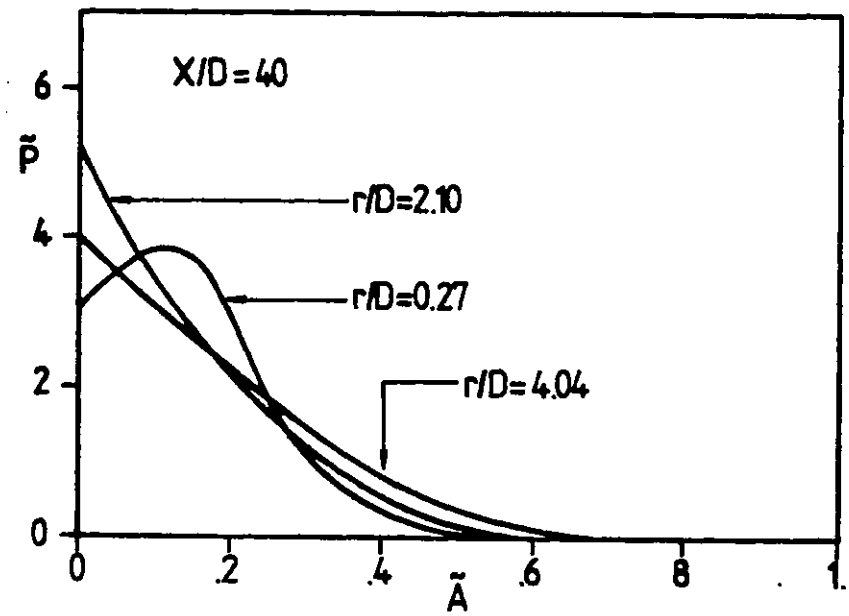

Fig.7.4-3 Population distribution function with respect to age

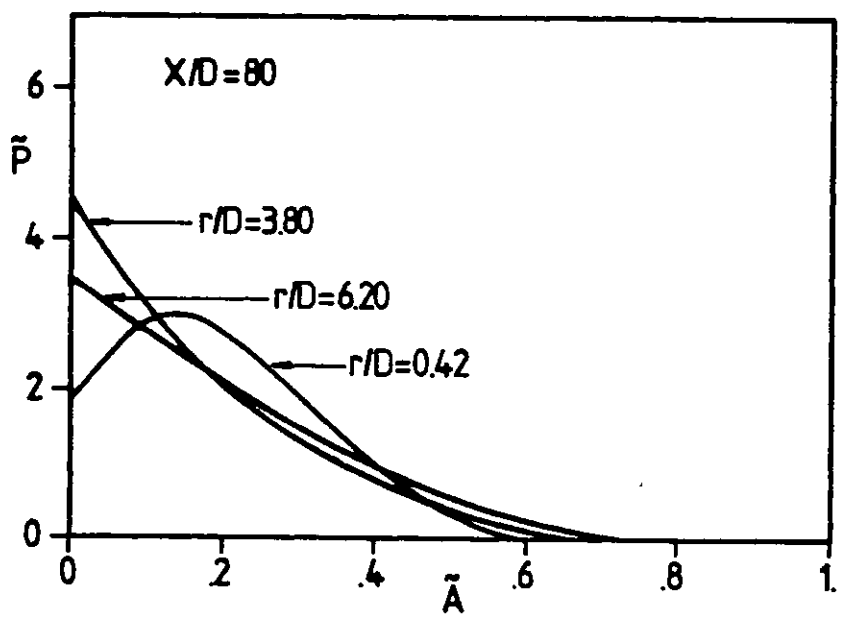

Fig.7.4-4 Population distribution function with respect to age

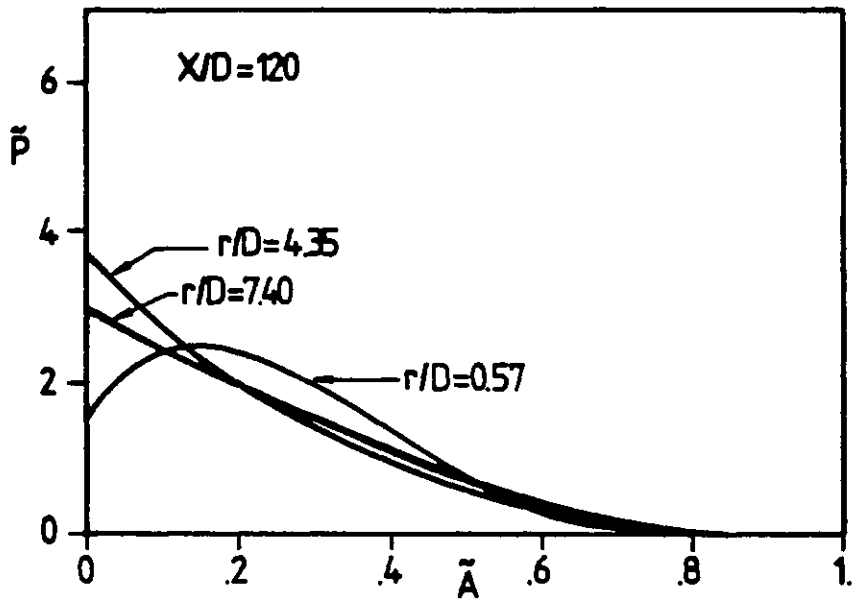

Fig.7.4-5 Population distribution function with respect to age

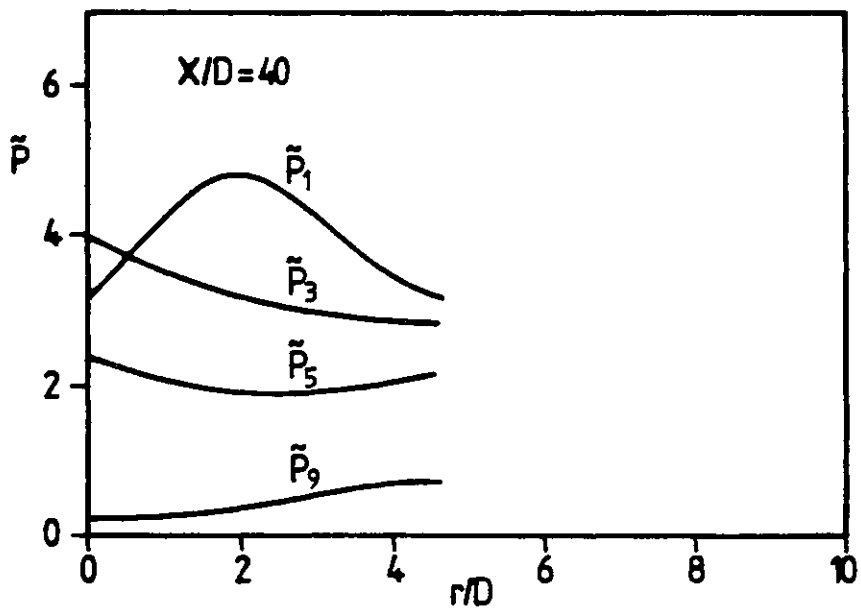

Fig.7.4-6 Radial variation of population of folds belonging to a particular age-interval

attains the maximum value round r/D=2.12 as described above. For the population of folds having age between 0.10 and 0.15, $\tilde{P}_3$, the curve decays monotonically from the axis (r/D=0) towards the outer edge of the jet. The value of $\tilde{P}_5$ (for $0.20 \leq A \leq 0.25$) first decreases as the value of r/D increases and then rises slightly in the outer part of the jet. However, the population of older folds (for $0.40 \leq A \leq 0.45$), $\tilde{P}_9$, increases steadily with the radial distance.

The variation of folds population, obtained at X/D=80, are presented in Fig.7.4-7. The patterns of $\tilde{P}_1$, $\tilde{P}_3$ and $\tilde{P}_5$ are similar to their counterparts in the previous figure, while the trend of $\tilde{P}_9$ is somewhat different. The results in Fig.7.4-8, for X/D=120, bear much resemblence to those in Fig.7.4-7, apart from the gentler change in the magnitude of each curve.

Thirdly, the radial distribution of average age at X/D=40, 80 and 120 are provided in Fig.7.4-9. The noticeable point is that the folds in the mid-region of the jet have the lowest average age, since the fold formation rate is highest there and the newly born folds are more prominent. Also it can be observed that the level of average age increases in the further downstream region of the jet, where the mean velocity of the flow approaches the velocity of co-flowing air stream.

7.4.3 The mean temperature and species concentration

The general features of the diffusion flame considered are described by the turbulent mean temperature and species concentration, namely the concentration of H_2, O_2 and H_2O.

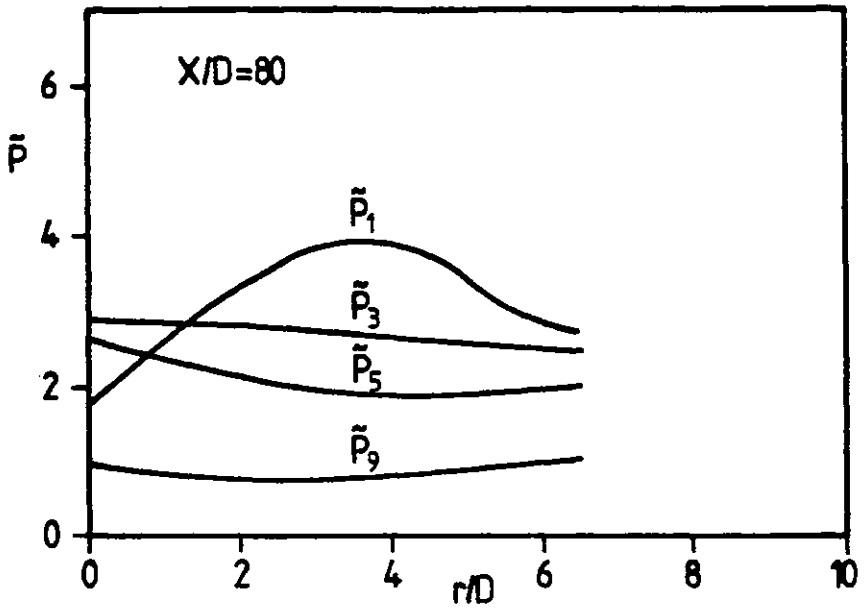

Fig.7.4-7 Radial variation of population of folds belonging to a particular age-interval

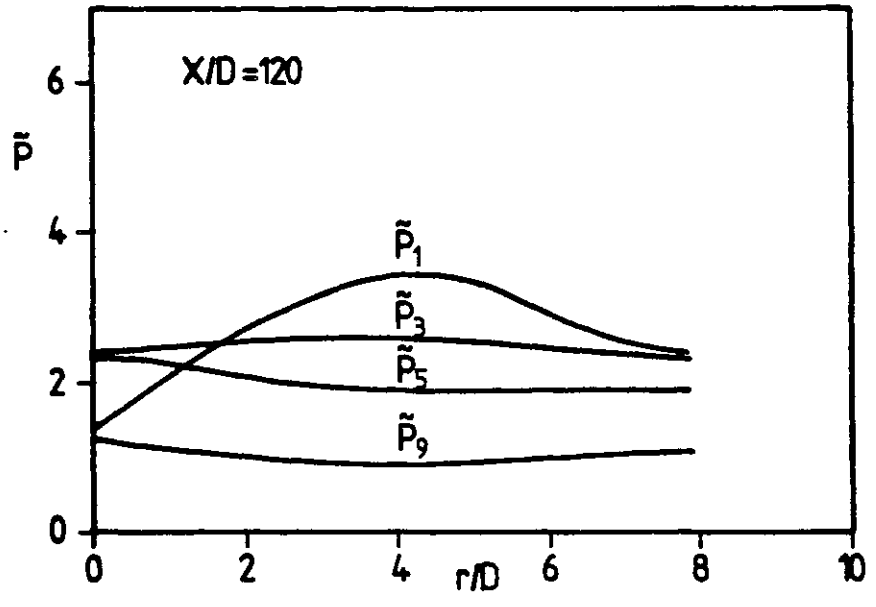

Fig.7.4-8 Radial variation of population of folds belonging to a particular age-interval

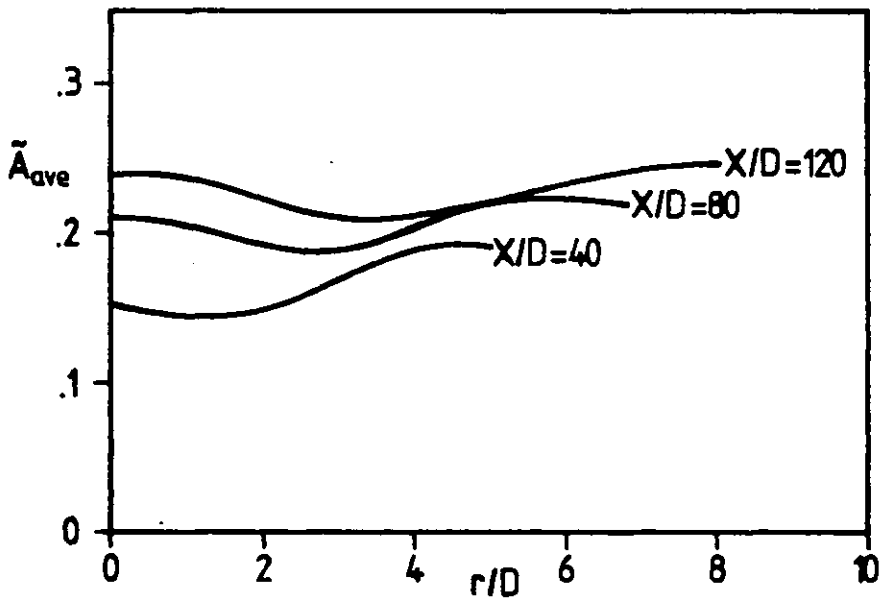

Fig.7.4-9 Radial profiles of average age across the jet

The concentration of minor species, radicals and nitric oxides have not been considered in the present reaction scheme.

The axial distribution of mean temperature and mean species concentration (in molar fraction) are plotted in Fig.7.4-10 with the experimental results of Kent and Bilger (1973). It can be observed that the concentration of fuel and oxygen are under-predicted for X/D larger than 40, and the temperature is also slightly underpredicted. Nevertheless, the agreement between the predictions and measurements is believed to be reasonably good.

The radial distribution of mean temperature and species concentration, at X/D=40, 80, 120 and 160 respectively, will be provided in Figs.7.4-11 to 7.4-14.

The results obtained at X/D=40 are demonstrated in Fig.7.4-11. The calculated peak temperature is lower than the measured value by 200^{0}K, and the predicted peak location has been shifted towards the outer region of the jet by the distance of one jet radius approximately. The hydrogen concentration and water vapour concentration have been well predicted from the jet axis until r/D=3. For the region of r/D greater than 3, the concentration of water vapour is overpredicted, while the amount of oxygen is underpredicted. The overlapping of fuel and oxygen, which is the characteristics of turbulent diffusion flames, has been shown in the present calculation. However, the calculated value at the over-lapping point ($\approx$0.05) is lower than the measured one ($\approx$0.08).

The results in Fig.7.4-12 are obtained at X/D=80. The

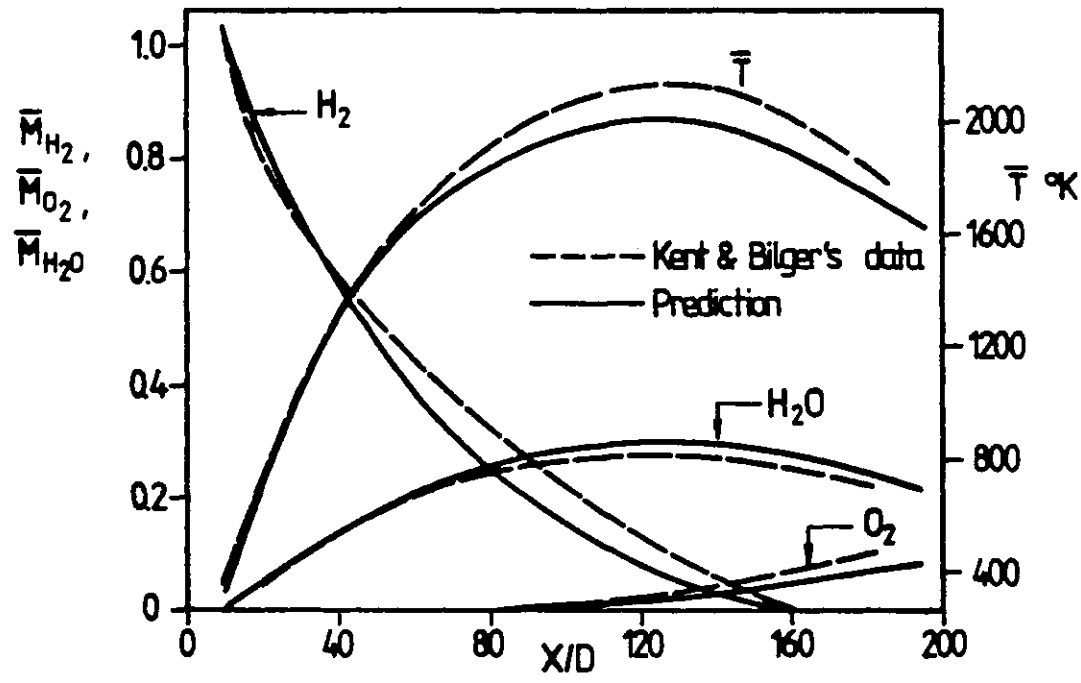

Fig.7.4-10 Axial distribution of mean temperature and mean composition

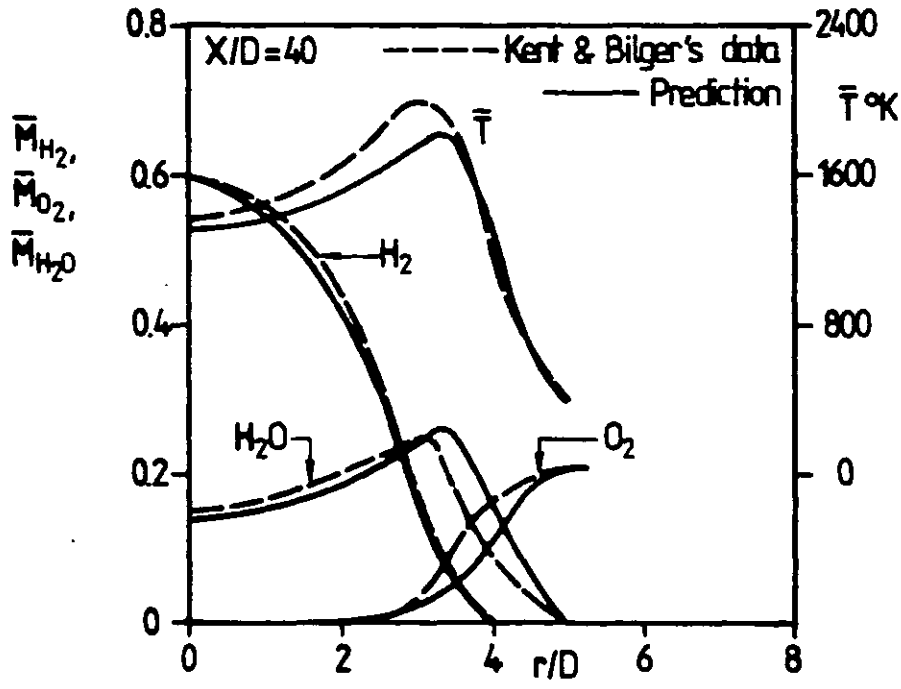

Fig.7.4-11 Radial distribution of mean temperature and mean composition

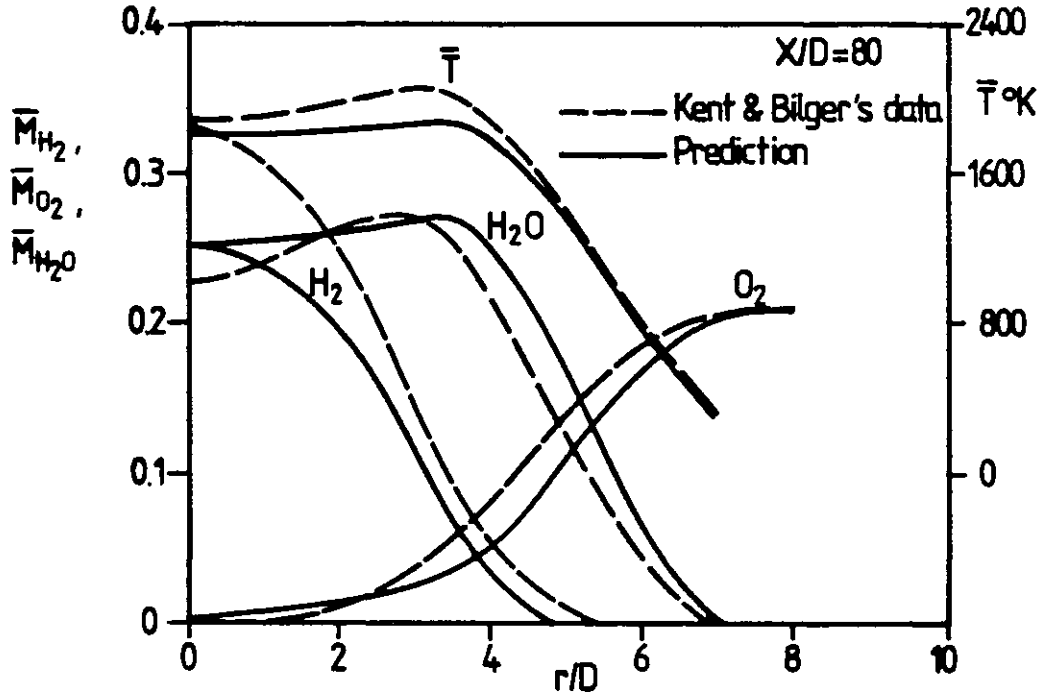

Fig.7.4-12 Radial distribution of mean temperature and mean composition

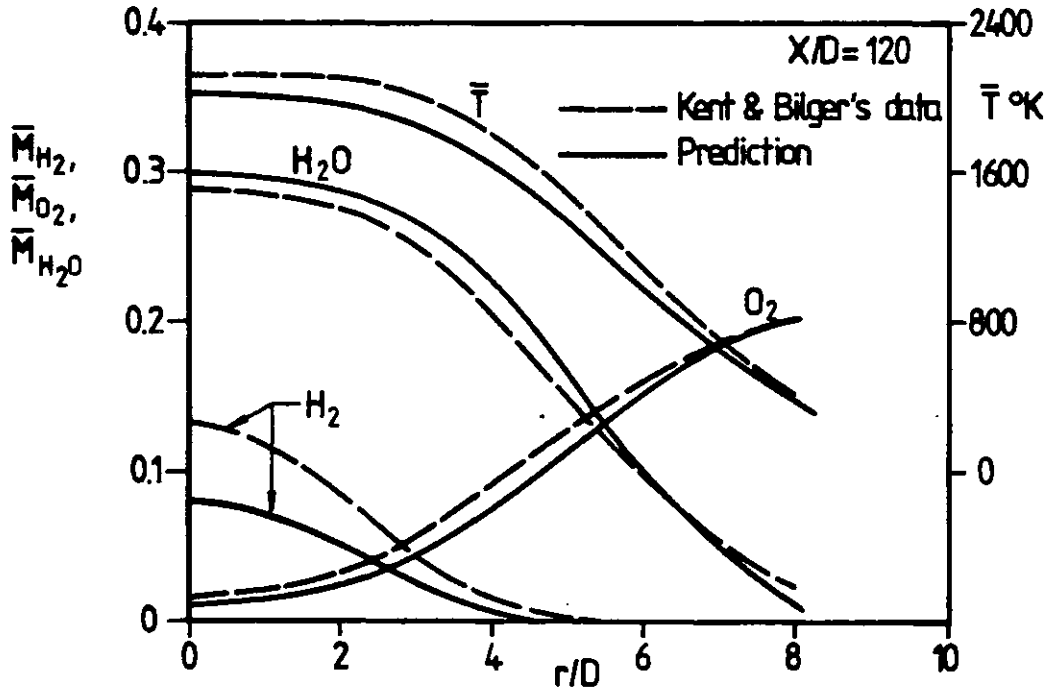

Fig.7.4-13 Radial distribution of mean temperature and mean composition

temperature at the axis is now higher (≈1800°K) and the computed peak temperature reaches 1880°K at r/D=3.5. The measured maximum temperature is located at r/D=3.0 and has the magnitude of 2040°K approximately. The amount of water vapour is overpredicted for r/D greater than 3, while the oxygen concentration is lower than the experimental counterpart. The fuel concentration is underpredicted in whole part of the jet.The degree of overlapping in the prediction (≈0.045) is again lower than the measurement.

Similarly, the same set of quantities are provided in Fig.7.4-13 for X/D=120. The axial temperature has now achieved the highest value in both prediction and measurement, signifying that the flame zone is around the jet axis. The concentration of hydrogen and oxygen have been underpredicted, while the amount of water vapour was overpredicted from the jet axis until r/D=6. The measured degree of mixing (or overlapping) is still higher than the calculated value, as in other positions.

The hydrogen content is nearly exhausted at X/D=160, as indicated in Fig.7.4-14. The oxygen has already penetrated into the central zone of the jet and the temperature is highest in the axial position, all these phenomena suggest that the flame tip is located near X/D=160. The amount of oxygen is still underpredicted across the jet, while the water vapour is overpredicted for $0 \leq r/D \leq 5$ and underpredicted for $r/D > 5$.

Finally, the flame and temperature contours from the predictions and measurements are presented in Fig.7.4-15.

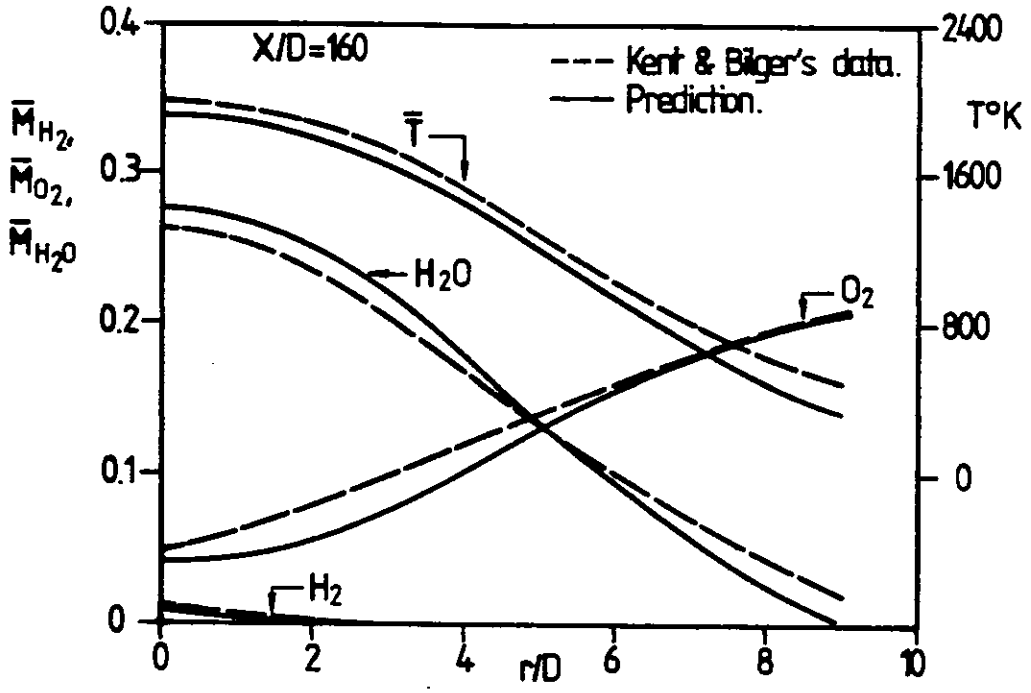

Fig.7.4-14 Radial distribution of mean temperature and mean compositions

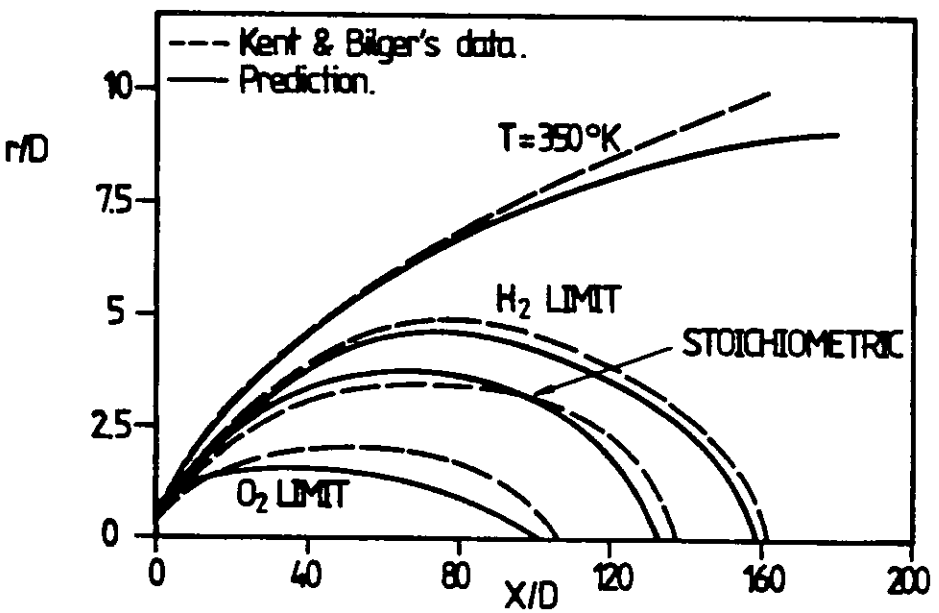

Fig.7.4-15 Flame contours. H_2 limit is for mole fraction of 1 per cent and O_2 limit for 0.5 per cent

The smooth variation in all predicted curves indicates the correct tendency obtained from the present theory. However, the major discrepancies between the computation and Kent and Bilger's data appear in the O_2 limit, where under-prediction persists.

7.4.4 The root mean square fluctuation of temperature

The RMS fluctuation of temperature will be presented here as a further demonstration of the applicability and power of ESCIMO theory. The axial distribution of temperature fluctuation is now plotted in Fig.7.4-16 together with the prediction made by Kent and Bilger (1976). The measurements are not available for this flame as mentioned by Kent and Bilger (1976).

Kent and Bilger (1976) has assumed a Gaussian turbulent pdf in the mixture fraction with a prescribed fluctuation intensity to calculate the temperature fluctuation. Inspection of Fig.7.4-16 reveals that the results obtained with both approaches follow the similar trend although higher fluctuation level has been detected from the current study. The decay of the fluctuating intensities between X/D=50 and X/D=80 are observed from both curves and the shape is in qualitative agreement with the measurements of Lockwood and Odidi (1975) in the methane-air free jet diffusion flame.

The radial variation of temperature fluctuations, obtained at X/D=40, 80, and 120 respectively, are now shown in Fig.7.4-17. The locations of the peak in each curve shift toward the central part of the jet in the further downstream region in a similar way to the mean temperature profile. The

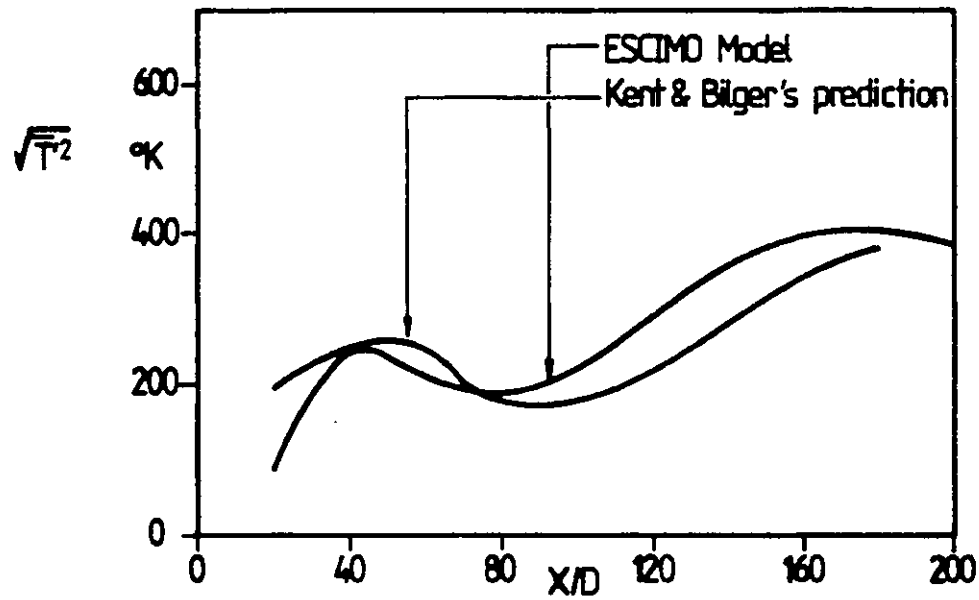

Fig.7.4-16 Axial distribution of temperature fluctuations

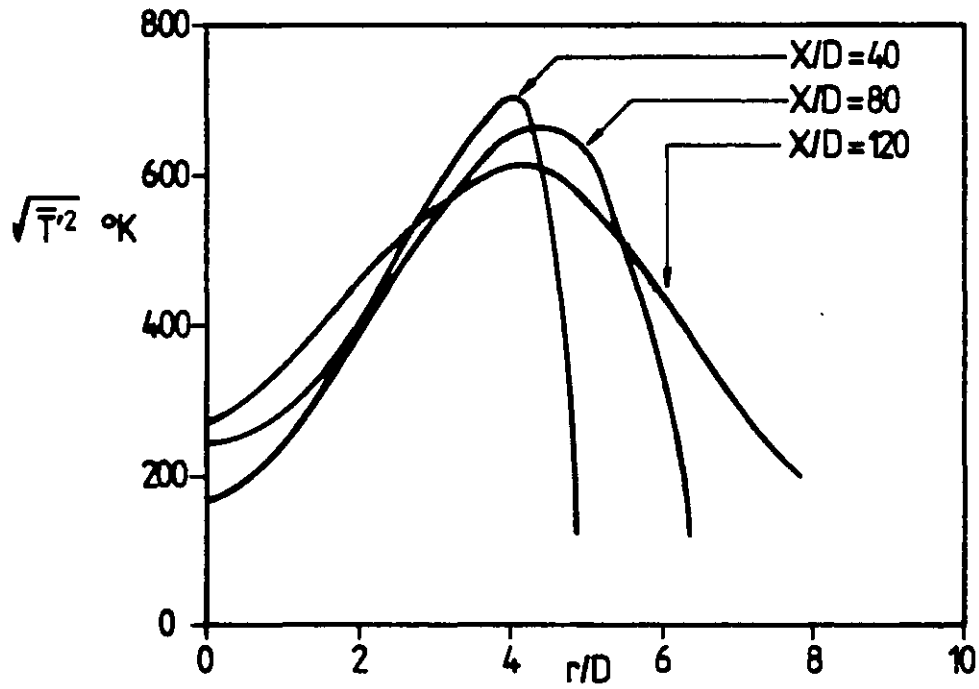

Fig.7.4-17 Radial distribution of temperature fluctuations at various locations

maximum fluctuation intensity decreases and the profile broadens as the value of X/D further increases, indicating the diffusive spreading of the flame zone. The experimental data have not been reported by Kent and Bilger.

7.4.5 The root mean square fluctuation of species concentration

The concentration fluctuation intensities of hydrogen and oxygen, at X/D=40, 80 and 120, are presented through Figs.7.4-18 to 7.4-20 respectively. The mean concentration profiles are also shown in the graphs so that the relative magnitude of fluctuation can be recognized.

In Fig.7.4-18, the RMS value of hydrogen concentration fluctuation is equal to 0.175 at the jet axis and reaches the maximum value of 0.235 at r/D=1.75. It can be observed that the RMS fluctuation value of H_2 molar fraction is higher than the mean value when the latter quantity is low, e.g., in the region where r/D>3.25. On the other hand, the fluctuation level of O_2 concentration is greater than the mean value in the range $0.5 \leq r/D \leq 3.75$, i.e.,when the mean oxygen concentration is lower than 0.06. The fluctuation intensities approach zero as the mean value of O_2 concentration reaches the free-stream value.

Similarly, the results obtained at X/D=80 are plotted in Fig.7.4-19. The RMS value of H_2 concentration fluctuation is now lower than the counterpart in the preceding graph, but the variation is similar in each case. The profile of O_2 fluctuation also exhibits a peak value of 0.06 near the intersection point of mean H_2 and mean O_2 concentration curves.

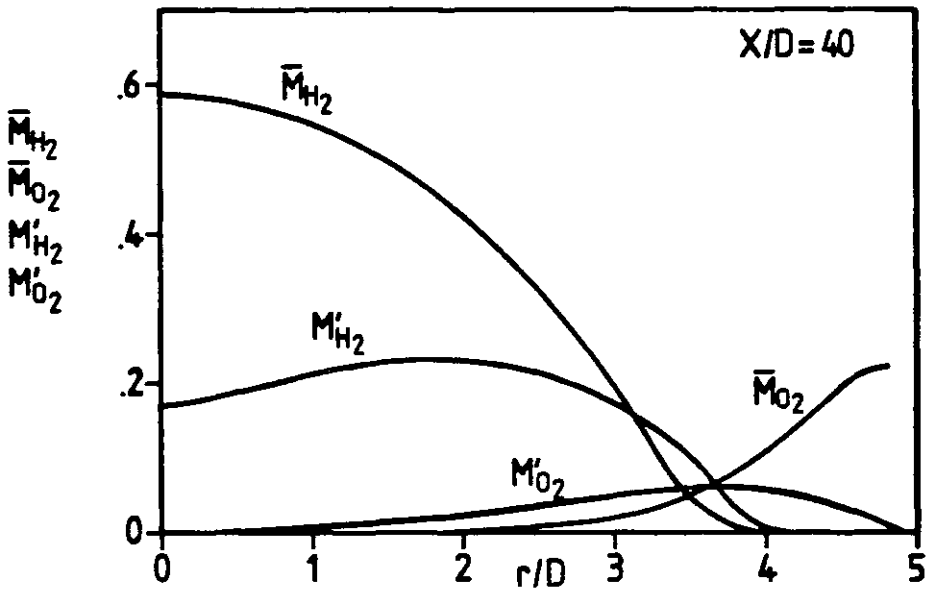

Fig.7.4-18 Concentration fluctuation of hydrogen and oxygen

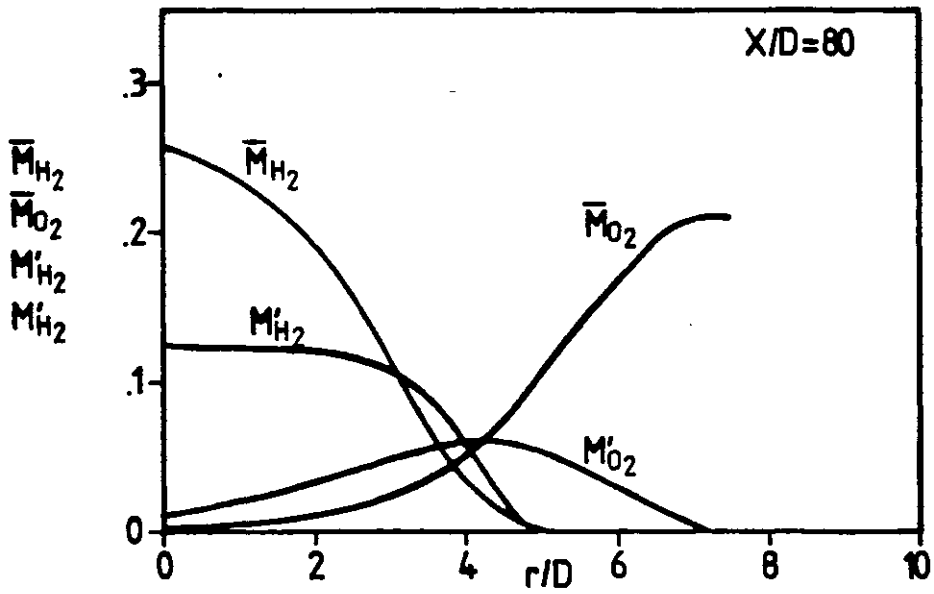

Fig.7.4-19 Concentration fluctuation of hydrogen and oxygen

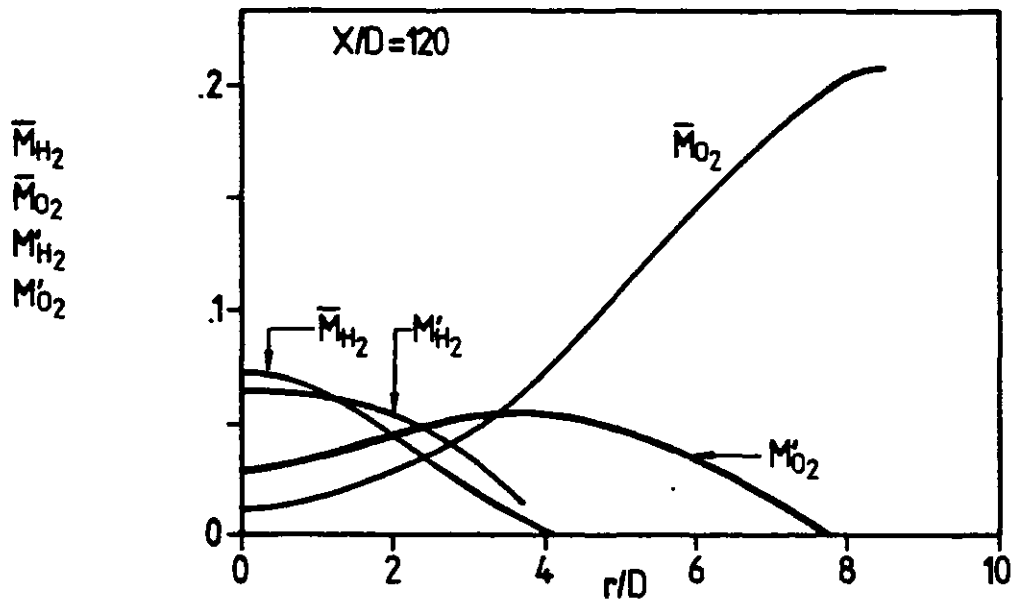

Fig.7.4-20 Concentration fluctuation of hydrogen and oxygen

In Fig.7.4-20 the RMS values of H_2 concentration fluctuation, at X/D=120, further decrease below the level of 0.1, but the relative fluctuation intensities (the ratio of RMS value to the mean value) are higher now. The location of the maximum RMS value, for H_2 fluctuation, is now situated at the jet axis where the temperature is highest (as shown in Fig.7.4-13).

Finally, the RMS values of H_2O concentration fluctuation, at X/D=40, 80, 120 and 160, are demonstrated in Figs.7.4-21-7.4-22. The profiles of concentration fluctuation spread outwards as the value of X/D increases, which is the result of the diffusion process. It can also be observed that the peak of fluctuation is located in the inner region of the jet (r/D=2.5) at X/D=160.

7.4.6 The probability density function of temperature

The temperature pdf is one of the most interesting quantities associated with the detail structure of turbulent flames, since it depends on the composition of the mixture and the enthalpy as well.

The temperature pdfs at the centre line of the jet, for four X/D values, will first be demonstrated in Fig.7.4-23. Then, the radial evolution of temperature pdfs at the corresponding X/D positions will be presented from Figs.7.4-24 to 7.4-27 respectively.

In Fig.7.4-23, the axial temperature pdfs calculated at X/D=40, 55, 80, 120 were shown by four diagrams. The location of the maximum value shifts towards the high temperature direction as the value of X/D increases and

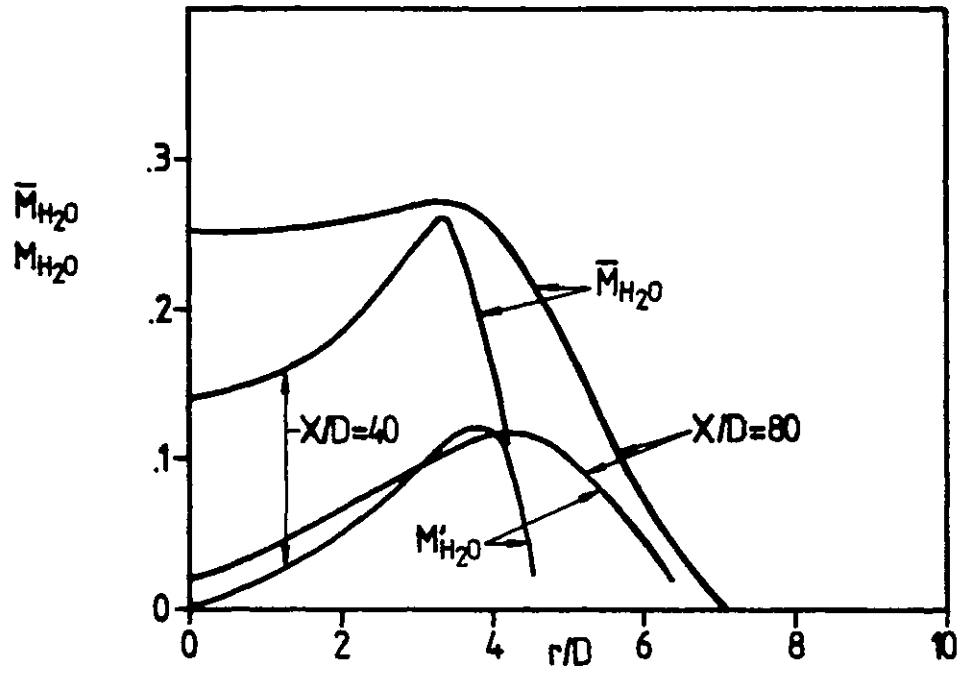

Fig.7.4-21 Radial distribution of water vapour concentration and its fluctuation

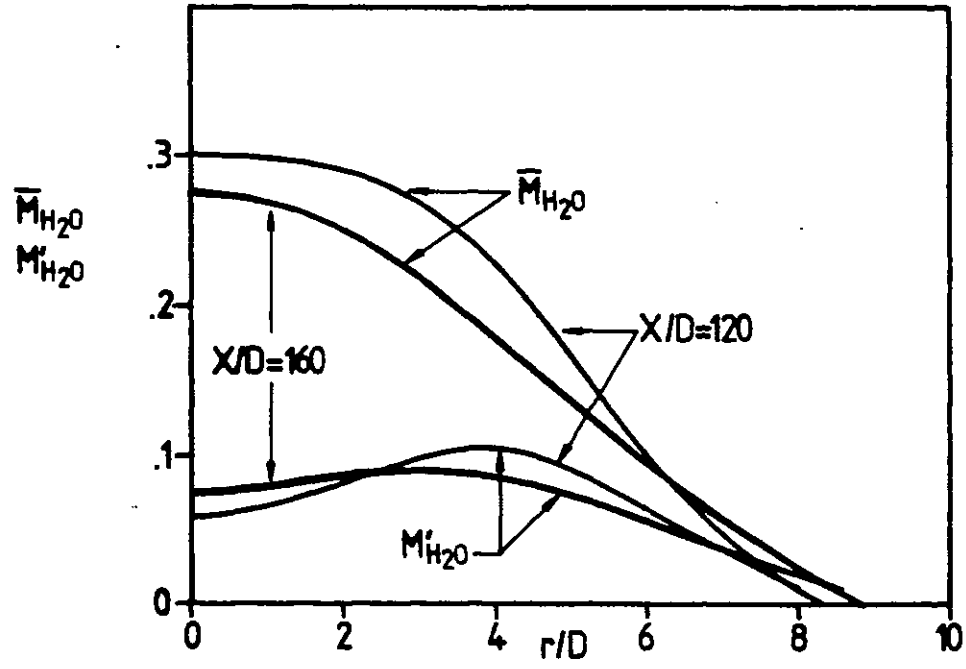

Fig.7.4-22 Radial distribution of water vapour concentration and its fluctuation

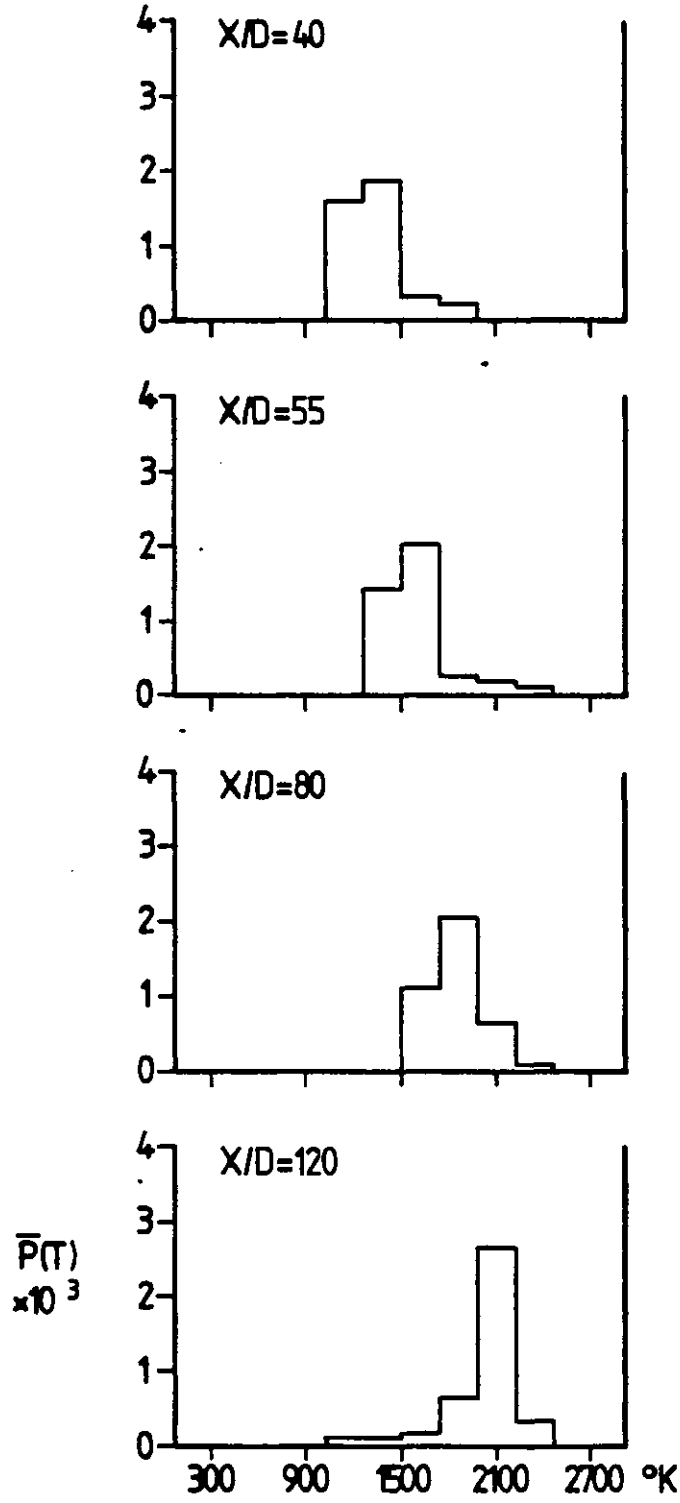

Fig.7.4-23 Probability density function of temperature at flame axis

this is consistent with the variation of mean axial temperature represented in Fig.7.4-10. It should be noted that no contribution of free stream fluid (at T=300°K) is present in any of these diagrams and the pdf profiles are unimodal.

The radial evolution of pdfs at X/D=40 are plotted in Fig.7.4-24 where the four curves stand for the distribution at r/D=0.69, 1.86, 3.21 and 4.20 respectively. The temperature corresponding to the maximum distribution in each curve is approximately equal to the mean value. A small but finite contribution of free stream property appears in the profile of r/D=3.21, i.e. near the outer edge of the jet.

The pdf profiles at X/D=55 are drawn in Fig.7.4-25 with the results from Kennedy and Kent (1981) who have measured the pdfs of the mixture fraction with the aid of optical devices and converted to temperature pdfs. There is a larger intermittent spike (T=300°K) in the outer edge of the flow (e.g., at r/D=4.16) in Kennedy and Kent's data. The present predictions produce a narrower distribution (hence smaller fluctuation) in the outer region of the jet where the influence of free stream conditions are stronger.

The pdf profiles at X/D=80 are shown in Fig.7.4-26 and it can be seen again that the mean temperature coincides with the corresponding value where the distribution is maximum. The contribution of free stream properties, at r/D=2.95, is still small.

In Fig.7.4-27, where X/D=120, the probability of finding

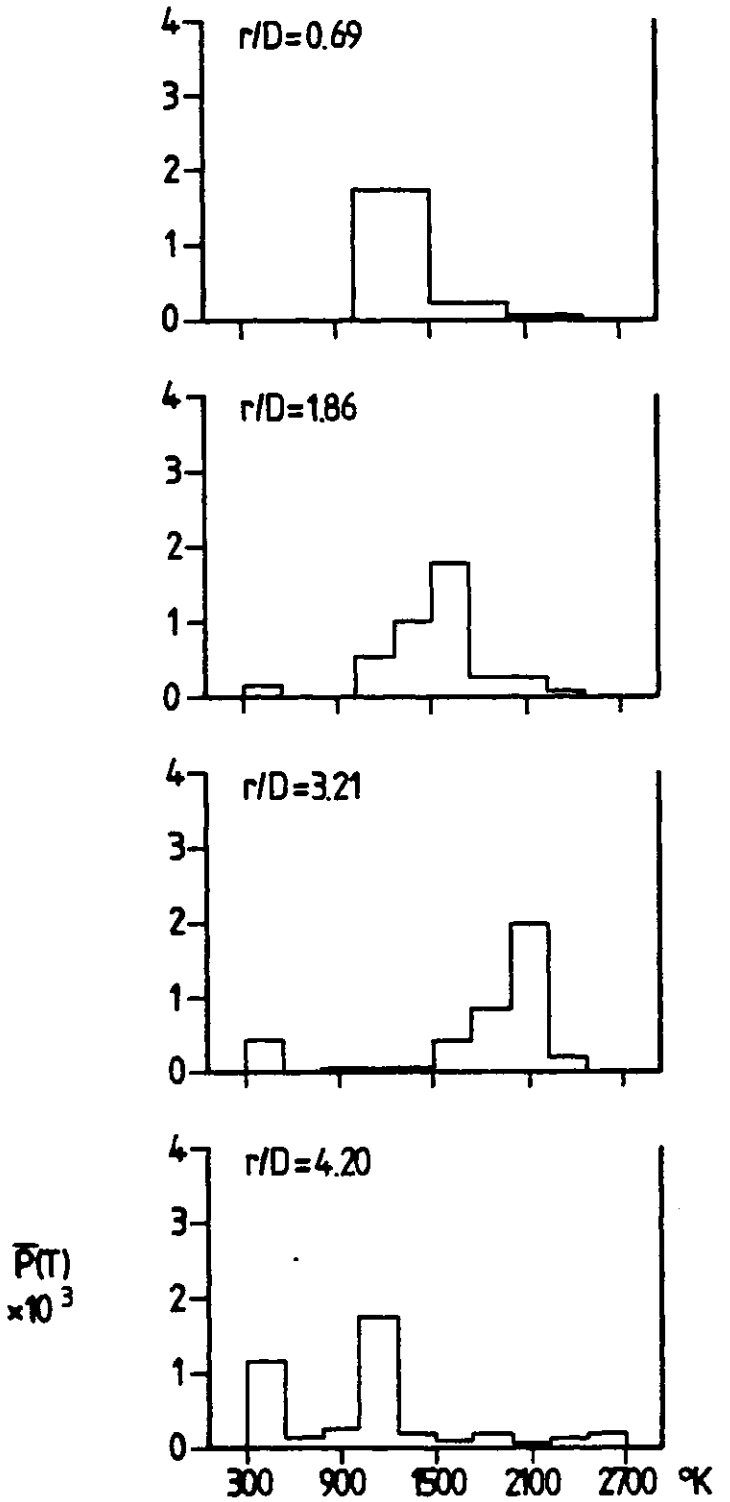

Fig.7.4-24 Probability density function of temperature at X/D=40

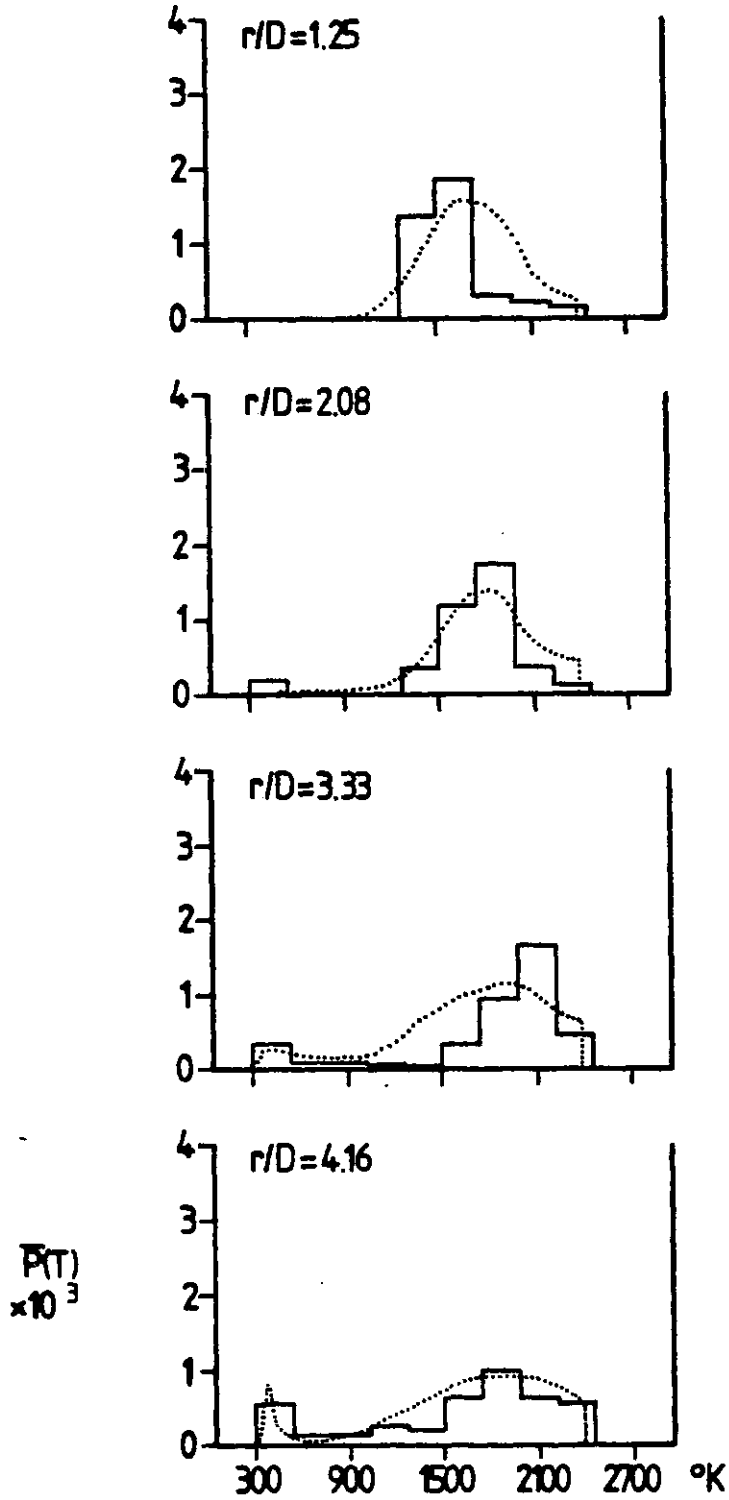

Fig.7.4-25 Probability density function of temperature at X/D=55
(——— present predictions,
····· measurements of Kennedy and Kent)

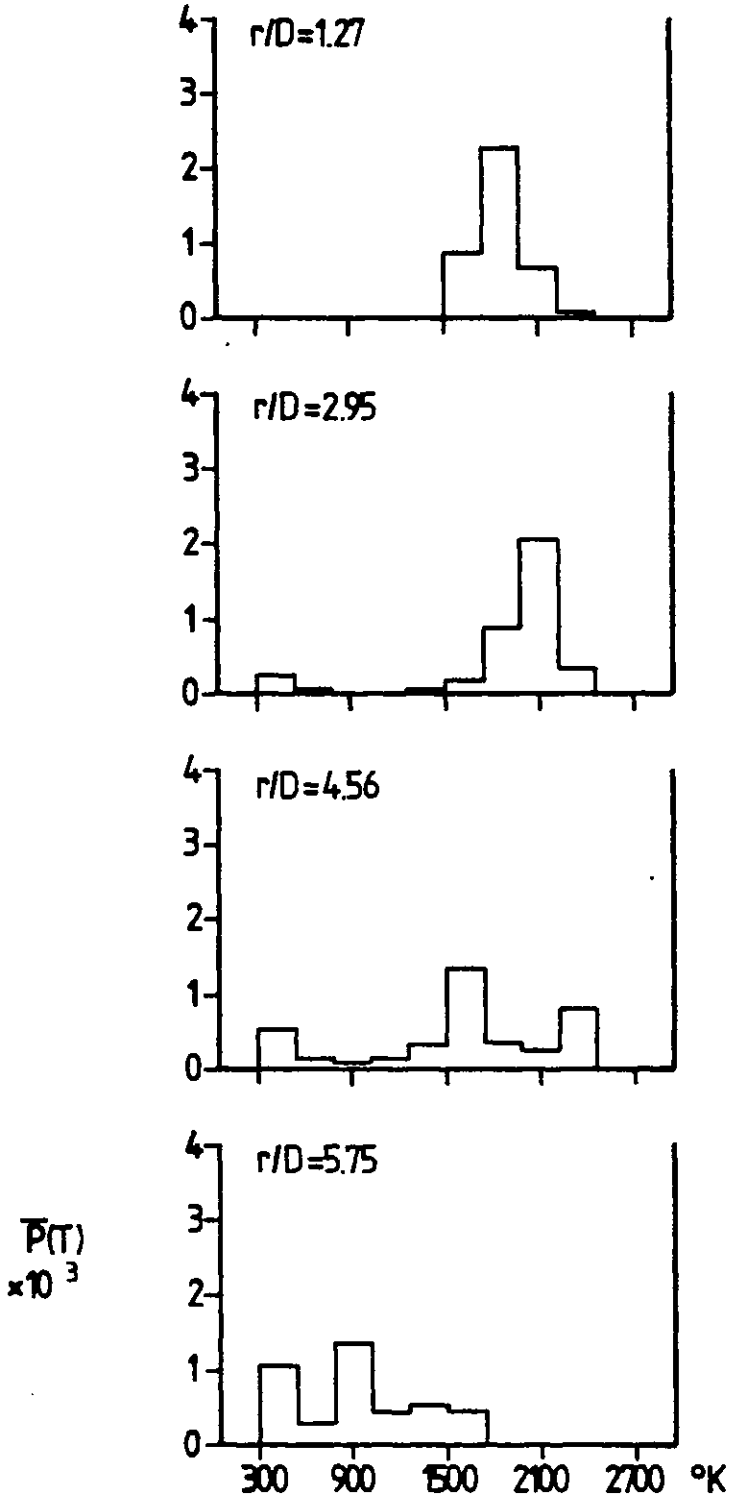

Fig.7.4-26 Probability density function of temperature at X/D=80

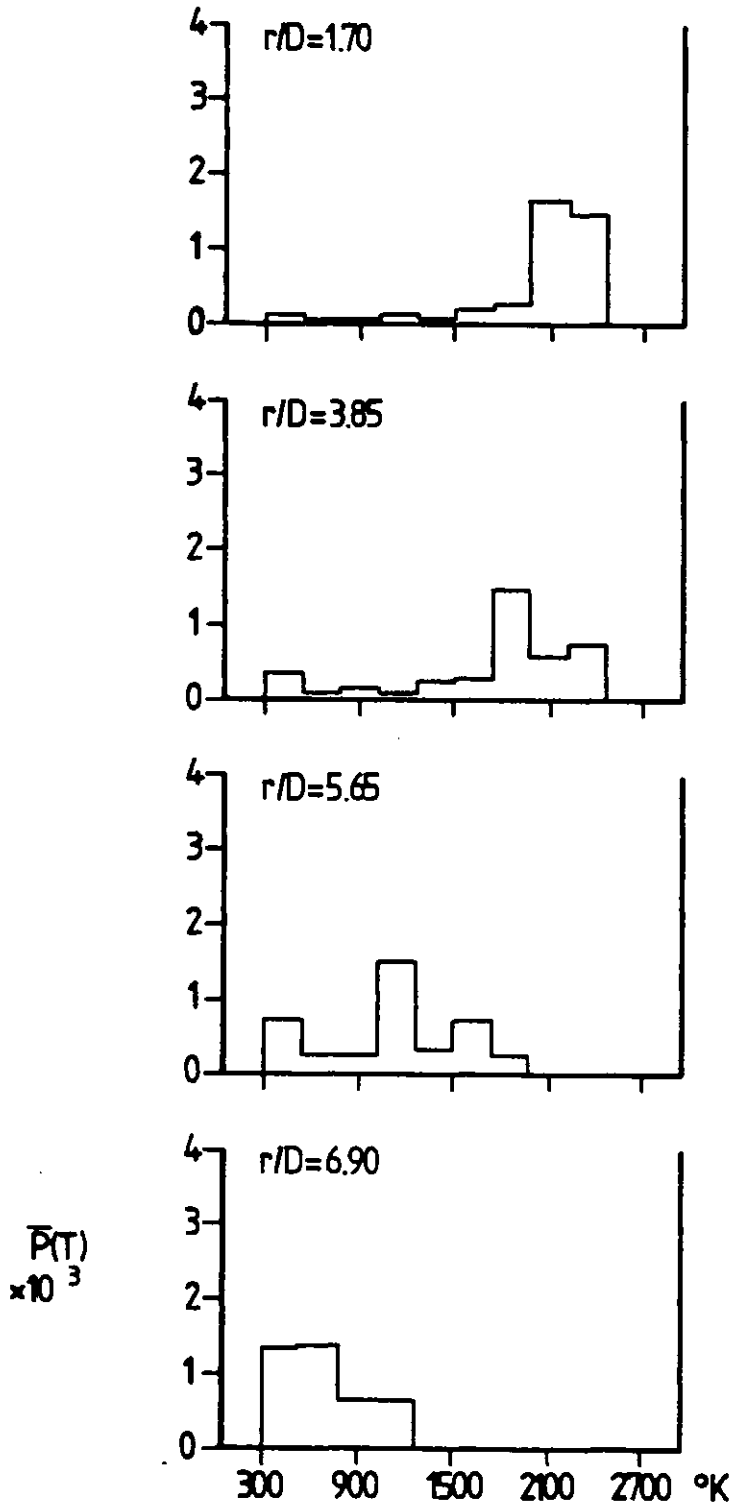

Fig.7-4-27 Probability density function of temperature at X/D=120

the temperature near the ambient condition is greater at the outer edge of the jet, at r/D=5.65. Furthermore, the pdf at r/D=6.90 is composed of lower temperature intervals (from 300°K~1300°K), indicating that the mean temperature is well below the flame temperature there.

7.4.7 The probability density function of species concentration

The radial variation of pdf of the mass fraction of hydrogen, for X/D=40, and 80 respectively, are presented in Figs.7.4-28 and 7.4-29. In Fig.7.4-28, the pdf profile is broader in the inner region of the jet (e.g., at r/D=0.69 and 1.86) and narrows as the mean value of hydrogen diminishes in the outer region (e.g., at r/D=4.20). The similar trend can also be detected in Fig.7.4-29, where the quantitative contribution of fuel is smaller.

The same variation regarding the pdf of mass fraction of oxygen are demonstrated in Figs.7.4-30 and 7.4-31. It can be observed that the profile is mainly concentrated around the lower limit of oxygen content for r/D value up to 3.11, where the mean value is small compared with the free stream value. The profile shifts towards the higher limit only in the outer region of the jet, e.g., at r/D=4.20. The evolution pattern at X/D=80 is also similar as shown in Fig.7.4-31.

The pdf of mass fraction of H_2O, at X/D=40, 80 and 120, are presented through Figs.7.4-32 to 7.4-34. It is evident that the shape of the pdf is neither Gaussian nor symmetric. The profile moves towards the lower bound in the outer region of the jet, for all X/D-values, indicating

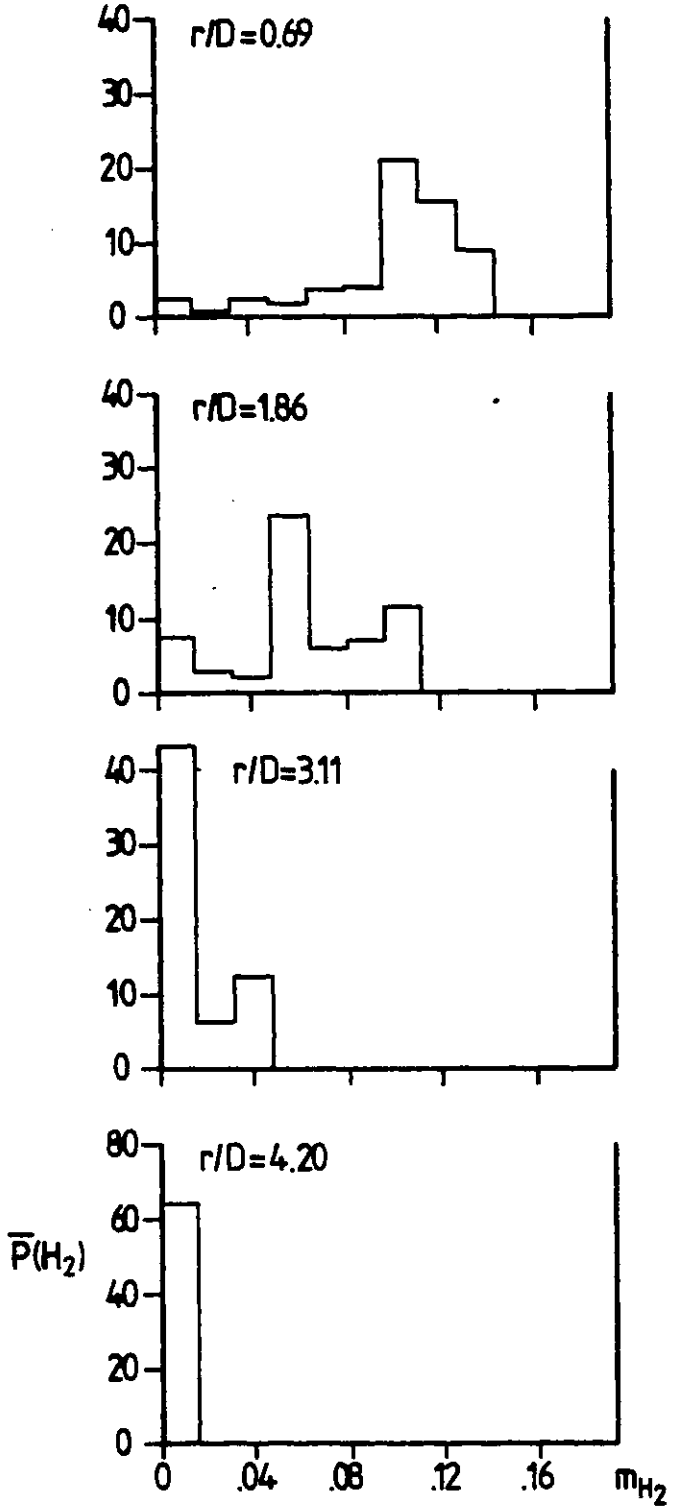

Fig.7.4-28 Probability density function of mass fraction of H_2 at X/D=40

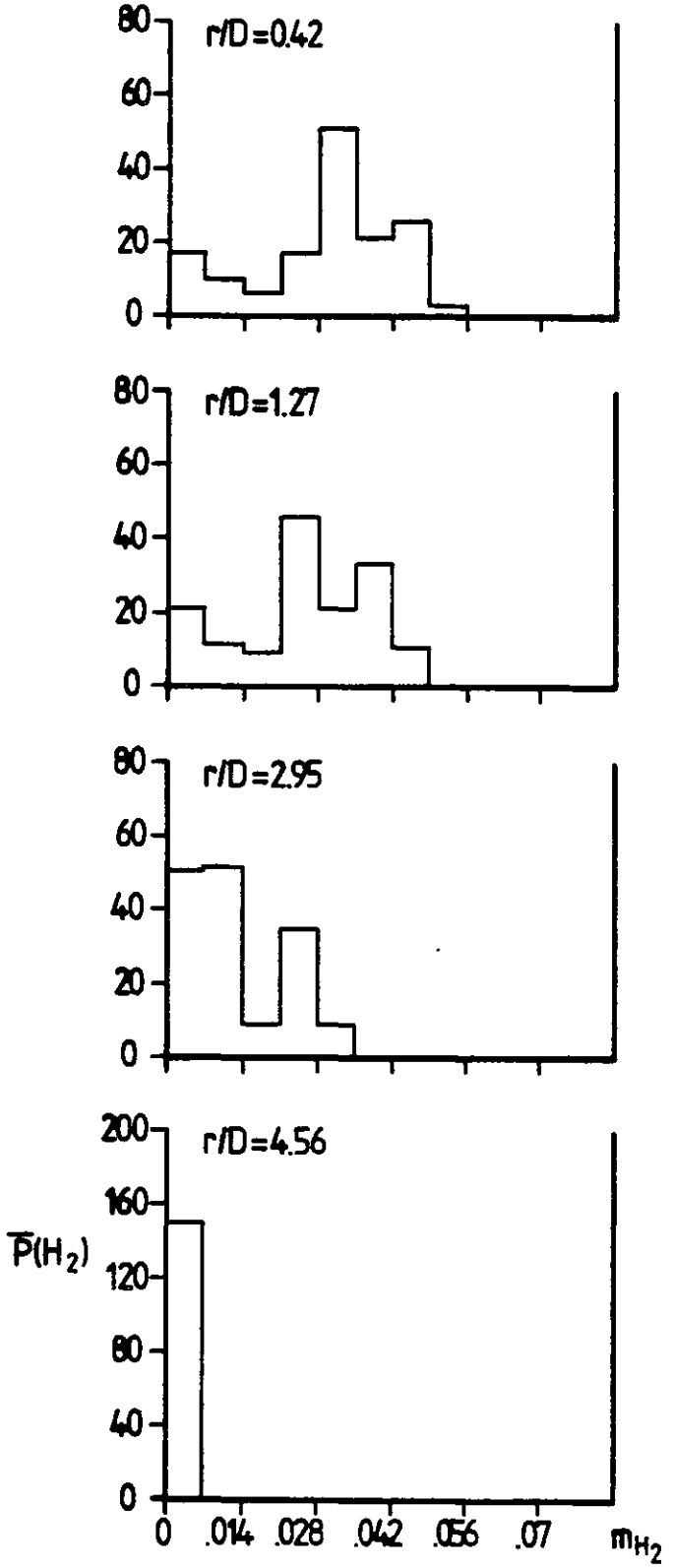

Fig.7.4-29 Probability density function of mass fraction of H_2 at X/D=80

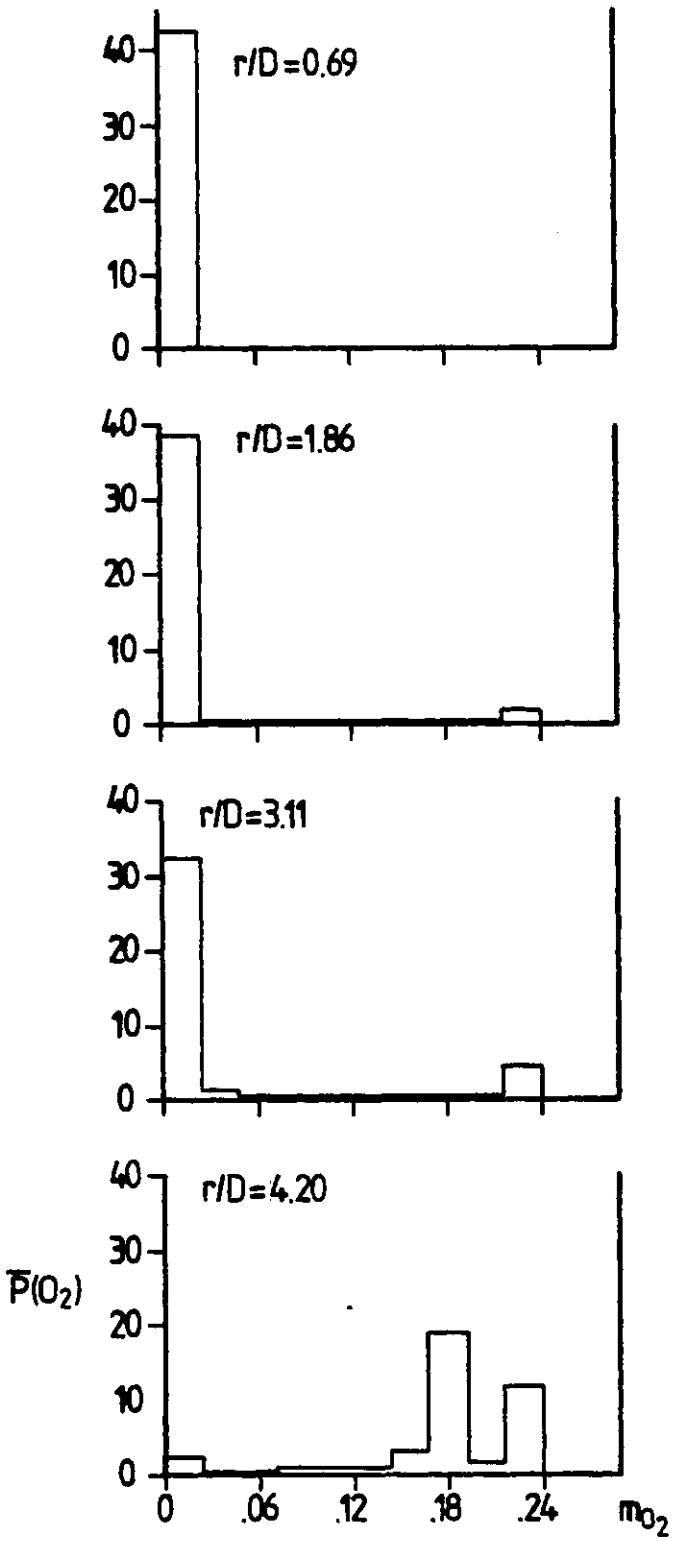

Fig.7.4-30 Probability density function of mass fraction of O_2 at X/D=40

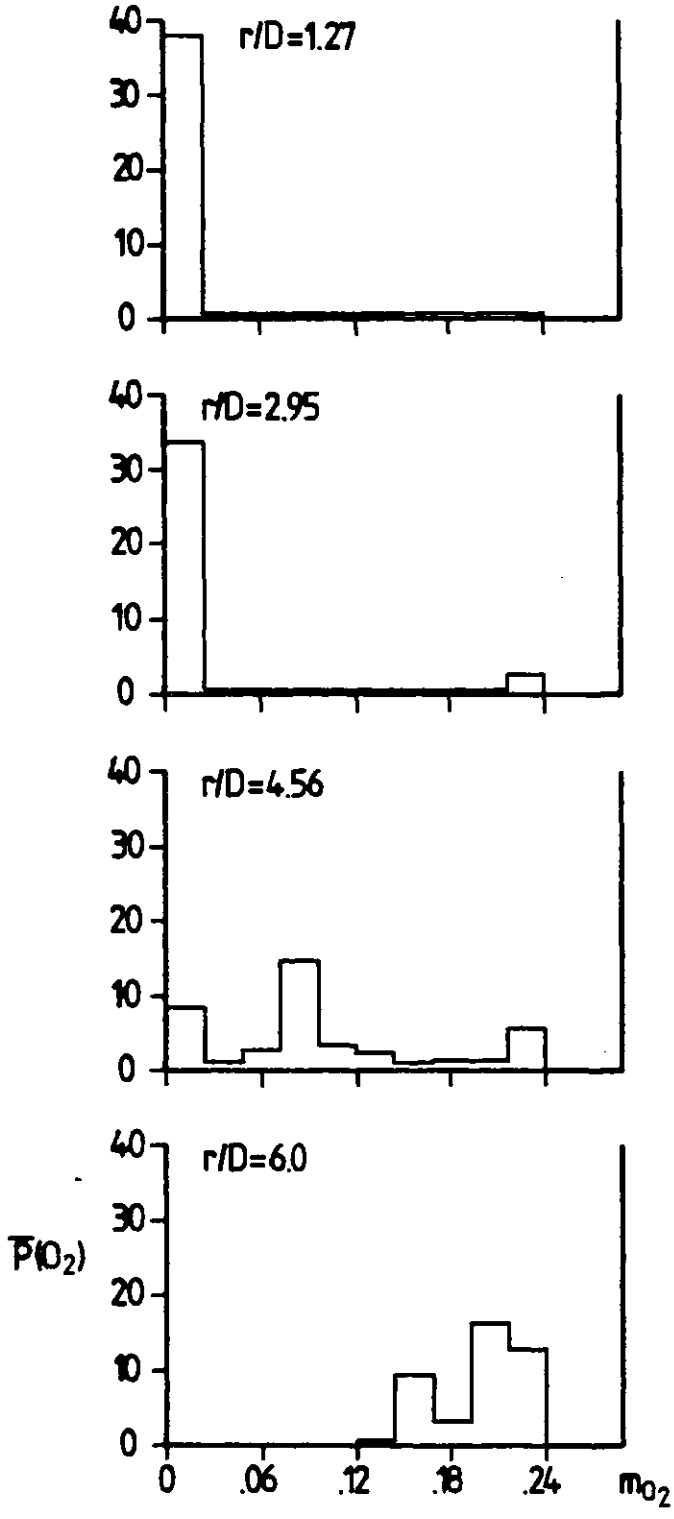

Fig.7.4-31 Probability density function of mass fraction of O_2 at X/D=80

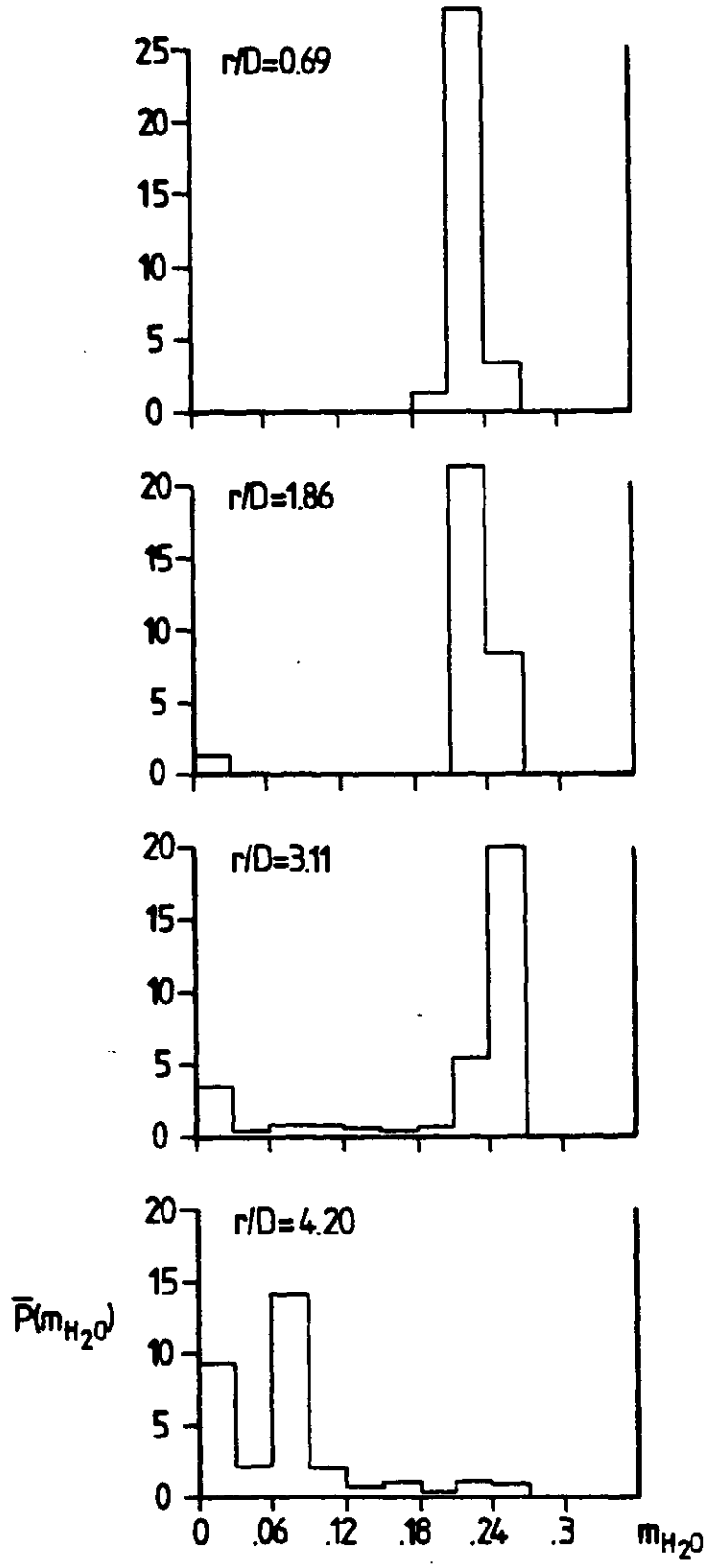

Fig.7.4-32 Probability density function of mass fraction of H_2O at X/D=40

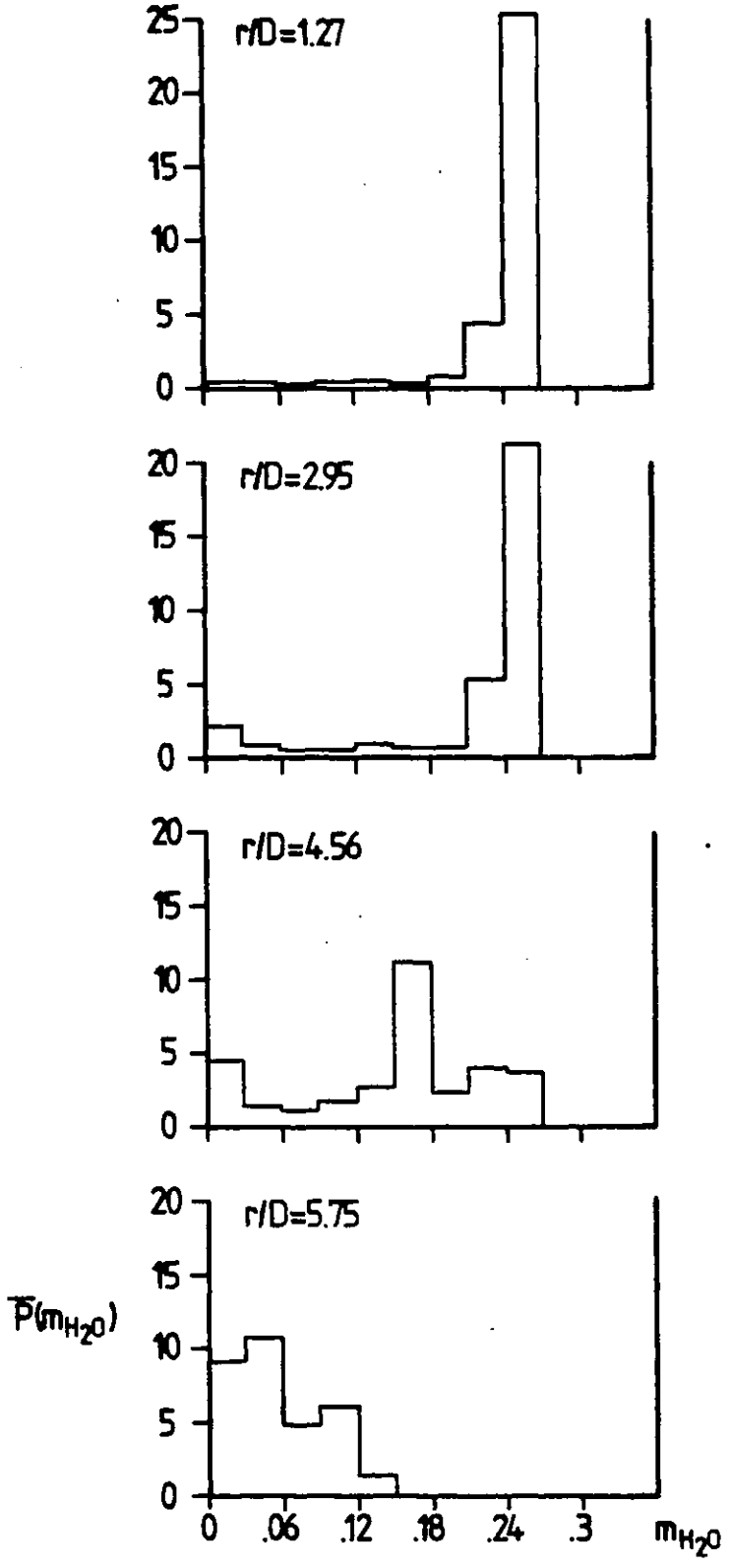

Fig.7.4-33 Probability density function of mass fraction of H_2O at X/D=80

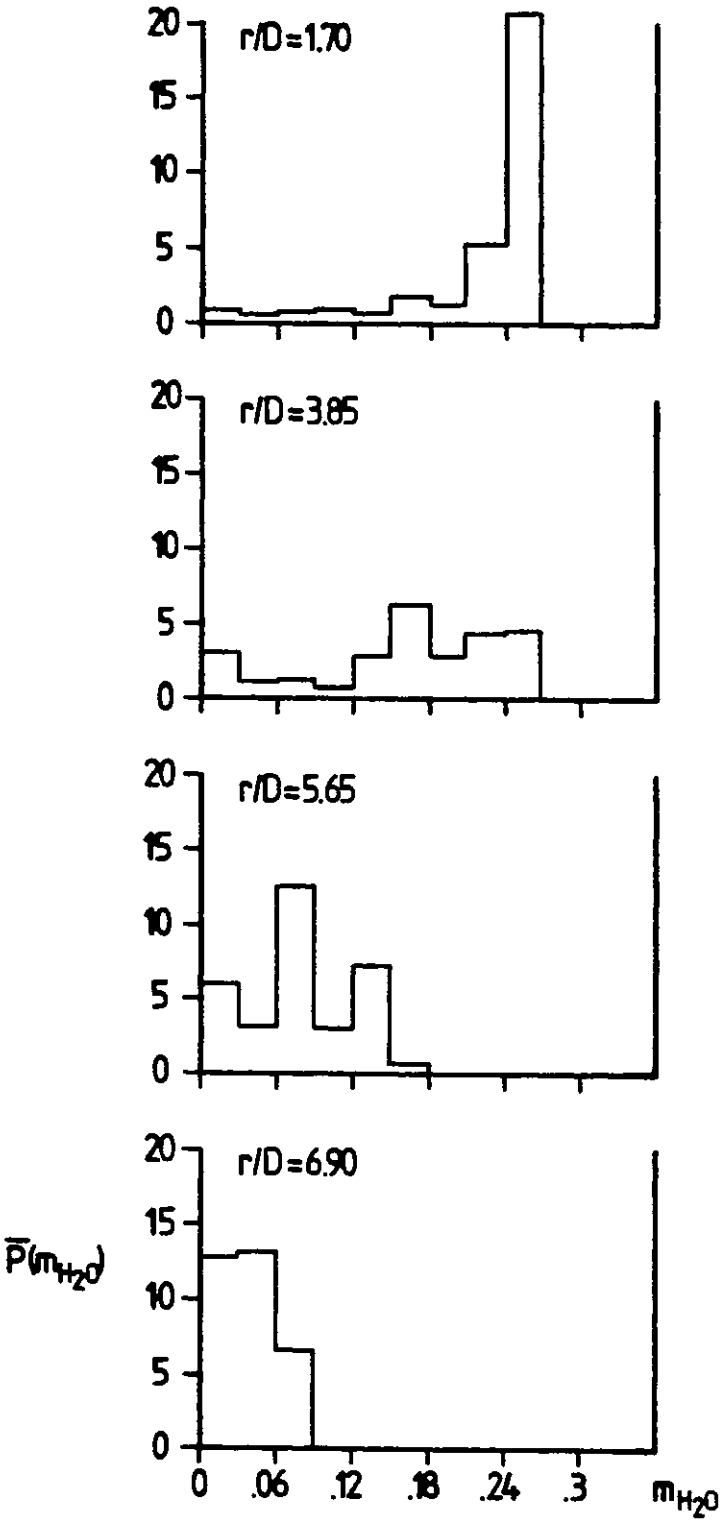

Fig.7.4-34 Probability density function of mass fraction of H_2O at X/D=120

that the mass fraction of H_2O diminishes gradually there.

7.5 Discussion of results

The population distribution of folds

It has been observed that the radial variation of $\tilde{P}\sim\tilde{A}$ distribution diminishes in the further downstream region of the jet, as revealed from Figs.7.4-3 to 7.4-5. The reason is that the velocity difference across the jet becomes smaller as X increases, which results in more uniform ageing rate (c.f. Eqn.3.7-15). Therefore, one can expect that the $\tilde{P}\sim\tilde{A}$ curve will be a function of longitudinal distance x only, if the velocity (and also density) is uniform in the cross-stream direction as in the case of plug flow reactor.

However, the shape of the $\tilde{P}\sim\tilde{A}$ curve is dependent on the hypothesis about the distribution of fold formation rate. The results obtained from the present chapter show a similar trend as those from the mixing layer calculation in chapter 6, since it is supposed that the fold formation rate is proportional to the gradient of local mean velocity. Actually, the population of the youngest folds will not be the most dominant one, at least in some points, when the fold formation rate is low in the central region of the jet. The influence of the formation rate on the $\tilde{P}\sim\tilde{A}$ profiles will be presented and discussed separately in the next chapter.

The turbulent mean quantities

From the results presented in the previous section,

several remarks can be made about the comparison between the predictions and measurements.

Firstly, the general trend in the variation of mean temperature and species concentration have been satisfactorily predicted based on the simple chemical reaction scheme. The discrepancy between the present computations and experimental data is almost the same as in the work of Janicka and Kollman (1979) where a multistep non-equilibrium reaction scheme was employed.

Secondly, the degree of coexistence of reactants (i.e., H_2 and O_2) is an important feature of turbulent diffusion flames and it is one of the purposes and contributions of the ESCIMO theory to predict this quantity. However, the amount of overlapping was found to be under-predicted here and hence attention has been paid to seek further improvements. Therefore, various values of the parameters, C_Z, C_F, C_S have been tested and larger overlapping obtained. The results produced from the parametric studies will appear in the next chapter.

Thirdly, the oxygen content was underestimated in the results of Sec.7.4 and it also happened to the theoretical calculations of Janicka and Kollman (1979). Since the Shvab-Zeldovich assumptions (in particular the assumption of equal molecular diffusivities for mass and energy) are adopted in both calculations, one may speculate that the preferential diffusion effect of hydrogen (high mobility of hydrogen molecules) is the cause of this disagreement.

The root mean square fluctuation quantities

The maximum temperature fluctuation in the jet centre line is around 450°K, as indicated by Fig.7.4-16. The fluctuation level is believed to be reasonable, although experimental data for this case are not available. The indirect supporting evidence of the statement is the measurements of Lenz and Günther (1980) in methane-air free jet diffusion flame where the maximum axial temperature fluctuation is about 400°K. It is well understood that the peak temperature in H_2-air flame is higher than the counterpart in CH_4-air flame (by 300°K~400°K) and hence the fluctuation temperature is expected to be larger for the former flame (under the same turbulence level).

The decay of temperature fluctuation between X/D of 40 and 80 has not yet been confirmed by experimental data, although the same feature ocurred in the theoretical results of Lockwood and Naguib (1975) for the town-gas flame and those of Kent and Bilger (1976) for the present case.

In the radial profiles of temperature fluctuation indicated by Fig.7.4-17, the peak value has reached 600°K~700°K . The value is also thought to be realistic, because the maximum value of 600°K in RMS fluctuation has been observed in the turbulent methane-air diffusion flames (c.f. Lenz and Günther (1980)).

The relative fluctuation intensities of hydrogen and oxygen concentration are greater than unity in the region where the mean values are small, as shown in Figs.7.4-18

to 7.4-20. The same phenomena were detected in the calculations of Becker (1975) for turbulent propane-air diffusion flames. In the concentration fluctuations obtained by Becker (1975), a finite amount of RMS value exists in the region where the mean quantity is equal to zero.

The probability density functions

It can be seen from the comparison between present predictions and the pdf deduced from Kennedy and Kent (1981), shown in Fig.7.4-25, that there is a stronger intermittency effect near the edge of the jet from the experimental observation. The influence of the free stream appears in the ESCIMO theory through the fold-composition at birth only, and it becomes less significant in the older folds because of molecular diffusion and fold stretching.

The shape of the pdf profiles is directly related to the fold size, stretching rate and population distribution of folds. Since all the results obtained in this chapter are based on a single set of parameters only, more parametric studies are necessary before drawing any final conclusion about the model. The presentation of parametric studies is to appear in chapter 8.

7.6 The turbulent methane-air diffusion flame

The systematic experimental investigation on the turbulent methane-air free jet diffusion flames have been performed during the last decade by Lenze and Günther (1975), Lenz and Günther (1980). The experimental burner was of a nozzle type with a diameter of 8mm. The velocity of fuel jet at the jet exit plane is equal to 70m/sec, corresponding to a Reynolds number of 3.7×10^4. The flame was stabilised with an annular oxygen supply of a few litres per hour. Lenz and Günther (1980) claimed that the oxygen from the annular supply can be neglected compared to the oxygen content of the entrained air, especially in the downstream region where most measurements were made. They believed that the oxygen affects only the flame root.

The experimental data include the axial and radial distribution of species concentration, the mean temperature distribution, the temperature fluctuation and the pdf of temperature at flame axis.

The measuring system of fluctuating temperature consisted of a thermocouple whose frequency response was determined at each measurement point and compensated with an electrical network. The signal from the RMS voltmeter was passed through a spectrum analyser and a pdf analyser to reveal any marked peaks in the spectrum and to determine the skewness and flatness of the pdf.

7.7 The computational aspects

The grid system

The grid distribution in the x, ω and $\tilde{A}$ coordinate are

the same as those described in Sec.7.3, except the definition of the transformation function $F\{x\}$. It is inadequate to assign the velocity of surrounding air, for the present case, $U_{air}(\approx 0)$, as the reference velocity. Alternatively, the reference velocity is given by:

$$U_{ref} = \frac{U_e}{3(1+0.01x/D)} \quad , \quad (7.7\text{-}1)$$

where U_e is the velocity of the jet at the nozzle exit.

The value of U_{ref} is now a function of x and it decays approximately at the same rate as the velocity at the centre line of the jet, U_c, viz:

$$U_{ref} \approx \frac{U_c}{3} \quad . \quad (7.7\text{-}2)$$

Therefore, $F\{x\}$ is now defined as:

$$F\{x\} \equiv \frac{U_e}{3x(1+0.01x/D)} \quad . \quad (7.7\text{-}3)$$

and $\frac{\partial F}{\partial x}$ is obtained by its first derivative as:

$$\frac{\partial F}{\partial x} = \frac{-U_e(1+0.02x/D)}{3[x(1+0.01x/D)]^2} \quad . \quad (7.7\text{-}4)$$

The input data

The fuel jet in the experimental conditions of Lenze and Günther's (1975) work is mainly composed of methane and nitrogen, with small amount of other hydrocarbon fuels. The volumetric composition of the fuel jet is reproduced here for the sake of clarification:

Species	Volumetric fraction %
CH_4	81.3
C_2H_6	2.85
C_3H_8	0.60
CO_2	0.90
N_2	14.35
O_2	0.01

Table 7.7-1 Composition of the natural gas

Some simplifications have however been made in the numerical predictions, i.e., the fuel jet is treated as composed of CH_4 and N_2 only. Since the species conservation equation is based on the mass fraction instead of the volume (or molar) fraction, the following mass fraction of methane and nitrogen have been used as the initial conditions at the jet exit:

$$m_{CH_4,e} = 0.713 \quad , \quad (7.7\text{-}5)$$

$$m_{N_2,e} = 0.287 \quad . \quad (7.7\text{-}6)$$

The errors introduced by this approximation is believed to be of the same order as those of the simple chemical reaction scheme.

The thermodynamics properties

The specific heat, Cp, of each species is again calculated according to Eqn.(4.4-8) and the coefficients given by Table 4.4-1. The species considered in this case

include CH_4, O_2, N_2, H_2O and CO_2, the intermediate species of the chemical reaction (e.g., H_2 and CO) being neglected.

The products of the chemical reaction are assumed to consist of water vapour and carbon dioxide only and the amount of each species is determined by:

$$m_{H_2O} = 0.45\ m_{pr} \quad , (7.7\text{-}7)$$

$$m_{CO_2} = 0.55\ m_{pr} \quad , (7.7\text{-}8)$$

since the following one-step reaction scheme is assumed:

$$CH_4 + 2O_2 + 7.52N_2 \rightarrow CO_2 + 2H_2O + 7.52N_2 \quad , (7.7\text{-}9)$$

where m_{H_2O} and m_{CO_2} represent the mass fraction of H_2O and CO_2 respectively.

The heat of combustion for methane is taken as equal to 5×10^7J/Kg in the computation, according to the data from Perry and Chilton (1973).

7.8 Presentation of results

7.8.1 The hydrodynamic results

The axial distribution of mean velocity, $\overline{U}_c$, is presented in Fig.7.8-1 together with the measurements obtained by Wittmer (1980) with the Laser-anemometry. It can be seen that the mean velocity is well predicted until X/D=40, while the rate of decay is overpredicted afterwards.

Fig.7.8-2 shows the turbulent kinetic energy and the velocity fluctuations for the same flame. It is not possible to calculate the axial velocity fluctuation and radial velocity fluctuation separately from the present k-ε model,

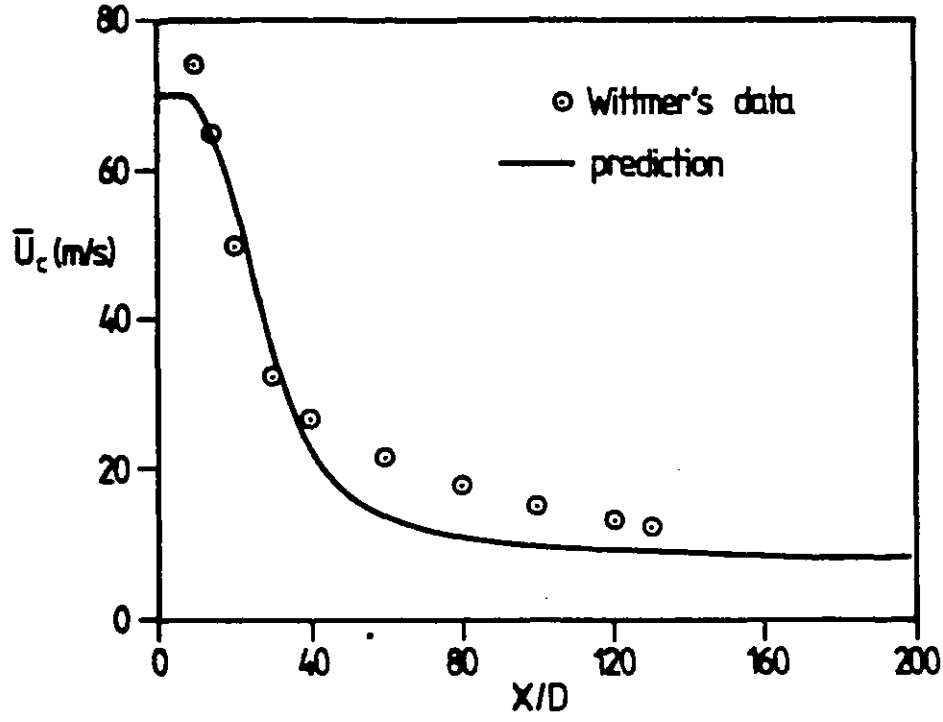

Fig.7.8-1 Variation of axial-velocity in the methane-air flame

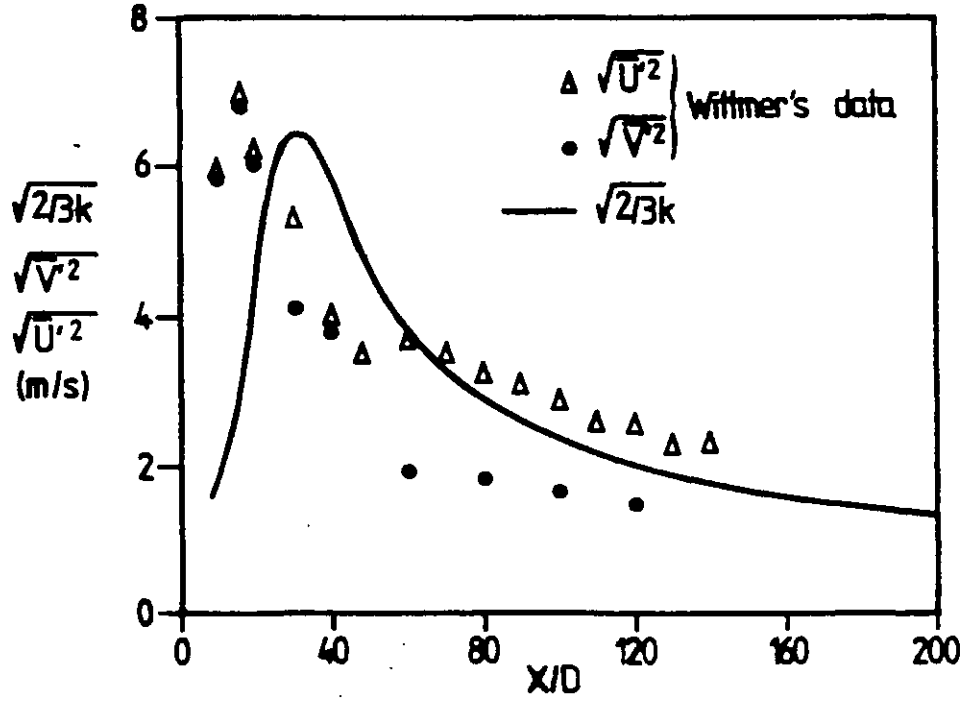

Fig.7.8-2 Variation of axial turbulence-intensities in methane-air flame

therefore it is assumed that the turbulence is isotropic and the "equivalent velocity fluctuation", $\sqrt{2/3k}$, is now compared with the measured values of $\sqrt{\overline{u'^2}}$ and $\sqrt{\overline{v'^2}}$.

The main discrepancies between the predictions and the experimental data exist in the region of $0 < X/D < 60$, where the predicted location of peak fluctuation is situated further downstream ($X/D \simeq 30$) to the position found by Wittmer (at $X/D \simeq 16$). Nevertheless, the maximum fluctuation level is only slightly underpredicted by the turbulence model The value of $\sqrt{2/3k}$ is lying between the $\sqrt{\overline{u'^2}}$ and $\sqrt{\overline{v'^2}}$ for X/D ratios greater than 80, i.e., in the fully developed region of the jet.

7.8.2 <u>The population distribution of folds</u>

Figures 7.8-3, 4 and 5 present the population distribution with respect to age, at three different X/D values, for the methane-air diffusion flame. In Fig.7.8-3, the $\tilde{P}$~$\tilde{A}$ distributions obtained at three radial locations, for X/D=40, are denoted by separate curves. It can be observed that the population distributions at r/D=2.4 and 5.3 are close to the exponential decay function, while the result at r/D=0.2 (near the jet axis) behaves in a different way. This feature is the consequence of the distribution of fold formation rate and the local mean velocity. The fold formation rate is assumed to vary with the gradient of mean velocity ($\overline{U}$) and hence it reaches the maximum value near the mid-point between the jet axis and outer boundary. The larger is the fold formation rate, the more popular are the youngest folds. The influence of the mean velocity itself mainly

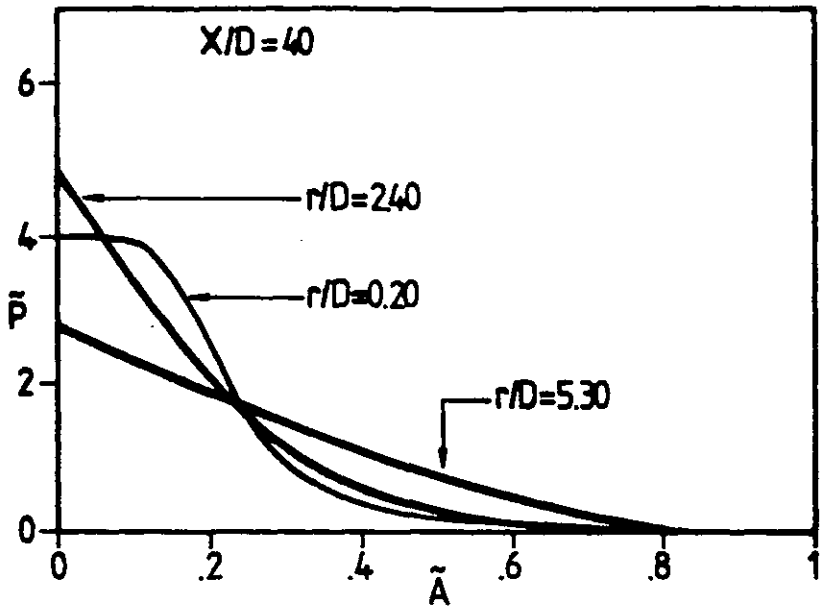

Fig.7.8-3 Population distribution function at various positions in the jet region

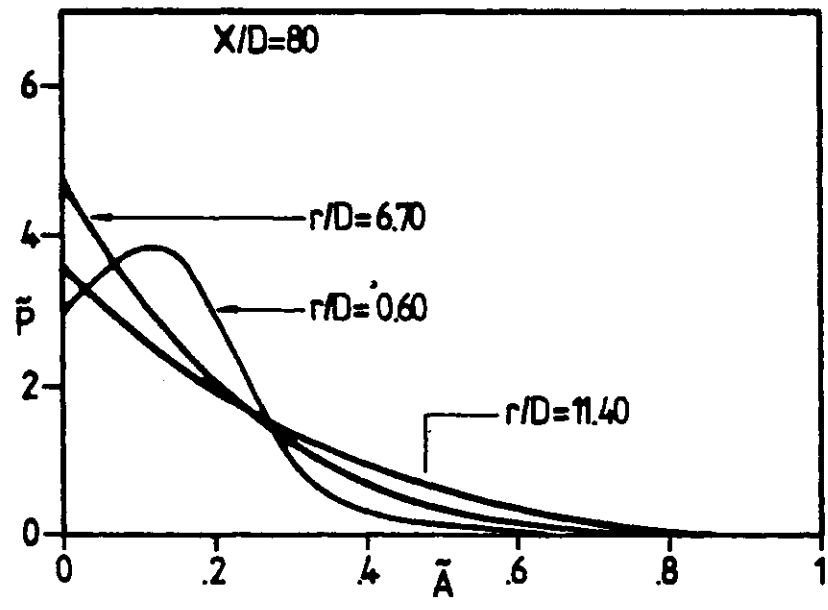

Fig.7.8-4 Population distribution function at various positions in the jet region

appears in the aging term (see Eqn.3.4-24) and the latter quantity is larger when the mean velocity diminishes. Therefore, the steepest curve at r/D=2.4 is caused by the large formation rate and moderate aging effect, while the distinctive curve at r/D=0.2 is the result of relatively small formation rate and aging effect.

The results demonstrated in Fig.7.8-4 are obtained at X/D=80, again at three different radial locations. Now the peak value of $\tilde{P}\sim\tilde{A}$ distribution is located at $\tilde{A}\simeq 0.12$, for r/D=0.6. Similar features are also detected in the results from X/D=120 which are shown in Fig.7.8-5.

The radial variation of folds-population is shown in Figs.7.8-6, 7 and 8 for X/D values of 40, 80 and 120 respectively. It is evident in Fig.7.8-6, that the highest population of youngest folds ($\tilde{P}_1$) appears around r/D=2, where the fold formation rate is large. On the other hand, the value of $\tilde{P}_3$ (for folds having $\tilde{A}$ value between 0.1 and 0.15) has its maximum at the jet-axis and decreases monotonically towards the outer edge. The variation of $\tilde{P}_5$ (for $\tilde{A}$ value varying between 0.2 and 0.25) is very small across the jet and $\tilde{P}_9$ (for $\tilde{A}$ value lying between 0.4 and 0.45) increases with the radial distance from the axis. The results obtained at X/D=80 and 120 are similar to those in Fig.7.8-6, apart from the fact that the profiles have spreaded in radial direction.

The radial distribution of "average age", for three X/D values, are plotted in Fig.7.8-9. The average age is larger in the outer region of the jet where the mean velocity is

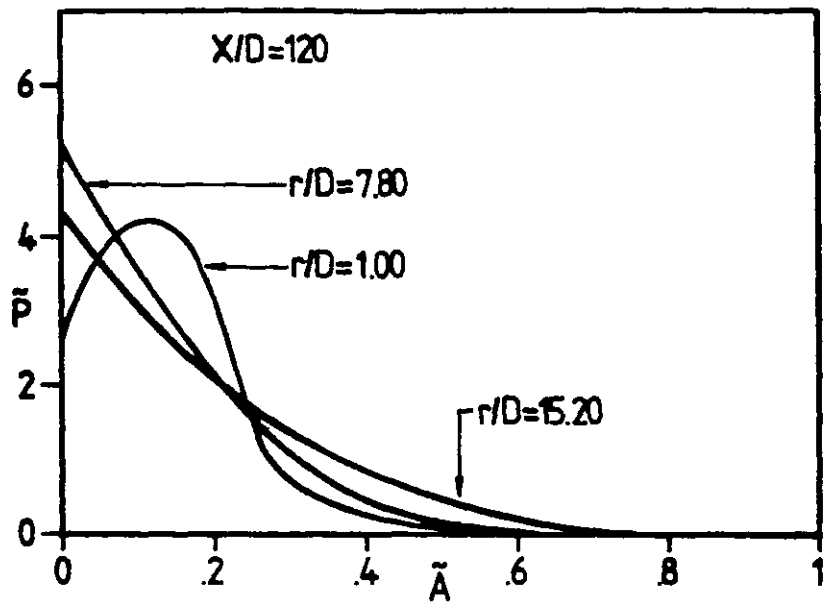

Fig.7.8-5 Population distribution function at various positions in the jet region

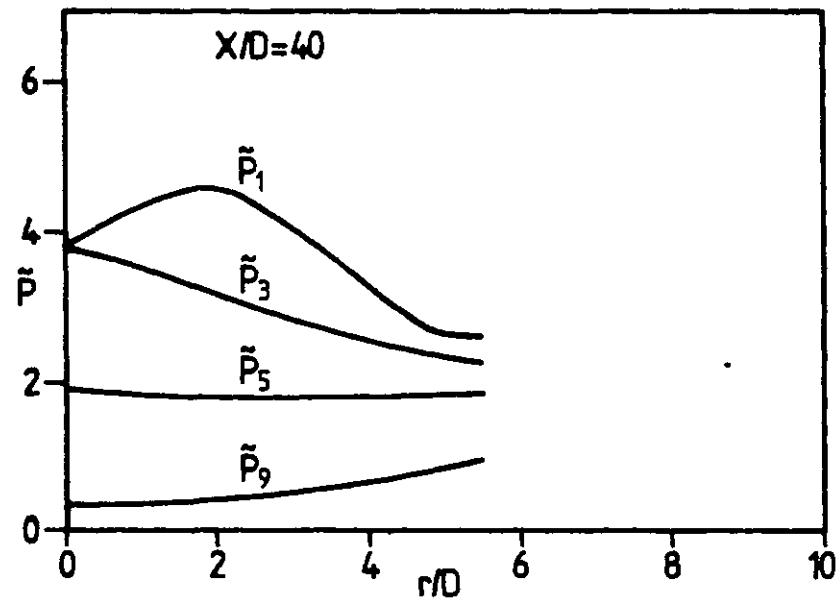

Fig.7.8-6 Radial variation of population of folds belonging to a particular age interval

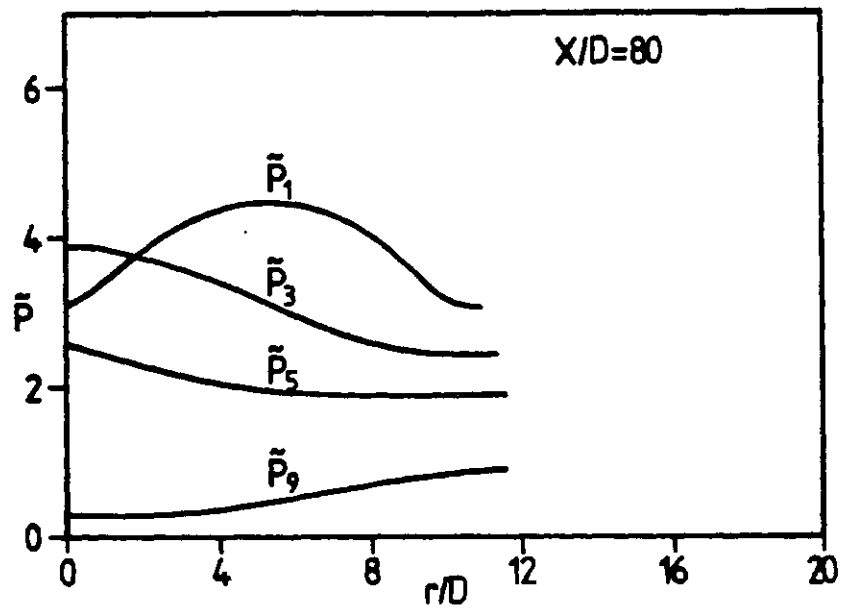

Fig.7.8-7 Radial variation of population of folds belonging to a particular age-interval

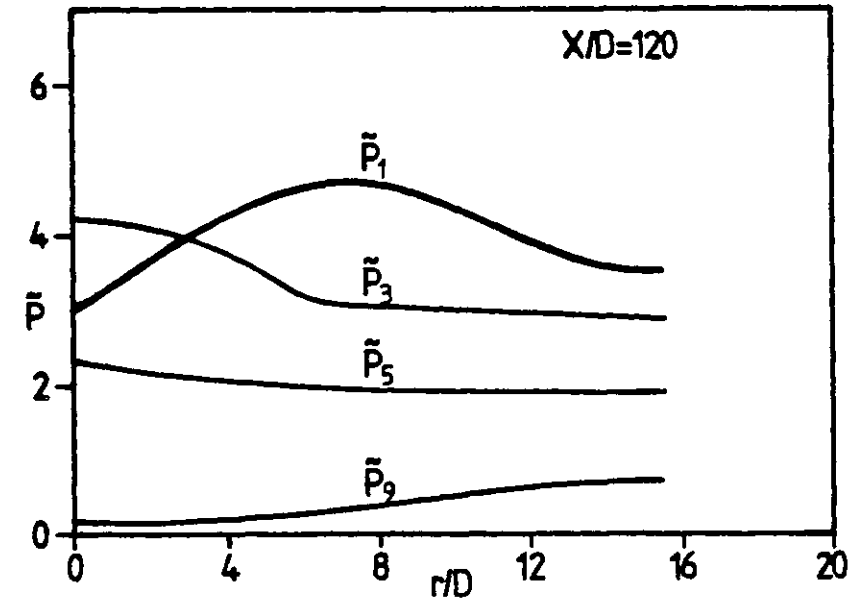

Fig.7.8-8 Radial variation of population of folds belonging to a particular age-interval

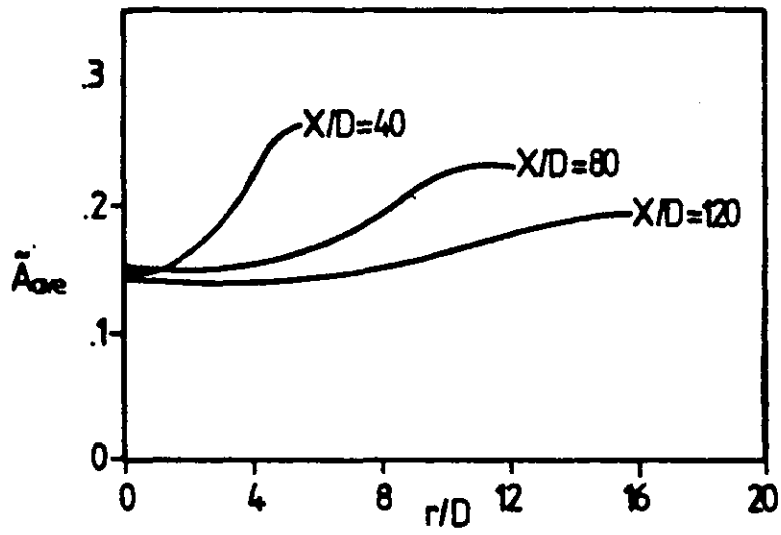

Fig.7.8-9 Radial profiles of average age

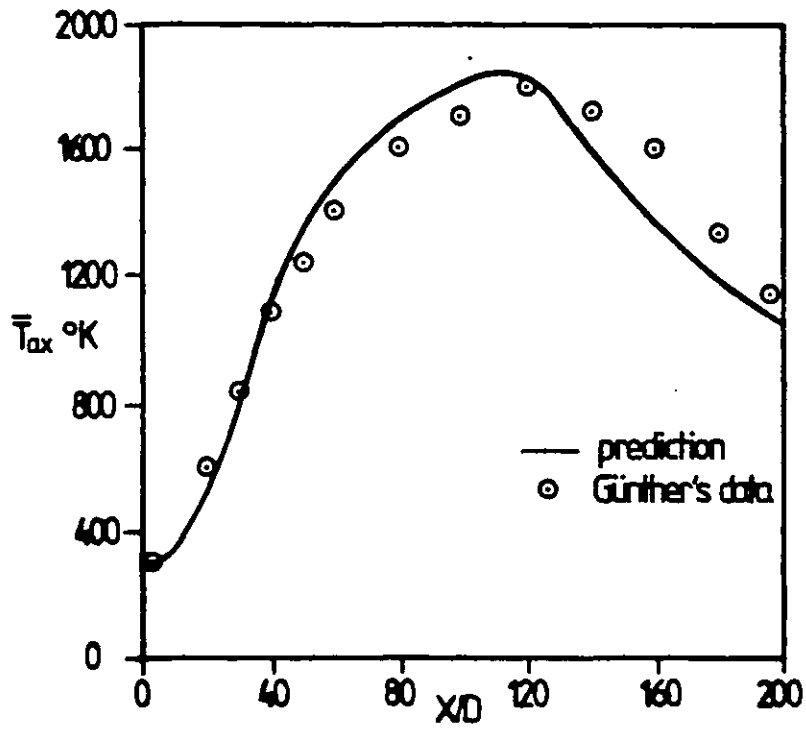

Fig.7.8-10 Axial distribution of mean temperature

slower. The difference in the average age diminishes as the value of X/D increases, since the velocity gradient is smaller in the further downstream region of the jet.

7.8.3 The mean temperature and species concentration

The distribution of mean axial temperature along the jet centre-line is plotted in Fig.7.8-10 together with the experimental data of Lenz and Günther (1980). It can be noticed that the axial temperature is slightly over-predicted from X/D=40 until X/D=120 and underpredicted afterwards. The calculated maximum temperature is equal to 1840°K, which is close to the measured value of 1800°K. The computed location of the peak value is equal to 112 diameters from the nozzle exit, while the measurements show that it is situated at X/D=120.

The axial variation of species concentration is shown in Fig.7.8-11 with the experimental results from Lenz and Günther (1975). The concentration of CH_4 is overpredicted in the region of $10 \leq X/D \leq 40$, while the agreement is satisfactory from X/D=60 to X/D=120. The concentration of H_2O has been well predicted from X/D=20 to X/D=100, but some discrepancies occur between X/D=120 and X/D=160. The amount of CO_2 is generally overestimated in the present calculation, since the existence of CO and H_2 have been ignored. The experimental data revealed that the mole fraction of CO and H_2 along the flame axis vary between 0.02 and 0.065, indicating that the influence of these species is just enough to cause the discrepancies between the predictions and measurements.

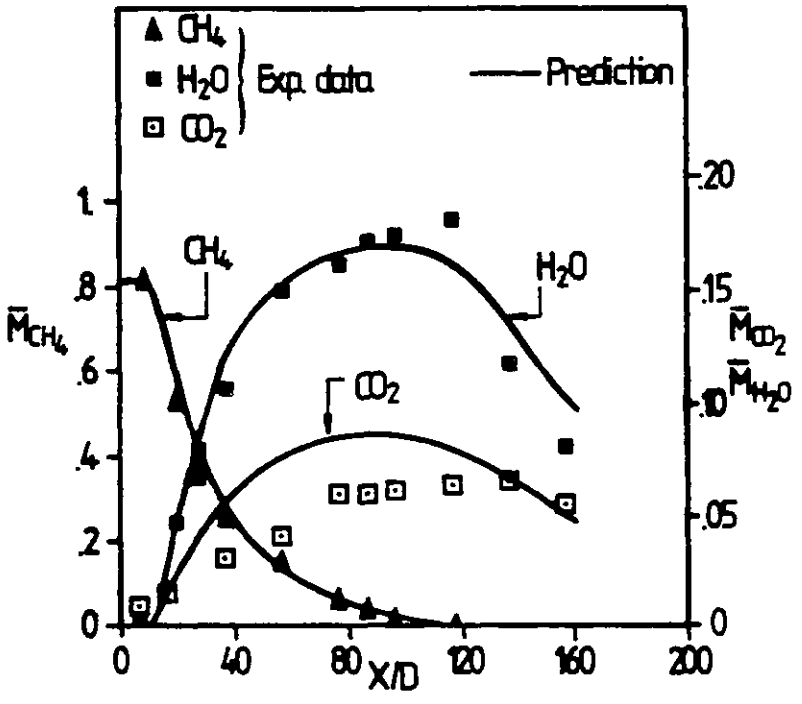

Fig.7.8-11 The axial variation of mean compositions in methane-air flame

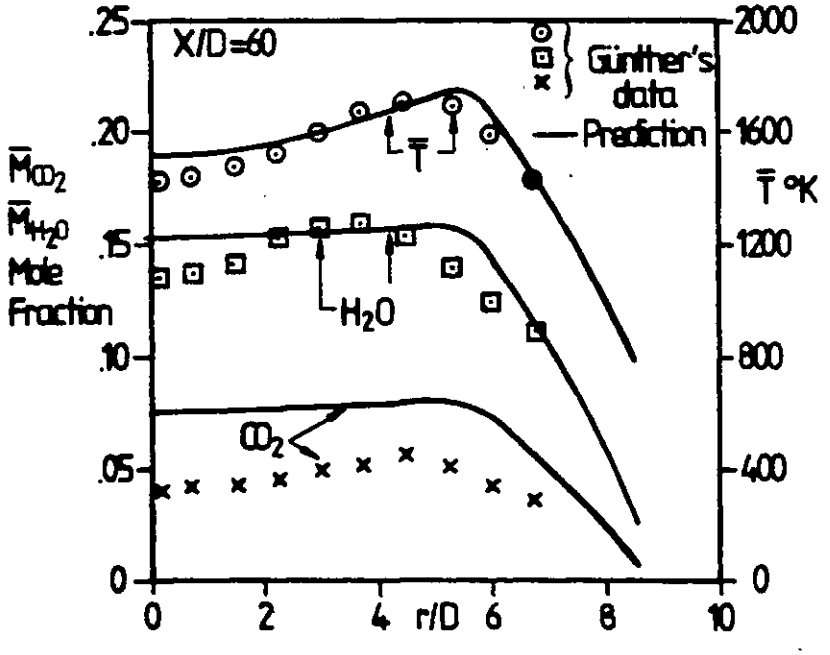

Fig.7.8-12 The radial variation of mean temperature and products concentration

The radial profiles of mean temperature, H_2O and CO_2 concentration, at X/D=60, are demonstrated in Fig.7.8-12. The quantitative agreement between the calculated and measured temperature is satisfactory. The flame front (denoted by the position of the highest temperature) appeared at r/D=5.5 in the predictions, but the measurements show the corresponding value is equal to 4.5 only. The concentration of H_2O is overpredicted in the regions of $0 \leq r/D \leq 2$ and $5 \leq r/D \leq 6.5$, while the content of CO_2 is everywhere overpredicted. Lenz and Günther's measurements have confirmed that the volume fraction of CO gas can reach the value of 0.045 at this station.

Similarly, the correspondent results at X/D=90 are presented in Fig.7.8-13. The mean temperature is well predicted according to the measurements available (the data for r/D greater than 6.5 have not been provided). The calculated H_2O concentration is now lower than the experimental values, but the amount of CO_2 is still overpredicted by 2~3% in volume fraction across the flame zone. It should be noted that the CO concentration is equal to 0.05 near the axis and gradually diminishes towards the outer edge of the flame, according to Lenz and Gunther's results.

Also, the predictions made at X/D=120 are demonstrated in Fig.7.8-14. No experimental data has been found for this cross-section and hence only qualitative assessment can be done. The temperature and concentration of main products achieve the maximum values at the jet centre-line, signifying that the flame tip is now located at the axis.

The radial profiles of methane and oxygen concentration, at X/D=60, are plotted separately in Fig.7.8-15, since the

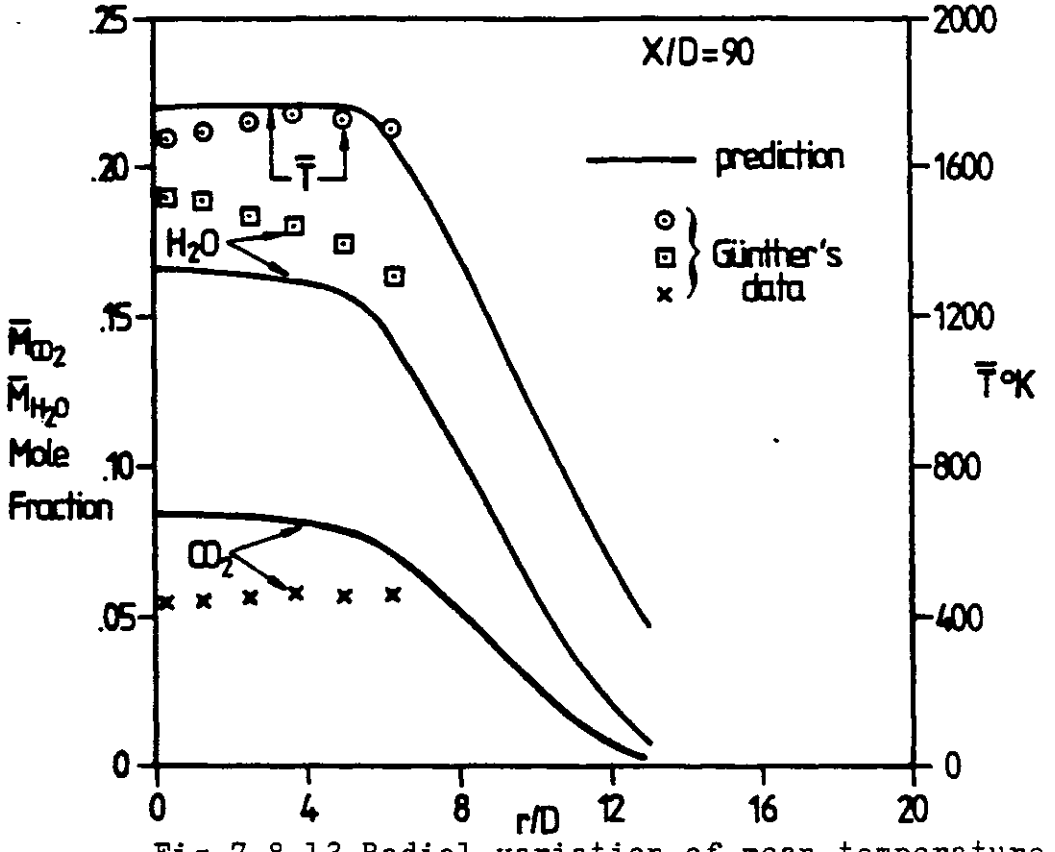

Fig.7.8-13 Radial variation of mean temperature and products

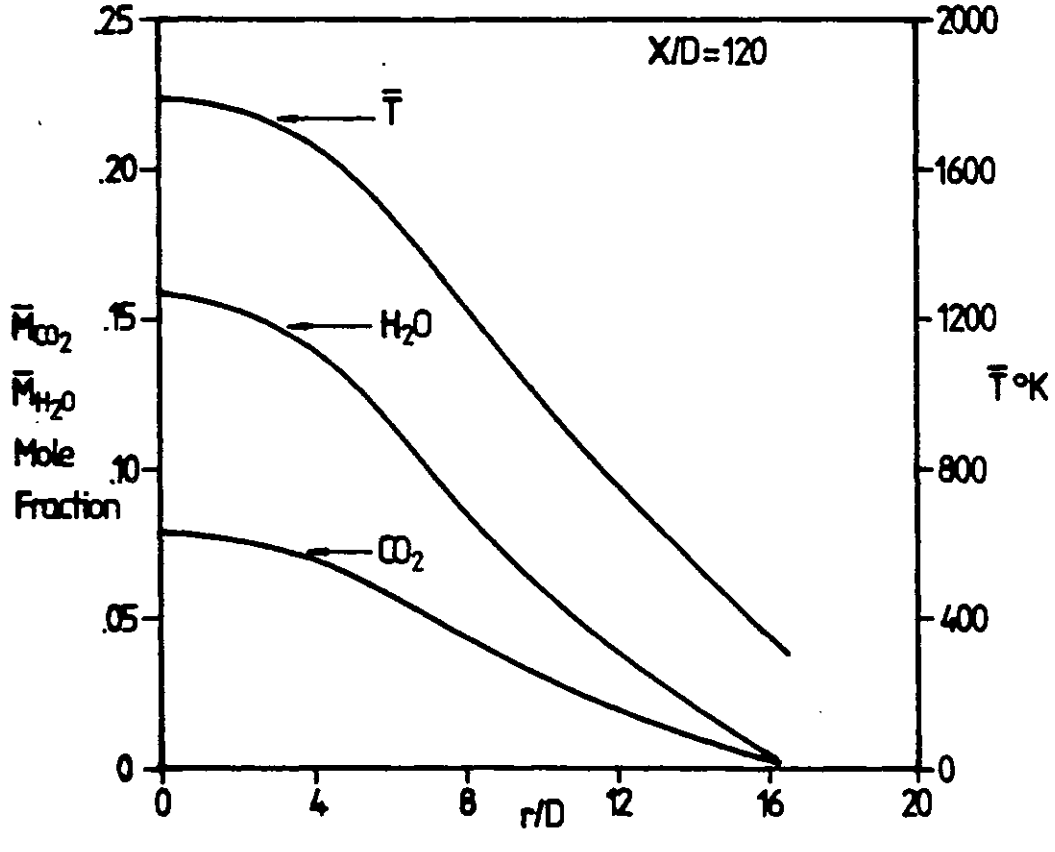

Fig.7.8-14 Radial variation of mean temperature and products

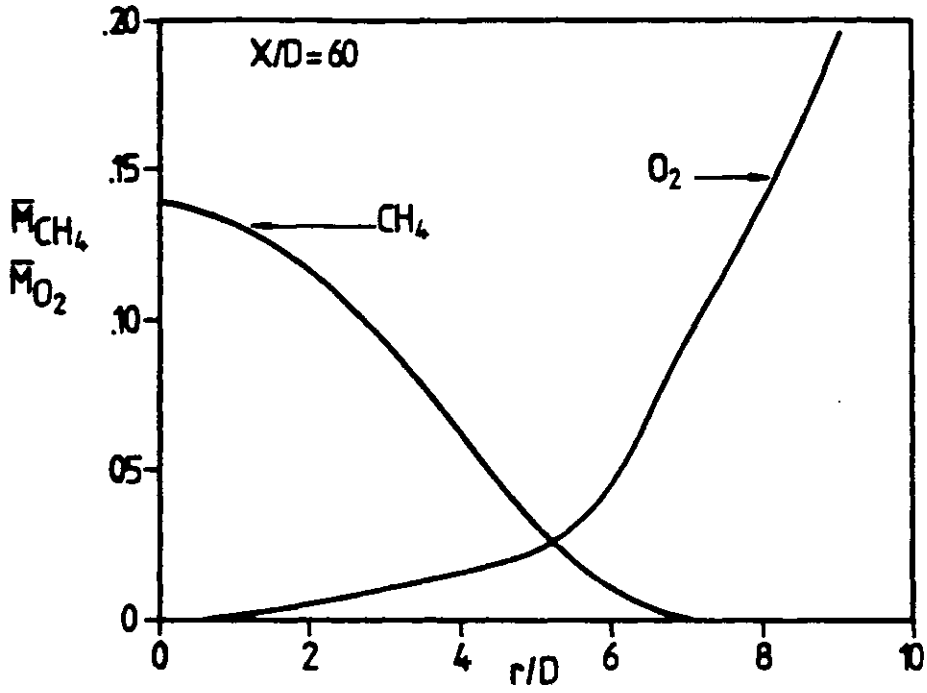

Fig.7.8-15 Radial profile of methane and oxygen concentration

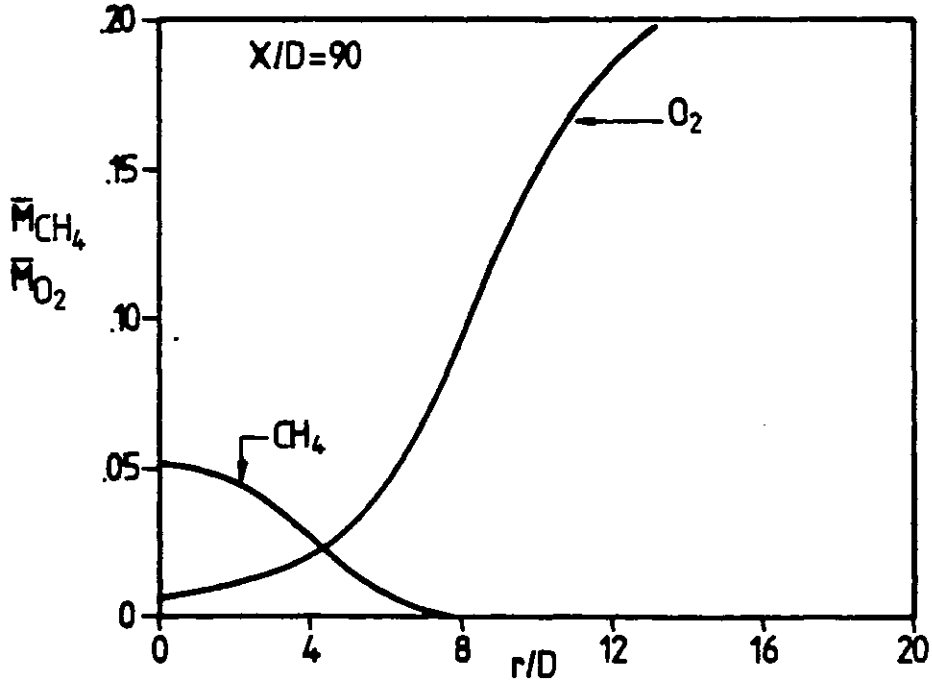

Fig.7.8-16 Radial profile of methane and oxygen concentration

overlapping feature of fuel and oxygen deserves more attention. It can be observed that the amount of reactants at the intersection points of two curves is equal to 0.025.

Finally, the radial variation of reactants concentration obtained at X/D=90 are provided in Fig.7.8-16. The degree of the cross-over of two curves is almost the same as that in the previous figure.

7.8.4 The root mean square fluctuation of temperature

The axial distribution of temperature fluctuation (the rms values) is shown in Fig.7.8-17 with the data of Lenz and Günther (1980). The predicted curve reveals a peak value of 400°K at X/D=160, which is consistent with the measurements. The predictions follow the same trend of the experimental observations for X/D values larger than 80. The decay of fluctuation level between X/D=20 and X/D=40 in the measurements has not been demonstrated by present calculations. On the other hand, there is a slight double hump between x/D=50 and X/D=80 in the computed curve.

The radial distribution of temperature fluctuation, at X/D=60, is provided in Fig.7.8-18 with the measured data. The maximum fluctuation intensity occurs at the outer region of the jet (outside the main reaction zone) and achieves the value of 600°K which is slightly higher than the predicted one (≈560°K). However, the present predictions overestimate the fluctuation intensities for r/D smaller than 5, while the rate of decay becomes faster in the region of r/D greater than 7.

The calculated temperature fluctuations at X/D=90 and

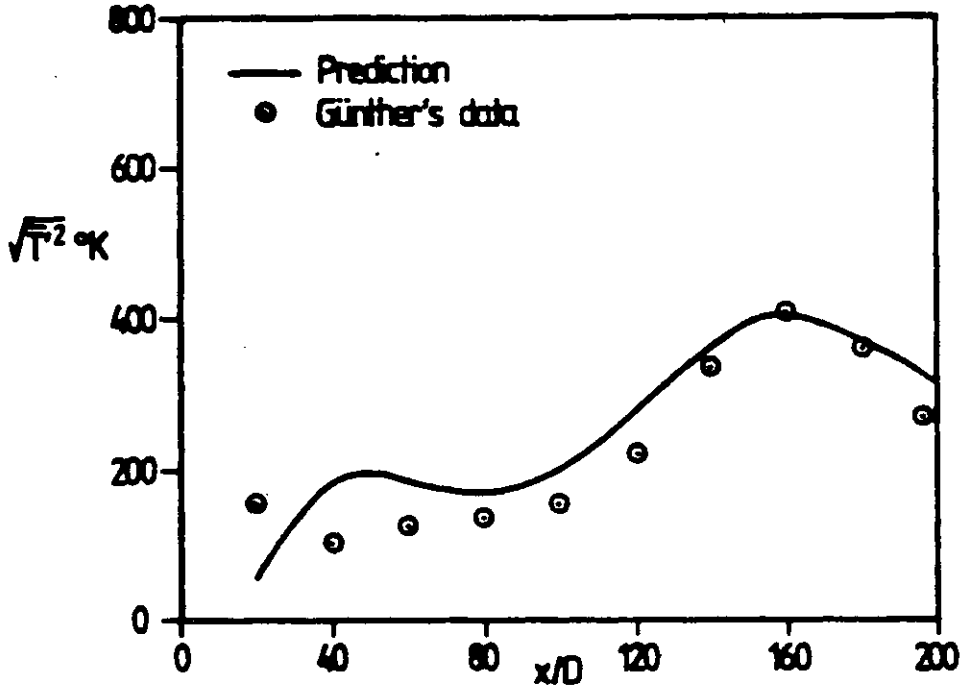

Fig.7.8-17 Axial distribution of rms temperature fluctuation

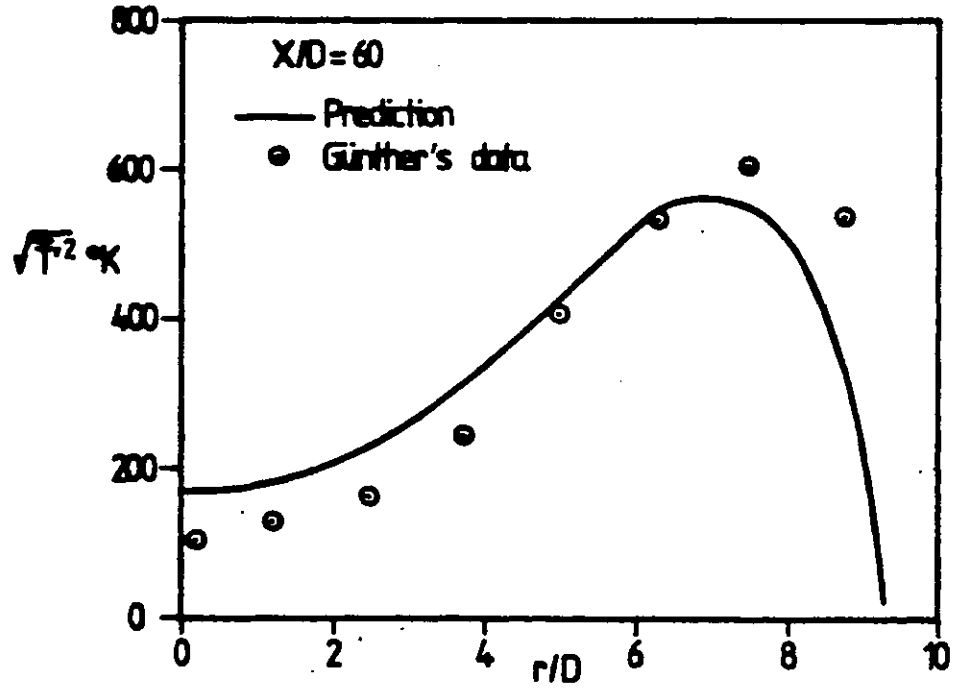

Fig.7.8-18 Radial distribution of rms temperature fluctuation

X/D=120 are shown in Fig.7.8-19. Inspection of the graph reveals that the highest fluctuation quantities nearly remain constant in the downstream region of the flow. However, the radial profile becomes more uniform and broadens as the value of x increases.

7.8.5 The root mean square fluctuation of species concentration

The RMS fluctuations of methane and oxygen concentration, at X/D=60, 90 and 120 respectively, are presented in Figs.7.8-20 to 7.8-22. The concentration fluctuation of methane reaches the maximum value of 0.047 at r/D=1.5, in Fig.7.8-20, while the highest fluctuation of oxygen occurs at r/D=5.6, which is inside the main reaction zone. It can be seen that the relative fluctuation intensities of oxygen are greater than unity from the axis up to r/D=6.3.

The location of highest concentration fluctuation in methane is situated at the flame axis, in Fig.7.8-21, indicating that the axial fluctuation intensities become larger now. However, the maximum fluctuation of oxygen still takes place around r/D=7.0.

In Fig.7.8-22, the fluctuation level of methane concentration is lower as a consequence of smaller mean value. Larger fluctuation value is observed on the axis for the oxygen species and the peak value (at r/D≈5) is now around 0.0425.

7.8.6 The probability density functions of temperature

The probability density functions of temperature at flame axis, for X/D values of 40, 110, 120 and 130, are

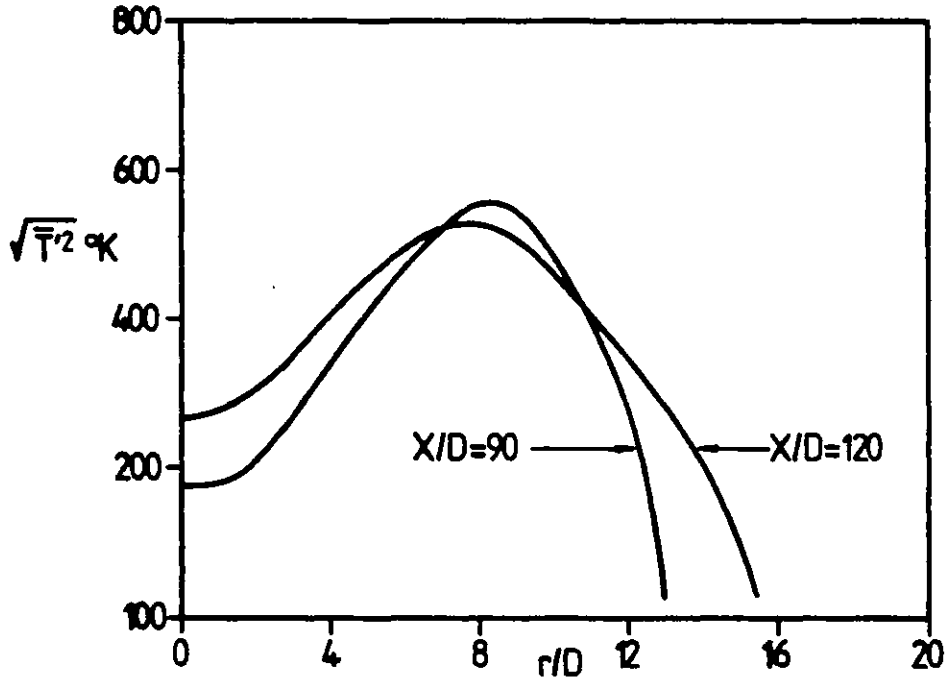

Fig.7.8-19 Radiál distribution of rms temperature fluctuation

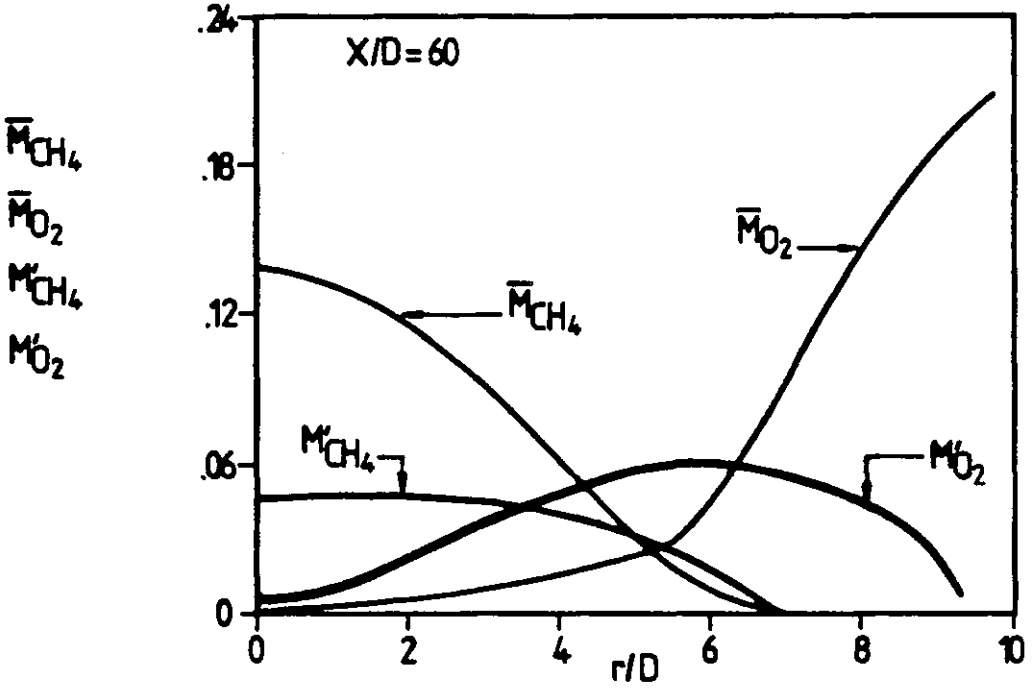

Fig.7.8-20 Concentration fluctuation of methane and oxygen

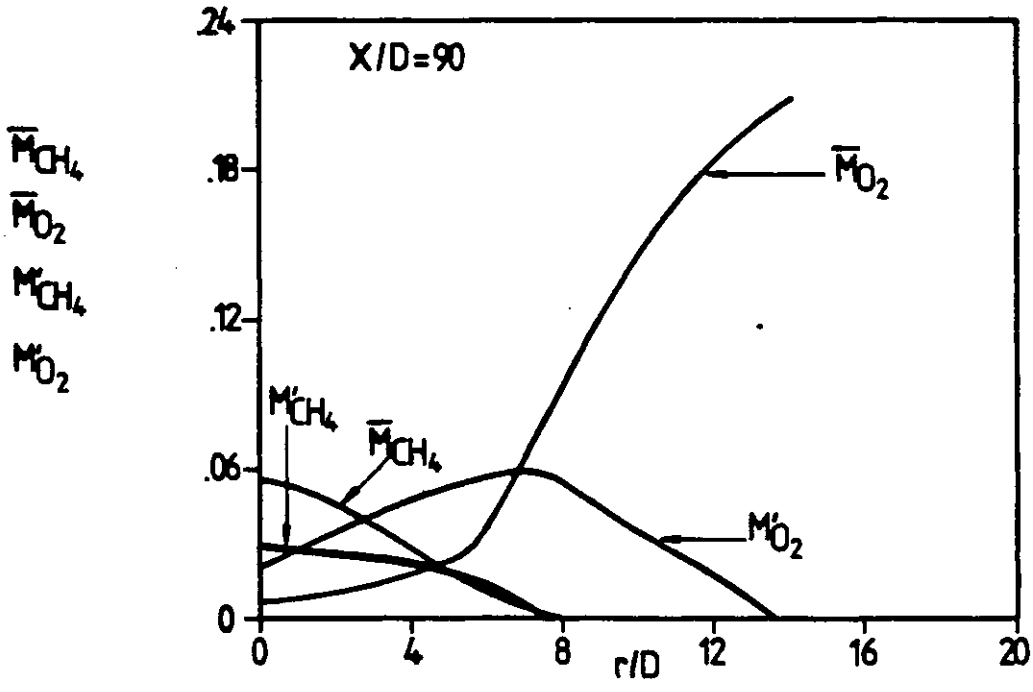

Fig.7.8-21 Concentration fluctuation of methane and oxygen

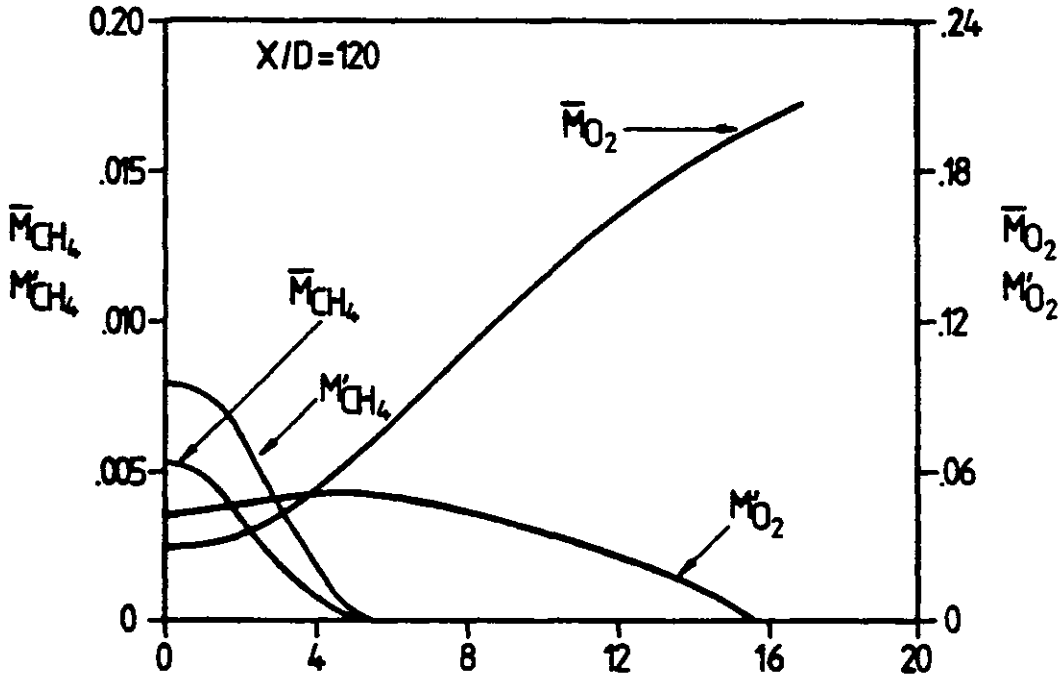

Fig.7.8-22 Concentration fluctuation of methane and oxygen

shown in Fig.7.8-23. The experimental results of Lenz and Günther (1980) are also presented (by the broken lines) for comparison. The predictions show that the pdf profiles shift with the value of mean temperature at different positions. There is no contribution of the low temperature gases ($300^{\circ}K<T<800^{\circ}K$) being observed in the present calculation.

The radial evolution of pdf profiles at X/D=40 is plotted in Fig.7.8-24. Obviously, the pdfs are not Gaussian and there is a finite amount of cold air existing in the outer edge of the jet, e.g., at r/D=2.38 and 4.66. The peak value of the distribution curve corresponds to the mean temperature at the point in question.

The similar results for X/D=110 are presented in Fig. 7.8-25 where the amount of cold air becomes more significant near the outer boundary of the jet, i.e., at r/D=14.0. Further results obtained at X/D=120 and 130 are demonstrated by Figs.7.8-26 and 7.8-27 respectively.

7.8.7 The probability density functions of species concentration

The radial evolution of pdf profiles for the mass fraction of fuel, at X/D=40 and 60, are presented in Figs.7.8-28 and 7.8-29 respectively. It can be seen in the diagrams of Fig.7.8-28 that the mass fraction of fuel decreases as the value of r/D increases. The pdf profile is broad in the centre of the jet and becomes narrow near the edge where the amount of fuel is almost exhausted. Similar phenomena are observed in Fig.7.8-29, apart from the fact that smaller fuel contents are present.

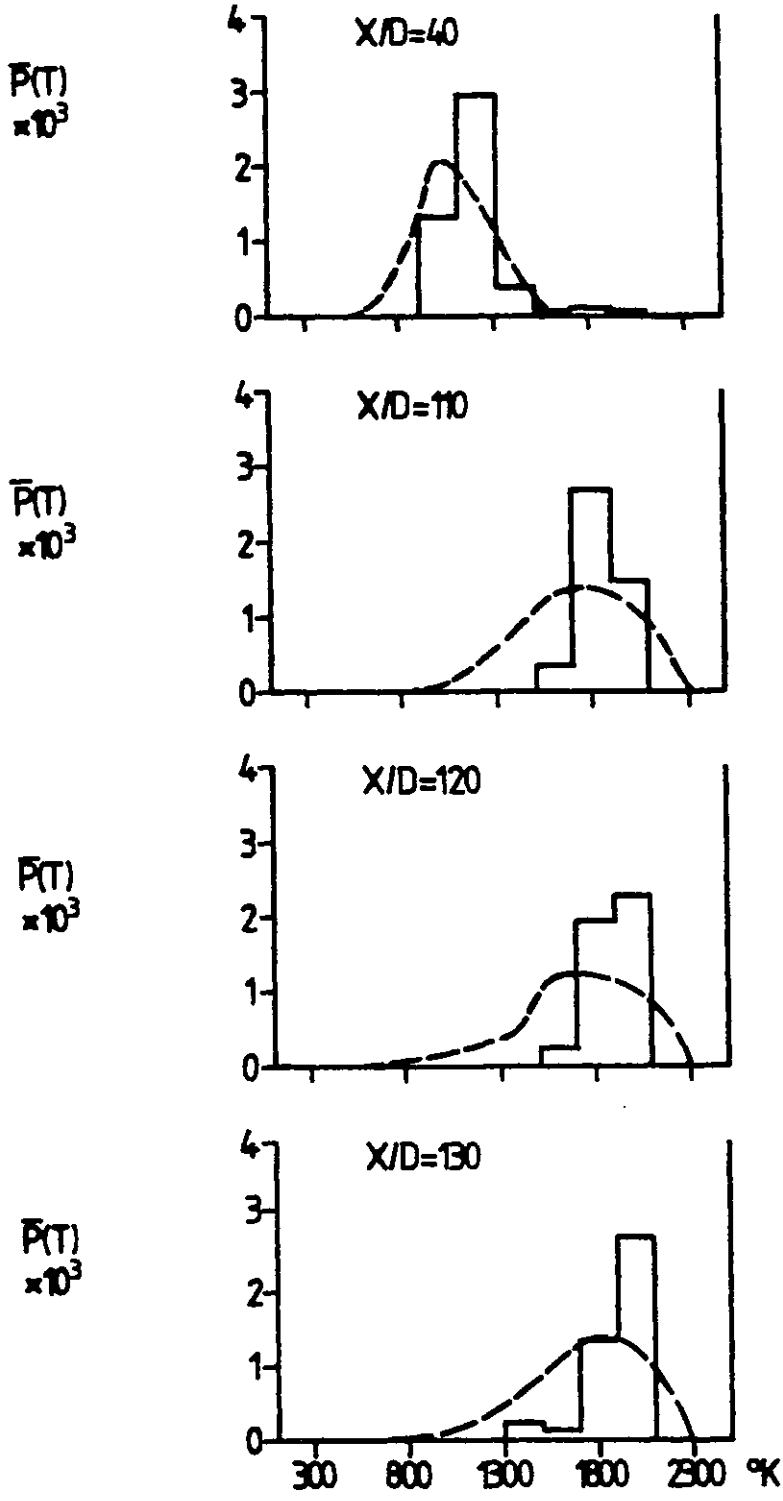

Fig.7.8-23 Probability density functions of temperature at flame axis
(——— Predictions,
----- Measurements)

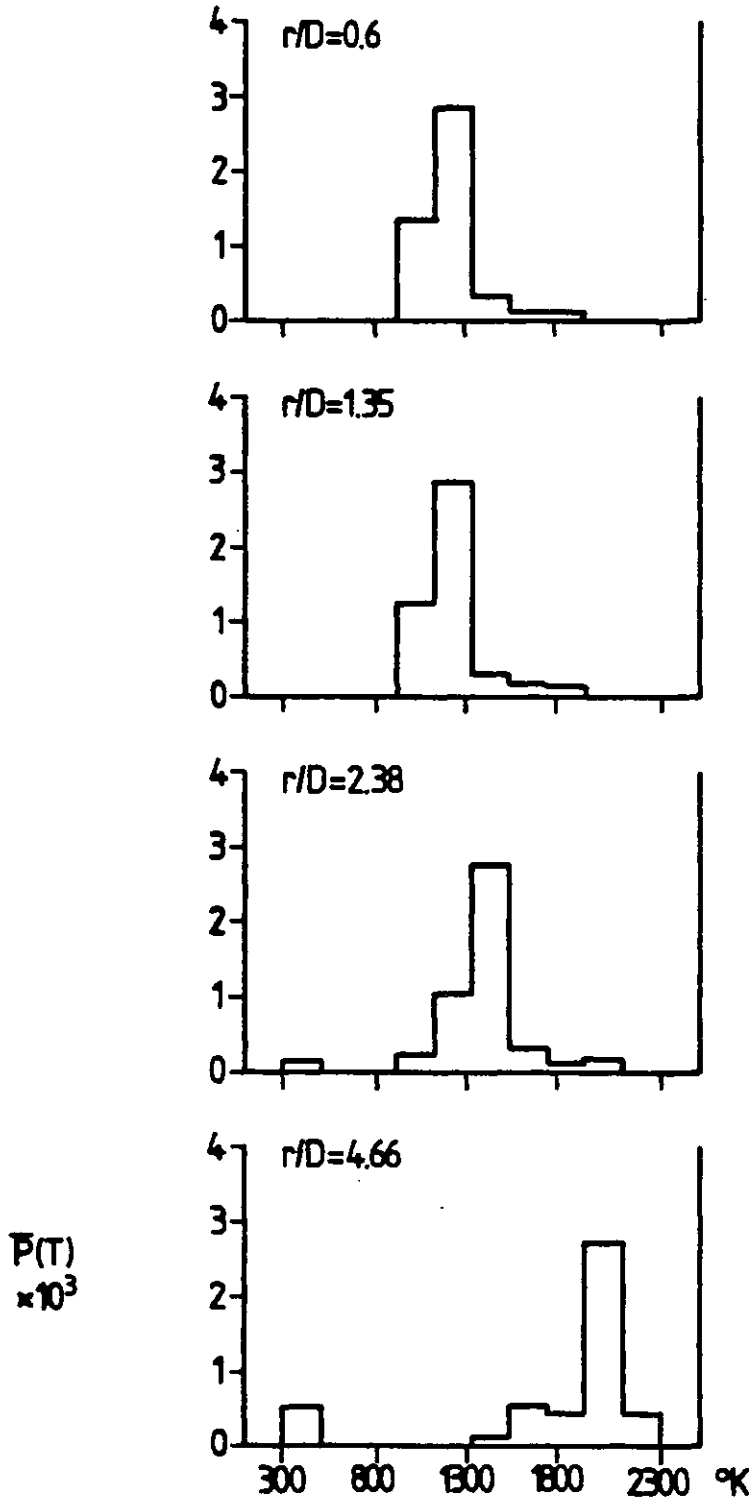

Fig.7.8-24 Probability density functions of temperature at X/D=40

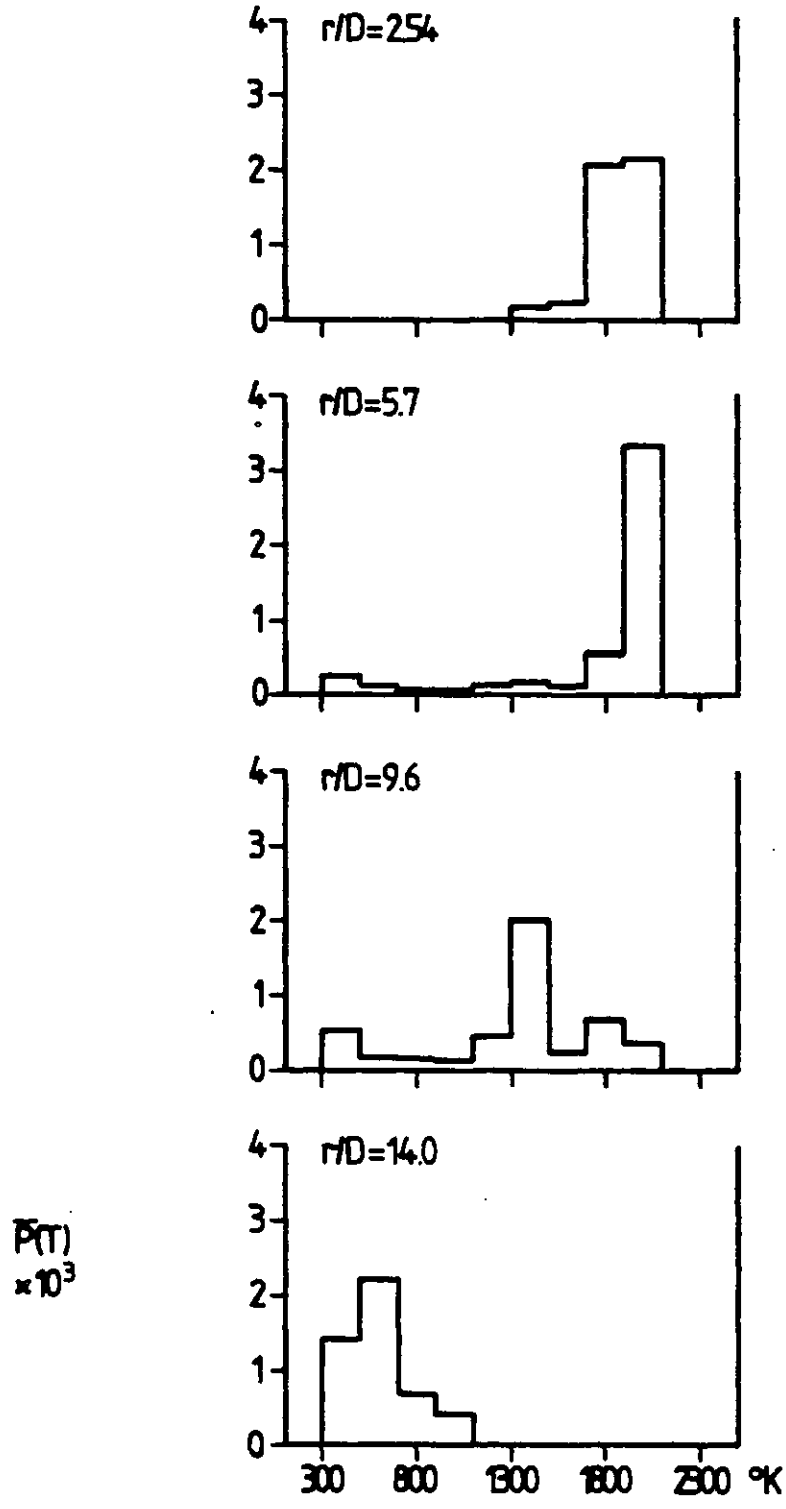

Fig.7.8-25 Probability density functions of temperature at X/D=110

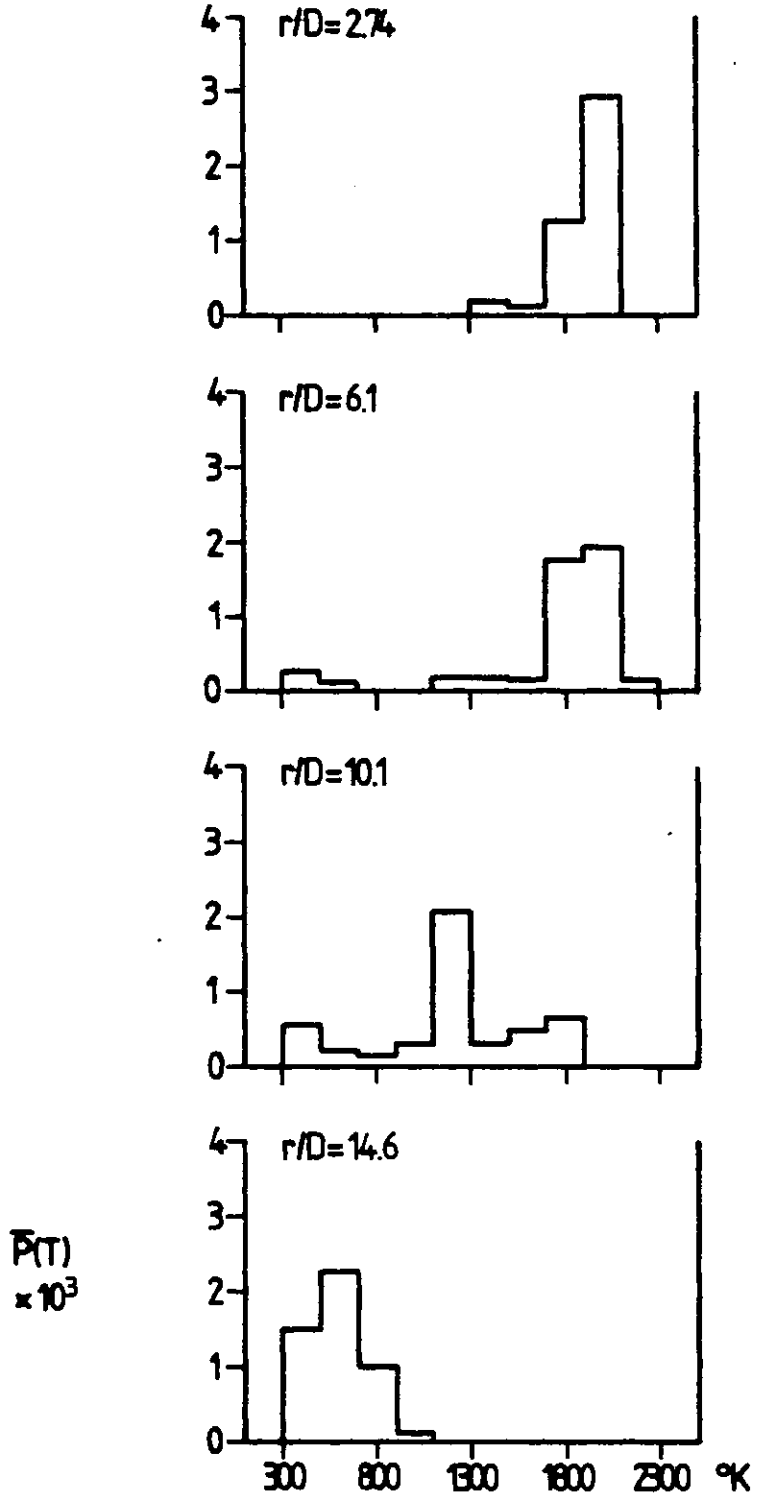

Fig.7.8-26 Probability density functions of temperature at X/D=120

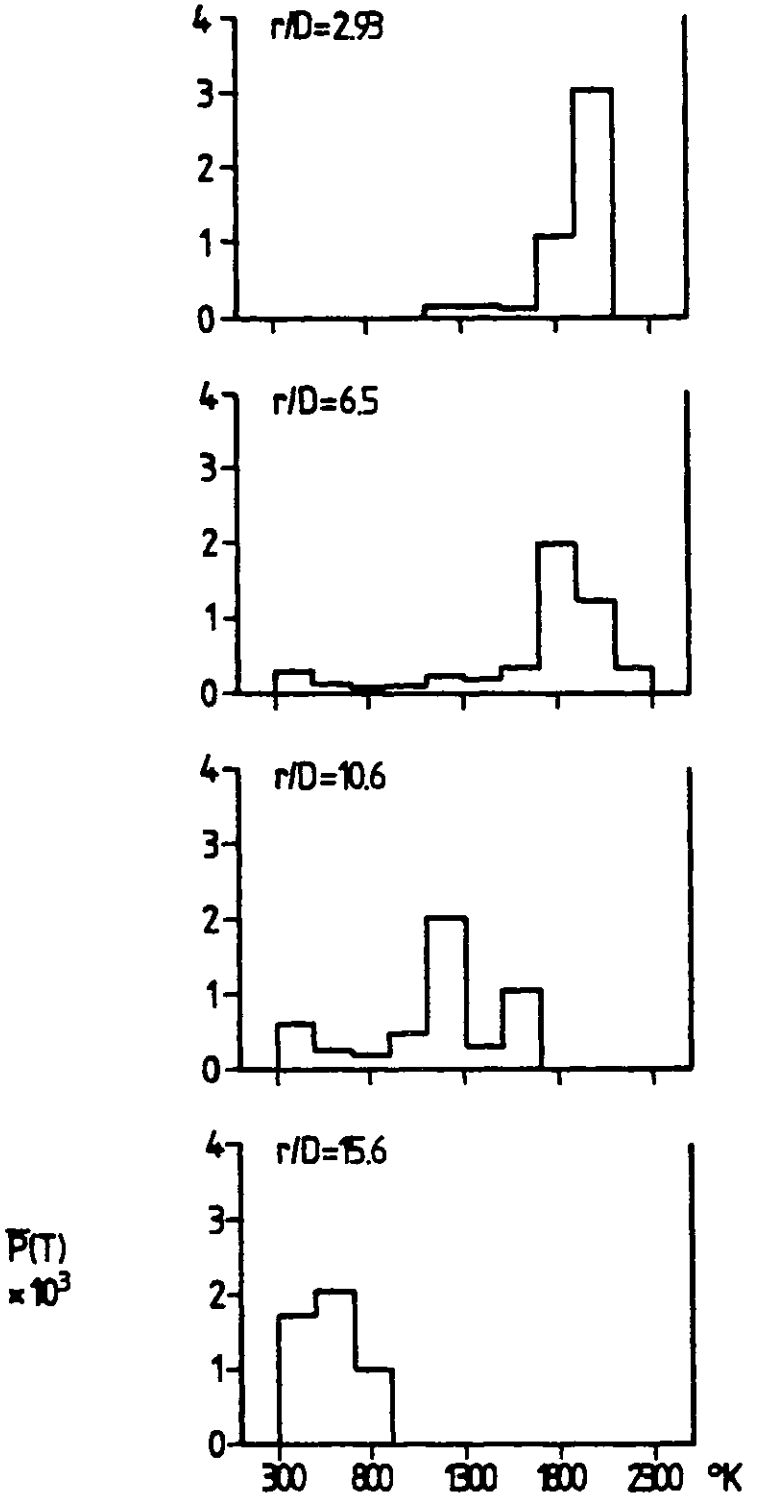

Fig.7.8-27 Probability density functions of temperature at X/D=130

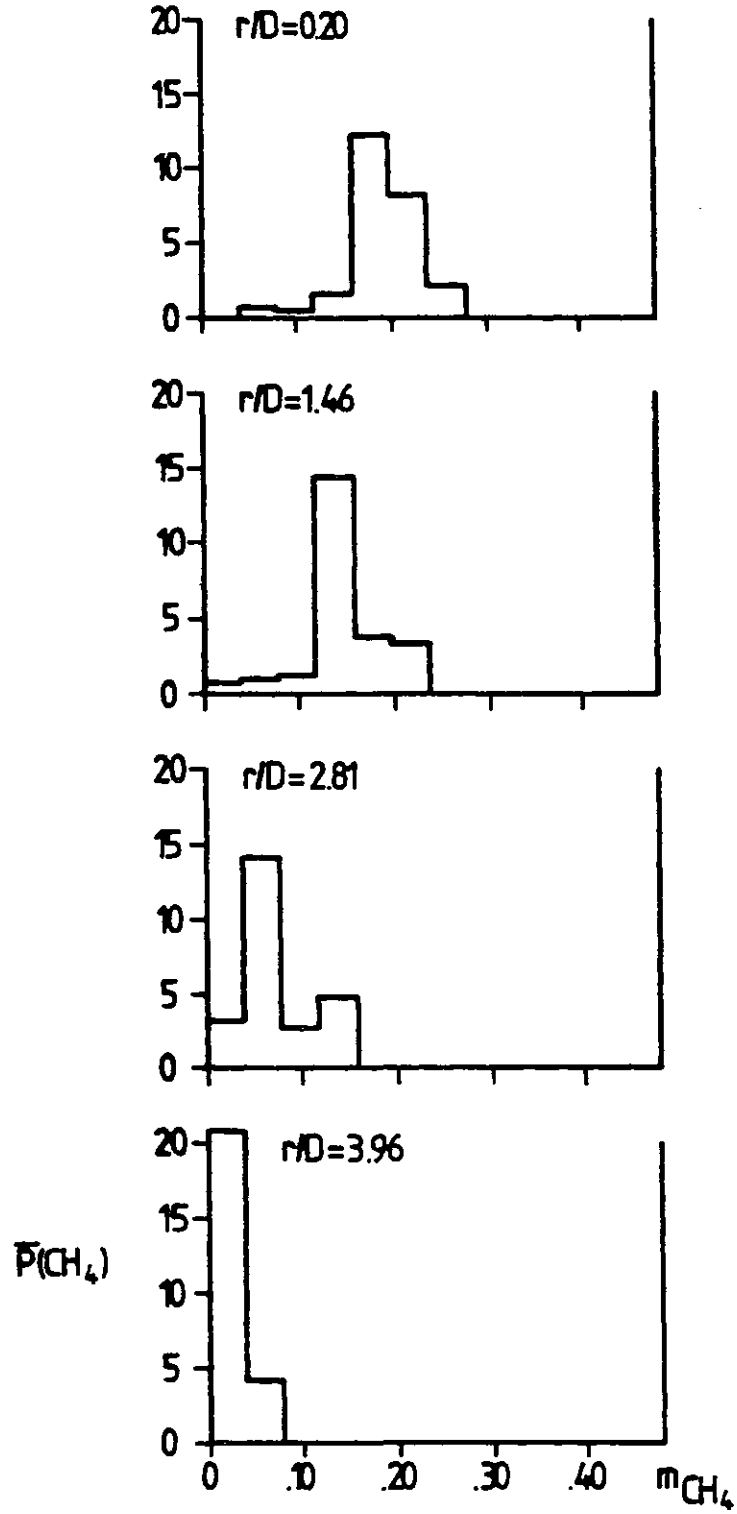

Fig.7.8-28 Probability density functions of mass fraction of methane at X/D=40

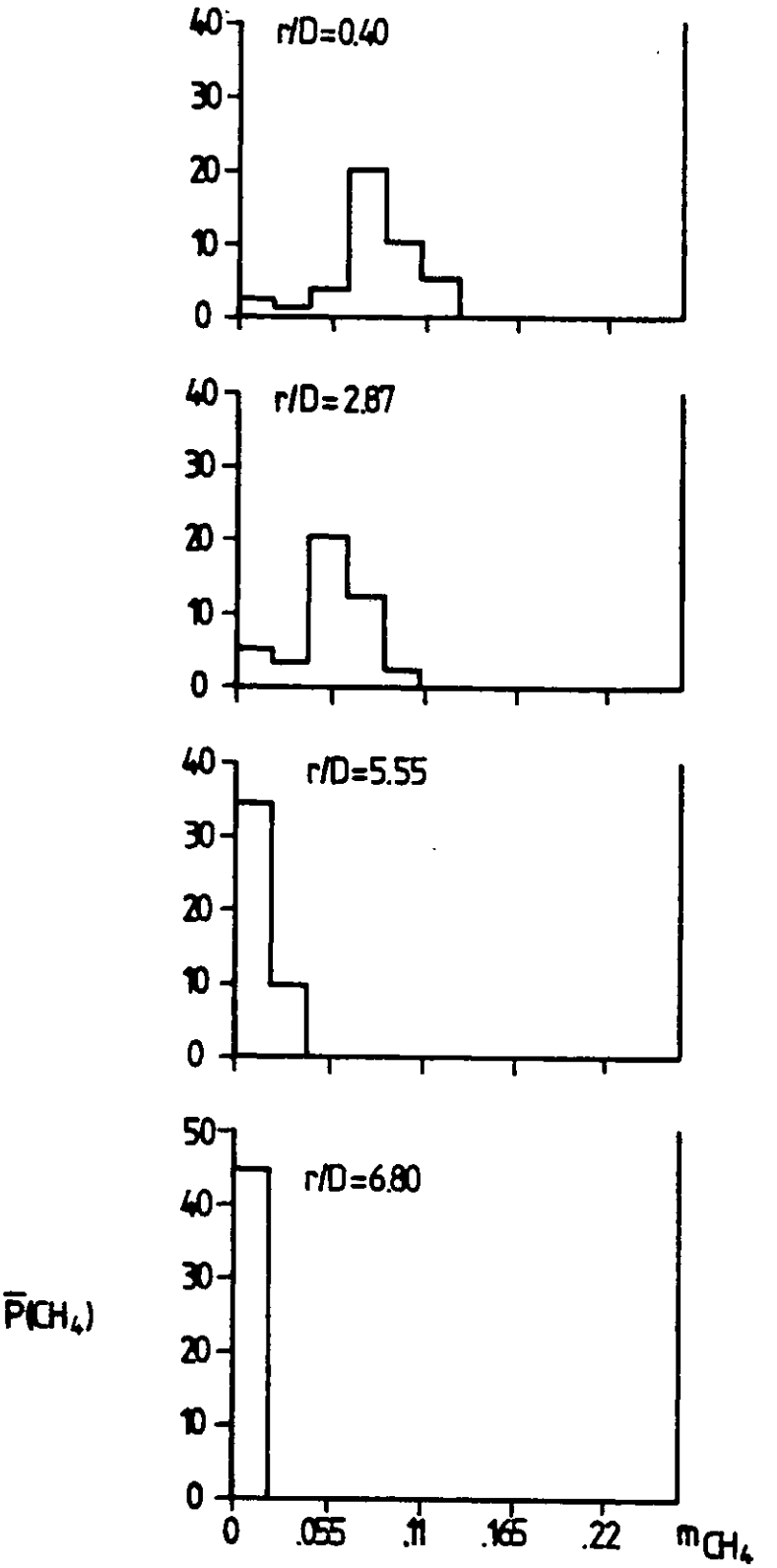

Fig.7.8-29 Probabilty density functions of mass fraction of methane at X/D=60

Figs.7.8-30 and 7.8-31 show the pdf curves for the mass fraction of oxygen at X/D=40 and 60 respectively. The pdf profiles at X/D=40 are mainly located near the lower bound of the domain until r/D=3.51, where a small but finite contribution from the free stream exists. At r/D=5.05, the peak value of the pdf moves towards the central part of the domain, while the proportion of free-stream property also increases. The evolution pattern in Fig.7.8-31 bears the resemblance to the previous graph, where higher mass fraction of oxygen is situated in the outer edge of the jet, e.g., at r/D=8.50.

7.9 Discussion of results

The turbulent mean quantities

The axial distribution of mean temperature in Fig.7.8-10, and the radial variation in Figs.7.8-12 and 7.8-13 have been found to agree fairly with the experimental measurements. It can be inferred that the gross nature of the flame was correctly predicted, although the primitive chemical scheme is incorporated with the ESCIMO model.

There exists some discrepancies between the predictions and the measurements on the species concentration, especially the amount of CO_2 is overpredicted. The main reason is that only water vapor and carbon dioxide are included in the calculation of products, while a finite contents of hydrogen and carbon monoxide do present in actuality during the reaction process. The calculated value of CO_2 will be smaller if CO is included as a product in the reaction scheme and hence better agreement with the experimental

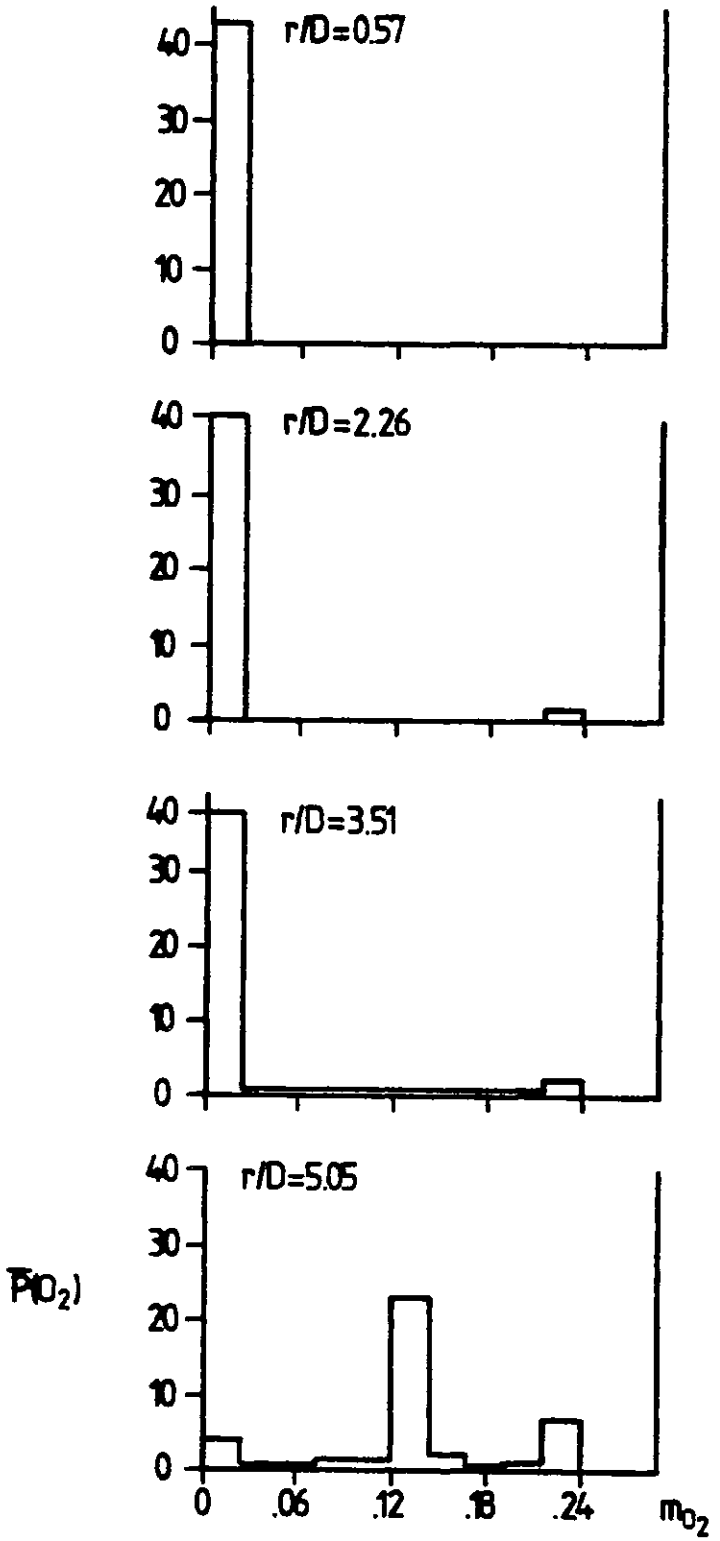

Fig.7.8-30 Probability density functions of mass fraction of oxygen at X/D=40

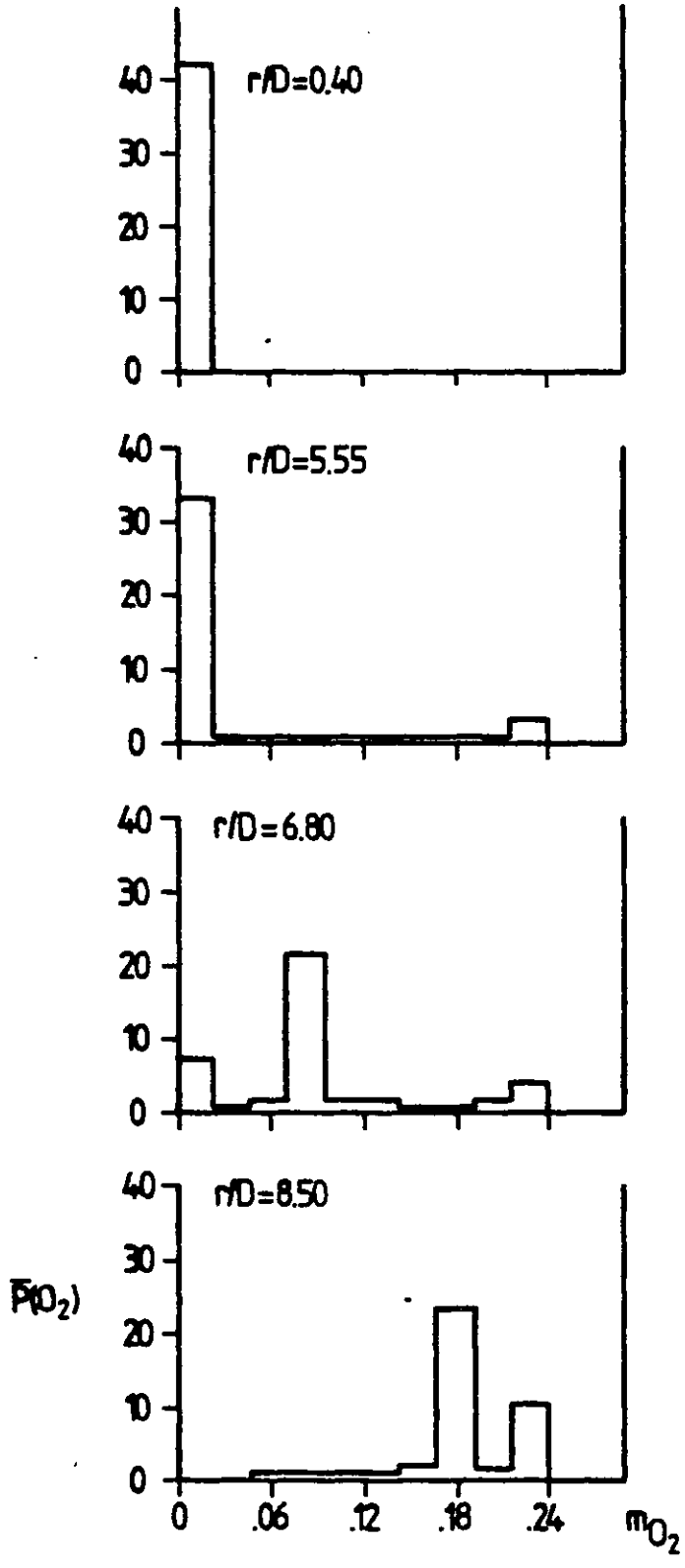

Fig.7.8-31 Probability density functions of mass fraction of oxygen at X/D=60

data can be achieved.

Dryer and Westbrook (1979) have mentioned that typical hydrocarbons (such as methane, propane etc.) burn in a sequential manner. That is, the fuel is partially oxidised to CO and H_2,which are not appreciably consumed until all of the hydrocarbon species have disappeared. The two-step reaction scheme has been used by Dryer and Glassman (1972) for methane oxidation in a turbulent flow reactor and is given by:

$$CH_4 + 3/2\ O_2 \rightarrow CO + 2H_2O \quad , \quad (7.9\text{-}1)$$

$$CO + 1/2\ O_2 \rightarrow CO_2 \quad , \quad (7.9\text{-}2)$$

where the chemical reaction rates were derived empirically.

However, the author has decided to adopt the global reaction mechanism at the present stage of development of ESCIMO theory, because additional transport equations with non-linear source terms (for the production rate) will have to be solved in the biographic analysis and the computer time will be enlarged considerably. On the other hand, the earlier work of Tam (1981) has demonstrated the capability of handling detail multistep reaction machanism in a well-stirred reactor.

The root mean square fluctuation quantities

The successful predictions on temperature fluctuations as indicated by Figs.7.8-17 and 7.8-18 further substantiates the potential power of the present model. Lenz and Günther (1980) have discussed the cause of larger temperature fluctuation at X/D=20 than that of X/D=40 and they supposed that the influence of flame stabilization by the annular

oxygen supply can still be felt there.

The fluctuating temperatures of an open methane diffusion flame at a Reynolds number of 9200 have been measured in the work of Ballantyne and Moss (1977) with the aid of fine wire thermocouple. The peak RMS temperature fluctuation is of the order of 450°K which is lower than the results obtained by Lenz and Günther, probably because the Reynolds number is lower and so is the turbulence intensity.

The quantitative validation of predicted fluctuations level on the species concentration can not be made, since the relevant experimental data are not reported in the literature. But one can be sure that the present theory is capable of calculating the important and interesting quantities in turbulent flames.

The probability density functions

From the comparison between the calculated pdf and measured pdf in Fig.7.8-23, it can be observed that the experimental curves are broader. Since the shape of pdf is more closely related to the various parameters such as C_F, C_Z and C_S than the mean quantities, it will be necessary to investigate the influence of each constant before making the concrete remarks.

The intermittent effect is observed from the pdf profiles near the free stream boundary, e.g.,in Fig.7.8-24, at r/D=4.66 and X/D=40. This feature is included in the fold composition at birth, as described in Sec.7.5, and hence it is expected that the fold formation rate and stretching rate will have considerable influence on it.

7.10 Closure

The application of ESCIMO theory to turbulent hydrogen-air diffusion flame and methane-air diffusion flame have been made. A single set of parameters is employed for both cases and the results have been compared with the experimental data available in the literature.

Generally speaking, the quantitative agreement between the predictions and the measurements is reasonably good, including the fluctuating quantities as well as the turbulent mean values. However, some discrepancies do exist in the comparison between calculated and measured probability density functions of temperature.

Therefore, it is important to investigate the influence of different presumptions and parameters on the results, especially the fluctuation levels and the shape of pdf profiles. The systematic presentation of the sensitivity analaysis and grid independence tests will appear in the next chapter.

CHAPTER 8

THE PARAMETRIC STUDIES

8.1 Introduction

In the previous chapter, the predictions on the turbulent diffusion flames have been made with the aid of some simplified assumptions to compromise between the realism and economy. Several empirical constants related to the fold composition, fold size at birth and, the stretching rate have been chosen during the computations.

The purpose of the present chapter is to check whether the final results are sensitive to those presumptions and empirical constants. Hence, the description of all test cases performed in this chapter will be provided in Sec.8.2, followed by the report on the influence of various hypothesis about the distribution of fold formation rate in Sec.8.3. Subsequently, the influence of fold composition at formation time, fold size at birth and the stretching rate will be discussed in Secs.8.4, 8.5 and 8.6 respectively.

The effects of grid-size in x, ω and $\tilde{A}$ coordinate will also be investigated and depicted in Sec.8.7 to ensure that all results are practically grid independent. Finally, a short closure will appear at the end.

8.2 The test cases performed

A systematic study has been performed in such a way that each test case is different from the "standard run" by one parameter only. The standard run stands for the case

described in the previous chapter. The list of all test runs is given by the following table:

Run No	Mode	C_F	C_Z	C_S	NA	N	λ_3
1	(i)	2.	0.328	0.5	20	20	0.01
2	(ii)	2.	0.328	0.5	20	20	0.01
3	(iii)	2.	0.328	0.5	20	20	0.01
4	(i)	1.	0.328	0.5	20	20	0.01
5	(i)	3.	0.328	0.5	20	20	0.01
6	(i)	2.	0.164	0.5	20	20	0.01
7	(i)	2.	0.082	0.5	20	20	0.01
8	(i)	2.	0.328	2.0	20	20	0.01
9	(i)	2.	0.328	0.1	20	20	0.01
10	(i)	2.	0.328	0.5	10	20	0.01
11	(i)	2.	0.328	0.5	6	20	0.01
12	(i)	2.	0.328	0.5	20	30	0.01
13	(i)	2.	0.328	0.5	20	40	0.01
14	(i)	2.	0.328	0.5	20	20	0.02
15	(i)	2.	0.328	0.5	20	20	0.03
16	(i)	2.	0.328	0.5	20	20	0.005

Table 8.2-1 The test cases of parametric studies (Run No.1 is the standard run) for methane-air diffusion flame.

In contrast to the full scale parametric studies of methane-air diffusion flame, only a selective number of runs will be presented for the hydrogen-air diffusion flame. The

same definition of "Run No" will be used for hydrogen-air flame and the cases are Run nos 1, 2, 3, 5, 6 and 8.

8.3 The influence of fold formation rate

The population distribution functions

The population distributions with respect to age, for methane-air diffusion flame, obtained from various presumptions on the fold formation rate are now presented through Figs.8.3-1 to 8.3-4.

In Fig.8.3-1, the $\tilde{P}$~$\tilde{A}$ distribution exhibits a stronger characteristic of exponential decay at r/D=3.8, where the fold formation rate reaches its climax. In Run No.2, the fold formation rate is assumed to be proportional to the mean velocity and hence the peak value is always located at the jet axis. Therefore, the steepest curve in Fig.8.3-2 is the one which corresponds to the distribution near the axis, i.e.,at r/D=0.42. Both the fold formation rate and the ageing effect are small at r/D=8.3, which result in a rather flat distribution. Similarly, the maximum fold formation appears at r/D=8.3, for Run No.3 (Fig.8.3-3), and the curve again shows the exponential behaviour.

The influence of fold formation rate on the radial variation of average age is demonstrated in Fig.8.3-4. It can be observed that the average age increases as the distance from the jet axis enlarges, for all three runs. The average age calculated from Run No.3 does not increase rapidly in the outer edge of the jet, since the fold formation rate there is higher than that of the other runs.

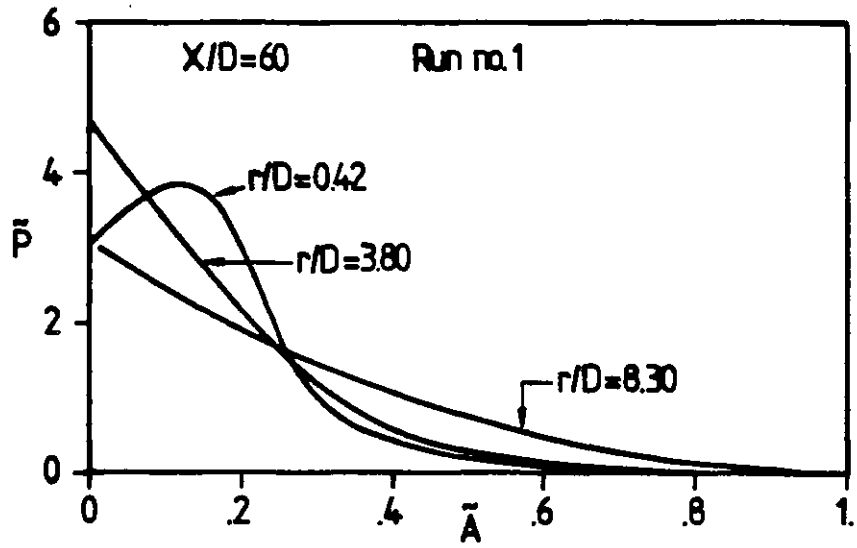

Fig.8.3-1 Population distribution functions of methane-air diffusion flame

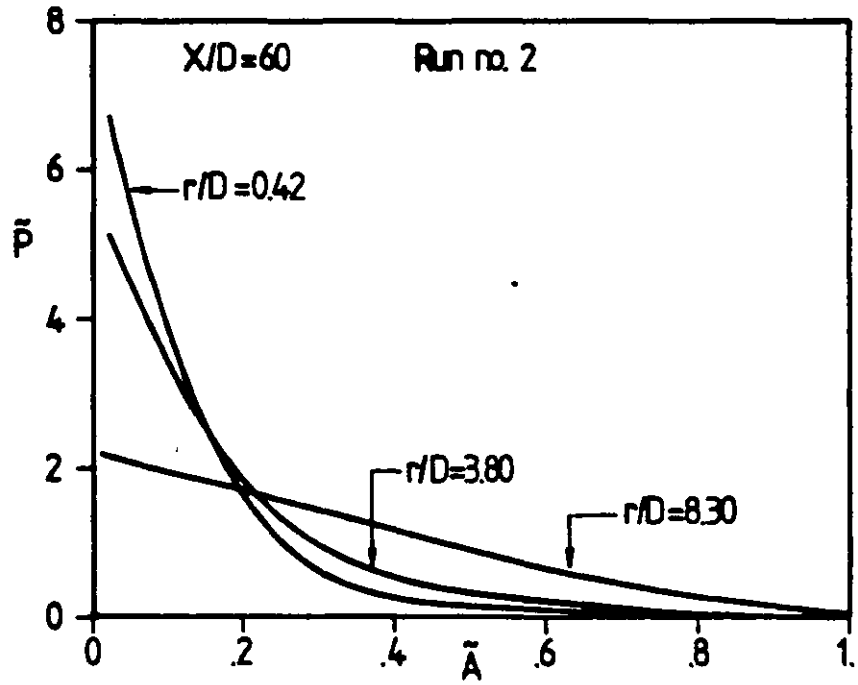

Fig.8.3-2 Population distribution functions of methane-air diffusion flame

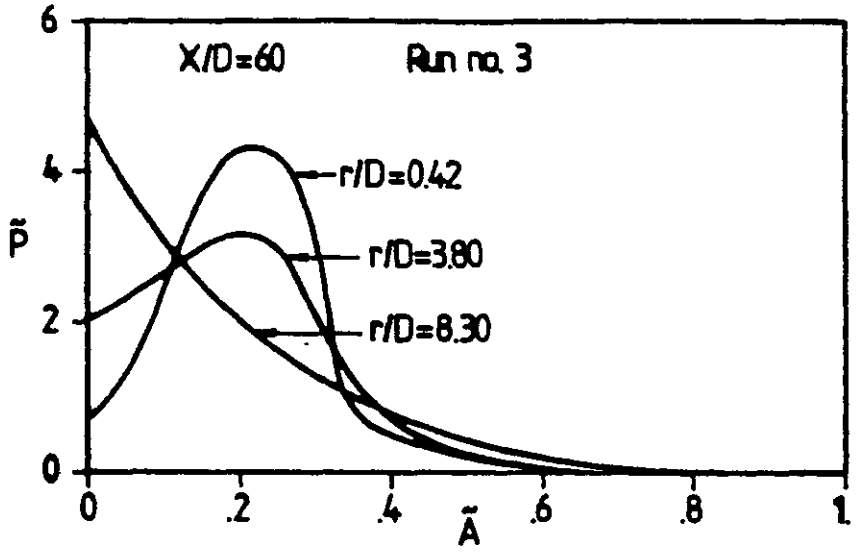

Fig.8.3-3 Population distribution functions of methane-air diffusion flame

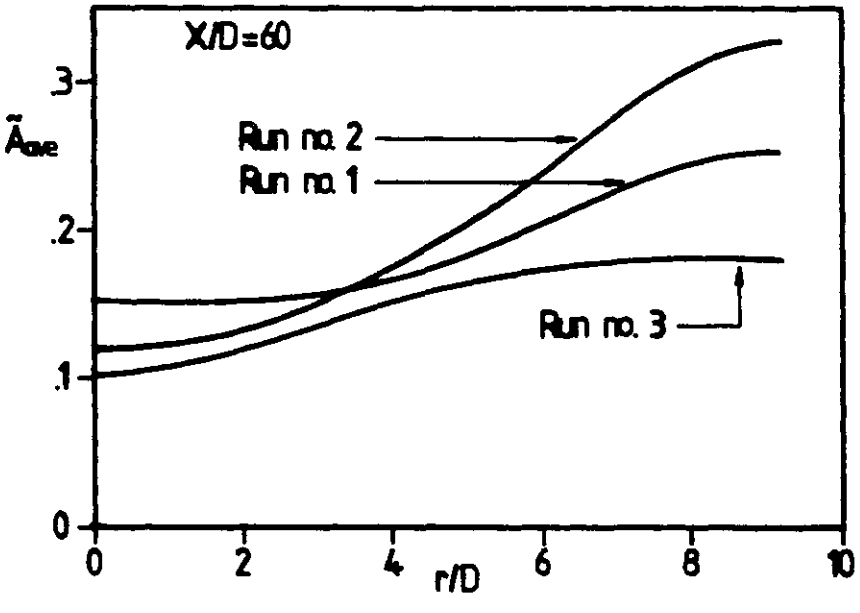

Figure 8.3-4 The radial variation of average age for methane-air diffusion flame

The turbulent mean quantities

The mean temperature of methane-air diffusion flame, at X/D=60, calculated from Runs Nos.1, 2 and 3 are presented in the following table for comparison. The longitudinal station of X/D=60 has been chosen here because more comprehensive experimental data are available (Lenz and Günther, 1980).

Radial Location r/D	Turbulent Mean Temperature °K		
	Run No.1	Run No.2	Run No.3
0.40	1520	1520	1520
1.46	1540	1540	1550
2.87	1590	1570	1630
4.45	1680	1670	1740
5.55	1740	1760	1770
6.80	1430	1430	1410
8.50	787	786	783

Table 8.3-1 Influence of fold formation rate on mean temperature

Table 8.3-1 shows that the effect of various distributions about fold formation rate on the mean temperature is rather small. The maximum discrepancy between each run is only around 70°K (e.g.,at r/D=4.45), which is less than 4% of the flame temperature

The mean molar fraction of methane, at X/D=60, is selected as a representative to demonstrate the influence of different formation rates on the species concentration. The results are provided in the following table:

Radial Location r/D	Mean CH_4 Molar Fraction		
	Run No.1	Run No.2	Run No.3
0.40	0.138	0.137	0.139
1.46	0.126	0.126	0.126
2.87	0.0962	0.0970	0.0938
4.45	0.052	0.0510	0.0470
5.55	0.0165	0.0161	0.0135
6.80	0.0015	0.0013	0.0013
8.50	0.0	0.0	0.0

Table 8.3-2 Influence of fold formation rate on mean CH_4 molar fraction

Again it can be noticed that the results obtained from each case are very close to each other. Hence the attention is now turned to the fluctuation quantities.

Similar to the case for methane-air flame, the influence of various fold formation rates on the mean temperature for hydrogen-air flame, at X/D=80, is demonstrated in Table 8.3-3.

Radial Location r/D	Turbulent Mean Temperature ^oK		
	Run No.1	Run No.2	Run No.3
0.42	1830	1860	1810
1.68	1840	1900	1830
3.36	1860	1980	1860
4.56	1580	1580	1580
5.25	1210	1200	1210
5.75	900	900	900
6.20	680	690	680

Table 8.3-3 Influence of fold formation rate on mean temperature

It can be observed that the mean temperature are not very sensitive to the distribution of fold formation rate, except in the peak value (at r/D=3.36). The peak temperature obtained in Run No.2 is equal to 1980°K, which is 120°K higher than the counterpart from the other two runs.

The mean molar fraction of hydrogen, at X/D=80, calculated from three different fold formation rates are presented in Table 8.3-4. The main discrepancies again happen at r/D=3.36, where the value in Run No.2 is substantially lower (around 27% difference).

The root mean square fluctuation quantities

Fig.8.3-5 shows the fluctuating temperatures calculated from three different fold formation rates, at X/D=60. The measurements of Lenz and Günther are also presented for the sake of comparison. It can be observed that the difference between each case is now more significant and the predictions from Run No.3 fit the experimental data very well. In the case of Run No.3, the fold formation rate is assumed to vary linearly with the ω-value, i.e., the fold formation rate is minimum in the jet axis and reaches the maximum value near the outer edge of the jet.

The rms fluctuation of methane (in molar fraction) calculated from Run Nos.1, 2 and 3, at X/D, are shown in Table 8.3-5 given below:

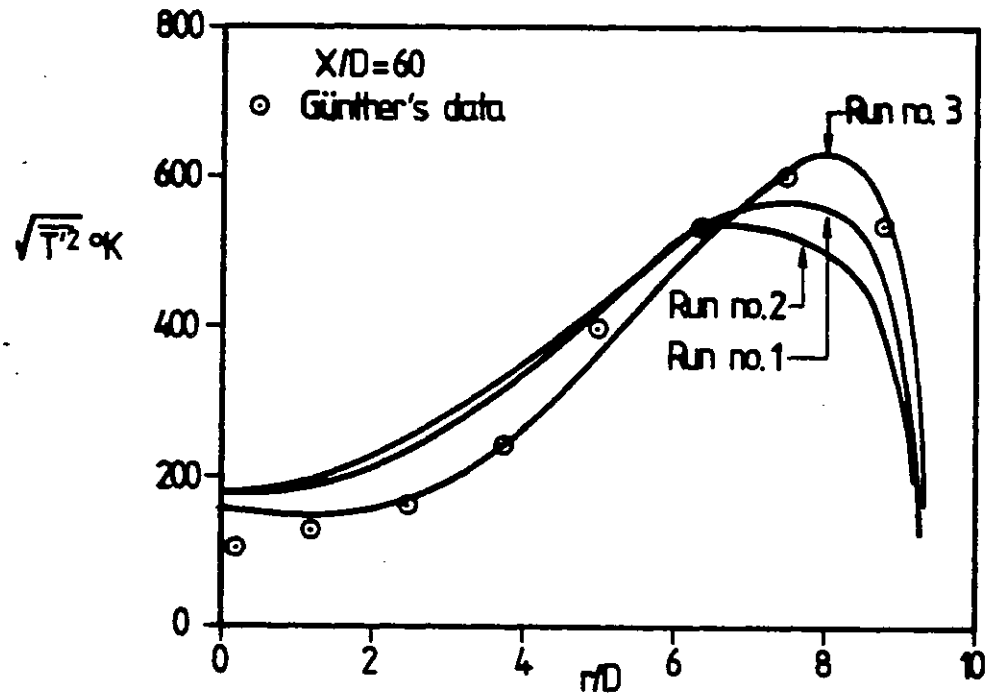

Fig.8.3-5 Influence of fold formation rate on temperature fluctuation

Radial Location r/D	Mean H_2 Molar Fraction		
	Run No. 1	Run No 2	Run No. 3
0.42	0.250	0.253	0.250
1.68	0.209	0.204	0.213
3.36	0.0815	0.0592	0.0819
4.56	0.007	0.005	0.007
5.25	0.0	0.0	0.0
5.75	0.0	0.0	0.0
6.20	0.0	0.0	0.0

Table 8.3-4 Influence of fold formation rate on mean H_2 molar fraction

Radial Location r/D	RMS fluctuation of CH_4		
	Run No.1	Run No.2	Run No.3
0.40	0.0464	0.0451	0.0412
1.46	0.0468	0.0511	0.0357
2.87	0.0455	0.0485	0.0311
4.45	0.0360	0.0365	0.0311
5.55	0.0256	0.0254	0.0238
6.80	0.0037	0.0035	0.0032
8.50	0.0	0.0	0.0

Table 8.3-5 Influence of fold formation rate on rms fluctuation of CH_4 concentration

Considerable difference between each run was found, especially at r/D=1.46 and 2.87 where the maximum relative

discrepancy reaches the order of 30%. In Run no.2 the concentration fluctuations at r/D=1.46 and 2.87 are greater than the value at r/D=0.40, while the peak of concentration fluctuation is situated at r/D=0.40 in the case of Run no.3. It is worth mentioning here that the fold formation rate is large in the central region of the jet and small near the outer edge for Run no.2, exactly oppposite to Run no.3. In the case of Run no.1, the fold formation rate has its peak value situated between the jet axis and the outer boundary, since it is proportional to the mean velocity gradient. Thus, the population of youngest folds is the most prominent one in the near axis region for Run no.2 and results in higher fluctuation level (the non-uniformity of properties inside the fold has not yet evened out).

The probability density functions

The pdf profiles of temperature obtained from Run no.1 and Run no.2, at X/D=60, are illustrated in Fig.8.3-6. The difference is not visible in the near-axis region (e.g.,r/D =0.40) and the results actually collapse on the same profile. However, some discrepancies do exist in other positions, especially in the higher values of P(T).

The pdf profiles are composed of two parts for the newly formed folds, namely the values which stand for the properties of fresh layer and re-engulfed layer respectively. For the very old folds, a single spike representing the fold-average value is dominant. A broad distribution exists for those medium age folds in which the molecular diffusion effect is still taking place. Hence, the population average

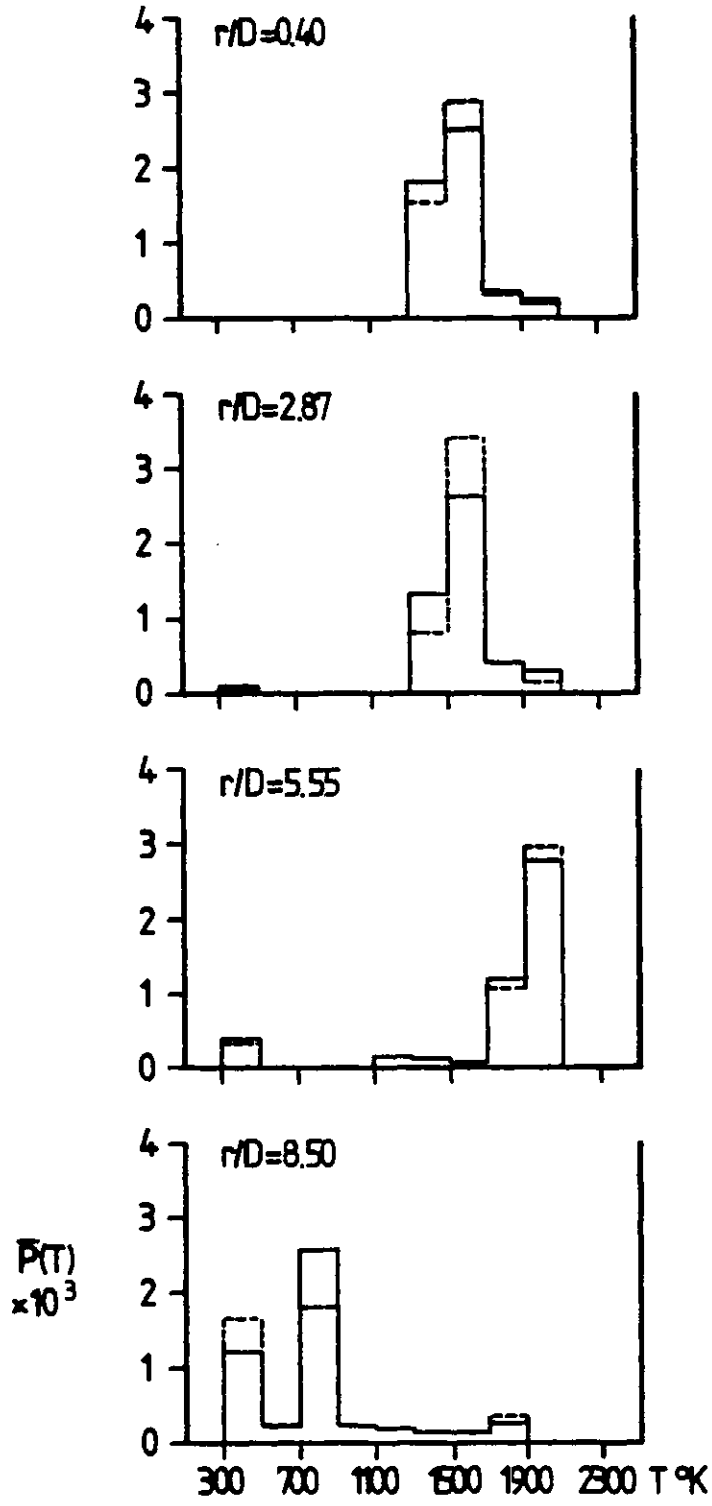

Fig.8.3-6 Influence of fold formation rate on pdf of temperature at X/D=60 (—— Run no.1, ---- Run no.2)

pdf is dependent on the population distribution of various folds.

8.4 The influence of fold composition

The turbulent mean quantities

The radial distribution of mean temperature, at X/D=60, obtained by three different empirical constants for the fold composition are compared and listed in Table 8.4-1.

The peak temperature (at r/D=5.55) varies from 1660°K (for C_F=3.0) to 1850°K (for C_F=1.0) when the composition of fold at birth is altered. In other words, the flame temperature is far below the adiabatic temperature (≈2150°K for methane-air flame) when the re-engulfed layer has the

Radial Location r/D	Mean Temperature °K		
	Run No.1	Run No.4	Run No.5
0.40	1520	1520	1510
1.46	1540	1550	1520
2.87	1590	1630	1550
4.45	1680	1760	1610
5.55	1740	1850	1660
6.80	1430	1450	1360
8.50	787	792	775

Table 8.4-1 Influence of fold composition on the mean temperature

properties far different from the local mean values. The flame temperature becomes higher if the properties in the re-engulfed layer are closer to the mean values. The experimental flame temperature from Lenz and Günther is around 1740°K which is close to the value from Run No.1.

The influence of C_F values on the mean concentration of methane, at X/D=60, is now presented in Table 8.4-2.

Radial Location r/D	Mean CH_4 Molar Fraction		
	Run No 1	Run No 4	Run No 5
0.40	0.138	0.141	0.135
1.46	0.126	0.129	0.124
2.87	0.0962	0.0965	0.0947
4.45	0.0502	0.0475	0.0511
5.55	0.0165	0.0111	0.0189
6.80	0.0015	0.0	0.0042
8.50	0.0	0.0	0.0

Table 8.4-2 Influence of fold composition on mean CH_4 molar fraction

Inspection of Table 8.4-2 reveals that higher C_F value yields larger concentration of methane across the jet and hence it is expected that the overlapping of methane and oxygen also increases as a consequence.

The influence of initial fold composition on the mean temperature and compositions, for hydrogen-air flame, is now demonstrated in Fig.8.4-1. When larger C_F value (C_F=3.0 in Run no.5) is employed, the mean concentration of hydrogen

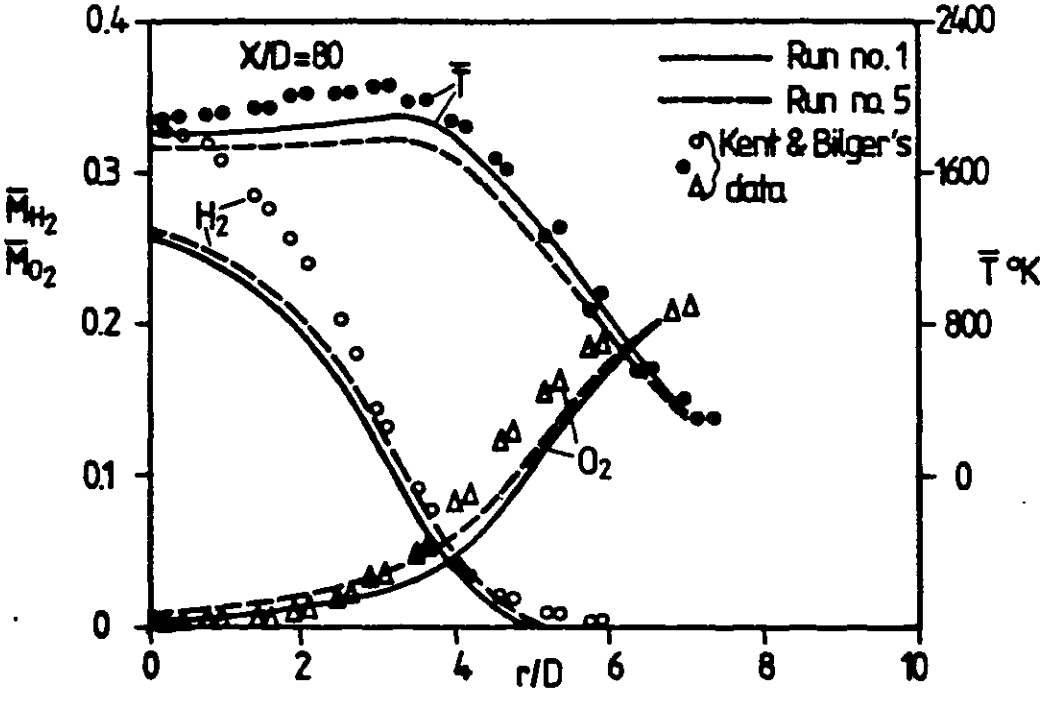

Fig.8.4-1 Influence of fold composition on the mean temperature and compositions for hydrogen-air flame

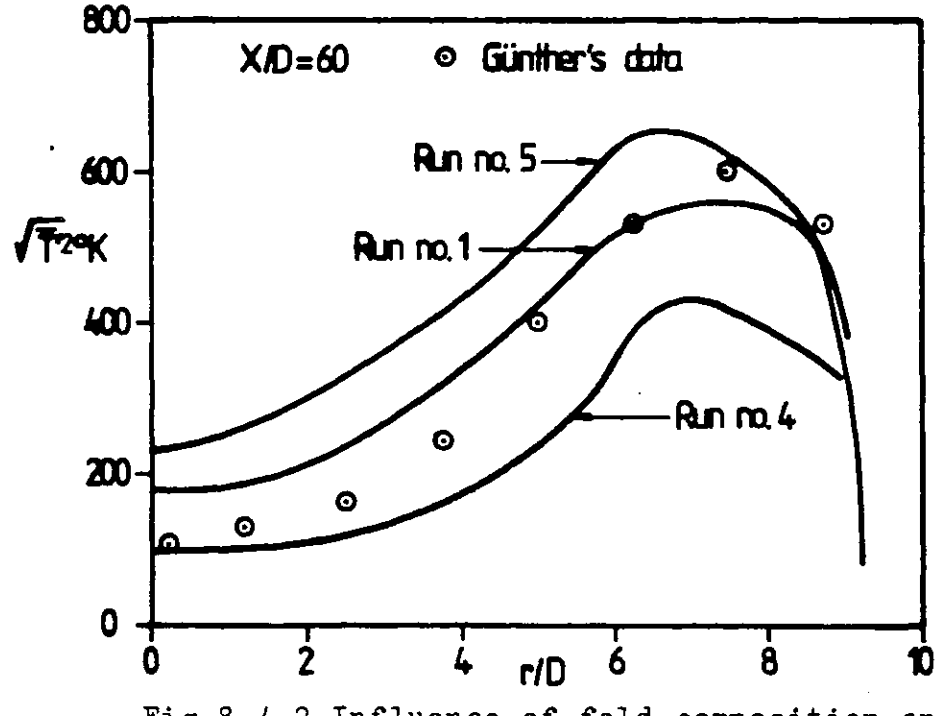

Fig.8.4-2 Influence of fold composition on temperature fluctuation for methane-air flame

and oxygen increase. The degree of overlapping for fuel and oxidant is slightly enhanced, but it is still lower than the measured value. On the other hand, the temperature profile has been reduced by about 80°K~100°K in the case of higher C_F value.

The root mean square fluctuation quantities

The rms values of temperature fluctuations for three runs are plotted in Fig.8.4-2 to demonstrate the influence of different fold compositions. It is evident that the fluctuation intensities are sensitive to the value of C_F, i.e., larger C_F will result in higher fluctuation. The present comparison with the experimental data suggests that the value of C_F=2.0 produces reasonable agreement.

The influence of fold composition on the concentration fluctuation of CH_4 is demonstrated in Table 8.4-3.

Radial Location r/D	RMS fluctuation of CH_4		
	Run no 1	Run no 4	Run no 5
0.40	0.0464	0.0257	0.0612
1.46	0.0468	0.0282	0.0597
2.87	0.0455	0.0297	0.0578
4.45	0.0360	0.0229	0.0458
5.55	0.0256	0.0142	0.0340
6.80	0.0037	0.0	0.0105
8.50	0.0	0.0	0.0

Table 8.4-3 Influence of fold composition on rms fluctuation of CH_4 concentration

The probability density functions

Fig.8.4-3 shows the pdf of temperature obtained from two different values of C_F (C_F=2.0 and 3.0), at X/D=60. The pdf profiles calculated from larger C_F value exhibit a broader characteristic in the inner part of the jet, i.e., at r/D=0.40 and 2.87. This is consistent with the structure inside the fold, since larger C_F value means greater variation of properties are present for each fold.

The results obtained from run no.4 (C_F=1.0) are plotted separately with those of run no.1 in Fig.8.4-4 for the sake of clarity. The pdf profiles now become narrower as expected, indicating that the non-uniformity of properties has diminished.

8.5 The influence of fold size

The turbulence mean quantities

The mean temperature of methane-air flame obtained from three different values of fold size at birth, for X/D values of 60, are listed and compared in Table 8.5-1

The peak temperature of the flame (at r/D≈5.55) varies from 1740°K (C_Z=0.328) to 1910°K (C_Z=0.082) when the initial fold size changes by a factor of four. It can be seen that the results from run no.1 are closer to the experimental data, since the measured flame temperature is around 1740°K.

The smaller the fold is at birth, the faster the evening out of the fluctuation level is under the conditions that other parameters remain fixed. Hence, the peak temperature will be closer to the equilibrium adiabatic temperature when

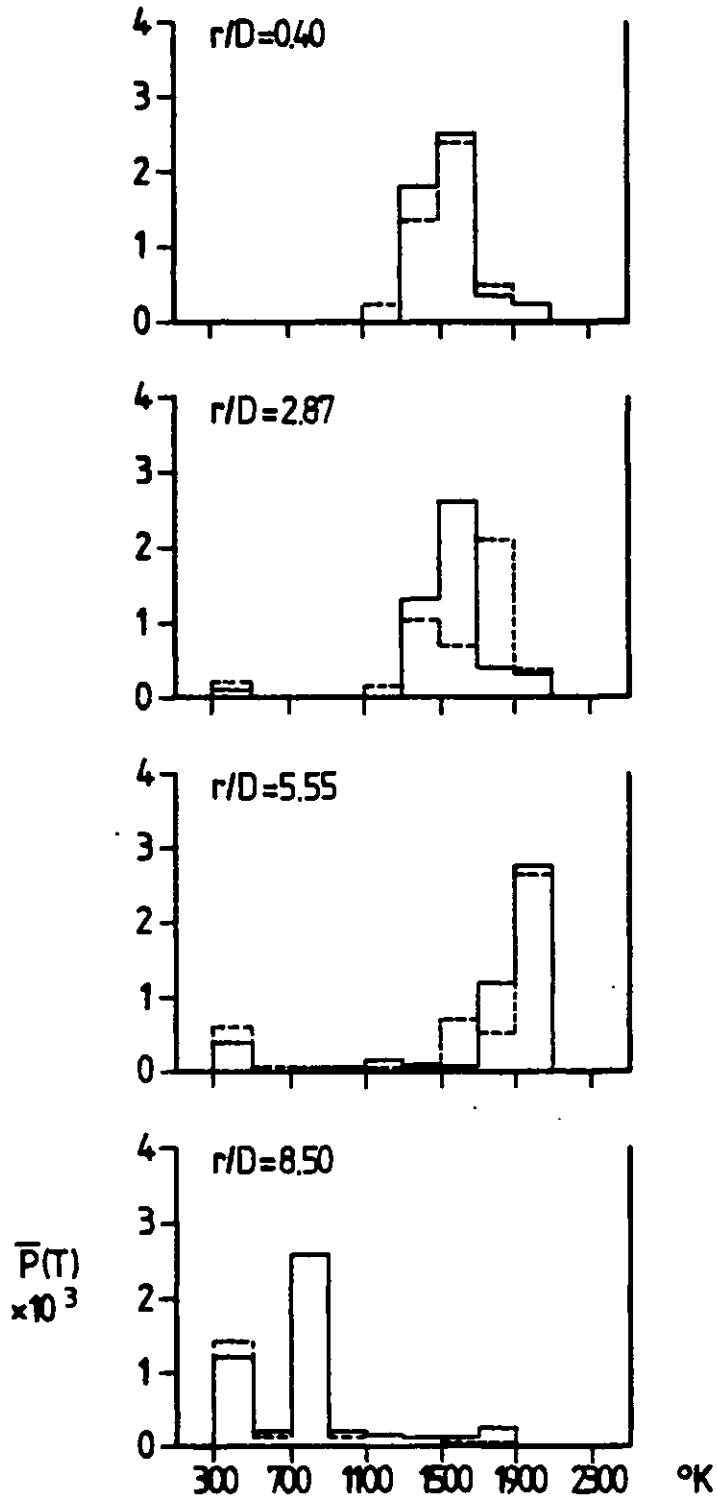

Fig.8.4-3 Influence of fold composition on pdf of temperature at X/D=60
(—— Run no.1, ---- Run no.5)

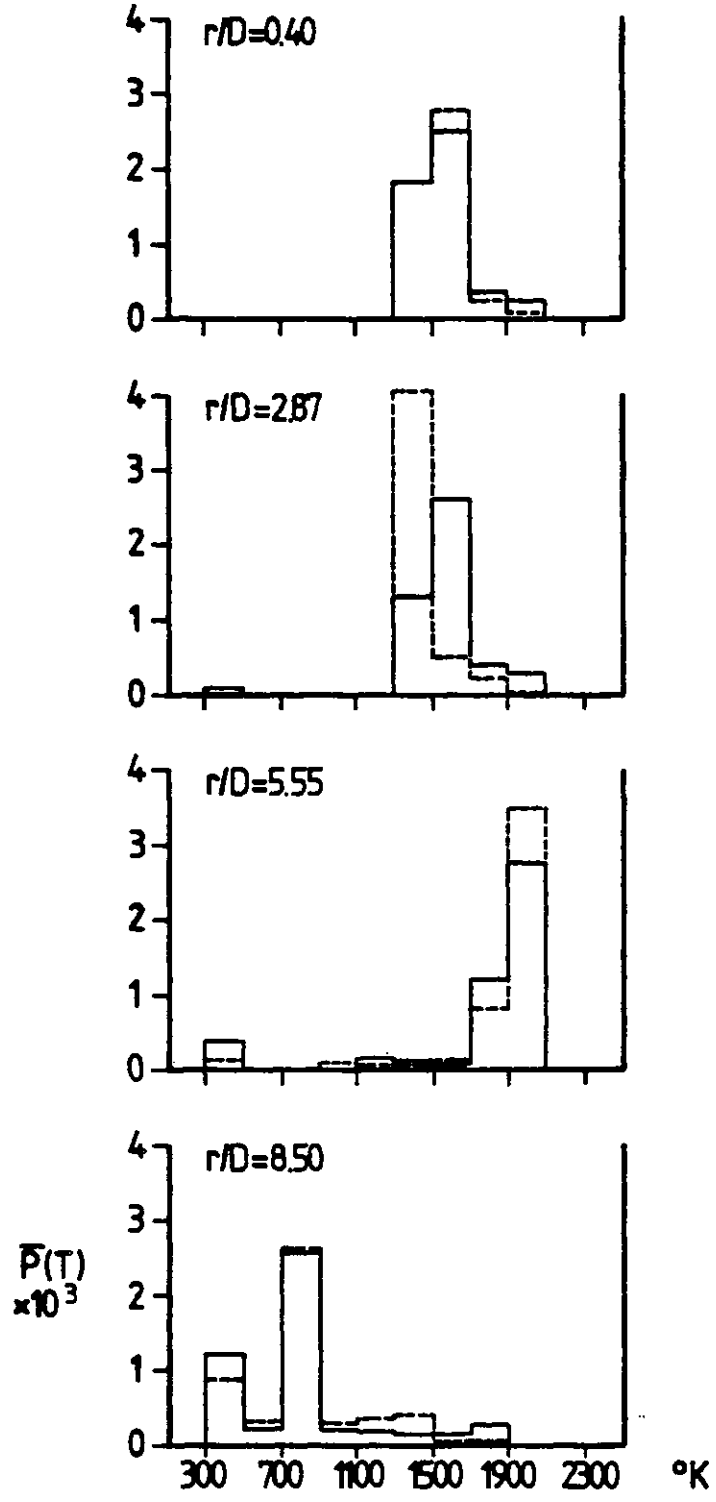

Fig.8.4-4 Influence of fold composition on pdf of temperature at X/D=60
(—— Run no.1, ---- Run no.4)

Radial Location r/D	Mean temperature °K		
	Run no 1	Run no 6	Run no 7
0.40	1520	1520	1520
1.46	1540	1560	1550
2.87	1590	1630	1640
4.45	1680	1750	1800
5.55	1740	1830	1910
6.80	1430	1440	1390
8.50	787	792	776

Table 8.5-1 The influence of fold size on the mean temperature

the fold is rather small.

The influence of initial fold size on the mean concentration of CH_4 is now demonstrated in Table 8.5-2.

Radial Location r/D	Mean CH_4 molar fraction		
	Run No.1	Run No.6	Run No.7
0.40	0.138	0.140	0.140
1.46	0.126	0.128	0.127
2.87	0.0962	0.0960	0.104
4.45	0.0502	0.0477	0.0439
5.55	0.0165	0.0117	0.0054
6.80	0.0015	0.0005	0.0
8.50	0.0	0.0	0.0

Table 8.5-2 The influence of fold size on mean CH_4 molar fraction

It can be observed that the major discrepancies between each run occur in the flame zone (e.g., at r/D≈5.55) where the concentration of CH_4 decreases significantly as the value of C_Z becomes smaller.

The mean temperature and compositions claculated from two different fold sizes, for the hydrogen-air flame, are shown in Fig.8.5-1. The mean temperature is higher in the case of the smaller fold size (C_Z=0.164 in Run No.6) and closer to the experimental data. However, the concentration of hydrogen and oxygen are lower around the flame zone (3<r/D<4.5) and less amount of cross-over is observed.

The root mean square fluctuation quantities

The radial distribution of temperature fluctuations calculated from three different values of C_Z, at X/D=60, are plotted in Fig.8.5-2. It is evident that the fluctuation intensities are sensitive to the initial fold size, i.e., larger fold size will result in higher fluctuation level. The C_Z value of 0.328 in Run No.1 yields better quantitative agreement between the predictions and measurements.

The root mean square fluctuation of methane concentration obtained by Run Nos.1, 6 and 7, at X/D=60, are given in Table 8.5-3.

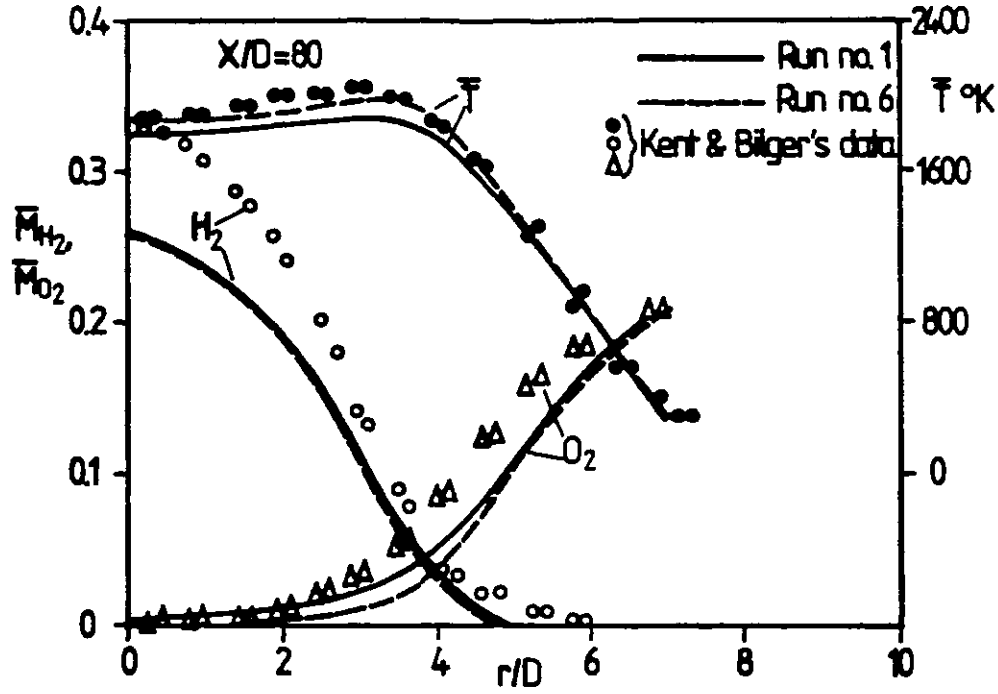

Fig.8.5-1 Influence of fold size on the mean temperature and compositions for hydrogen-air flame

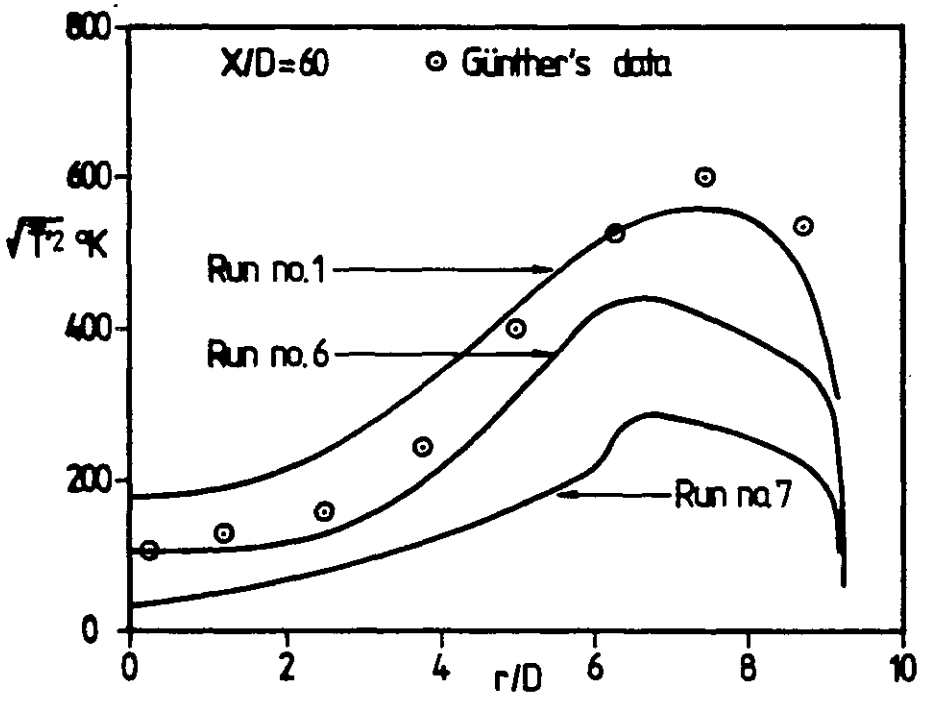

Fig.8.5-2 Influence of fold size on temperature fluctuation for methane-air flame

Radial Location r/D	RMS fluctuation of CH_4		
	Run No.1	Run No.6	Run No.7
0.40	0.0464	0.0274	0.0097
1.46	0.0468	0.0323	0.0150
2.87	0.0455	0.0361	0.0235
4.45	0.0360	0.0300	0.0217
5.55	0.0256	0.0210	0.0152
6.80	0.0037	0.0021	0.0059
8.50	0.0	0.0	0.0

Table 8.5-3 Influence of fold size on rms fluctuation of CH_4 concentration

Table 8.5-3 reveals that the concentration fluctuation diminishes when the initial fold size is small. In the mean time, the location of maximum fluctuation shifts from the jet axis towards the outer region as the value of C_Z decreases.

The probability density functions

The influence of fold size on the pdf of temperature, at X/D=60, is demonstrated in Figs.8.5-3 and 8.5-4. The shape of the pdf profile becomes narrower and concentrated around the mean value when the fold size is smaller. For example, at r/D=2.87, the maximum value of P(T) varies from 2.65×10^{-3} in Run No.1 (C_Z=0.328) to 4.08×10^{-3} in Run No.7 (C_Z=0.082), while the corresponding value in Run No.6 (C_Z=0.164) lies between the two extremes and is equal to 3.28×10^{-3}. In the meantime, the contribution of the cold ambient air diminishes (e.g., at r/D=5.55 and 8.50) as the

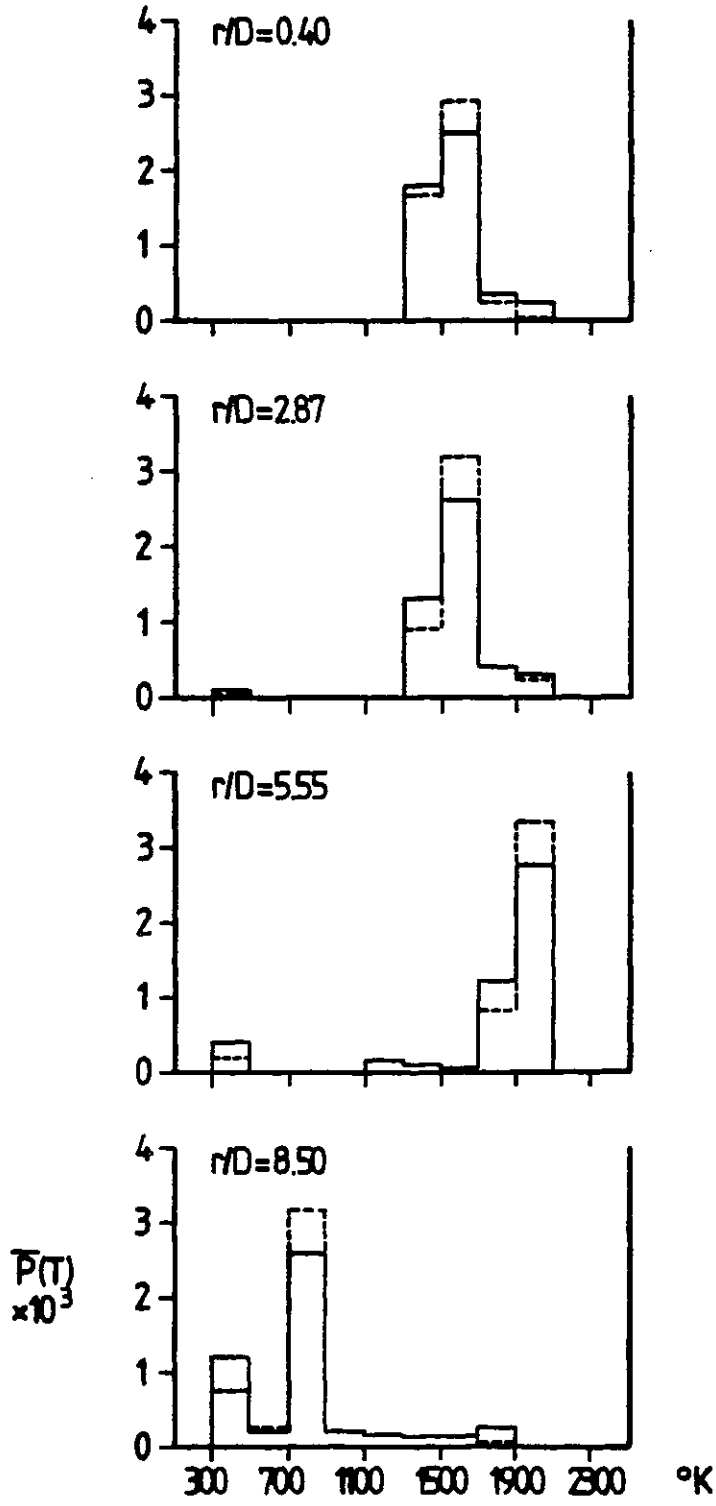

Fig.8.5-3 Influence of fold size on pdf of temperature at X/D=60
(—— Run no.1, ---- Run no.6)

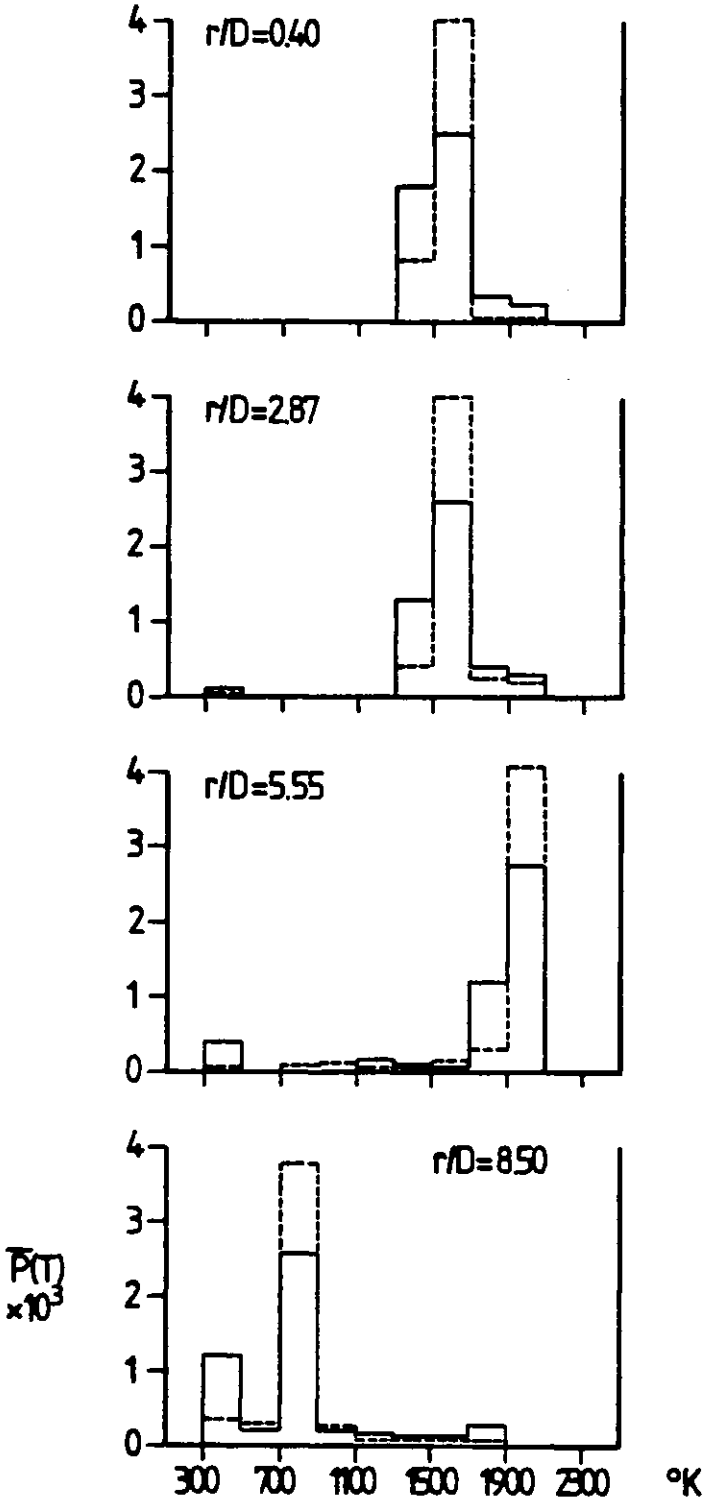

Fig.8.5-4 Influence of fold size on pdf of temperature at X/D=60
(—— Run no.1, ---- Run no.7)

value of C_Z decreases. On the other hand, the distribution in the high temperature domain (between 1900°K and 2100°K) is stronger for lower C_Z values, e.g., the P(T) values at r/D=5.55 for Run nos.6 and 7.

8.6 The influence of fold stretching rate

The turbulent mean quantities

The mean temperature calculated from three different values of fold stretching rate, at X/D=60, are compared and listed in Table 8.6-1.

It is obvious that the flame temperature (at r/D≈5.55) is significantly lower (T=1600°K) in the case of rather moderate stretching effect (e.g.,Run No.9, C_S=0.1). The difference between the peak temperature is about 17% when the value of C_S changes from 2.0 to 0.1, i.e., by a factor of 20. The value of C_S=0.5 in Run No.1 gives the best agreement with experimental data for the present test case.

Radial Location r/D	Mean Temperature °K		
	Run No.1	Run No.8	Run No.9
0.40	1520	1520	1520
1.46	1540	1540	1530
2.87	1590	1610	1550
4.45	1680	1740	1590
5.55	1740	1870	1600
6.80	1430	1440	1410
8.50	787	794	777

Table 8.6-1 Influence of fold stretching rate on the mean temperature

The influence of the stretching rate on the flame temperature is expected, since slower stretching results in greater proportion of cold fresh air inside the fold (the diffusion is slower) and hence reduces the average temperature.

The effects of the stretching rate on the mean concentration of methane, at X/D=60, are demonstrated in Table 8.6-2.

Radial Location r/D	Mean CH_4 molar fraction		
	Run no 1	Run no 8	Run no 9
0.40	0.138	0.141	0.135
1.46	0.126	0.129	0.123
2.87	0.0962	0.0974	0.0940
4.45	0.0502	0.0490	0.0517
5.55	0.0165	0.0104	0.0225
6.80	0.0015	0.0007	0.0022
8.50	0.0	0.0	0.0

Table 8.6-2 Influence of fold stretching rate on mean CH_4 molar fraction

There is a considerable influence of stretching rate on the amount of methane near the flame zone (i.e., at r/D=5.55) where the value of molar fraction varies from 0.0104 to 0.0225, i.e., by a factor of 2.2. Thus, the degree of overlapping of fuel and oxygen in the flame zone is considerably enlarged when a low stretching rate is applied.

The influence of stretching rate on the mean temperature

and compositions, for the hydrogen-air flame, is illustrated in Fig.8.6-1. The temperature obtained from larger stretching rate (C_S=2.0 in Run no 8) exhibit a better agreement with the experimental data. However, the overlapping of hydrogen and oxygen again becomes smaller and the results are similar to those obtained from Run no 6 (c.f. Fig.8.5-1).

The root mean square fluctuation quantities

The temperature fluctuations obtained from three different values of stretching rate, at X/D=60, are plotted in Fig.8.6-2 with the experimental data. It can be observed that the highest fluctuation level rises from 440°K to 710°K as C_S changes from 2.0 to 0.1. It is evident from the graph that the results from Run no.1 yield a better agreement with the measurements on the overall comparison.

Next, the effects of stretching rate on the concentration fluctuation of methane, at X/D=60, are presented in Table 8.6-3.

Radial location r/D	RMS fluctuation of CH_4		
	Run no 1	Run no 8	Run no 9
0.40	0.0464	0.0225	0.0624
1.46	0.0468	0.0272	0.0630
2.87	0.0455	0.0308	0.0579
4.45	0.0360	0.0256	0.0425
5.55	0.0256	0.0201	0.0277
6.80	0.0037	0.0025	0.0045
8.50	0.0	0.0	0.0

Table 8.6-3 Influence of fold stretching rate on rms fluctuation of CH_4 concentration

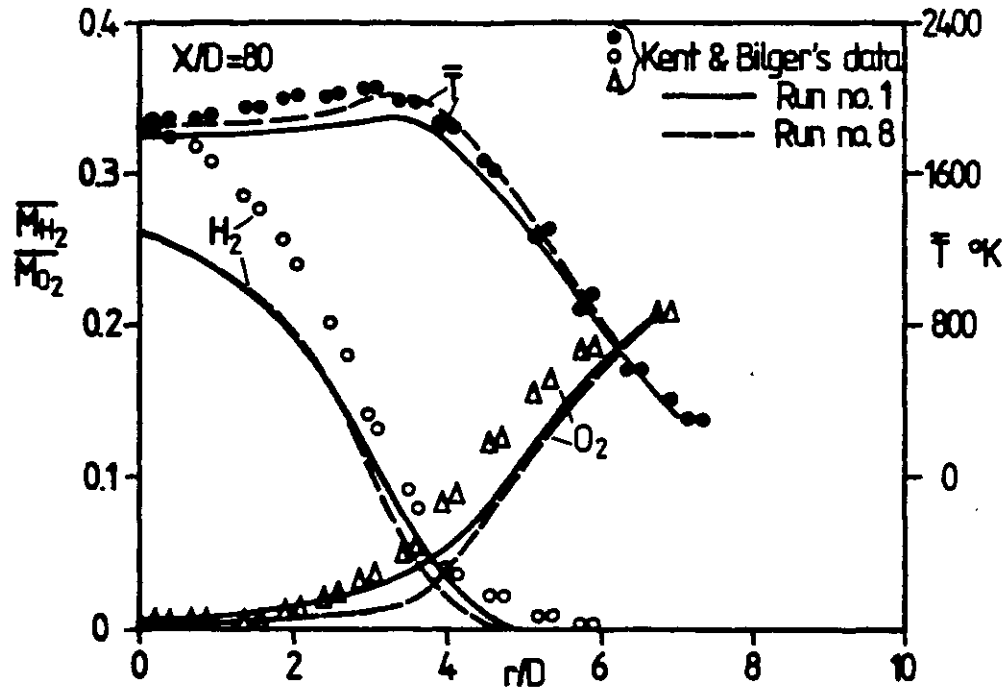

Fig.8.6-1 Influence of fold stretching rate on the mean temperature and compositions for hydrogen-air flame

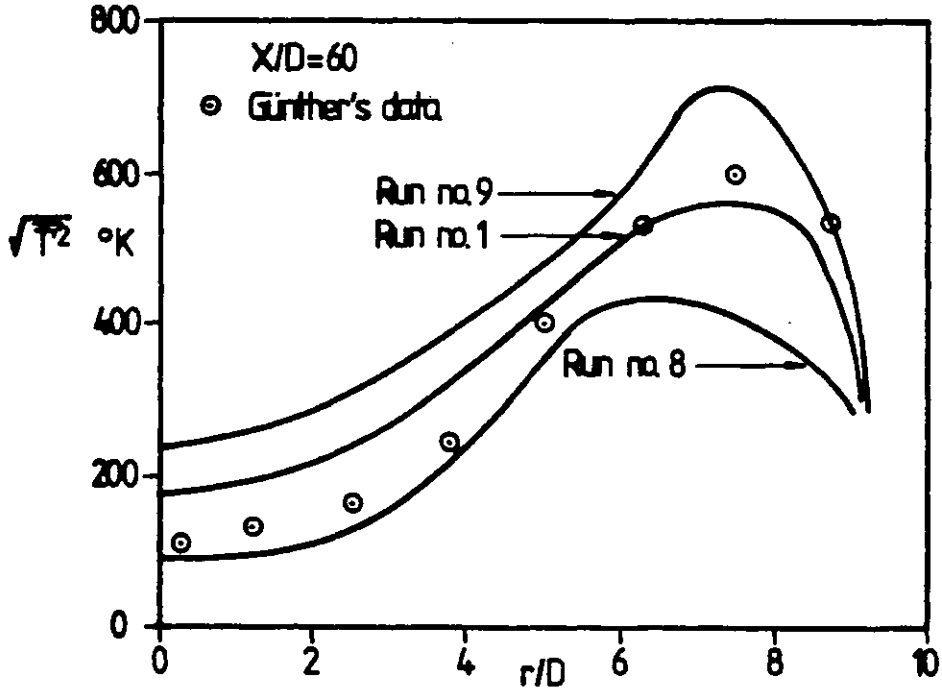

Fig.8.6-2 Influence of fold stretching rate on temperature fluctuation for methane-air flame

The table reveals that the concentration fluctuation level enhances when the stretching rate diminishes. The most distinguished difference occurs around r/D=0.40, where the value from run no.9 is approximately equal to 2.8 times its counterpart in run no.8.

The probability density functions

The influence of fold stretching rate on the pdf of temperature are shown in Figs.8.6-3 and 8.6-4 respectively. In Figs.8.6-3 the higher stretching rate results in narrower pdf and higher peak, indicating that the fluctuation level is lower. On the other hand, the slower stretching rate significantly broadens the pdf profiles as shown in Fig. 8.6-4.

8.7 The influence of grid size

8.7.1 The number of age-interval

The newly introduced coordinate in the present work is the age-coordinate and hence the number of sub-division, NA, should be chosen carefully to yield the grid independent results without overspending the computing resources.

Three different numbers of age-interval have been employed as mentioned in Sec.8.2, where the grid-distribution for each run is given by:

Run no 1 (NA=20): uniform distribution

Run no 10 (NA=10): 0., 0.05, 0.1, 0.15, 0.2, 0.3, 0.4, 0.5, 0.6, 0.8, 1.

Run no 11 (NA=6): 0., 0.1, 0.2, 0.3, 0.4, 0.7, 1.

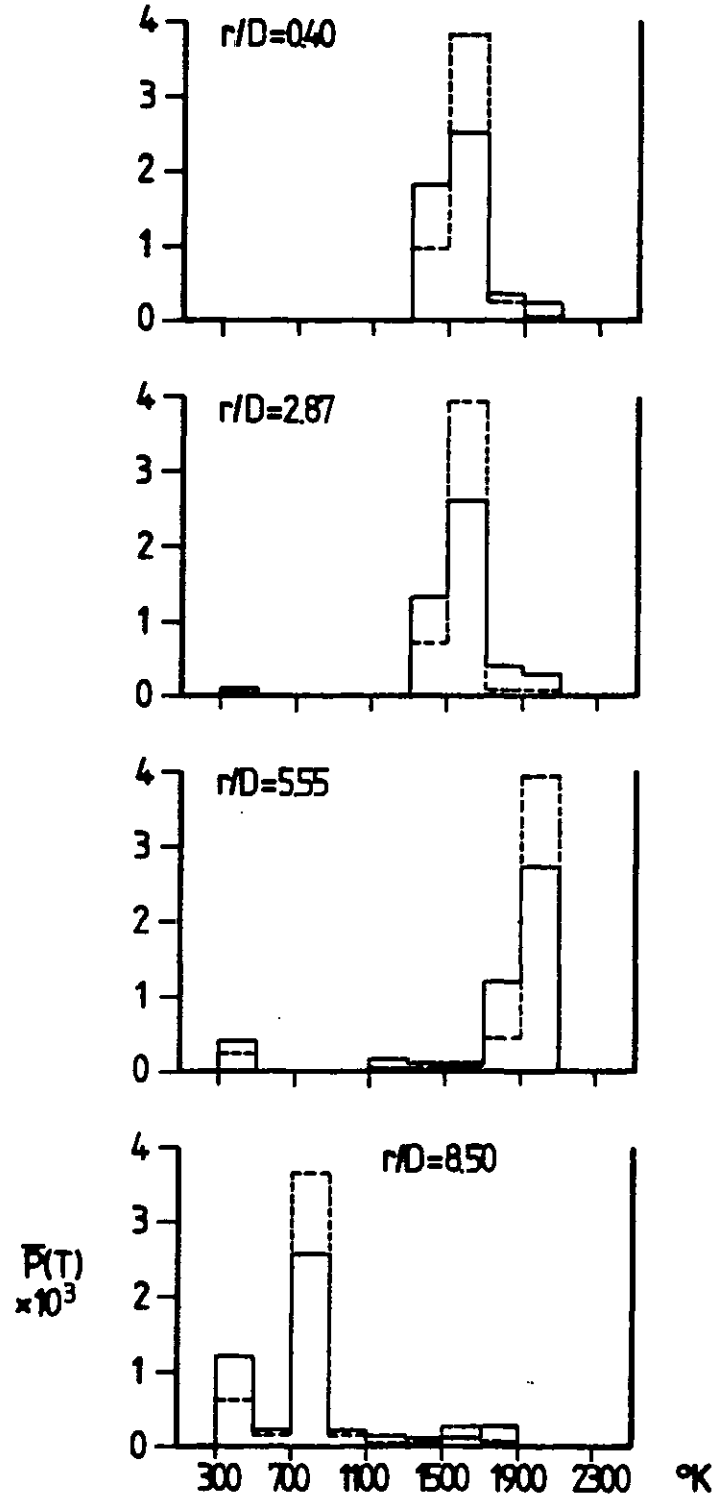

Fig.8.6-3 Influence of fold stretching rate on pdf of temperature at X/D=60 (—— Run no.1, ---- Run no.8)

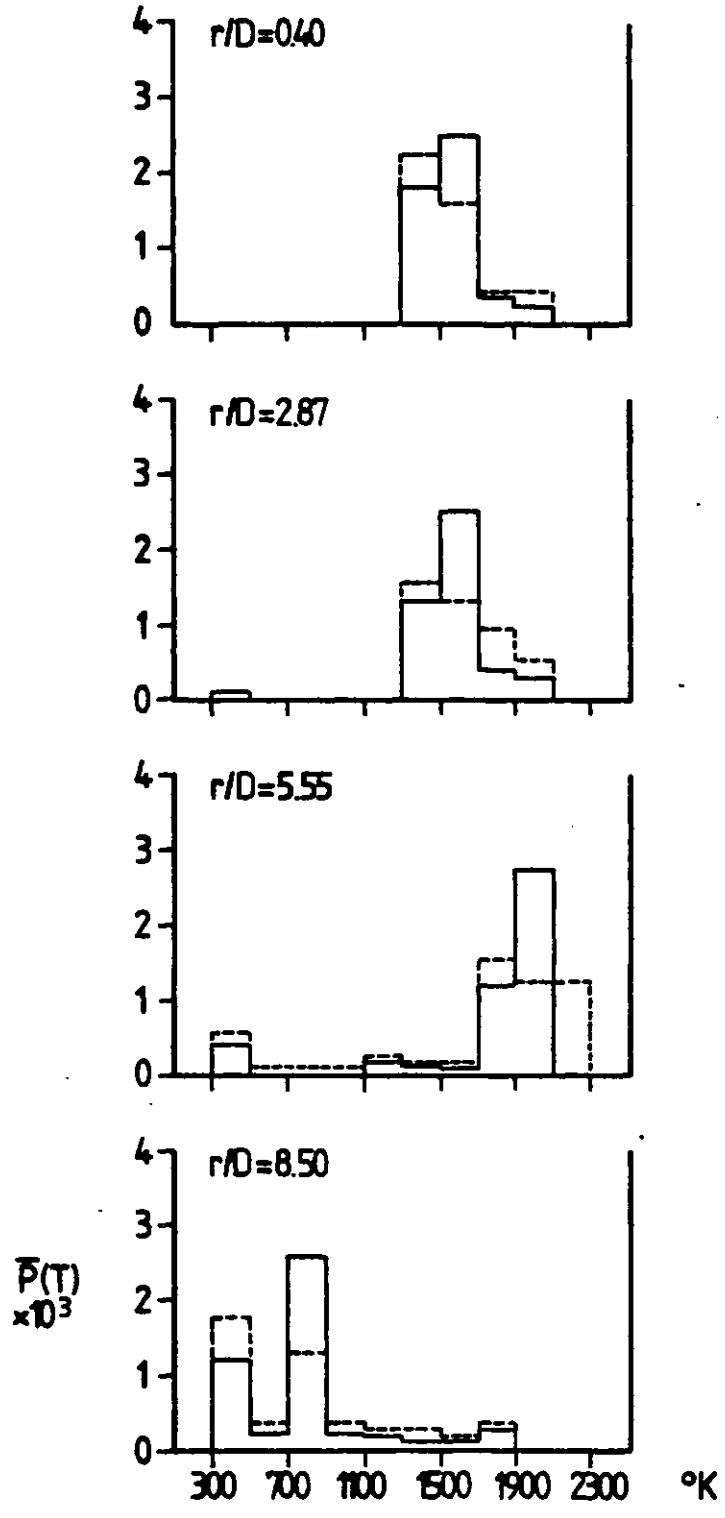

Fig.8.6-4 Influence of fold stretching rate on pdf of temperature at X/D=60 (—— Run no.1, ---- Run no.9)

The influence of NA on various quantities will be described below.

The turbulent mean quantities

The mean temperature calculated from various distributions of age-interval, at X/D=60, is now presented in Table 8.7-1.

Radial location r/D	Mean temperature ^{0}K		
	Run no 1	Run no 10	Run no 11
0.40	1520	1520	1530
1.46	1540	1540	1560
2.87	1590	1590	1600
4.45	1680	1680	1690
5.55	1740	1740	1760
6.80	1430	1430	1430
8.50	787	787	789

Table 8.7-1 Influence of age-interval on mean temperature

Table 8.7-1 reveals that the mean temperatures calculated from NA=20 and NA=10 are actually the same. However, further comparison for other quantities is needed before making any conclusion.

Next, the influence of age-interval on the mean concentration of CH_4, at X/D=60, is demonstrated in Table 8.7-2.

It is again evident that the mean concentration of methane calculated from NA=20 and NA=10 are actually the same, while those obtained from NA=6 only differ very slightly from the former ones. Thus, the attention is now turned to

Radial location r/D	Mean CH_4 molar fraction		
	Run no 1	Run no 10	Run no 11
0.40	0.138	0.138	0.138
1.46	0.126	0.126	0.126
2.87	0.0962	0.0962	0.0962
4.45	0.0502	0.0502	0.0499
5.55	0.0165	0.0165	0.0156
6.80	0.0015	0.0015	0.0012
8.50	0.0	0.0	0.0

Table 8.7-2 Influence of age-interval on mean CH_4 molar fraction

the rms fluctuation quantities.

The root mean square fluctuation quantities

The temperature fluctuations computed from Run Nos.1, 10 and 11 are now compared and listed in Table 8.7-3.

Radial Location r/D	Temperature fluctuations ^{o}K		
	Run No.1	Run No.10	Run No.11
0.40	181	181	147
1.46	200	200	188
2.87	255	255	211
4.45	375	375	370
5.55	475	475	455
6.80	550	545	516
8.50	510	509	504

Table 8.7-3 Influence of age-interval on temperature fluctuations

The discrepancies between the results from Run No.10 and Run No.11 are still significant, but further comparison between Run No.1 and Run No.10 shows that grid independent results have been achieved.

The effects of age-interval on the concentration fluctuation of methane, at X/D=60, are provided in Table 8.7-4.

Table 8.7-4 reveals that the concentration fluctuations calculated from NA=10 (Run No.10) are actually grid-independent. Therefore, ten intervals for the age-space are sufficient to yield grid-independent results.

Radial Location r/D	RMS fluctuations of CH_4		
	Run No.1	Run No.10	Run No.11
0.40	0.0464	0.0462	0.0366
1.46	0.0468	0.0468	0.0417
2.87	0.0455	0.0455	0.0417
4.45	0.0360	0.0360	0.0341
5.55	0.0256	0.0256	0.0245
6.80	0.0037	0.0037	0.0034
8.50	0.0	0.0	0.0

Table 8.7-4 Influence of age-interval on rms fluctuation of CH_4 concentration

The probability density functions

Finally, the influence of the number of age-interval is shown in Fig.8.7-1. The difference between the pdf profiles from Run no 1 and Run no 10 is not visible and hence both of them collapse on the same distribution (indicated by the solid line). The results from Run no 11 are different from the other two runs only in some part of the domain where the dash line appears (the dash line does not appear when it is coincident with the full line).

8.7.2 The number of cross-stream grids

The influence of the number of cross-stream grids, N, will now be presented in a similar way to the preceding subsection. It should be mentioned here that the tabulated form is employed instead of the graphic form, because the values from each run are so close to each other that they are almost undistinguishable graphically.

The turbulent mean quantities

The mean temperature of methane-air flame calculated from N=20 (Run no 1), 30 (Run no 12) and 40 (Run no.13) are presented in Table 8.7-5. The temperatures are obtained from the linear interpolation procedure if the positions of grid nodes (for the case of Run no 12 and Run no 13) do not fall exactly on the selected radial locations, which are taken for Run no 1.

The discrepancies between the results from each run are small, except in the outer region of the jet (e.g. at r/D= 8.50) where the temperature gradient is rather steep.

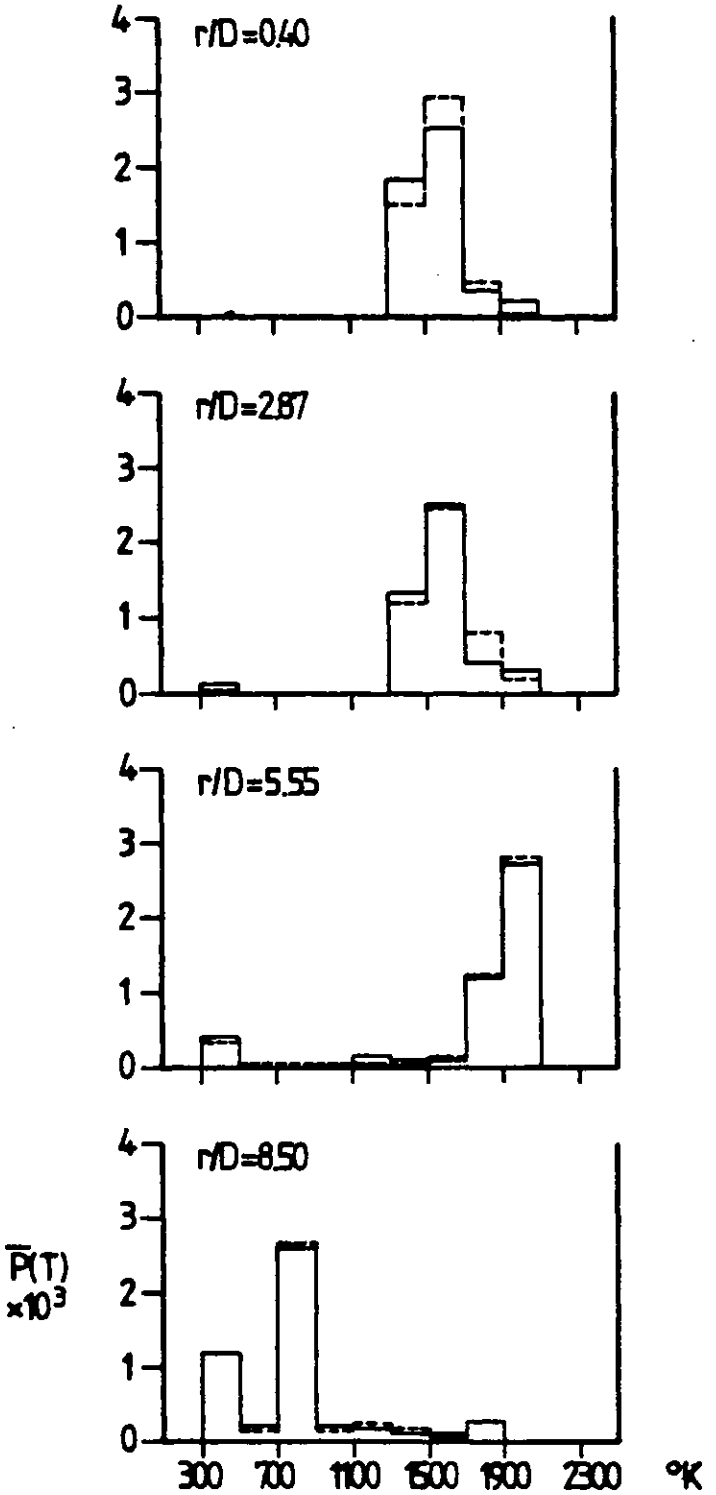

Fig.8.7-1 Influence of age interval on pdf of temperature
(—— Run no.1 and Run no.10,
---- Run no.11)

Radial location r/D	Mean temperature °K		
	Run no 1	Run no 12	Run no 13
0.40	1520	1540	1550
1.46	1540	1560	1570
2.87	1590	1600	1610
4.45	1680	1680	1680
5.55	1740	1730	1730
6.80	1430	1460	1480
8.50	787	870	880

Table 8.7-5 Influence of cross-stream grids on the mean temperature

The influence of the cross-stream grids on the mean concentration of methane, at X/D=60, are presented in Table 8.7-6.

Radial location r/D	Mean CH_4 molar fraction		
	Run no 1	Run no 12	Run no 13
0.40	0.138	0.130	0.128
1.46	0.126	0.119	0.117
2.87	0.0962	0.0920	0.0904
4.45	0.0502	0.0505	0.0492
5.55	0.0165	0.0195	0.0201
6.80	0.0015	0.0025	0.0030
8.50	0.0	0.0	0.0

Table 8.7-6 Influence of the cross-stream grids on the mean CH_4 molar fraction

It can be seen that the results obtained from the first run only differ slightly from the fine-grid computations. Therefore, twenty grid nodes in the cross-stream direction are practically sufficient to yield the grid independent results.

The root mean square fluctuation quantities

The temperature fluctuations computed by three different numbers of cross stream grids, for methane-air flame at x/D =60, are provided in Table 8.7-7. The difference between each set of results is small, except in the outer region of the jet (e.g., at r/D=8.50) where some degree of

discrepancy exists.

Radial location r/D	Temperature fluctuation °K		
	Run no 1	Run no 12	Run no 13
0.40	181	182	183
1.46	200	199	200
2.87	255	256	255
4.45	375	375	374
5.55	475	461	471
6.80	550	538	539
8.50	510	515	520

Table 8.7-7 Influence of cross-stream grids on temperature fluctuation

Radial location r/D	RMS fluctuation of CH_4		
	Run no 1	Run no 12	Run no 13
0.40	0.0464	0.0466	0.0466
1.46	0.0468	0.0455	0.0449
2.87	0.0455	0.0441	0.0436
4.45	0.0360	0.0357	0.0355
5.55	0.0256	0.0263	0.0268
6.80	0.0037	0.0072	0.0076
8.50	0.0	0.0	0.0

Table 8.7-8 Influence of cross-stream grids on rms fluctuation of CH_4 concentration

The influence of cross-stream grids on the concentration fluctuation of methane is demonstrated by Table 8.7-8. It is noticeable that the results have not been significantly altered when more cross-stream grids are employed.

The probability density functions

Figure 8.7-2 shows the effect of cross-stream grids on the pdf of temperature. The difference between the pdfs from Run no 1 and those from Run no 12 is still visible in some parts of the domain (marked by the broken line), but no further variation can be observed when the number of grids increased from 30 to 40.

8.7.3 The size of forward marching step

It is usually essential to employ small marching step in the present solution algorithm to produce accurate results, since no iteration procedure has been employed for the solution of hydrodynamic variables and mixture fraction. The number of marching steps in Run nos 1, 14, 15 and 16 to reach 200 diameters downstream of the jet nozzle are equal to 500, 240, 160 and 1000 respectively. The influence of marching step on various quantities are presented in the following paragraphs.

The turbulent mean quantities

The radial profiles of mean temperature from three runs are plotted in Fig.8.7-3 with the experimental data. Considerable discrepancies can be observed between each curve, indicating that the results calculated from larger marching steps, such as in Run nos 14 and 15, are not yet grid

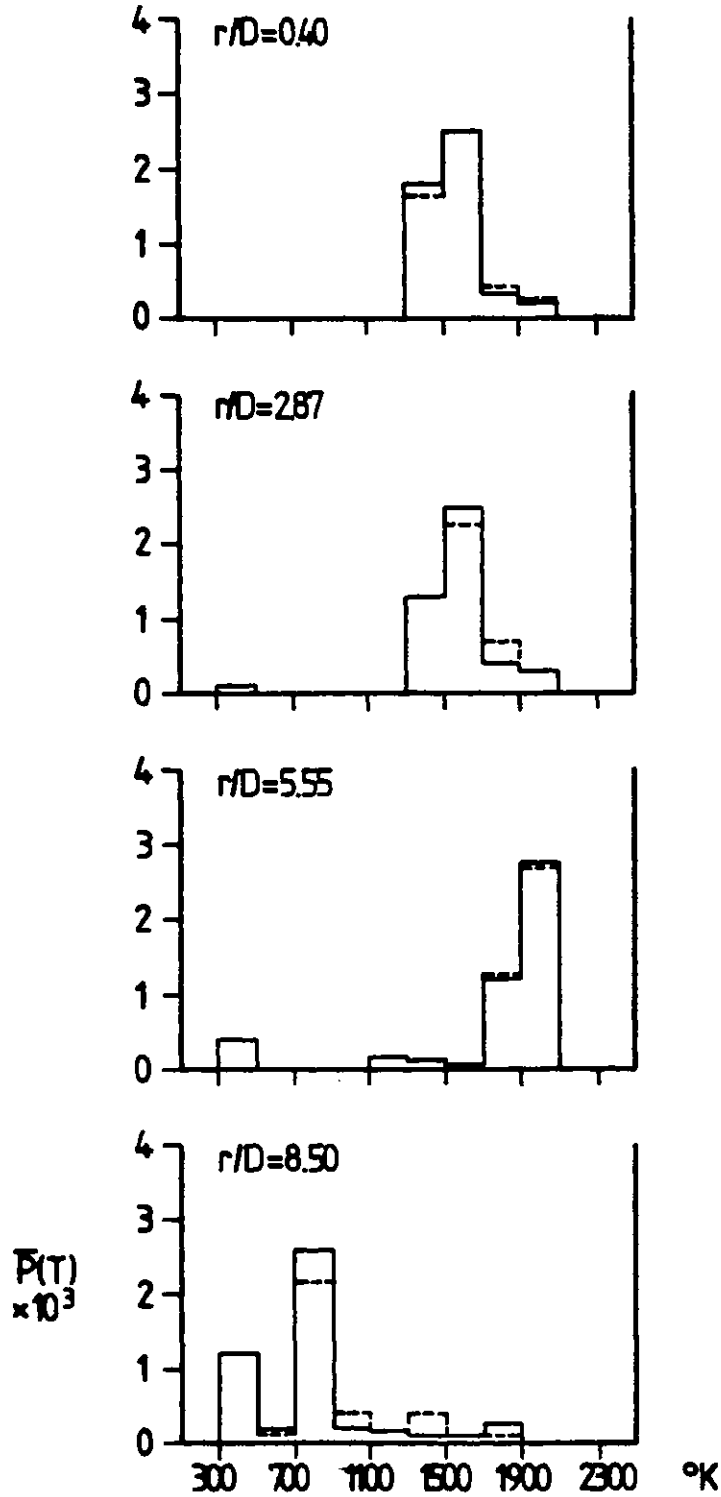

Fig.8.7-2 Influence of cross-stream grids on pdf of temperature at X/D=60
(—— Run no.1, ---- Run nos.12 and 13)

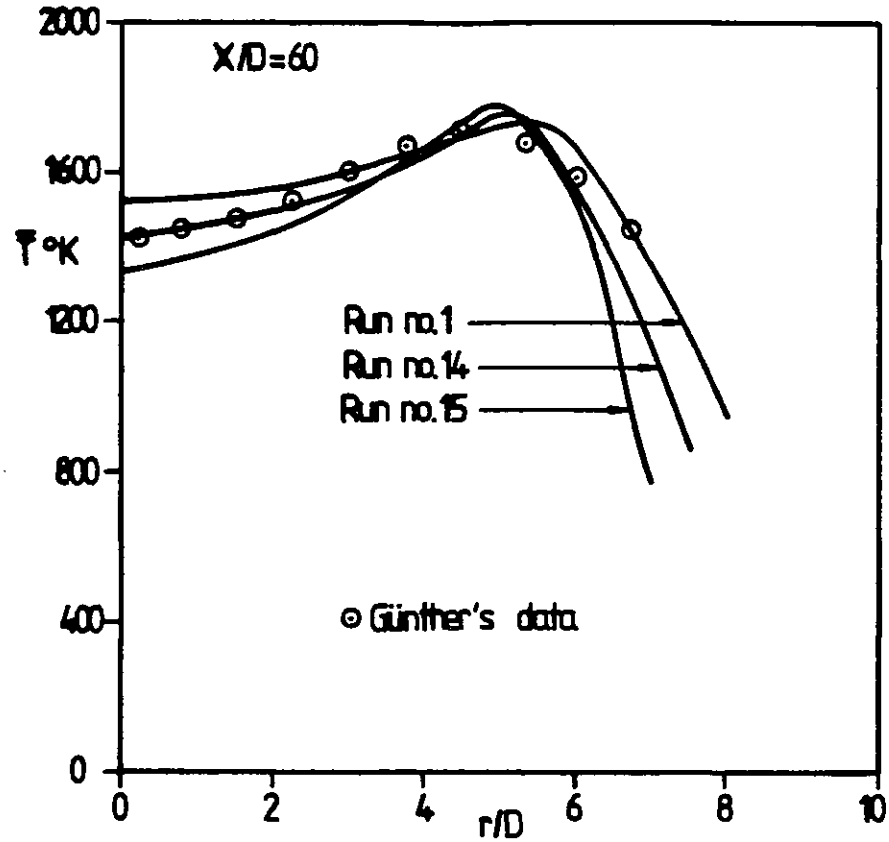

Fig.8.7-3 Influence of marching step on the mean temperature

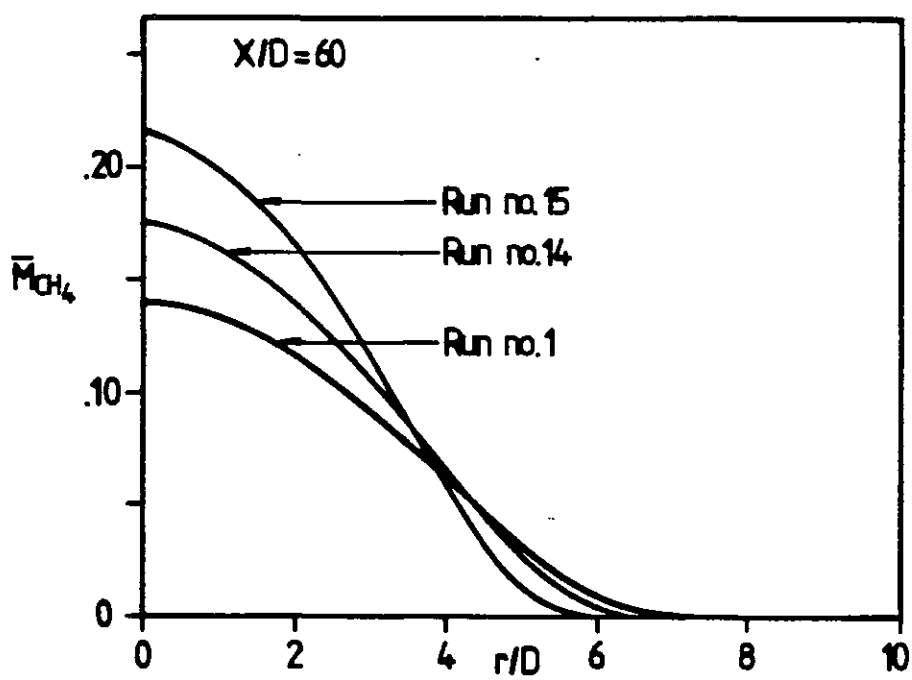

Fig.8.7-4 Influence of marching step on the mean concentration of fuel

independent. However, it has been recognized that the results remain unchanged if an even smaller marching step than that of Run no 1 (say, λ_3=0.005) is adopted in the computation.

Fig. 8.7-4 presents the radial distribution of methane concentration calculated by different marching steps. The profiles corresponding to the larger marching steps exhibit a steeper characteristic.

The root mean square fluctuation quantities

The influence of the number of marching steps on the temperature fluctuations, at X/D=60, is demonstrated in Fig.8.7-5. The spreading of the fluctuation profile is larger and closer to the measurements in the case of Run no 1, in which a small marching step is employed.

The concentration fluctuations of methane calculated from each run are provided in Fig.8.7-6. The difference between each curve is visible for Run nos 1, 14 and 15, but it is again negligible for Run nos 1 and 16.

The probability density functions

Finally, the influence of marching step on the pdf of temperature is plotted in Fig.8.7-7. The results obtained from Run no 14 are not presented here for the sake of clarity. It is evident that the pdfs computed from Run nos 1 and 16 are coincident, indicating that the value of numerical factor λ_3=0.01 is sufficient to produce grid independent results.

8.8 Closure

The parametric studies performed in the present chapter reveals that the fluctuation quantities and probability density

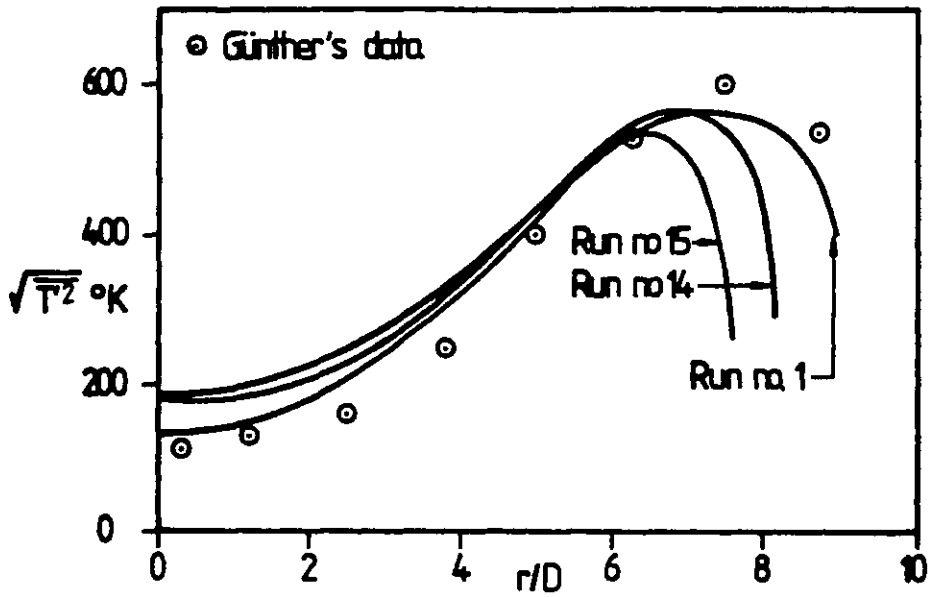

Fig.8.7-5 Influence of marching step on temperature fluctuation at X/D=60

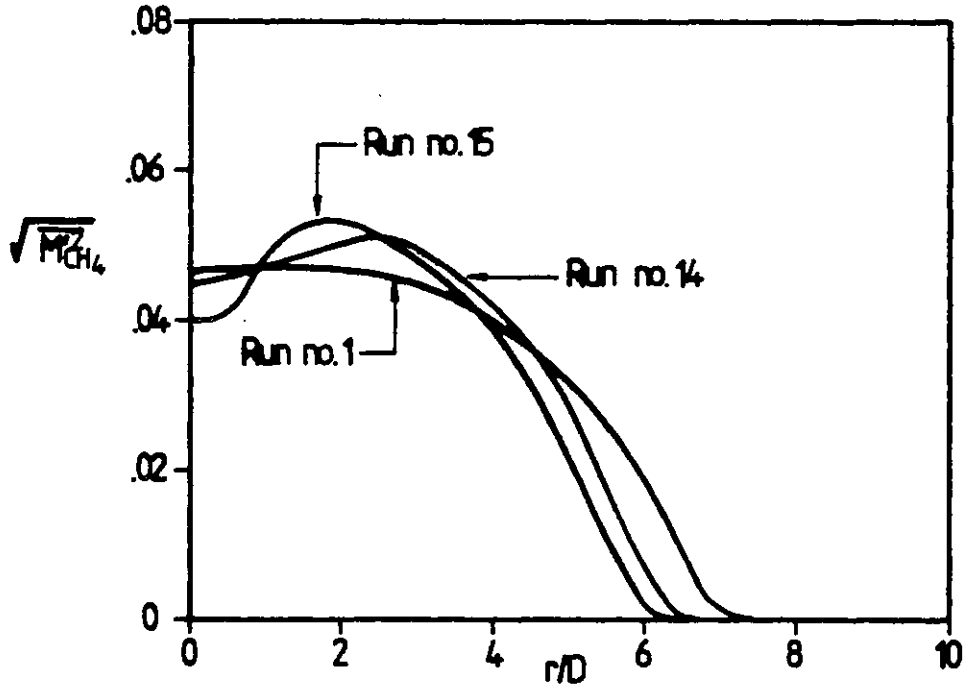

Fig.8.7-6 Influence of marching step on concentration fluctuation at X/D=60

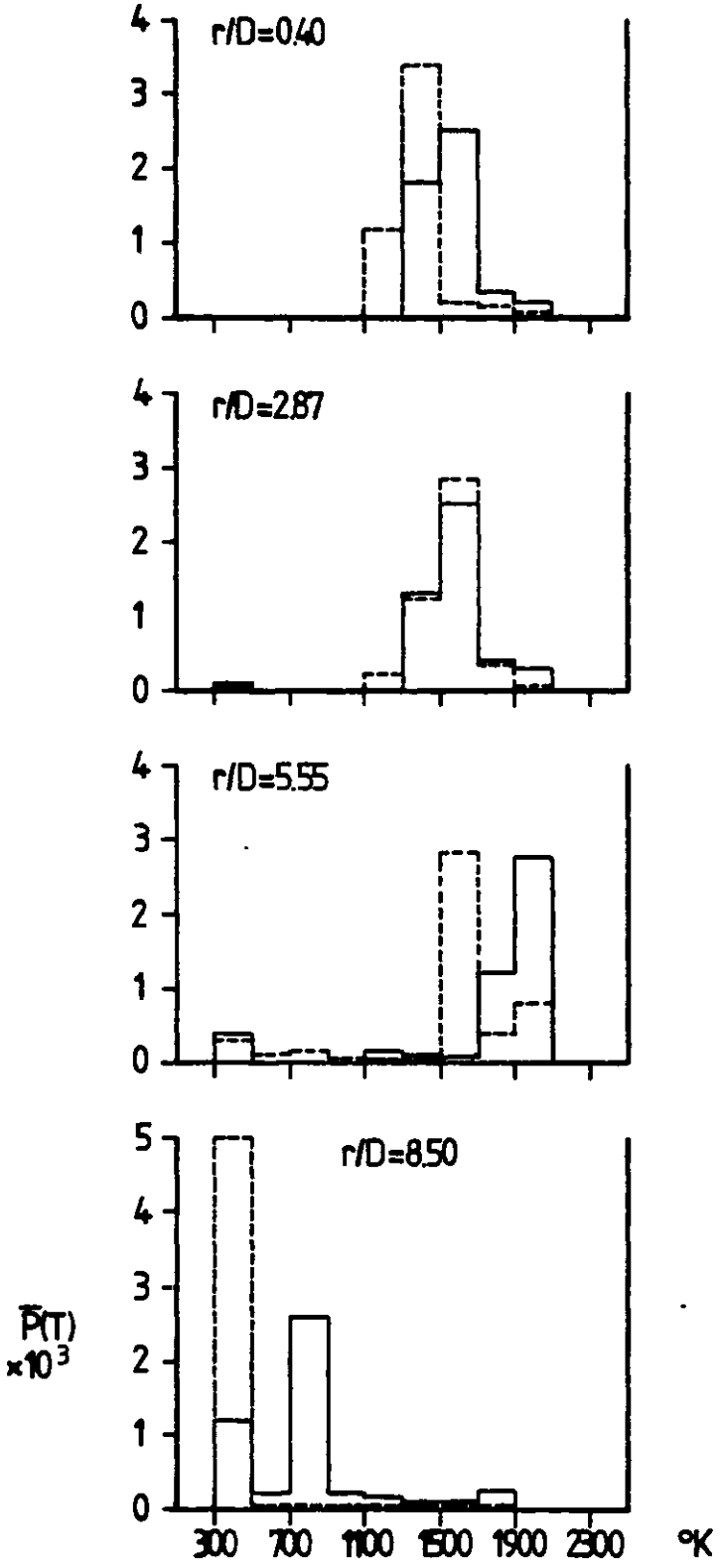

Fig.8.7-7 Influence of marching step on pdf of temperature at X/D=60
(—— Run nos.1 and 16,
---- Run no.15)

functions are generally more sensitive to the presumptions made in the ESCIMO theory than the turbulent mean properties.

It has been demonstrated that satisfactory agreement between the predictions and measurements can be achieved when proper values of various parameters are chosen, for both hydrogen-air flame and methane-air flame. The encouraging fact is that same set of parameters is capable of predicting the important phenomena for the turbulent combustion in the two different fuel-air reaction systems investigated.

Nevertheless, the discrepancies between the theoretical calculations and the experimental data on the overlapping of reactants and the probability density functions of temperature do imply that the well known intermittency effects of turbulence have to be included more explicitly. Otherwise, more extreme values of some parameters (say, the stretching rate) need to be employed during the computation.

CHAPTER 9

CONCLUSIONS

9.1 Achievements of the present study

The main achievements of the present study and the conclusions are summarized below.

The Demographic Aspects of the "ESCIMO" Theory

(a) The mathematical formulation for the governing partial differential equations of folds-population has been set up for the two-dimensional boundary layer flows. In addition to the turbulent convection and diffusion terms included in the equations, the source terms contain the simple-aging, birth rate and re-engulfment rate respectively. The age-coordinate is discretized into a number of intervals in the finite difference schemes which result in a set of equations, each one describing the population of folds belong to a particular age-interval.

(b) The non-dimensional age and non-dimensional population distribution have been introduced and the finite difference equations have been transformed and expressed in terms of these variables. The upwind differencing in the non-dimensional age-coordinate is adopted to ensure the physical plausibility of the results.

(c) The major hypothesis employed in the calculation of folds-population is the distribution of fold formation rate in the cross-stream direction. The total amount of

fold formation rate is however related to the entrainment rate through the proportion of fresh layer in newly formed folds. Various distributions have been made and their influence on the population distribution extensively investigated. The validity of each distribution can only be assessed indirectly (through the combined demographic and biographic analysis) in the present stage, since the direct experimental evidence is not available.

The Combined Demographic and Biographic Analyses

(a) The only variable needs to be solved in the biographic part is the mixture fraction, since the chemical reaction is relatively fast and the molecular diffusivities of all species are assumed to be equal. The resultant equation has been solved by the "profile method", because the computer time is only 25% compared with that of "time-marching method". The accuracy of the profile method is satisfactory, since the results calculated from the "time-marching method" virtually reproduced the same quantitative pictures.

(b) The trajectories of the folds are supposed, in the present work, to be coincident with the constant-mixture fraction contours. The birth place of different folds is located with the aid of the age, which is related to the distance through the definition. The folds are subject to the stretching effect (caused by the turbulent flow) while they are moving downstream. The link between the demographic and biographic part of the theory has now been established in a self-consistent way.

(c) The turbulent reacting plane mixing layer is chosen as the first case to verify the credibility of the theory. Both the flow configuration and the chemical kinetics are simple enough to avoid the distraction. The predictions include the turbulent mean properties, the fluctuation intensities and the probability density functions. The quantitative agreement between the present computations and the measurements of Batt (1977) is generally fair.

(d) The other two test cases are the turbulent hydrogen-air jet diffusion flame and methane-air jet diffusion flame. It has been shown from the comparison between the theoretical calculations and experimental data that most of the important features can be predicted. However, some quantitative discrepancies do appear in the mean compositions (say, fuel and oxygen) and temperature, pdf pf temperature, indicating that some improvements on the turbulence model itself are still required.

(e) The sensitivity analyses performed in this work have shown the influence of various presumptions, such as the distribution of fold formation rate, initial fold composition, fold size at birth and stretching rate, on the predictions. It is worth mentioning here that the same set of parameters and constants can produce reasonably good results for all cases considered. The successful performance in the computation of fluctuation quantities is of more importance to the development of present model, since the mean quantities can be fairly calculated from less sophisticated method as well.

(f) The main aim of this work is to use a new and more fundamental approach to tackle the conventional combustion problems. The increase of computations is the price to be paid off and it can be perceived that even larger computer time is required if the complex chemical-kinetics scheme is to be employed. But the number of equations to be solved in the biographic part only increases linearly with the number of species considered, which is still moderate in comparison with the moment closure method and pdf method. The fact that the computational amount in demographic part is not influenced by the chemistry scheme reveals another important feature of the "ESCIMO" theory.

9.2 Suggestions for future work

In order to make the present model more complete and applicable to complex-flow situations, the following steps need to be realised:

(a) To include the intermittency effects in the turbulence model, so that the "ESCIMO" theory can be incorporated with a more realistic description of turbulence phenomena. It has been shown by the experimental evidence that, in the outer part of any turbulent mixing layer and jet, the fluid found by a fixed sampling probe is turbulent only for a proportion of time which diminishes from 100 to 0% as the distance from the mid-region increases.

A possible approach is to treat the "turbulent" and

"non-turbulent" portion as two separate phases. The mathematical treatments can then follow closely those of the real two-phase flows (Spalding, 1982). The interphase friction laws, interphase mass-transfer and interphase heat-transfer laws will need to be modified for this problem, based on the experimentally observed effective Prandtl number and the "form drag" associated with the movement of fluid parcels.

An extra pressure term will be needed in the momentum equation of turbulent fluid (say, the first phase in the two-phase approach) to express the effect of turbulent separation.

Another major outcome of this intermittency model is that the engulfment rate (related to entrainment rate) can be calculated now and hence the presumption concerning the distribution of fold formation rate is no more required. This consequence will further promote the physical reality of ESCIMO model and result in better quantitative agreement with the experimental data.

The GENMIX2P computer code (Spalding,1981a) and PHOENICS code (Spalding,1981b) are both capable of performing the computational task, since the mechanism of solving two-phase flows are already built in.

(b) To apply the present theory to the flows of elliptic type, where the recirculation zone exists inside the flow domain. The tracing of the folds will become the major issue in the development work, since the folds may come from all directions around the point being considered.

The first possible approach is to treat the recirculation zone separately, and to take into account of the folds which are created within a small distance only (e.g., the average radius of the recirculation zone).

(c) To extend the present theory in three-dimensional combustion problems, such as the gas turbine combustors and internal combustion engines. It is necessary to devise an efficient solution procedure for these flow cases. The full biographic analysis needs to be employed (e.g., using the time-marching method), when the chemical reaction rate is moderate or slower than the turbulent mixing process. In order to economise the computational cast, some sacrifice will have to be made on the demographic side. For instance, the number of folds-group has to be reduced to the minimum allowable level (say, three or four groups).

(d) To incorporate the pollutant formation schemes, such as those of nitrogen oxides, into the present theory. The chemical reaction mechanism of nitrogen oxides has been investigated and established by many researchers, the review paper of Bowman (1975) provided a good collection of information. The process of pollutant formation is kinetically controlled and the assumption of chemical equilibrium is not valid.

(e) To perform the experimental work in simple turbulent shear flows, such as mixing layers and jets, in order to measure (or deduce) the fold formation rate and the

fold composition. A possible way is to measure the electrical conductivity (and hence the concentration of ions) in the salt-water solution, in which the salt solution is injected into the water jet at various positions.

REFERENCES

ALBER,I.E. and BATT,R.G. (1975)
"Diffusion-limited chemical reactions in a turbulent shear layer".
AIAA Journal, Vol.14, no.1, pp.70-76.

BALLANTYNE,A. and BRAY,K.N.C. (1976)
"Investigation into the structure of jet diffusion flames using time-resolved optical measuring techniques".
Sixteenth symposium (Int.) on combustion, pp.777-787.
The Combustion Institute, Pittsburgh.

BALLANTYNE,A. and MOSS,J.B. (1977)
"Fine wire thermocouple measurements of fluctuating temperature".
Combustion Science and Technology, Vol.17, pp.63-72.

BATT,R.G. (1977)
"Turbulent mixing of passive and chemically reacting species in a low-speed shear layer".
J.Fluid Mech., Vol.82, Part 1, pp.53-95.

BECKER,H.A. (1975)
"Effects of concentration fluctuations in turbulent diffusion flames". Fifteenth symposium(Int.) on Combustion,pp.601-615.
The Combustion Institute, Pittsburgh.

BILGER,R.W. (1976)
"Turbulent jet diffusion flames"
Prog.Energy Combust.Sci., Vol.1, pp.87-109.

BILGER,R.W. (1979)
"Effects of kinetics and Mixing in Turbulent Combustion"
Comb.Sci.Technol., Vol.19, p.89.

BILGER,R.W. (1980)
"Turbulent flows with Nonpremixed Reactants".
In Turbulent Reacting Flows, ed.Libby,P.A. and Williams,F.A.
Springer-Verlag, Berlin.

BONNIOT,C., BORGHI,R. and MAGRE,P. (1978)
"Turbulent combustion in a stirred combustor".
Paper presented at AIAA meeting, Los Angeles.

BORGHI,R. (1974)
"Chemical reactions calculating in turbulent flows: application to a co-containing turbojet plume".
Adv.Geophys., Vol.18B, pp.349-365.

BORGHI,R. (1979)
"Models of turbulent combustion for numerical predictions"
Paper presented at Von-Karman Institute of Fluid Dynamics Meeting, Rhode Saint Genese, Belgium, 1979.

BOWMAN,C.T. (1975)
"Kinetics of pollutant formation and destruction in combustion".
Prog.Energy.Combust.Sci., Vol.1, pp.33-45.

BRAY,K.N.C. and MOSS,J.B. (1977)
"A unified statistical model of the premixed turbulent flame".
Acta Astronautica, Vol.4, p.291.

BRAY,K.N.C. (1979)
"The interaction between turbulence and combustion".
Seventeenth Symposium (Int.) on Combustion, The Combustion Institute, Pittsburgh, pp.223-233.

BRAY,K.N.C. (1980)
"Turbulent flows with premixed reactants".
In Turbulent Reacing Flows,ed. Libby,P.A. and Williams,F.A.
Springer-Verlag, Berlin.

BROWN,G.L. and ROSHKO,A. (1974)
"On density effects and large structure in turbulent mixing layers".
J.Fluid Mech., Vol.64, pp.775-816

DONALDSON,C.DuP. (1974)
In "Turbulent mixing in non-reactive and reactive flows".
ed. Murthy,S.N.B., p.131, Plenum, New York, London.

DONALDSON,C.DuP. and HILST,G.R. (1972)
"Effect of inhomogeneous mixing on atmospheric photochemical reaction".
Environ.Sci.Technol., Vol.6, p.812.

DOPAZO,C. (1975)
"Probability density function approach for a turbulent axisymmetric heated jet. Centerline evolution".
Phys.Fluids Vol.18, pp.397-404.

DRYER,F.L. and GLASSMAN,I. (1972)
"High temperature oxidation of CO and CH_4".
Fourteenth Symposium (Int.) on Combustion, The Combustion Institute, Pittsburg, p.987.

DRYER,F.L. and WESTBROOK,C.K. (1979)
"Chemical kinetic modelling for combustion applications".
Paper presented at the Propulsion and Energetics Panel 54th Specialist's Meeting, Cologne, West Germany, October 1979. NATO AGARD Conference Proceedings no.275, University of Claifornia, Lawrence Livermore National Laboratory Report UCRL-81777, September 1977.

ELGHOBASHI,S.E., PRATT,D.T., SPALDING,D.B. and SRIVATSA,S.K.(197
"Unsteady combustion of fuel spray in jet-engine afterburners".
Third Air-Breathing Engines Conference, Munich, Germany, March, 1976.

FAN,W.C. (1982)
Private communication at Imperial College Computational Fluid Dynamics Unit.

FIEDLER,H.E. (1974)
"Transport of heat across a plane turbulent mixing layer"
Adv. in Geophys., Vol.18, pp.93-109.

FIEDLER,H.E. (1975)
"On turbulent structure and mixing mechanism in free turvulent shear flows".
In Turbulent Mixing in Nonreactive and Reactive Flows, A Project Squid Workshop, pp.381-410, Plenum.

GANJI,A.T. and SAWYER,R.F. (1980)
"Turbulence, combustion, pollutant and stability characterisation of a premixed step combustor".
NASA CR 3230.

GIBSON,M.M. and MORGAN,B.B. (1970)
"Mathematical model of combustion of solid particles in a turbulent stream with recirculation".
Journal of the Institute of Fuel, Vol.43, pp.517-523.

HARLOW,F.H. and NAKAYAMA,P. (1968)
"Transport of turbulent energy decay rate".
Los Alomos Scientific Lab., University of California, Report LA-3854.

HAWTHORNE,W.R., WEDDELL,D.S. and HOTTEL,H.C. (1949)
Third Symposium on Combustion, Flame and Explosion phenomena, p.267, Williams and Wilkins, Baltimore.

HUTCHINSON,P., KHALIL,E.E. and WHITELAW,J.H. (1978)
"Turbulent combustion" ed. Kennedy,L.A., Vol.58 of Progress in Astronautics and Aeronautics, AIAA, p.211.

JANICKA,J., KOLBE,W. and KOLLMAN,W. (1978)
"The solution of a pdf-transport equation for turbulent diffusion flames", in Proceedings of the 1978 Heat Transfer and Fluid Mechanics Institute, ed. Crowe,C.T., Grosshandler, W.L., Stanford University Press, p.298, Stanford.

JANICKA,J. and KOLLMAN,W. (1979)
"A two-variables formalism for the treatment of chemical reactions in turbulent H_2-air diffusion flames".
Seventeenth Symposium (int.) on Combustion. The Combustion Institute, Pittsburgh, pp.421-430.

JONES,W.P. and WHITELAW,J.H. (1978)
"Coupling of turbulence and chemical reaction".
Workshop on Modelling of Combustion in Practical Systems, Los Angeles.

KAYS,W.M. (1969)
"Convective heat and mass transfer".
McGraw-Hill Book Company, New York.

KENNEDY,I.M. and KENT,J.H. (1981)
"Scalar measurements in a co-flowing turbulent diffusion flame".
Combustion Sci. Technol., Vol.25, pp.109-119.

KENT,J.H. (1970)
"A Noncataltic Coating for Platimum-Rhodium Thermocouples".
Combustion and Flame, Vol.14, p.279

KENT,J.H. and BILGER,R.W. (1973)
"Turbulent diffusion flames"
Fourteenth (Int.) Symposium on Combustion, p.615-625.
The Combustion Institute, Pittsburgh.

KENT,J.H. and BILGER,R.W. (1976)
"The prediction of turbulent flame fields and nitric oxide formation".
Sixteenth (Int.) Symposium on Combustion. The Combustion Institute, pp.1643-1656.

KOLBE,W. and KOLLMAN,W. (1980)
"Prediction of turbulent diffusion flames with a four-equation turbulence model".
Acta Astronautica, Vol.7, pp.91-104, Pergamon Press.

LAUNDER,B.E. and SPALDING,D.B. (1972)
"Mathematical models of turbulence".
Academic Press, London.

LAUNDER,B.E. and SPALDING,D.B. (1973)
"The numerical computation of turbulent flows".
Computer Methods in Applied Mechanics and Engineering, Vol.3, pp.269-289.

LENZ,W. and GÜNTHER,R. (1980)
"Measurements of fluctuating temperature in a free-jet diffusion flame".
Combustion and Flame, Vol.37, pp.63-70.

LENZE,B. and GÜNTHER,R. (1975)
"Ausbrand und warmeent-wicklung in erdgas-diffusions-flamen".
Brennstoff-Warme-Kraft, Vol.17, pp.387-394

LIBBY,P.A.,BRAY,K.N.C. and MOSS,J.B. (1979)
"Effects of finite reaction rate and molecular transport in premixed turbulent combustion".
Combustion and Flame, Vol.34,n.3, p.285.

LIBBY,P.A. and WILLIAMS,F.A. (1981)
"Some implications of recent theoretical studies in turbulent combustion".
AIAA Journal, Vol.19, p.261.

LOCKWOOD,F.C. and NAGUIB,A.S. (1975)
"The predictions of the fluctuations in the properties of free, round-jet, turbulent, diffusion flames".
Combustion and Flame, Vol.24, pp.109-124.

LOCKWOOD,F.C. and ODIDI,A.O.O. (1976)
"Measurement of mean and fluctuating temperature and of ion concentration in round free-jet turbulent diffusion and premixed flames".
Fifteenth Symposium (Int.) on Combustion. The Combustion Institute, Pittsburgh, p.561.

LOCKWOOD,F.C. (1977)
"The modelling of premixed and diffusion turbulent combustion".
Combustion and Flame, Vol.29, n.2, p.111

MAO,K.W. and TOOR,H.L. (1970)
"A diffusion model for reactions with turbulent mixing"
AICHE J., Vol.16, p.49

MARBLE,F.E. and ADAMSON,T.C. (1954)
"Selected combustion problems", Vol.2, p.68,
London:Butterworth's.

MASON,H.B. and SPALDING,D.B. (1973)
"Prediction of reaction rates in turbulent premixed boundary layer flows"
Combustion Institute European Symp., pp.601-606

O'BRIEN,E.E. (1971)
"Turbulent mixing of two rapidly reacting chemical species"
Phys.Fluids Vol.14, pp.1326-1331.

PATANKAR,S.V. and SPALDING,D.BRIAN (1967)
"A finite-difference procedure for solving the equations of the two-dimensional boundary layer".
Int.J.of Heat and Mass Transfer, Vol.10, pp.1389-1411.

PERRY,R.H. and CHILTON,C.H. (1973)
"Chemical Engineers' Handbook".
McGraw-Hill Book Company. New York, 5th ed.

POHLHAUSEN,K. (1921)
Z.Angew.Match.Mech., Vol.1, p.252.

POPE,S.B. (1976)
"The probability approach to the modelling of turbulent reacting flows".
Combustion and Flame, Vol.27, p.299

RICHTER,W. and QUACK,R. (1974)
"A mathematical model of a low-volatile pulverized fuel flame".
Heat Transfer in Flames, ed. Afgan,N.H. and Beer,J.M., pp.95-110, Scripta Book Co.

ROBERTS,P.T. and MOSS,J.B. (1981)
"A wrinkled flame interpretation of the open turbulent diffusion flame".
Eighteenth Symposium (Int.) on Combustion, pp.941-950.
The Combustion Institute, Pittsburgh.

SERAG-ELDIN,M.A. (1977)
"The numerical prediction of the flow and combustion processes in a three-dimensional can combustor".
Ph.D. Thesis, University of London.

SCHLICHTING,H. (1979)
"Boundary-Layer Theory".
McGraw-Hill Book Co., 7th.ed.

SMITH,G.D. (1978)
"Numerical Solution of Partial Differential Equations: Finite Difference Mehtods".
Oxford University Press, Oxford. 2nd.ed.

SPALDING,D.BRIAN (1958)
"Approxiamte solutions of transcient and two-dimensional flame phenomena: Constant-enthalpy flames".
Proc.of the Royal Society A, Vol.245, pp.352-372.

SPALDING,D.BRIAN (1970a)
"Mathematische Modelle Turbulenten Flammen".
In Vorträge der VDI-Tagung Karlsruhe, 1969;
Verbrennung und Feuerungen. VDI-Bericht No.146;
VDI Verlag, Dusseldorf, pp.25-30.

SPALDING,D.BRIAN (1970b)
"Notes on the Parmix Program"
Imperial College, Heat Transfer Report BL/TN/A/35.

SPALDING,D.BRIAN (1971a)
"Concentration fluctuations in a round turbulent free jet".
Chemical Engineering Science, Vol.26, pp.95-107.

SPALDING,D.BRIAN (1971b)
"Mixing and chemical reaction in steady confined turbulent flames".
Thirteenth Synposium (Int.) on Combustion, p.649,
The Combustion Institute, Pittsburgh.

SPALDING,D.BRIAN (1976a)
"Mathematical models of turbulent flames: a review"
Combustion Science and Technology, Vol.13, pp.3-25.

SPALDING,D.BRIAN (1976b)
"The ESCIMO theory of turbulent combustion".
Imperial College, Mechanical Engineering Department
Report No.HTS/76/13

SPALDING,D.BRIAN (1978a)
"GENMIX: a general computer program for two-dimensional parabolic phenomena".
Pergamon Press, Oxford, U.K.

SPALDING,D.BRIAN (1978b)
"Chemical reactions in turbulent fluids".
Proceedings of Levich Birthday Conference, Advance Publications, Vol.1, pp.321-338.

SPALDING,D.BRIAN (1979a)
"Theories of turbulent reacting flows".
Paper presented at AIAA Conference, New Orleans, 1979.
Imperial College, Heat Transfer Section Report No. HTS/79/1.

SPALDING,D.BRIAN (1979b)
"The influences of laminar transport and chemical kinetics on the time-mean reaction rate in a turbulent flame".
Seventeenth Symposium (Int.) on Combustion, pp.431-440.
The Combustion Institute, Pittsburgh.

SPALDING,D.BRIAN (1981a)
"GENMIX 2P: Notes and Listing".
Imperial College of Science and Technology, Department of Mechanical Engineering Report No.HTS/81/1.

SPALDING,D.BRIAN (1981b)
"A general purpose computer program for multi-dimensional one and two-phase flow".
Mathematics and Computers in Simulation, Vol.XXIII, pp.267-276, North Holland Press.

SPALDING,D.BRIAN (1982)
"Chemical reaction in turbulent fluids".
4th Physicochemical Hydrodynamics Conference,
New York City, June 1982.

STEPHENSON,P.L. (1972)
"Development of models for predicting laminar and turbulent flames".
Ph.D. Thesis, University of London.

SUNYACH,M. and MATHIEU,J. (1969)
"Mixing zone of a two-dimensional jet".
Int.J.Heat and Mass Transfer, Vol.12, pp.1679-1697.

TAM,L.T. (1981)
"The theory of turbulent flow with complex chemical kinetics".
Ph.D. Thesis, University of London.

VASSILATOS,G. and TOOR,H.L. (1965)
AICHE J.,Vol.11, p.666.

VON KARMAN,T. (1921)
Z.Agnew.Match.Mech., Vol.1, p.233.

WEGENER,P.P. (1959)
"Supersonic nozzle flow with a reacting gas mixture"
The Physics of Fluids, Vol.2, pp.264-275.

WINANT,C.D. and BROWAND, (1974)
"Vortex pairing: the mechanism of turbulent mixing-layer growth at moderate Reynolds number."
J.Fluid Mech., Vol.63, pp.237-255.

WITTMER,V. (1980)
"Geschwindigkeit und Temperatur in einer turbulenten Freistrahl-Diffusionsflammen".
Ph.D. Thesis, University of Karlsruhe, West Germany.

WYGNANSKI,I. and FIEDLER,H. (1969)
"Some measurements in the self-preserving jet".
J.Fluid Mech., Vol.38, Part 3, pp.577-612.

NOMENCLATURE

SYMBOL	MEANING	LOCATION OF FIRST APPEARANCE
a,b,c	Coefficients of the general partial-differential equation	Eqns.(3.2-16), (3.2-17) and (3.2-19)
A	Age of the fold (≡time since formation)	Eqn.(2.6-1)
$\tilde{A}, A^*$	Non-dimensional age of the fold	Eqns.(3.4-1) and (4.2-8)
A^*_{cj}	Non-dimensional age at the centre of the j-th age interval	Eqn.(4.6-1)
C	Coefficients in the partial differential equation of the biographic analysis	Eqn.(4.2-8)
C_1, C_2	Empirical constants appearing in the transport equation for ε	Eqn.(3.2-4)
C_F	Empirical constant related to the fold composition at birth	Eqn.(4.3-2)
C_p	Specific heat	Eqn.(4.4-6)
$C_{p,j}, C_{p,mix}$	Specific heat of species j and the mixture	Eqns.(4.4-6) and (4.4-8)
C_S	Empirical constant related to the stretching rate	Eqn.(4.3-9)
C_Z	Empirical constant related to the fold size	Eqn.(4.3-1)

C_μ	Empirical constant in equation for the turbulent viscosity	Eqn.(3.2-6)
d	Source term of the general partial differential equation	Eqn.(3.2-21)
D	Diameter of the jet	Sec.7.4-2
$\mathscr{D}$	Diffusion coefficient	Eqn.(4.2-1)
f	Mixture fraction	Eqn.(2.5-1)
F	Transformation function in equation for the non-dimensional age	Eqn.(3.4-1)
g	Gravitational acceleration	Eqn.(3.2-1)
G_k	Rate of generation of the turbulent kinetic energy per unit volume	Eqn.(3.2-3)
h	Enthalpy	Eqn.(4.4-5)
H_{fu}	Heat of combustion in fuel	Eqn.(4.4-6)
i	Index of the control volume in the cross-stream direction	Sec.3.7
I	Turbulence intermittency factor	Eqn.(6.8-1)
j	Index of the age-interval and variable domain	Sec.3.5
k	Turbulent kinetic energy per unit volume	Sec.2.1
k_D, k_R	Rate constants in forward and reverse chemical reaction	Eqn.(6.3-9)

K_1, K_2, K_3	Constants in the equation of specific heat	Eqn.(4.4-9)
K_c	Equilibrium constant in chemical reaction	Eqn.(6.3-10)
ℓ	Turbulence length scale	Eqn.(4.3-2)
m_j	Mass fraction of species j	Eqn.(4.4-8)
$\dot{m}'''_E, \dot{m}'''_I$	Mass flow rate per unit area	Eqn.(3.2-23)
M_j	Molar fraction of species j	Sec.7.4-3
N	Number of grids in the cross-stream direction	Sec.3.7
NA	Number of age-intervals	Eqn.(6.3-8)
N_p	Number of grids in the fold biography analysis	Sec.6.3-1
N_ϕ	Number of intervals in the equation of pdf	Eqn.(5.5-5)
NM1	Number of control volumes in the cross-stream direction (≡N-1)	Fig.3.7-1
$[NO_2], [N_2O_4]$	Concentration of NO_2 and N_2O_4 gas	Eqn.(6.3-9)
p	Pressure	Eqn.(4.4-7)
P	Population distribution function w.r.t. age	Eqn.(3.3-1)
$\tilde{P}$	Non-dimensional population distribution function w.r.t. non-dimensional age	Eqn.(3.4-18)
$\tilde{P}_1, \tilde{P}_2, \tilde{P}_3, \cdots, \tilde{P}_{NA}$	Values of $\tilde{P}$ prevailing at each age-interval	Eqns.(3.5-1) to (3.5-3)

P_ϕ	Probability density function w.r.t. variable ϕ in a fold	Eqn.(5.5-1)
$\overline{P}_\phi$	Population-average value of P_ϕ	Eqn.(5.5-2)
$Q_{i-\frac{1}{2}}, Q_{i+\frac{1}{2}}$	Quantities related to the diffusion coefficient	Eqns.(3.7-7) and (3.7-8)
r	Radius	Eqn.(3.2-1)
R	Stretching rate	Eqn.(4.3-9)
R_u	Universal gas constant	Eqn.(4.4-7)
s	Stoichiometric ratio	Eqn.(2.5-2)
S_i, S_i'	Linearised source terms of the general partial differential equation	Eqn.(3.7-9)
t	Time	Eqn.(4.2-1)
T	Temperature	Eqn.(4.4-6)
u	Mean axial velocity	Eqn.(3.2-1)
U_e	Axial velocity at the jet exit	Eqn.(7.7-1)
$\sqrt{\overline{U'^2}}$	Root mean square value of of the fluctuation of U	Sec.7.8.1
v	Mean radial velocity	Eqn.(3.2-1)
$\sqrt{\overline{v'^2}}$	Root mean square value of the fluctuation of v	Sec.7.4.1
W_j	Molecular weight of species j	Eqn.(6.3-12)
X	Longitudinal distance	Eqn.(3.2-1)
y	Radial distance	Eqn.(3.2-9)
z	Distance across fold	Eqn.(4.2-4)
Z	Fold thickness	Eqn.(4.2-6)
Z_o	Z at the instant of fold formation	Eqn.(4.2-7)

GREEK SYMBOL	MEANING	LOCATION OF FIRST APPEARANCE
$\alpha_i, \beta_i, T_i, \zeta_i$	Coefficients in the calculation of TDMA procedure for the i-th grid node	Eqn.(3.7-10)
$\Gamma_{\phi,eff}$	Effective exchange coefficient for ϕ	Eqn.(3.2-8)
Δ and δ	Indicate a finite-difference	Secs.3.5 and 3.7
ε	Dissipation rate of turbulent kinetic energy per unit volume	Sec.2.2
η	Normalized distance across the fold	Eqn.(4.2-5)
η_T	Normalized distance across the mixing layer calculated from the temperature profile	Eqn.(6.4-1)
$\lambda_1, \lambda_2, \lambda_3$	Numerical factors in the calculation of forward marching step in x-direction	Sec.6.3.1
θ	Normalized temperature across the mixing layer	Sec.6.5
μ	Viscosity; subscript ℓ, t, e indicates laminar, turbulent or effective viscosity	Sec.3.2
ρ	Density	Eqn.(3.2-1)
Σ	Summation	Eqn.(4.4-8)

τ	Time scale	Sec.6.8
ϕ	General variable	Eqn.(3.2-8)
ψ	Stream function ($\equiv\int_o^y r\rho u dy$)	Eqn.(3.2-9)
ξ_1,ξ_2,ξ_3	Arguments in the sinusoidal profile of mixture fraction	Eqn.(4.5-1)
ω	Normalized stream function	Eqn.(3.2-10)

SUBSCRIPTS	MEANING
b	Birth place of the fold
c	Centre of the finite difference cell
D	Downstream neighbouring cell
e	At the nozzle exit of jet
eff	Effective quantity
E	External boundary of the computational domain
fu	Fuel
I	Internal boundary of the computational domain
i,j	Indicates location on the finite-difference cell
in	Inert species
ℓ	Laminar quantity
max	Maximum
min	Minimum
o	Reference value

ox	Oxygen
p	Potential flow
pr	Products
st	Stoichiometric point
t	Turbulent quantity
U	Upstream neighbouring cell
∞	Value in the free stream
1,2	Reference values

SUPERSCRIPTS	MEANING
′	Fluctuating component of a property
′′	Per unit area
•	Per unit time
‾	Population-average value, or time average value
~	Fold average value
═	Time average value including the intermittency factor

APPENDIX A

Flow chart of the computer program

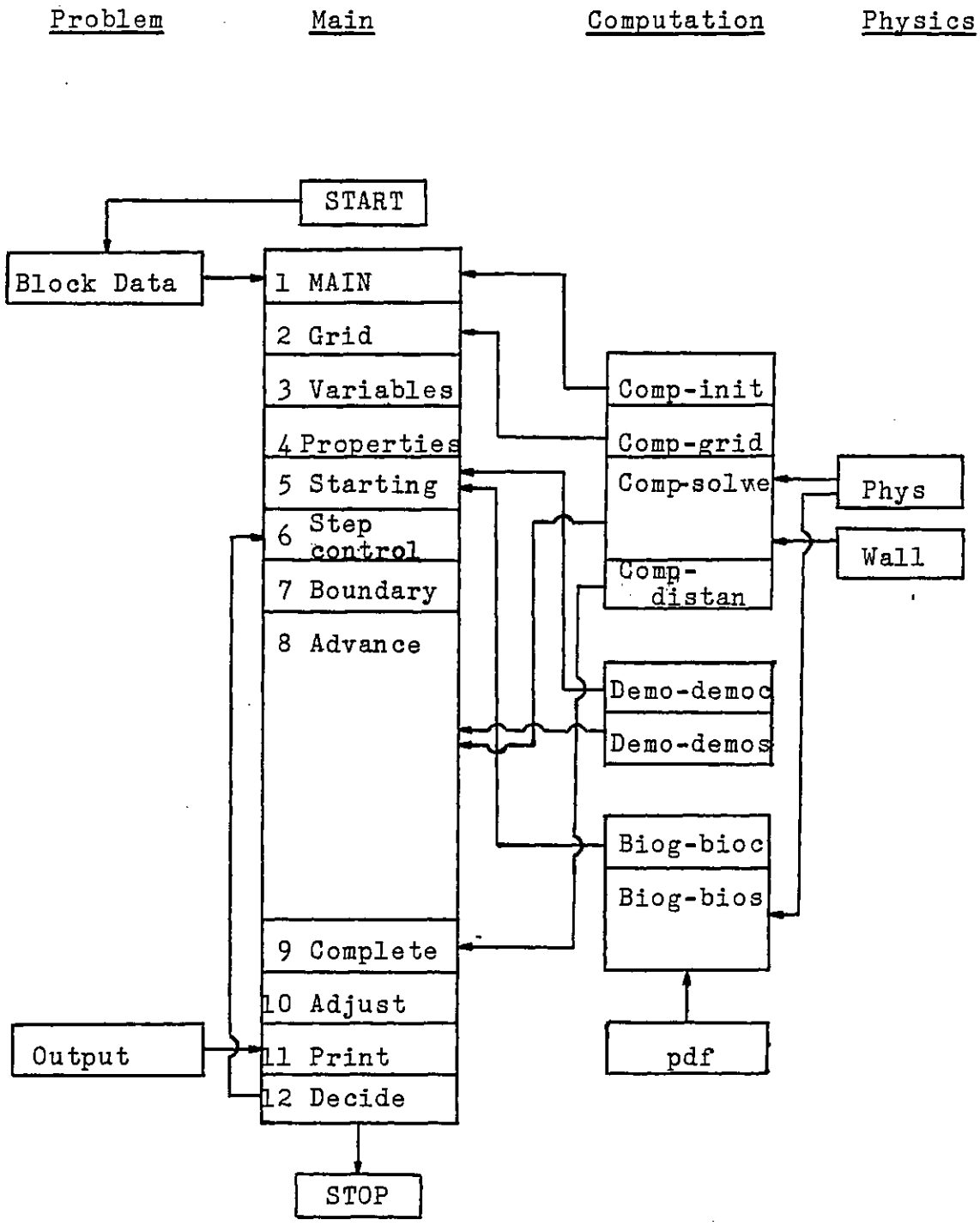

Flow chart of the computer program

APPENDIX B

Computer Listing for the calculation of H_2-Air Flame

```
 COMMON/COMA/
1 ADPEI(60),BIG,BOM(60),CSALFA,DIF(60),DIFU(60),DP,DX,DXLAST,
2 EMU(60),F(60,29),IBEX(29),IBIN(29),IDIMF,IFIN,ISTEP,ITEST,J,
3 JUSTEX,JUSTIN,KEX,KIN,KRAD,KSOURC,MOMSOU,N,NEWPR,NF,NM1,NM2,
4 NM3,NOVEL,OM(60),OMINT(60),PEI,PSIE,PSII,R(60),RECRU(60),
5 RECYDF(60),RHO(60),RJTOTE(29),RJTOTI(29),RME,RMI,SI(60),SIP(60),
6 TAUE,TAUI,TINY,U(60),XD,XU,Y(60),YE,YI,A1(60),B1(60),
7 PEE,FP(60,29)
 COMMON/COMA/
1 ADPEI(60),BIG,BOM(60),CSALFA,DIF(60),DIFU(60),DP,DX,DXLAST,
2 EMU(60),F( 1740),IBEX(29),IBIN(29),IDIMF,IFIN,ISTEP,ITEST,J,
3 JUSTEX,JUSTIN,KEX,KIN,KRAD,KSOURC,MOMSOU,N,NEWPR,NF,NM1,NM2,
4 NM3,NOVEL,OM(60),OMINT(60),PEI,PSIE,PSII,R(60),RECRU(60),
5 RECYDF(60),RHO(60),RJTOTE(29),RJTOTI(29),RME,RMI,SI(60),SIP(60),
6 TAUE,TAUI,TINY,U(60),XD,XU,Y(60),YE,YI,A1(60),B1(60),
7 PEE,FP( 1740)
 COMMON/COMB/
1 AK,AGRAV,AHEX,AHIN,ARRCON,AUEX,BHEX,BHIN,BUEX,
2 CD,CEBU,CHEX,CHIN,CMU,CMUCD,CUEX,C1MOD4,
2 CFU(60),CMIX(60),COX(60),CPR(60),CN2(60),CH2O(60),
2 AFU1,AFU2,AFU3,AOX1,AOX2,AOX3,AN21,AN22,AN23,AH2O1,AH2O2,
3 C1MOD5,C2MOD4,C2MOD5,DA1,DA2,DISSK(60),DPDX,DXINC,DXMAX,
4 DXPSI,DXRAT,DXRE,DXY,ELEXP,ENTHA,ENTHB,ENTHC,ENTHD,
4 ELCON,ELCON0(4),ELCONK(8),
5 EWALL,FACE,FACEXP,FACI,FJKA,FJKD,FJ2A,FJ2D,FLOB,FLOC,FR,
6 FRA,FUA,FUB,FUC,FUD,GAMMA,GASCON,GENK(60),H,HDIV,HEX0,HFU,
7 HIN0,ILPLOT,INERT,IRUN,ITPLOT,JEL,JF,JH,JK,JOX,JP,JPR,JTE,
8 J2,KASE,KIND,KUDIF,LASTEP,LENGTH,MODEL,MOD4C1,NPLOT,
9 NPROF,NSTAT,OMPOW,OXA,OXB,OXC,OXD,PEILIM,PHIA,PHIB,PHIC,
1 PHID,PREEXP,PRESS,PRL(29),PRLAM,PRTURB,RATE,RATI,RECPRL(29),
2 RECPRT(29),REY,SIGK,SIG2,STOICH,TA,TAUDK,TB,TC,TD,TWALL,UA,
3 UB,UBAR,UC,UD,UDIF,UEX0,UFAC,UFLUX,ULIM,VISFU,VISMIX,VISOX,
4 VISPR,WALCON,WFU,WMIX,WOX,WPR,XEND,XHEX0,XHIN0,XOUT,XUEX0,
5 XULAST,YREF1,YREF2,UREF,
6 JA1,JA2,JA3,JA4,JA5,JA6,JA7,JA8,JA9,JA10,JAL,UMIN,UMAX,
7 JA11,JA12,JA13,JA14,JA15,JA16,JA17,JA18,JA19,JA20
 COMMON/DEM1/
1 AGE(21),AGEC(20),DAGE(20),RECDA(20),NAGE,NAGEP1,MODFOR,
2 FOLM0,PEINEW,RECXD,UMXXD,XDUMX,DUDYB(60),PA0(60),PA(60,20),
3 JA1M1,JA1P1,ENTR(60),ARRAY(20,8),
4 AVTEM(60),DTST,XM0(60),IBIO,FSTOIC,SIW(60),SIPW(60),AVOX(60),
5 INDEX(3010),XP(3010),RATEA1(60),RATEA2(60),TEMAV(60),
6 AVRAT1(60),AVRAT2(60),RBURN(60),FUAV(60),AVFU(60),OXAV(60),
7 FN2(60),FH2O(60),FMFU(60),FMOX(60),FMN2(60),FMH2O(60),WN2,
8 WH2O,FSR(60),FUM(60),OXM(60),ENTHFO(60),TEMM(60),TFLU(60),
9 OXFLU(60),FUFLU(60),TEMAVS(60),AVTEMS(60),
1 FUAVS(60),AVFUS(60),OXAVS(60),AVOXS(60),
2 PHI(60),PHIBV(60),PDF1(60),PDFIT(60),PDFITA(60),
3 PHIBVA(60),AVPFA(60,60),AVPDF(60,60),SUMPDF(60),
4 IPDF,ISTAGE,OMA(60),TEML,TEMR,FUL,FUR,OXL,OXR,
5 F1,F2,FAMP,PHIL,PHIR,NDIFOM,NPDF,NPDFM1,PHIDIF,
```

```
     6 OMLEFT,OMRIGT,DDELAJ,PHIMAX,PHIMIN,EMIX,
     7 FFIAVS(60),AVFFIS(60),FRFLU(60),FMAX(60),
     8 EMPC1,EMPC2,EMPC3,FVAL(60),POPAGE(60)
      COMMON/DEM2/
     1 CCO2(60),ACO21,ACO22,ACO23,FCO2(60),FMCO2(60),WCO2,
     2 PROL,PROR,PROM(20),PRAV(60),AVPR(60),PRAVS(60),
     3 AVPRS(60),PRFLU(60),PRFLUM(60)
      INTEGER SEARCH
      BLOCK DATA
C/FEB.1977 ---------- G E N M I X ---------- COPYRIGHT, D.B.SPALDING ---
C     "GENMIX, A GENERAL COMPUTER PROGRAM FOR TWO-DIMENSIONAL
C      PARABOLIC PHENOMENA", BY D. B. SPALDING
C     REPORT NO. HTS/77/9, FEBRUARY 1977,
C     IMPERIAL COLLEGE, MECHANICAL ENGINEERING DEPARTMENT, LONDON,SW72BX
C
C      APPENDIX A (BASIC PROGRAM) - COMBUSTION OF METHANE AND AIR IN
C                  A DIVERGENT DUCT EXHAUSTING INTO THE ATMOSPHERE.
C-----------------------------------------------------------------------
CHAPTER 1  1  1  1  1  1  1  1  PRELIMINARIES  1  1  1  1  1  1  1  1
$INCLUDE 9,COMA1.FTN
$INCLUDE 9,COMB.FTN
C
C/I=TA1411 RECFJK ADDED, F(I,JK) MADE ABS IN PHYS DO 151 LOOP.
C/I=TA0211/P=OPL779A/UN=UMEMH02.
C     02.11.78 REPLACE ALMG BY ELCON0, REPLACE ELCOND BY ELCONK
C     24.10.78 GENERAL CORRECTIONS
C     29.8.78  NEW VERSION INTRODUCING LENGTH AND DELETING KONFIG
C/ SEPT.1977 -- GENMIX-T, HTS/77/9, APPXA -- COPYRIGHT, D.B.SPALDING ---
C     GENMIX-T, TURBULENCE MODELS TEACHING PROGRAM,
C     WITH CHEMICAL REACTION.
C     BASED ON APPENDIX A OF THE HTS REPORT NO. HTS/77/9.
C
C/ SEPT.1981 -- THE ESCIMO MODEL OF TURBULENT COMBUSTION
C     IS INCORPORATED INTO THE GENMIX-T PROGRAM.
C     THE NEW SUBROUTINES ARE CALLED DEMO,BIOG  AND PDF.
C     ---------- CONFIGURATION INDEX
C       KASE =0   STANDARD GENMIX, APPENDIX A.
C            1    PIPE OR CHANNEL
C            2    MIXING LAYER
C            3    PLANE JET
C            4    AXI-SYMMETRICAL (ROUND) JET
C            5    RADIAL (FAN) JET
C            6    PLANE PLUME
C            7    AXI-SYMMETRICAL (ROUND) PLUME
C
C     ---------- INITIALISE DATA
      DATA KUDIF/-1/
C     -----------------------------------------------------------------
      DATA KASE,IRUN/4,0/
      DATA ITEST/1/
      DATA BIG,TINY/1.E20,1.E-10/
```

```
C
C-----------------------------------------------------------------------
CHAPTER 2  2  2  2  2  2  2  GRID AND GEOMETRY  2  2  2  2  2  2  2  2
C     ------------------------------ GRID
      DATA N,OMPOW/20,2.0/
C     ----- SET IDIMF= DIMENSION FOR I, ENSURE THAT IDIMF.GE.N
      DATA IDIMF/60/
C     ----- SET KRAD=1 FOR PLANE, 2 FOR AXIAL, 3 FOR POINT SYMMETRY
      DATA KRAD,CSALFA/2,1./
C     ------------------------------ GEOMETRY
      DATA HIN0,XHIN0,AHIN,BHIN,CHIN/0.0,4*0./
      DATA HEX0,XHEX0,AHEX,BHEX,CHEX/0.00381,4*0./
      DATA HDIV/0.002/
      DATA XU,XEND,XOUT/3*0.0/
      DATA LASTEP,XULAST/1000,0.6096/
C     ----- FOR KIND=3, XU, XHEX0 AND XHIN0 =.25 (MAIN CH.2)
C
C-----------------------------------------------------------------------
CHAPTER 3  3  3  3  3  3  3  DEPENDENT VARIABLES  3  3  3  3  3  3  3
C     ----- SET NF= NUMBER OF DEPENDENT VARIABLES, EXCLUDING VELOCITY
      DATA NF/15/,JP,JK,J2,JA1,JA2,JA3,JA4,JA5,JA6,JA7,JA8,
     2 JA9,JA10,JH,JF,JEL,JOX,JTE,JPR/1,2,3,4,5,6,7,8,9,10,11,12,13,
     3 14,15,16,17,18,19/
C     -----SET NOVEL=1 FOR NO VELOCITY, NOVEL=2 OTHERWISE
      DATA NOVEL/2/
C
C-----------------------------------------------------------------------
CHAPTER 4  4  4  4  4  4  4  4  PROPERTY DATA  4  4  4  4  4  4  4  4
C     -------------------- S.I. UNITS
      DATA AGRAV,GASCON/9.8,8314./
C     ----- SET MODEL=1 FOR LAMINAR FLOW,
C     ----- SET MODEL=2 FOR "MIXING-LENGTH" MODEL OF TURBULENCE
C     ----- SET TURBULENCE MODEL
C           MODEL=1   LAMINAR
C                 2   MIXING LENGTH,
C                         LENGTH=1  STANDARD GENMIX
C                                =2  NIKURADSE"S LENGTH SCALE
C                                =3  UNIFORM LENGTH SCALE
C                 3   PRANDTL(ENERGY)
C                 4   KOLMOGOROV (ENERGY-FREQUENCY),
C                         MOD4C1=1   C1 FROM MIXING-LAYER RULE
C                                2   C1 FROM NO-DIFFUSION RULE
C                                3   C1 AND C2 ARE SAIY"S VALUES
C                 5   HARLOW (ENERGY-DISSIPATION)
      DATA MODEL,LENGTH/5,1/
      DATA MOD4C1/1/
      DATA AK,FR,CEBU,EWALL/.435,.033,.4,9./
      DATA TAUDK,SIGK,ELEXP,SIG2/.3,1.,2.38,1.314/
C     ----- SIG2 MAY BE RECOMPUTED IN CH.4 OF MAIN F 4 AND 5
C
C     -- MIXING-LENGTH CONSTANT FOR KASE=0, STANDARD GENMIX
```

```
C      ----- INITIAL VALUE WITHIN DUCT
       DATA ELCON/.09/
C      ----- VALUES FOR FREE BOUNDARY OUTSIDE DUCT, SET IN MAIN, CH.7
C      ----- THESE VALUES DEPEND ON CONFIGURATION, INDEX IS KIND
       DATA ELCON0/.075,.1,.14,.075/
C
C      -- MIXING-LENGTH CONSTANT FOR OTHER KASES, INDEX IS KASE
C      -- SET IN MAIN, CH.4
       DATA ELCONK/.14,.11,.251,.1985,.3514,.1985,.251,.09/
C
C      --- SET INERT=1 FOR INERT FLUID, INERT=2 FOR CHEMICALLY REACTIVE
       DATA INERT/2/
C      ------------------------------ MATERIALS
C      ---------- THERMODYNAMIC
       DATA AFU1,AFU2/13849.,1.69452/
       DATA AOX1,AOX2,AOX3/1081.3,0.03373,-2.4542E7/
       DATA AN21,AN22,AN23/1021.3,0.1346,-1.79E6/
       DATA AH201,AH202/1698.06,0.572/
       DATA WFU,WOX,WPR,WMIX/2.,32.,28.,29./
       DATA WN2,WH2O/28.,18./

       DATA HFU/1.206E8/
C      ---------- CHEMICAL
       DATA STOICH,ARRCON,PREEXP/8.,8.E3,1./
C      ---------- TRANSPORT
       DATA VISFU,VISOX,VISPR,VISMIX/4*1.E-6/
       DATA PRLAM,PRTURB/0.7,0.9/
       DATA H,UFAC/.9,.01/
C
C-----------------------------------------------------------------------
CHAPTER 5  5  5  5  5  5  5  STARTING VALUES  5  5  5  5  5  5  5  5
       DATA PRESS/1.E5/
C      ----- STREAM B IS PURE FUEL
       DATA UB,TB,FUB,OXB/151.,300.,1.,0./
C      ----- STREAM C IS AIR
       DATA UC,TC,FUC,OXC/151.,300.,1.,0./
C      ----- SET KEX AND KIN FOR INITIAL BOUNDARY TYPE,
C      ----- 1 FOR WALL, 2 FOR FREE BOUNDARY, 3 FOR SYMMETRY AXIS
       DATA KEX,KIN/2,3/
C
C-----------------------------------------------------------------------
CHAPTER 6  6  6  6  6  6  6  6 STEP CONTROL 6  6  6  6  6  6  6  6  6
       DATA FRA,DXMAX,DXRAT/1.,1.,5./
C      ----- ENTRAINMENT CONTROL
       DATA ULIM,PEILIM,FACEXP/.05,.01,.5/
C      ----- STARTING VALUES
       DATA FACE,FACI,RATE,RATI/4*1./
C
C-----------------------------------------------------------------------
CHAPTER 7  7  7  7  7  7  7  7  BOUNDARY CONDITIONS  7  7  7  7  7  7
C      ---------- STREAM A, THROUGH CENTRAL PIPE
```

```
      DATA UA,TA,FUA,OXA/151.,300.,1.,0./
C     ---------- STREAM D, SURROUNDING ATMOSPHERE
      DATA TD,FUD,OXD/300.,0.,0.232/
C     ----- UD IS SUPPLIED BY WAY OF THE UEX FUNCTION
C     ---------- VELOCITY ALONG OUTER BOUNDARY
      DATA UEX0,XUEX0,AUEX,BUEX,CUEX/15.1,4*0./
C     ---------- WALL TEMPERATURE OF OUTER TUBE
      DATA TWALL/299./
C
C-----------------------------------------------------------------------
CHAPTER 11 11 11 11 11 11 11 11 11 11  PRINT  11  11  11  11  11  11
C     --- SET ILPLOT=2 FOR  DOWN-STREAM PLOT, =1 FOR NO PLOT
C     --- SET ITPLOT=2 FOR CROSS-STREAM PLOT, =1 FOR NO PLOT
      DATA ILPLOT,ITPLOT/2,2/
C     --- SET NSTAT, NPROF, NPLOT TO NUMBER OF STEPS BETWEEN OUTPUT OF
C     --- STATION VALUES, PROFILES AND CROSS-STREAM PLOTS RESPECTIVELY
      DATA NSTAT,NPROF,NPLOT/12,12,10000/
C     ----- AFTER XU=XOUT, NSTAT AND NPROF ARE SET =24 AT MAIN, CH.11
C     ----------INPUT RELATED TO ESCIMO MODEL
      DATA NAGE,NAGEP1,JA1,JAL,FOLM0/10,11,4,13,0.5/
      DATA UMAX,UMIN/151.,15.1/
      DATA XM0/60*0.5/
      DATA F/1740*0./,PA0,PA/1260*0./,DUDYB/60*1.E-6/
      DATA MODFOR/3/
      DATA AGE/0.,.05,.1,.15,.2,.3,.4,.5,.65,.8,1./
      DATA IBIO,FSTOIC/1,0.0282/
      DATA EMPC1,EMPC2,EMPC3/2.,2.,0.5/
      DATA IPDF/1/
      DATA NPDF/11/
      END
```

```
      PROGRAM MAIN
C/ SEPT.1977 -- GENMIX-T, HTS/77/9, APPXA -- COPYRIGHT, D.B.SPALDING --
CHAPTER 1  1  1  1  1  1  1  1  PRELIMINARIES  1  1  1  1  1  1  1  1
$INCLUDE 9,COMA1.FTN
$INCLUDE 9,COMB.FTN
C
C     ------------------------------------------------------------------
C     ----- FUNCTIONS FOR BOUNDARY CONDITIONS
      HEX(X)=HEX0+X*(AHEX+X*(BHEX+X*CHEX))
      HIN(X)=HIN0+X*(AHIN+X*(BHIN+X*CHIN))
      UEX(X)=UEX0+X*(AUEX+X*(BUEX+X*CUEX))
C
C-----------------------------------------------------------------------
CHAPTER 2  2  2  2  2  2  2  GRID AND GEOMETRY  2  2  2  2  2  2  2  2
C     SEE DATA
C     ----- KIND IS AN INDEX WHICH DENOTES A PARTICULAR GEOMETRY TYPE
      KIND=4
      IF(KRAD.EQ.1) KIND=2
      IF(KRAD.EQ.2.AND.CSALFA.EQ.1.) KIND=1
      IF(KRAD.EQ.2.AND.CSALFA.EQ.0.) KIND=3
C     ----- MODIFICATIONS TO DATA
      IF(KIND.NE.3) GO TO 21
      XU=.25
      XHEX0=.25
      XHIN0=.25
   21 CONTINUE
C
      SNALFA=SQRT(1.-CSALFA**2)
C     ----- STARTING VALUES
      IEND=IFIX(XEND*1.E6)
      IOUT=IFIX(XOUT*1.E6)
C     -------------------- SUBROUTINE COMPUTE, ENTRY INIT
      CALL INIT
C     ------------------------------ GRID
      DO 20 I=1,N
   20 OM(I)=(FLOAT(I-1)/FLOAT(NM1))**OMPOW
C
C     -------------------- SUBROUTINE COMPUTE, ENTRY GRID
      CALL GRID
C
C-----------------------------------------------------------------------
CHAPTER 3  3  3  3  3  3  3  DEPENDENT VARIABLES  3  3  3  3  3  3  3
C     SEE DATA
C     U(I)= VELOCITY
C     F(I,JH)= STAGNATION ENTHALPY
C     F(I,JP)= PHI= OXIDANT CONCENTRATION - F(I,JF)*STOICH
C     F(I,JA1).....F(I,JAL) = FOLD POPULATIONS
C     F(I,JF)= FUEL CONCENTRATION
C     F(I,JOX)= OXIDANT CONCENTRATION
C     F(I,JTE)= TEMPERATURE
C     F(I,JPR)= PRODUCT CONCENTRATION
```

```
C      F(I,JK)= KINETIC ENERGY OF TURBULENCE
C      F(I,J2)= FREQUENCY= DISSIPATION RATE/(DENSITY*ENERGY) FOR MODEL 4
C          OR = EPSILON= DISSIPATION RATE/DENSITY FOR MODEL 5
C      F(I,JEL)= TURBULENCE LENGTH SCALE
C
C-----------------------------------------------------------------------
CHAPTER 4  4  4  4  4  4  4  4  PROPERTY DATA  4  4  4  4  4  4  4  4
C      SEE DATA
C      IF(MODEL.LE.2) NF=JAL+1
C      IF(MODEL.EQ.3) NF=JAL+2
C      IF(MODEL.GT.3) NF=JAL+3
       RECWFU=1./WFU
       RECWOX=1./WOX
       RECWPR=1./WPR
       RECWMX=1./WMIX
       DO 40 J=1,NF
       PRL(J)=PRLAM
       RECPRL(J)=1./PRLAM
    40 RECPRT(J)=1./PRTURB
       DO 401 I=1,N
       CFU(I)=AFU1+AFU2*TA
       COX(I)=AOX1+AOX2*TB+AOX3/(TB**2)
       CN2(I)=AN21+AN22*TC
       CPR(I)=CN2(I)
   401 CH2O(I)=AH201+AH202*TC
       GAMMA=CFU(1)/(CFU(1)-GASCON*RECWMX)
C
       CMU=SQRT(TAUDK)
       CD=TAUDK*CMU
       CMUCD=CMU*CD
C      ----- LATER MODIFY CMU AND CMUCD FOR KASE 4 TO FIT ROUND JET DATA
       WALCON=CD/AK
       RECPRT(JK)=1./SIGK
       IF(MODEL.LT.3) GO TO 44
C      ---------- MODELS 4 AND 5
       C2MOD5=1.5+1./ELEXP
       C1MOD5=C2MOD5-AK**2*TAUDK/(CMUCD*SIG2)
       IF(MODEL.EQ.5) GO TO 42
C      ---------- MODEL 4 (3 VERSIONS)
       C2MOD4=C2MOD5-1.
C      ----- C1 FROM MIXING-LAYER RULE
       IF(MOD4C1.EQ.1) C1MOD4=C1MOD5*C2MOD4/C2MOD5
C      ----- C1 FROM THE NO-DIFFUSION RULE
       IF(MOD4C1.EQ.2) C1MOD4=C1MOD5-1.
C      ----- C1 AND C2 ARE SAIY"S VALUES
       IF(MOD4C1.NE.3) GO TO 41
       C1MOD4=0.47
       C2MOD4=1.00
C      ----- MODELS 4 AND 5,  SIG2 FROM THE NEAR-WALL RULE
    41 SIG2=AK**2/(TAUDK*(C2MOD4-C1MOD4))
       GO TO 43
```

```
   42 SIG2=AK**2/(TAUDK*(C2MOD5-C1MOD5))
   43 RECPRT(J2)=1./SIG2
   44 CONTINUE
C
C-----------------------------------------------------------------------
CHAPTER 5  5  5  5  5  5  5  STARTING VALUES  5  5  5  5  5  5  5  5
C     SEE DATA
      WB=1./(FUB*RECWFU+OXB*RECWOX+(1.-FUB-OXB)*RECWPR)
      RHOB=PRESS*WB/(TB*GASCON)
      WC=1./(FUC*RECWFU+OXC*RECWOX+(1.-FUC-OXC)*RECWPR)
      RHOC=PRESS*WC/(TC*GASCON)
      FLOB=RHOB*UB*(HDIV-HINØ)
      FLOC=RHOC*UC*(HEXØ-HDIV)
      IF(KRAD.EQ.1) GO TO 55
      XSIN=XU*SNALFA
      HCOS=.5*CSALFA
      FLOB=FLOB*(XSIN+HCOS*(HDIV+HINØ))
      FLOC=FLOC*(XSIN+HCOS*(HEXØ+HDIV))
   55 CONTINUE
      OMDIV=FLOB/(FLOB+FLOC+TINY)
      TMIN=.5*AMIN1(TA,TB,TC,TD,TWALL)
C     ------------------- SEQUENCE TO PUT CELL BOUNDARY AT OMDIV.
      IF(OMDIV.LE.1.E-1Ø.OR.OMDIV.GE.(1.-1.E-1Ø)) GO TO 53
      DO 52 I=3,NM1
      IF(OMINT(I)-OMDIV) 52,53,57
   57 IDIV=I+1
      GO TO 58
   52 CONTINUE
   58 FAC=OMDIV/OMINT(IDIV-1)
      DO 59 I=2,IDIV
   59 OM(I)=OM(I)*FAC
C     ------------------- SUBROUTINE COMPUTE, ENTRY GRID
      CALL GRID
   53 CONTINUE
C     ---------- INSERTION INTO ARRAYS
      ENTHB=TB*(CFU(1)*FUB+COX(1)*OXB+CPR(1)*(1.-FUB-OXB))+
     1 .5*UB**2+HFU*FUB
      ENTHC=TC*(CFU(1)*FUC+COX(1)*OXC+CPR(1)*(1.-FUC-OXC))+
     1 .5*UC**2+HFU*FUC
      PHIB=OXB-FUB*STOICH
      PHIC=OXC-FUC*STOICH
      DO 5Ø1 I=1,N
      IF(OM(I).GT.OMDIV) GO TO 5Ø3
      U(I)=UB
      F(I,JH)=ENTHB
      F(I,JP)=PHIB
      F(I,JF)=FUB
      GO TO 5Ø1
  5Ø3 U(I)=UC
      F(I,JH)=ENTHC
      F(I,JP)=PHIC
```

```
      F(I,JF)=FUC
  501 F(I,JA1)=1./(AGE(2)-AGE(1))
      DO 502 I=1,NM1
      F(I,JK)=.03*UB**2
  502 F(I,J2)=CD*F(I,JK)*SQRT(F(I,JK))/(.03*HEX0)
      F(N,JK)=0.1
      F(N,J2)=CD*F(N,JK)*SQRT(F(N,JK))/(.03*HEX0)
      DO 504 I=1,N
      DISSK(I)=0.
  504 GENK(I)=0.
C     -- INITIAL VALUES FOR THE F(I,JK) AND F(I,J2) ARRAYS ARE IN PHYSU.
C
      IF(KASE.NE.0) ELCON=ELCONK(KASE)
C*****************************************************************
CALL FOR STARTING PREPARATIONS IN SUBROUTINE DEMO FOR CONSTANT AGE SIZES
C
      CALL DEMOC
      CALL BIOC
C*****************************************************************
C
C     ---------------------------------- ENTER MAIN LOOP AT CHAPTER 7
      GO TO 700
C
C-----------------------------------------------------------------------
CHAPTER 6  6  6  6  6  6  6  6  STEP CONTROL  6  6  6  6  6  6  6  6
C     SEE DATA
  600 DXY=FRA*Y(NM2)
      DXRE=DXY*PEI/(.5*(R(1)+R(N))*EMU(1)+TINY)
      DXINC=DXLAST*DXRAT
C
C     -------------------- DETERMINATION OF BOUNDARY TYPE
C     -------------------- I BOUNDARY
      IF(ISTEP.GE.IEND) GO TO 610
      KIN=1
      GO TO 611
  610 IF(PSII.LE.TINY) GO TO 612
      KIN=2
      GO TO 611
  612 KIN=3
C     -------------------- E BOUNDARY
  611 IF(ISTEP.GE.IOUT) GO TO 613
      KEX=1
      GO TO 614
  613 KEX=2
  614 CONTINUE
C
C     -------------------- ENTRAINMENT RATES
      IF(KIN.NE.2.AND.KEX.NE.2) GO TO 602
      KUDIF=ISTEP
      UMAX=U(1)
      UMIN=U(1)
```

```
      DO 615 I=2,N
      UMAX=AMAX1(UMAX,U(I))
  615 UMIN=AMIN1(UMIN,U(I))
      UDIF=UMAX-UMIN
C     ------------------------------ I BOUNDARY
      IF(KIN.NE.2) GO TO 601
      RATI=ABS((U(2)-U(1))/(UDIF*ULIM+TINY))
      RMI=(R(2)+R(3))*(EMU(2)+EMU(3))*RECYDF(2)*RATI/(1.+RATI)
      FACI=FACI*RATI**FACEXP
      FACI=AMAX1(0.1,AMIN1(FACI,10.))
      RMI=RMI*FACI
      IF(MODEL.EQ.2) RMI=AMIN1(RMI,0.4*UDIF*RHO(1)*R(1))
C     ------------------------------ E BOUNDARY
  601 IF(KEX.NE.2) GO TO 602
      RATE=ABS((U(NM1)-U(N))/(UDIF*ULIM+TINY))
      RME=-(R(NM2)+R(NM1))*(EMU(NM2)+EMU(NM1))*RECYDF(NM2)*RATE/
     1                                                    (1.+RATE)
      FACE=FACE*RATE**FACEXP
      FACE=AMAX1(.01,AMIN1(FACE,10.))
      RME=RME*FACE
      IF(MODEL.EQ.2) RME=AMAX1(RME,-0.4*UDIF*RHO(N)*R(N))
C
  602 DXPSI=PEI*PEILIM/(RMI-RME+TINY)
C
C     --------------- SET VALUE OF DX
      DX=AMIN1(DXY,DXRE,DXINC,DXPSI,DXMAX)
C
      IF(ISTEP.GE.IEND) GO TO 605
      IF(DX.LT.(XEND-XU)) GO TO 605
C     ----- RESET DX SO THAT XU WILL EXACTLY EQUAL XEND AT NEXT STEP
      DX=XEND-XU
      IEND=ISTEP+1
      JUSTIN=ISTEP+1
C
  605 IF(ISTEP.GE.IOUT) GO TO 606
      IF(DX.LT.(XOUT-XU)) GO TO 606
C     ----- RESET DX SO THAT XU WILL EXACTLY EQUAL XOUT AT NEXT STEP
      DX=XOUT-XU
      IOUT=ISTEP+1
      JUSTEX=ISTEP+1
C
  606 IF(PSII.GT.RMI*DX) GO TO 607
      IF(PSII.LE.TINY) GO TO 607
C     ----- RESET DX SO THAT AXIS IS REACHED AT NEXT STEP
      DX=PSII/RMI
      JUSTIN=ISTEP+1
C
C     ----- RESET DX SO THAT XU WILL NOT EXCEED XULAST
  607 DX=AMIN1(DX,XULAST-XU)
C
C     ---------- TRAP ZERO OR NEGATIVE DX
```

```
      IF(DX.GT.Ø.) GO TO 6Ø8
      IFIN=2
      GO TO 11ØØ
C
C     ------------------- DETERMINE XD
  6Ø8 XD=XU+DX
      DXLAST=DX
C
C     ----- IF CSALFA VARIES -
C           RECALCULATE IT, AND SNALFA AND HCOS, HERE, FOR X=XD
      GO TO 7Ø
C
C-----------------------------------------------------------------------
CHAPTER 7  7  7  7  7  7  7  7  BOUNDARY CONDITIONS  7  7  7  7  7  7
  7ØØ ASSIGN 751 TO ISTART
C     ---------- GENERAL BOUNDARY CONDITION INFORMATION
C     ---------- STREAM A, THROUGH CENTRAL PIPE
C     SEE DATA
      ENTHA=TA*(CFU(1)*FUA+COX(1)*OXA+CPR(1)*(1.-FUA-OXA))+
     1 .5*UA**2+HFU*FUA
      PHIA=OXA-FUA*STOICH
      RHOA=PRESS*WFU/(TA*GASCON+TINY)
      FLOA=RHOA*UA*HIN(XEND)
      FJKA=Ø.Ø3*UB**2
      IF(KRAD.EQ.2) FLOA=FLOA*(XEND*SNALFA+HCOS*HIN(XEND))
      PSII=FLOA
      PEI=FLOB+FLOC
      PSIE=PSII+PEI
C     ---------- STREAM D, SURROUNDING ATMOSPHERE
C     SEE DATA
      XUEXØ=XOUT
      UD=UEXØ
      XD=XU
      ENTHD=TD*(CFU(1)*FUD+COX(1)*OXD+CPR(1)*(1.-FUD-OXD))+
     1 .5*UD**2+HFU*FUD
      PHID=OXD-FUD*STOICH
C     ---------- OTHER RELATED INFORMATION
      HDUCID=HINØ
      ADUCTD=HEXØ-HDUCID
      IF(KRAD.EQ.2) ADUCTD=ADUCTD*(XSIN+HCOS*(HEXØ+HDUCID))
      AFLOWD=ADUCTD
   7Ø CONTINUE
C     --------------- BOUNDARY CONDITIONS FOR FORWARD STEP
C     ------------------------------------------  I BOUNDARY
      IF(KIN-2) 731,732,733
C     ------------------------------  WALL
  731 IF(ISTEP.GT.JUSTIN) GO TO 734
      U(1)=Ø.
      TAUI=Ø.
      RMI=Ø.
      DO 735 J=1,NF
```

```
      IBIN(J)=2
  735 RJTOTI(J)=0.
C     ------------------- ADJUST INNER HEIGHT
  734 HIND=HIN(XD-XHIN0)
      GO TO 740
C     ------------------------------  FREE BOUNDARY
  732 IF(ISTEP.GT.JUSTIN) GO TO 736
      TAUI=0.
      U(1)=UA
      VIMIX=FUA*RECWFU+OXA*RECWOX+(1.-FUA-OXA)*RECWPR
      F(1,JTE)=TA
      RHO(1)=PRESS/(VIMIX*F(1,JTE)*GASCON)
      RECRU(1)=1./(RHO(1)*U(1)+TINY)
      F(1,JH)=ENTHA
      F(1,JP)=PHIA
      F(1,JF)=FUA
      AREA=HDUCID
      IF(KRAD.EQ.2) AREA=AREA*(XU*SNALFA+HCOS*HDUCID)
      AFLOWD=AFLOWD+AREA
      IF(ISTEP.EQ.0) GO TO 740
  736 U(1)=U(1)+DX*AGRAV*(RHO(N)-RHO(1))*RECRU(1)
      F(1,JK)=FJKA
      IF(MODEL.LT.4) GO TO 740
      FJ2A=CD*SQRT(FJKA)/(ELCON*(Y(NM2)-Y(3)))
      IF(MODEL.EQ.5) FJ2A=FJ2A*FJKA
      F(1,J2)=FJ2A
      GO TO 740
C     ------------------------------ SYMMETRY AXIS
  733 IF(ISTEP.GT.JUSTIN) GO TO 740
      TAUI=0.
      RMI=0.
      PSII=0.
      HIND=0.
      U(1)=U(2)
      DO 737 J=1,NF
  737 F(1,J)=F(2,J)
C     ---------- NO SUBSEQUENT CHANGE NEEDED
  740 CONTINUE
C
C     ------------------------------------------  E BOUNDARY
      IF(KEX-2) 741,742,743
C     ------------------------------  WALL
  741 IF(ISTEP.GT.JUSTEX) GO TO 744
C     ---------- FIRST STEP ONLY
      U(N)=0.
      RME=0.
      TAUE=0.
      IBEX(JH)=1
      F(N,JOX)=OXC
      F(N,JPR)=1.-OXC-FUC
      DO 745 J=2,NF
```

```
      IBEX(J)=2
  745 RJTOTE(J)=0.
C     ----- ADJUST ENTHALPY TO FIT COMPOSITION
  744 CMIX(N)=CFU(N)*F(N,JF)+COX(N)*F(N,JOX)+CPR(N)*F(N,JPR)
      F(N,JTE)=TWALL
      F(N,JH)=CMIX(N)*F(N,JTE)+F(N,JF)*HFU
C     ------------------- ADJUST EXTERNAL HEIGHT
      HEXD=HEX(XD-XHEX0)
      F(N,JK)=0.
      F(N,J2)=0.
      GO TO 750
C     ------------------------------------------- FREE BOUNDARY
  742 IF(ISTEP.GT.JUSTEX) GO TO 746
      F(N,JH)=ENTHD
      F(N,JP)=PHID
      F(N,JF)=FUD
      F(N,JOX)=OXD
      FJKD=0.1
      F(N,JPR)=1.-F(N,JF)-F(N,JOX)
      VMIX=F(N,JF)*RECWFU+F(N,JOX)*RECWOX+F(N,JPR)*RECWPR
      F(N,JTE)=TD
      RHO(N)=PRESS/(VMIX*F(N,JTE)*GASCON)
      U(N)=UD
      RECRU(N)=1./(RHO(N)*U(N)+TINY)
C     ---------- ADJUSTMENT OF MIXING LENGTH CONSTANT
      IF(KASE.EQ.0) ELCON=ELCON0(KIND)
C     ---------- ADJUSTMENT OF DOWNSTREAM VELOCITY
  746 UD=UEX(XD-XUEX0)
      F(N,JK)=FJKD
      IF(MODEL.LT.4) GO TO 750
      FJ2D=CD*SQRT(FJKD)/(ELCON*(HEX0-HIN0))
      IF(MODEL.EQ.5) FJ2D=FJ2D*FJKD
      F(N,J2)=FJ2D
      GO TO 750
C     ---------- NO SYMMETRY AXIS
  743 CONTINUE
  750 GO TO ISTART, (751,800)
  751 ASSIGN 800 TO ISTART
      GO TO 900
C
C-------------------------------------------------------------------------
CHAPTER 8  8  8  8  8  8  8  8  ADVANCE  8  8  8  8  8  8  8  8  8  8
C     ------------------------  MOMENTUM SOURCES
C     ---------------------------------------- PRESSURE GRADIENT
  800 IF(KEX.NE.2) GO TO 821
      DP=(U(N)-UD)/RECRU(N)
      GO TO 823
C     ------------------------------- CONFINED FLOW
C     ----- CALCULATION OF AREA INCREASE
  821 AFLOWU=AFLOWD
      HDUCID=0.
```

```
      IF(KIN.EQ.1) HDUCID=HIND
      ADUCTD=HEXD-HDUCID
      IF(KRAD.EQ.2) ADUCTD=ADUCTD*(XD*SNALFA+HCOS*(HEXD+HDUCID))
      DA=ADUCTD-AFLOWU
      DP=DA/DADP
C     ---------- WALL SHEAR AND MASS ADDITION
      UBAR=0.
      DO 824 I=2,NM1
  824 UBAR=UBAR+(BOM(I)*U(I))
      IF(KIN.EQ.2) UBAR=(UBAR-U(1))*PEI/PSIE+U(1)
      UBAR=(UBAR-U(1))*PEI/PSIE+U(1)
      DP=DP+DX*(-TAUI*R(1)-TAUE*R(N)+2.*RME*UBAR)/ADUCTD
      DP=AMIN1(DP,.5*DPMAX)
C
  823 CONTINUE
C     ---------- COMP
      CALL DEMOS
      CALL SOLVE
C
C-----------------------------------------------------------------------
CHAPTER 9  9  9  9  9  9  9  9  COMPLETE  9  9  9  9  9  9  9  9  9  9
  900 CONTINUE
C
C     ---------- IGNITION SEQUENCE
      IF(ISTEP.GT.5) GO TO 931
      IF(INERT.EQ.1) GO TO 931
      T2=.5/STOICH
      DO 932 I=2,NM1
      F(I,JF)=T2*(ABS(F(I,JP))-F(I,JP))
  932 F(I,JOX)=F(I,JP)+STOICH*F(I,JF)
  931 CONTINUE
C
C     ---------- THERMODYNAMIC PROPERTIES
      PRESS=PRESS+DP
      PDGSCN=PRESS/GASCON
      DO 907 I=1,N
      F(I,JOX)=AMAX1(0.,F(I,JP)+STOICH*F(I,JF))
      F(I,JPR)=1.-F(I,JF)-F(I,JOX)
      ENTH=F(I,JH)-.5*U(I)**2-HFU*F(I,JF)
      IF(ISTEP.EQ.0) GO TO 940
      CFU(I)=AFU1+AFU2*AVTEM(I)
      COX(I)=AOX1+AOX2*AVTEM(I)+AOX3/(AVTEM(I)**2+TINY)
      CN2(I)=AN21+AN22*AVTEM(I)+AN23/(AVTEM(I)**2+TINY)
      CH2O(I)=AH2O1+AH2O2*AVTEM(I)
      CMIX(I)=CFU(I)*AVFU(I)+COX(I)*AVOX(I)+CN2(I)*FN2(I)+
     1 CH2O(I)*FH2O(I)
      GO TO 943
  940 CMIX(I)=CFU(I)*F(I,JF)+COX(I)*F(I,JOX)+CPR(I)*F(I,JPR)
  943 F(I,JTE)=ENTH/CMIX(I)
      IF(F(I,JTE).GT.TMIN) GO TO 941
      IF(I.EQ.1.OR.I.EQ.N) GO TO 941
```

```
      WRITE(6,942) F(I,JTE),I,ISTEP,TMIN
  942 FORMAT(27H *** TEMPERATURE, F(I,JTE)=,1PE10.3,6H AT I=,I4,7H ISTEP
     1=,I5/17H *** RESET =TMIN=,E10.3,23H *** MAIN CH.9 COMPLETE)
      F(I,JTE)=TMIN
  941 IF(ISTEP.LT.1) GO TO 944
      VMIX=AVFU(I)*RECWFU+AVOX(I)*RECWOX+FN2(I)/WN2+FH2O(I)/WH2O
      RHO(I)=PDGSCN/(AVTEM(I)*VMIX)
      GO TO 907
  944 VMIX=F(I,JF)*RECWFU+F(I,JOX)*RECWOX+F(I,JPR)*RECWPR
      RHO(I)=PDGSCN/(F(I,JTE)*VMIX)
  907 CONTINUE
      IF(KEX.EQ.1) F(N,JTE)=TWALL
      DPDX=DP/DX
C
C     ---------------------------- RADII AND Y"S
      IF(KRAD-2) 901,902,903
C     ----- KRAD=1, PLANE
  901 IF(KIN.EQ.2) HIND=ABS(PSII*RECRU(1))
      GO TO 909
C     ----- KRAD=2, AXIAL
  902 IF(KIN.NE.2) GO TO 908
      HIND=ABS(PSII*RECRU(1))
      HIND=2.*HIND/
     1          (XD*SNALFA+SQRT((XD*SNALFA)**2+2.*HIND*CSALFA)+TINY)
      GO TO 908
C     ----- KRAD=3, POINT SYMMETRY
  903 R(1)=0.
C     ----- CHANGE ABOVE STATEMENT IF NECESSARY FOR KRAD=3
      GO TO 909
  908 R(1)=XU*SNALFA+HIND*CSALFA
C     ------------------------------ COMP
  909 CALL DISTAN
C
C-------------------------------------------------------------------------
CHAPTER 10  10  10  10  10  10  10  ADJUST  10  10  10  10  10  10  10
C
      IF(KEX.EQ.2) GO TO 1022
      AFLOWD=Y(N)+HIND-HDUCID
      IF(KRAD.EQ.2) AFLOWD=AFLOWD*(XU*SNALFA+HCOS*(Y(N)+HIND+HDUCID))
      DA1=ADUCTD/AFLOWD-1.
C     ------------------- DEPENDENCE OF AREA ON PRESSURE
      RECGMP=1./(GAMMA*PRESS)
      DADP=0.
      IF(KIN.EQ.2) DADP=PSII*RECRU(1)*(RECRU(1)*RECRU(1)*RHO(1)-RECGMP)
      SUM=0.
      DPMAX=BIG
      DO 1025 I=2,NM1
      DPMAX=AMIN1(DPMAX,RHO(I)*U(I)**2)
 1025 SUM=SUM+BOM(I)*RECRU(I)*(RECRU(I)*RECRU(I)*RHO(I)-RECGMP)
      DADP=DADP+PEI*SUM
C     ------------------- ADJUSTMENT OF P"S, U"S ETC.
```

```
      IF(ABS(DA1).LT.1.E-3) GO TO 1022
      DP=DA1*AFLOWD/DADP
      DP=AMIN1(DP,.5*DPMAX)
      PRESS=PRESS+DP
      DPDX=DPDX+DP/DX
      RHOFAC=1.+DP*RECGMP
      DO 1027 I=2,NM1
      U(I)=U(I)-DP*RECRU(I)
 1027 RHO(I)=RHO(I)*RHOFAC
      IF(KIN.NE.2) GO TO 1029
      U(1)=U(1)-DP*RECRU(1)
 1029 RHO(1)=RHO(1)*RHOFAC
      RHO(N)=RHO(N)*RHOFAC
      RECRU(1)=1./(RHO(1)*U(1)+TINY)
      IF(KIN.NE.2) GO TO 1026
      HIND=ABS(PSII*RECRU(1))
      IF(KRAD.EQ.1) GO TO 1026
      HIND=2.*HIND/
     1       (XD*SNALFA+SQRT((XD*SNALFA)**2+2.*HIND*CSALFA)+TINY)
      R(1)=XU*SNALFA+HIND*CSALFA
 1026 CALL DISTAN
      AFLOWD=Y(N)+HIND-HDUCID
      IF(KRAD.EQ.2) AFLOWD=AFLOWD*(XU*SNALFA+HCOS*(Y(N)+HIND+HDUCID))
      DA2=ADUCTD/AFLOWD-1.
 1022 CONTINUE
C-----------------------------------------------------------------------
CHAPTER 11 11 11 11 11 11 11 11 11 11  PRINT  11  11  11  11  11  11
C     SEE DATA
 1100 CONTINUE
      IF(XU.LE.XOUT) GO TO 1101
      NSTAT=24
      NPROF=24
 1101 CONTINUE
      CALL DEMO2
      CALL OUTPUT
C
C-----------------------------------------------------------------------
CHAPTER 12  12  12  12  12  12  12  DECIDE  12  12  12  12  12  12  12
      IF(ISTEP.EQ.LASTEP) GO TO 1203
      IF(XU.LT.XULAST) GO TO 1202
 1203 IFIN=2
      CALL DEMO2
      CALL OUTPUT
 1202 IF(IFIN.EQ.1) GO TO 600
      STOP
      END
```

```
      SUBROUTINE OUTPUT
C/ SEPT.1977 -- GENMIX-T, HTS/77/9, APPXA -- COPYRIGHT, D.B.SPALDING --
$INCLUDE 9,COMA1.FTN
$INCLUDE 9,COMB.FTN
C
      DIMENSION LAB(25),OUT(25),TITLE(3,4),
     1XLPLOT(150),YLAXIS(17),YLPLOT(150,17),
     2XTPLOT(60),YTAXIS(9),YTPLOT(60,9),
     3DFE(20),DFI(20),FLUX(20),STANE(20),STANI(20)
C
CHAPTER A ---------------------- INITIAL DATA FOR PRINTOUT -----------
C     ------------------- CROSS-STREAM OUTPUT (PROFILE) DATA ----------
C     ----- ASSIGN KOUT= NO. OF VARIABLES, AND OUTPUT LABELS LAB(K)
      DATA KOUT/12/
      DATA LAB/"R/RØ","UVEL","TEMP","FUEL","OXYG","H2M",
     1 "O2M","H2OM","N2M","TEMF","FUFL","OXFL"/
C
C     -------------------- TRANSVERSE (CROSS-STREAM) PLOT DATA ---------
C     ----- ASSIGN NYT= NO. OF VARIABLES TO BE PLOTTED
C     --- INSERT DIMENSIONS, ENSURE THAT ITDIM.GE.N.AND.JTDIM.GE.NYT.
      DATA NYT/9/,ITDIM,JTDIM/60,9/
C     ----- ASSIGN LABELS FOR PLOT AXES
      DATA XTAXIS/"Y(I)"/
      DATA (YTAXIS(K),K=1,9)/"U VEL","TEMP","FUEL","OXYG","1FAG","2FAG"
     1,"3FAG","4FAG","5FAG"/
C
C     -------------------- LONGITUDINAL (DOWN-STREAM) PLOT DATA --------
C     ----- ASSIGN NYL= NO. OF VARIABLES TO BE PLOTTED
C     -- INSERT DIMENSIONS, ENSURE THAT ILDIM.GE.LASTEP.AND.JLDIM.GE.NYL
      DATA NYL/17/,ILDIM,JLDIM/150,17/
C     ----- ASSIGN LABELS FOR PLOT AXES
      DATA XLAXIS/"XU"/
      DATA (YLAXIS(K),K=1,17)/"U(1)","T(1)","FU(1)","OX(1)","N,R OR Y",
     1 "1,R(1)","2,PEI","3,RME","4,FLUXFU","5,DPDX","6,RATE","7,FACE",
     2 "A,FAG","B,FAG","C,FAG","D,FAG","E,FAG"/
C
C     -------------------- TITLE DATA
      DATA TITLE/"AXI-","SYMM","ETRI","CAL ","FLOW",
     1 "PLAN","E FL","OW "," ",
     2 "RADI","ALLY","-  T","WARD"," FLO","W",
     3 "VARI","ABLE"," CSA","LFA "," "/
C
CHAPTER B ---------------------------- HEADINGS ----------------------
      IF(ISTEP.GT.Ø) GO TO 1102
C     ------------------- MODIFIED DATA
      IF(MODEL.GT.2) GO TO 100
      KOUT=12
  100 CONTINUE
      WRITE(6,1103) (TITLE(I,KIND),I=1,5)
 1103 FORMAT(1H1,"GENMIX-T, SEPT.1977, TURBULENCE MODELS TEACHING PROGRA
     1M,"/" BASED ON APPENDIX A OF HTS REPORT NO. HTS/77/9, FEB.1977."/
```

```
     2 " COMBUSTION OF HYDROGEN AND AIR IN A JET, ",5A4)
C
      PRESS1=PRESS
      TEM=.5*(R(1)+R(N))
      EMU1=(VISFU*F(1,JF)+VISOX*F(1,JOX)+VISPR*F(1,JPR))*
     1                                                SQRT(F(1,JTE))
      REY=PEI/(EMU1*TEM)
      EQRAT=0.0
      IF(INERT.NE.1) EQRAT=FLOB*STOICH/(FLOC+TINY)/(OXC+TINY)
      AMACH=SQRT(PEI*UB/(GAMMA*PRESS*TEM))
C
      WRITE(6,1013) KASE,IRUN,KIND,KRAD,CSALFA,MODEL,LENGTH,MOD4C1,
     1 INERT,NOVEL
 1013 FORMAT(1H0,5H KASE,5H IRUN,5H KIND,5H KRAD,7H CSALFA,6H MODEL,
     1 7H LENGTH,7H MOD4C1,6H INERT,6H NOVEL/1X,I4,3I5,F7.3,I6,2I7,2I6)
C
      WRITE(6,1015)NAGE,JA1,JAL,FOLM0,UMAX,MODFOR,(AGE(L),L=1,NAGEP1,2)
 1015 FORMAT(/5(1H*),40HTHE ESCIMO MODEL OF TURBULENT COMBUSTION,
     + 5(1H*)/5(1H*),38HIS INCORPORATED IN THE PRESENT PROGRAM,
     + 2X,5(1H*)/5(1H*),21HDEMOGRAPHIC CONSTANTS,5(1H*)/1X,
     +37HNAGE  JA1   JAL   FOLM0 UMAX  MODFOR /1X,2I4,I6,2X,2F6.2,I4/
     +47H  AGE1   AGE3    AGE5    AGE7     AGE9    AGE11,/6F8.5)
      WRITE(6,1018) EMPC1,EMPC2,EMPC3
 1018 FORMAT(/5(1H*),20HBIOGRAPHIC CONSTANTS,5(1H*)/1X,
     1 25HEMPC1     EMPC2     EMPC3/1X,3E10.3)
      WRITE(6,1014) OMPOW,(OM(I),I=1,N)
 1014 FORMAT(1H0,18H OM(I), FOR OMPOW=,F6.3/(1X,1P6E11.3))
C
      WRITE(6,1010)
     1 HEX0,XHEX0,AHEX,BHEX,CHEX,
     2 HIN0,XHIN0,AHIN,BHIN,CHIN,
     3 UEX0,XUEX0,AUEX,BUEX,CUEX,
     4 XEND,XOUT,XULAST,HDIV,AGRAV
 1010 FORMAT(1H0,
     1 4X,4HHEX0,6X,5HXHEX0,7X,4HAHEX,7X,4HBHEX,7X,4HCHEX/1X,1P5E11.3/
     2 5X,4HHIN0,6X,5HXHIN0,7X,4HAHIN,7X,4HBHIN,7X,4HCHIN/1X,1P5E11.3/
     3 5X,4HUEX0,6X,5HXUEX0,7X,4HAUEX,7X,4HBUEX,7X,4HCUEX/1X,1P5E11.3/
     4 5X,4HXEND,7X,4HXOUT,5X,6HXULAST,7X,4HHDIV,6X,5HAGRAV/1X,1P5E11.3)
C
      WRITE(6,1011) UA,UB,UC,UD,TA,TB,TC,TD,
     2 PRESS,PREEXP,REY,EQRAT,AMACH,ULIM,PEILIM
 1011 FORMAT(1H0,4X,2HUA,7X,2HUB,7X,2HUC,7X,2HUD,
     1  7X,2HTA,7X,2HTB,7X,2HTC,7X,2HTD/1X,8F9.3/
     2 4X,5HPRESS,3X,6HPREEXP,6X,3HREY,4X,5HEQRAT,4X,5HAMACH,5X,4HULIM,
     2 3X,6HPEILIM/1X,1P7E9.2)
      IF(MODEL.LE.2) GO TO 1102
      WRITE(6,1012) AK,ELCON,TAUDK,ELEXP,SIGK,SIG2,
     2 CMU,CD,FJKA,FJ2A,FJKD,FJ2D
 1012 FORMAT(1H0,3X,2HAK,9X,5HELCON,6X,5HTAUDK,6X,5HELEXP,6X,4HSIGK,7X,
     1 4HSIG2/ 1P6E11.3/
     2 4X,3HCMU,8X,2HCD,9X,4HFJKA,7X,4HFJ2A,7X,4HFJKD,7X,4HFJ2D/6E11.3)
```

```
C
      IF(MODEL.EQ.4) WRITE(6,1017) C1MOD4,C2MOD4
 1017 FORMAT(1H ,3X,6HC1MOD4,5X,6HC2MOD4/2E11.3)
      IF(MODEL.EQ.5) WRITE(6,1016) C1MOD5,C2MOD5
 1016 FORMAT(1H ,3X,6HC1MOD5,5X,6HC2MOD5/2E11.3)
C
C
CHAPTER C ---------------- COMPUTE OUTPUT REQUIRED AT EACH STEP --------
 1102 CONTINUE
      UBAR=0.
      DO 110 I=2,NM1
  110 UBAR=UBAR+BOM(I)*U(I)
      UFLUX=PEI*UBAR
C
      NFLAST=JAL+3
      DO 115 J=1,NFLAST
      FLUX(J)=0.
      DO 116 I=2,NM1
  116 FLUX(J)=FLUX(J)+BOM(I)*F(I,J)
  115 FLUX(J)=PEI*FLUX(J)
C
      DO 117 J=1,NF
      DFI(J)=FLUX(J)/PEI-F(1,J)
  117 DFE(J)=DFI(J)+F(1,J)-F(N,J)
      UFLUX=UFLUX-PSIE*U(N)+U(1)*PSII
      FLUX(JH)=FLUX(JH)-PSIE*ENTHD+PSII*ENTHA
      FLUX(JP)=FLUX(JP)-PSIE*PHID+PSII*PHIA
      FLUX(JF)=FLUX(JF)-PSIE*FUD+PSII*FUA
      PRESSD=PRESS/PRESS1-1.
C
      IF(ISTEP.EQ.0.OR.ILPLOT.EQ.1) GO TO 1105
C     ----- ASSIGN VALUES FOR DOWNSTREAM PLOT
      IPRIPL=10
      XLPLOT(ISTEP)=XU
      YLPLOT(ISTEP,1)=U(IPRIPL)
      YLPLOT(ISTEP,2)=F(IPRIPL,JTE)
      YLPLOT(ISTEP,3)=F(IPRIPL,JF)
      YLPLOT(ISTEP,4)=F(IPRIPL,JOX)
      IF(KIND-1) 111,111,114
  111 YLPLOT(ISTEP,5)=R(N)
      GO TO 113
  114 YLPLOT(ISTEP,5)=Y(N)
  113 CONTINUE
      YLPLOT(ISTEP,6)=R(1)
      YLPLOT(ISTEP,7)=PEI
      YLPLOT(ISTEP,8)=RME
      YLPLOT(ISTEP,9)=FLUX(JF)
      YLPLOT(ISTEP,10)=DPDX
      YLPLOT(ISTEP,11)=RATE
      YLPLOT(ISTEP,12)=FACE
      YLPLOT(ISTEP,13)=F(IPRIPL,JA1)
```

```
      YLPLOT(ISTEP,14)=F(IPRIPL,JA2)
      YLPLOT(ISTEP,15)=F(IPRIPL,JA3)
      YLPLOT(ISTEP,16)=F(IPRIPL,JA4)
      YLPLOT(ISTEP,17)=F(IPRIPL,JA5)
 1105 CONTINUE
C
C     ----- TESTS FOR PRINTOUT
C     ----- IPRINT=1 GIVES SINGLE (STATION) VARIABLES,
C           IPRINT=2 ADDS THE ARRAY (PROFILE) VARIABLES,
C           IPRINT=3 ADDS THE CROSS-STREAM PLOTS.
      IPRINT=0
      IF(MOD(ISTEP,NSTAT).EQ.0) IPRINT=1
      IF(MOD(ISTEP,NPROF).EQ.0) IPRINT=2
      IF(ISTEP.EQ.0) GO TO 1020
      IF(MOD(ISTEP,NPLOT).EQ.0
     1 .OR.ISTEP.EQ.JUSTEX.OR.ISTEP.EQ.JUSTIN
     2 .OR.ITEST.NE.1.OR.IFIN.NE.1) IPRINT=3
 1020 IF(IPRINT.EQ.0) RETURN
C
CHAPTER D ------------------------------  STATION VARIABLES  ----------
      WRITE(6,1030) XU,ISTEP,
     1 JUSTIN,JUSTEX,DX,PRESSD,
     2 KIN,KEX,DXY,DPDX,
     3 PSII,PSIE,DXRE,PEI,
     4 RMI,RME,DXINC,YREF1,
     5 R(1),R(N),DXPSI,YREF2,
     6 ELCON,
     7 UFLUX,
     8 (FLUX(J),J=1,NF)
 1030 FORMAT(1H0,5H***  ,3HXU=,1PE10.3,2X,6HISTEP=,I5/
     1 2X,7HJUSTIN=,I10,1X,7HJUSTEX=,I10,5X,3HDX=,1PE10.3,
     1 8H PRESSD=,E10.3/
     2 5X,4HKIN=,I10,4X,4HKEX=,I10,4X,4HDXY=,E10.3,3X,5HDPDX=,E10.3/
     3 4X,5HPSII=,E10.3,3X,5HPSIE=,E10.3,3X,5HDXRE=,E10.3,
     3 4X,4HPEI=,E10.3/
     4 5X,4HRMI=,E10.3,4X,4HRME=,E10.3,2X,6HDXINC=,E10.3,2X,6HYREF1=,
     4 E10.3/
     5 4X,5HR(1)=,E10.3,3X,5HR(N)=,E10.3,2X,6HDXPSI=,E10.3,2X,6HYREF2=,
     5 E10.3/
     6 3X,6HELCON=,E10.3/
     7 3X,6HUFLUX=,E10.3/
     8 1X,8HFLUX(J)=,(5E11.3))
C
      IF(ISTEP.EQ.0) GO TO 1042
      UREF=UBAR
      RUREF=PEI/((R(1)+R(N))*.5*Y(N))
      URUREF=1./(UREF*RUREF)
C
      IF(KIN-2) 1061,1062,1063
 1061 TAUID=TAUI*URUREF
      DO 1025 J=1,NF
```

```
 1025 STANI(J)=(RJTOTI(J)-F(1,J)*RMI)/(R(1)*DFI(J)*RUREF+TINY)
      WRITE(6,1029) TAUID,(STANI(J),J=1,NF)
 1029 FORMAT(1H ,6HTAUID=,1PE10.3,10H STANI(J)=,(4E11.3))
      GO TO 1063
 1062 WRITE(6,1069) FACI,RATI
 1069 FORMAT(1H ,6H FACI=,1PE10.3,6H RATI=,E10.3)
C
 1063 IF(KEX-2) 1081,1082,1044
 1081 TAUED=TAUE*URUREF
      DO 1027 J=1,NF
 1027 STANE(J)=(RJTOTE(J)-F(N,J)*RME)/(R(N)*DFE(J)*RUREF+TINY)
      WRITE(6,1028) TAUED,(STANE(J),J=1,NF)
 1028 FORMAT(1H ,6HTAUED=,1PE10.3,10H STANE(J)=,(4E11.3))
      GO TO 1044
 1082 WRITE(6,1089) FACE,RATE
 1089 FORMAT(1H ,6H FACE=,1PE10.3,6H RATE=,E10.3)
      GO TO 1042
 1044 WRITE(6,1047) DA1,DA2
 1047 FORMAT(5H DA1=,1PE10.3,5H DA2=,E10.3)
C
CHAPTER E ------------------------------ CROSS-STREAM PROFILES  ---------
 1042 IF(IPRINT.EQ.1) GO TO 1050
      YN=Y(N)
      WRITE(6,1199) YN
 1199 FORMAT(6H Y(N)=,1PE10.2)
C
      WRITE(6,1099) (LAB(K),K=1,6)
      DO 1091 I=1,N
      OUT(1)=Y(I)/HEX0
      OUT(2)=U(I)
      OUT(3)=AVTEM(I)
      OUT(4)=AVFU(I)
      OUT(5)=AVOX(I)
      OUT(6)=FMFU(I)
C     ------------------------------ WRITE PROFILES
 1091 WRITE(6,1098) I,(OUT(K),K=1,6)
      IF(KOUT.LE.6) GO TO 1093
      WRITE(6,1099) (LAB(K),K=7,KOUT)
      DO 1092 I=1,N
      OUT(7)=FMOX(I)
      OUT(8)=FMH2O(I)
      OUT(9)=FMN2(I)
      OUT(10)=TFLU(I)
      OUT(11)=FUFLU(I)
      OUT(12)=OXFLU(I)
 1092 WRITE(6,1098) I,(OUT(K),K=7,KOUT)
 1093 CONTINUE
      IF(ISTEP.LT.5) GO TO 2003
      WRITE(6,2001) (J,J=1,NAGE)
 2001 FORMAT(/5X,5H*****,32HPOPULATION DISTRIBUTION OF FOLDS,
     1 5H*****/2X,3H I ,7H   FRAT,3X,5(7H  PA ( ,I2,2H) )/
```

```
     1 15X,5(7H  PA ( ,I2,2H) ))
       DO 2000 I=2,NM1
 2000 WRITE(6,2002) I,PA0(I)/RHO(I),(PA(I,J),J=1,NAGE)
 2002 FORMAT(1X,I3,1P6E11.3/15X,1P5E11.3)
       IF(IPDF.NE.1) GO TO 2003
       WRITE(6,2007)
 2007 FORMAT(1H1,5X,5H*****,30HPDF VALUES OF TEMPERATURE     ,
     1 5H*****)
       WRITE(6,2004) (K,K=1,NPDFM1)
 2004 FORMAT(/2X,3H I ,5(7H  PDF( ,I2,2H) )/
     1 5X,5(7H  PDF( ,I2,2H) ))
       DO 2005 I=2,NM1
 2005 WRITE(6,2006) I,(AVPDF(I,K),K=1,NPDFM1)
 2006 FORMAT(1X,I3,1P5E11.3/4X,1P5E11.3)
 2003 CONTINUE
C
       IF(IPRINT.LT.3.OR.ITPLOT.EQ.1) GO TO 1050
C      ----- ASSIGN CROSS-STREAM PLOTS
       DO 1073 I=1,N
       XTPLOT(I)=Y(I)
       YTPLOT(I,1)=U(I)
       YTPLOT(I,2)=F(I,JTE)
       YTPLOT(I,3)=F(I,JF)
       YTPLOT(I,4)=F(I,JOX)
       IF(MODEL.LE.2) GO TO 1073
       YTPLOT(I,5)=EMU(I)
       YTPLOT(I,6)=F(I,JEL)
       YTPLOT(I,7)=F(I,J2)
       YTPLOT(I,8)=F(I,JK)
C      YTPLOT(I,9)=OUT(11) ABOVE
 1098 FORMAT(1H ,I3,1P12E10.2)
 1099 FORMAT(1H0,3H  I,12(2X,A8))
 1073 CONTINUE
C      ---------------------- CROSS-STREAM PLOT OUTPUT
       WRITE(6,1096) XU,ISTEP
 1096 FORMAT(19H1CROSS-STREAM PLOT,,4H XU=,1PE10.3,7H ISTEP=,I4)
C
CHAPTER F ---------------------------- RETURN OR TERMINATE ---------------
 1050 IF(IFIN.EQ.1) RETURN
       WRITE(6,112) ISTEP,LASTEP,XU,XULAST,IFIN
  112 FORMAT(14H0TERMINATED AT//7H ISTEP=,I5,8H LASTEP=,I5,
     1 4H XU=,1PE11.3,8H XULAST=,E11.3,6H IFIN=,I3)
       IF(ILPLOT.EQ.1) RETURN
C
C      ---------------------- DOWNSTREAM PLOT OUTPUT
       WRITE(6,1054) XU,ISTEP
 1054 FORMAT(18H1DOWN-STREAM PLOT,,4H XU=,1PE10.3,7H ISTEP=,I4)
       RETURN
C      ------------------------------------------
       END
```

```
      SUBROUTINE DEMO
$INCLUDE 9,COMA1.FTN
$INCLUDE 9,COMB.FTN
C*****************************************************************
      ENTRY DEMOC
C*****************************************************************
      DO 3 L=1,NAGE
      DAGE(L)=AGE(L+1)-AGE(L)
      AGEC(L)=AGE(L)+Ø.5*DAGE(L)
    3 RECDA(L)=1./DAGE(L)
      AGE2=AGE(2)
      JA1P1=JA1+1
      JA1M1=JA1-1
      RETURN
C*****************************************************************
      ENTRY DEMOS
C*****************************************************************
C-------------CALCULATION OF ME/MO---------------------------------
C           CALCULATION OF FOLD FORMATION RATE  BASED
C           ON DIFFERENT ASSUMPTIONS  ABOUT THE DISTRIBUTION
C           ACROSS THE BOUNDARY LAYER
C           MODFOR=1  EXPONENTIAL DISTRIBUTION
C           MODFOR=2  LINEAR DISTRIBUTION
C           MODFOR=3  VELOCITY GRADIENT PROFILE DISTRIBUTION
C           MODFOR=4  VELOCITY PROFILE DISTRIBUTION
C           MODFOR=5  THETA DISTRIBUTION
C           OTHER DISTRIBUTION CAN BE INSERTED HERE
      SUM1=Ø.
      SUM2=Ø.
      FOLMØ=Ø.5
C----------ARRAY PAØ IS USED HERE AS TEMPORAY STORAGE FOR THE
C----------AREA OF EACH CELL.
      PAØ(2)=Ø.5*(Y(2)+Y(3))*R(2)
      PAØ(NM1)=(Y(N)-Ø.5*(Y(NM1)+Y(NM2)))*R(NM1)
      DO 4Ø I=3,NM2
   4Ø PAØ(I)=Ø.5*(Y(I+1)-Y(I-1))*R(I)
      GO TO (41,42,43,44,45),MODFOR
C----------EXPONENTIAL DISTRIBUTION OF INJECTED MASS
   41 DO 41Ø I=2,NM1
      OMI=OM(I)
      SUM1=SUM1+RHO(I)*(1.-OMI)*EXP(-OMI)*PAØ(I)*XMØ(I)
  41Ø SUM2=SUM2+RHO(I)*OMI*EXP(OMI-1.)*PAØ(I)*XMØ(I)
      ALFA1=RMI/SUM1
      ALFA2=-RME/SUM2
      DO 411 I=2,NM1
      OMI=OM(I)
  411 PAØ(I)=RHO(I)*(ALFA1*(1.-OMI)*EXP(-OMI)+ALFA2*OMI*EXP(OMI-1.))
      GO TO 49
C----------LINEAR DISTRIBUTION OF FOLD FORMATION
   42 DO 42Ø I=2,NM1
      SUM1=SUM1+RHO(I)*(1.-OM(I))*PAØ(I)*XMØ(I)
```

```
  420 SUM2=SUM2+RHO(I)*OM(I)*PA0(I)*XM0(I)
      ALFA1=RMI/SUM1
      ALFA2=-RME/SUM2
      DO 421 I=2,NM1
  421 PA0(I)=RHO(I)*(ALFA1*(1.-OM(I))+ALFA2*OM(I))
      GO TO 49
C-----------VELOCITY GRADIENT RATE
   43 DO 430 I=2,NM1
      DUDYB(I)=ABS(U(I+1)-U(I-1))/(Y(I+1)-Y(I-1))
  430 SUM1=SUM1+RHO(I)*DUDYB(I)*PA0(I)*XM0(I)
      ALFA1=(RMI-RME)/SUM1
      DO 431 I=2,NM1
  431 PA0(I)=RHO(I)*ALFA1*DUDYB(I)
      GO TO 49
C----------VELOCITY PROFILE DISTRIBUTION
   44 DO 440 I=2,NM1
  440 SUM1=SUM1+RHO(I)*U(I)*PA0(I)*XM0(I)
      ALFA1=(RMI-RME)/SUM1
      DO 441 I=2,NM1
  441 PA0(I)=RHO(I)*ALFA1*U(I)
      GO TO 49
C----------THETA DISTRIBUTION RATE
   45 OMSTAR=0.5
      IF(ISTEP.GT.1) OMSTAR=RMI/(RMI-RME+TINY)
      TEMI=(F(1,JH)-.5*U(1)**2)/CPR(1)
      TEMIP1=(F(2,JH)-.5*U(2)**2)/CPR(1)
      TTI=(TD-TEMI)/(TD-TA)
      TTIP1=(TD-TEMIP1)/(TD-TA)
      SUMM0=0.
      DO 450 I=2,NM1
      TTIM1=TTI
      TTI=TTIP1
      TEMIM1=TEMI
      TEMI=TEMIP1
      TEMIP1=(F(I+1,JH)-.5*U(I+1)**2)/CPR(1)
      TTIP1=(TD-TEMIP1)/(TD-TA)
      TPRIME=0.735*F(I,JEL)*ABS(TTIP1-TTIM1)/(Y(I+1)-Y(I-1))
      TPRIME=AMIN1(TPRIME,1.-TTI,TTI)+TINY
C     IF(OM(I).LT.OMSTAR) GO TO 10
      YSTAR=Y(I)/Y(N)
      IF(YSTAR.LT.OMSTAR) GO TO 10
      TREENG=TTI+TPRIME
      TFRESH=0.
      GO TO 11
   10 TREENG=ABS(TTI-TPRIME)
      TFRESH=1.
   11 XM0(I)=(TREENG-TTI)/(TREENG-TFRESH)
  450 SUM1=SUM1+RHO(I)*XM0(I)*PA0(I)
      ALFA1=(RMI-RME)/(FOLM0*SUM1)
      DO 451 I=2,NM1
  451 PA0(I)=RHO(I)*ALFA1*XM0(I)
```

```
  49  CONTINUE
      RETURN
C*************************************************************************
      ENTRY DEMO2
C*************************************************************************
      IF(IFIN.EQ.2) GO TO 50
      IF(ISTEP.LE.1.OR.MOD(ISTEP,NSTAT).NE.0) GO TO 70
   50 DO 51 J=1,NAGE
      DO 51 I=2,NM1
      PA(I,J)=F(I,J+JA1-1)
  51  CONTINUE
   70 CONTINUE
      RETURN
      END
```

```
      SUBROUTINE BIOG
$INCLUDE 9,COMA1.FTN
$INCLUDE 9,COMB.FTN
C*****************************************************************
      ENTRY BIOC
C*****************************************************************
C----------THE BIOGRAPHIC ANALYSIS IS PERFORMED
C----------IN THIS SUBROUTINE
C----------THE FOLLOWING "OPEN" STATEMENT IS VALID FOR
C----------PERKIN-ELMER 3220 COMPUTER ONLY.IT SHOULD
C----------BE MODIFIED IF OTHER MACHINE IS USED.
C----------THE RECORD LENGTH(RECL) SHOULD BE EQUAL TO
C----------OR GREATER THAN THE NUMBER OF ELEMENTS IN
C----------THE ARRAY(TO BE STORED)MULTIPLIED BY FOUR.
      OPEN(7,FILE="FOLD",ACCESS="DIRECT",STATUS="UNKNOWN",
     1 RECL=640,COUNTBY="RECORD",FORM="UNFORMATTED")
      PI=3.141596
      NDIFOM=20
      FSTOIC=0.0282
      DTST=2276.
      TST=DTST
      PDGSCN=PRESS/GASCON
      RHOAIR=PDGSCN*WPR/TD
      RHOFUL=PDGSCN*WFU/TA
      WOXPR=(WOX-WPR)*0.232
      WFUPR=WFU-WPR
      FS1=1.-FSTOIC
      VISDPR=VISMIX/PRLAM
      TWODPI=2./PI
      PHID=OXD-FUD*STOICH
      T2=0.5/STOICH
      T3=1./(PHIB-PHID+TINY)
      T4=-PHID*T3
      OXD1=1.-OXD
      RETURN
C*****************************************************************
      ENTRY BIOS
C*****************************************************************
      OMSTAR=0.
      IF(ISTEP.GT.1)OMSTAR=RMI/(RMI-RME+TINY)
C----------OMEGA-STAR DEVIDES THE SHEAR LAYER INTO TWO PARTS
C----------OF DIFFRENT ENTRAINED FRESH MASS . IT HAS TO BE CALCULATED
C----------IN CONSISTENT MANNER WITH FOLD FORMATION RATE.
      FFI=-(F(1,JP)-.232)/(PHID-PHIB)
      FFIP1=-(F(2,JP)-0.232)/(PHID-PHIB)
C------ LOOP FOR ALL LAYER GRID POINTS
      Y2=Y(2)
      ISTEP1=ISTEP+1
      DO 110 I=1,N
      DO 110 K=1,NPDF
      AVPFA(I,K)=0.
```

```
      AVPDF(I,K)=0.
  110 CONTINUE
      DO 100 I=2,NM1
C------ CALCULATION OF F- PRIME
      ELI=AMAX1(Y2,F(I,JEL))
      FFIM1=FFI
      FFI=FFIP1
      FFIP1=-(F(I+1,JP)-0.232)/(PHID-PHIB)
      FPRIME=EMPC1*ELI*ABS(FFIP1-FFIM1)/(Y(I+1)-Y(I-1))
      IF(FPRIME.GT.0.001.AND.FFI.EQ.1.) FFI=0.5*(FFIP1+FFIM1)
      IF(FPRIME.GT.0.001.AND.FFI.EQ.0.) FFI=0.5*(FFIP1+FFIM1)
      FPRIME=AMIN1(FPRIME,1.-FFI)+TINY
      IF(OM(I).LT.OMSTAR) GO TO 10
C------ DETERMINATION OF FRESH F AND REENGULFED F
      FFRESH=0.
      FREENG=FFI+FPRIME
      RHOFSH=RHOAIR
      GO TO 11
   10 FREENG=ABS(FFI-FPRIME)
      FFRESH=1.
      RHOFSH=RHOFUL
C------ DETERMINATION OF M0 VALUE
   11 FOLM0=(FREENG-FFI)/(FREENG-FFRESH+TINY)
      XM0(I)=FOLM0
      AVRAT1(I)=0.
      AVRAT2(I)=0.
      AVFU(I)=0.
      AVOX(I)=0.
      AVPR(I)=0.
      AVTEM(I)=0.
      AVTEMS(I)=0.
      AVFUS(I)=0.
      AVOXS(I)=0.
      AVPRS(I)=0.
      RBURN(I)=0.
      SUMPDF(I)=0.
      AVFFIS(I)=0.
      POPAGE(I)=0.
      CXFOR=0.5*(UMAX+UMIN)/UMAX
      DUDYB(I)=ABS(U(I+1)-U(I-1))/(Y(I+1)-Y(I-1))
C------ DETERMINATION OF FOLD DIVISION
C------DENSITY OF REENGULFED MASS
      IF(FREENG.GE.FSTOIC) GO TO 17
C------AIR SIDE
      RHORE=PDGSCN*(WOXPR*(FSTOIC-FREENG)/FSTOIC+WPR)/(TD+FREENG/FSTOIC*
     1                                                  (TST-TD))
      GO TO 19
C------FUEL SIDE
   17 RHORE=PDGSCN*(WFUPR*(FREENG-FSTOIC)/FS1+WPR)/(TA+(1.-FREENG)/FS1*
     1                                               (TST-TA))
   19 CONTINUE
```

```
C
C------ FOLD DISTANCES MEASURED FROM THE FRESH SIDE
      HFOL=EMPC2*ELI
      HDIVF=RHORE*FOLMØ*HFOL/(RHOFSH+RHORE*FOLMØ-RHOFSH*FOLMØ)
      HFRESH=HDIVF
      RHODIV=RHOFSH
      HREENG=HFOL-HFRESH
      OMDIVF=FOLMØ
C----------LEFT PART OF THE FOLD HAS THE HIGHER F-VALUE
      IF(FFRESH.EQ.1.) GO TO 24
      RHODIV=RHORE
      HDIVF=HFOL-HDIVF
      HFRESH=HFOL-HDIVF
      HREENG=HFOL-HFRESH
      OMDIVF=1.-FOLMØ
   24 RHOAV=(RHOFSH*HFRESH+RHORE*HREENG)/HFOL
      IF(FREENG.LE.FSTOIC) GO TO 25
      TREENG=TA+(1.-FREENG)/FS1*(TST-TA)
      TAV=(RHOFSH*TA*HFRESH+RHORE*TREENG*HREENG)/(RHOAV*HFOL)
      GO TO 26
   25 TREENG=TD+FREENG/FSTOIC*(TST-TD)
      TAV=(RHOFSH*TD*HFRESH+RHORE*TREENG*HREENG)/(RHOAV*HFOL)
   26 DIFCOF=VISDPR*SQRT(TAV)/RHOAV
      RSTR=EMPC3*DUDYB(I)+TINY
      OMDIVF=HDIVF*RHODIV/(HFOL*RHOAV)
      ADIF=DIFCOF/(2.*HFOL*HFOL)
C----------STORE THE FOLD CHARACTERISTICS AT BIRTH PLACE
C----------FOR EACH POINT ACROSS THE JET---------------
      ARRAY(I,1)=HFOL
      ARRAY(I,2)=OMDIVF
      ARRAY(I,3)=FFRESH
      ARRAY(I,4)=FREENG
      ARRAY(I,5)=RSTR
      ARRAY(I,6)=FFI
      ARRAY(I,7)=ADIF
      ARRAY(I,8)=U(I)
  1ØØ CONTINUE
      XMØ(1)=XMØ(2)
      XMØ(N)=XMØ(NM1)
      IF(KIN.NE.3) GO TO 1Ø1Ø
      DO 1Ø1 JJ=1,8
      ARRAY(1,JJ)=ARRAY(2,JJ)
  1Ø1 CONTINUE
      GO TO 1Ø2Ø
 1Ø1Ø ARRAY(1,1)=ARRAY(2,1)
      ARRAY(1,2)=ARRAY(2,2)
      ARRAY(1,3)=1.
      ARRAY(1,4)=1.
      ARRAY(1,5)=ARRAY(2,5)
      ARRAY(1,6)=1.
      ARRAY(1,7)=ARRAY(2,7)
```

```
      ARRAY(1,8)=ARRAY(2,8)
 1020 ARRAY(N,1)=ARRAY(NM1,1)
      ARRAY(N,2)=ARRAY(NM1,2)
      ARRAY(N,3)=0.
      ARRAY(N,4)=0.
      ARRAY(N,5)=ARRAY(NM1,5)
      ARRAY(N,6)=0.
      ARRAY(N,7)=ARRAY(NM1,7)
      ARRAY(N,8)=UD
      DO 1030 I=2,NM1
      FVAL(I)=-(F(I,JP)-0.232)/(PHID-PHIB)
 1030 FN2(I)=OXD1*(1.-FVAL(I))
C----------STORE THE FOLD INFORMATION INTO THE TAPE
C----------THE MASS STORAGE FACILITIES IS EMPLOYED--------
C----------HERE TO REDUCE THE IN-CORE STORAGE------------
      WRITE(7,REC=ISTEP1) ARRAY
      XP(ISTEP1)=XD
      KBORN=ISTEP1
C----------LOOP ON AGES STARTS NOW----------
      DO 1000 IA=1,NAGE
      IF(IA.GT.1) GO TO 800
      IBORN1=1
      GO TO 805
  800 IBORN1=1
      XFOR=XD*(1.-AGEC(IA))
      KSUM=ISTEP1+1
C----------SEARCH FOR THE BIRTH PLACE OF FOLDS AT
C----------PARTICULAR AGE IN THE POPULATION -------------
      DO 801 KK=1,ISTEP1
      K=KSUM-KK
      IF(XFOR.GT.XP(K)) GO TO 802
  801 CONTINUE
  802 KBORN=K+1
C----------READ THE REQUIRED INFORMATION FROM THE TAPE-------
      IF(KBORN.LT.KBORNP) READ(7,REC=KBORN) ARRAY
  805 KBORNP=KBORN
      DO 900 I=2,NM1
      RATEA1(I)=0.
      RATEA2(I)=0.
      FUAV(I)=0.
      OXAV(I)=0.
      PRAV(I)=0.
      TEMAV(I)=0.
      TEMAVS(I)=0.
      FUAVS(I)=0.
      OXAVS(I)=0.
      PRAVS(I)=0.
      FFIAVS(I)=0.
      DO 903 L=2,N
      IF(FVAL(I).GT.ARRAY(L,6)) GO TO 904
  903 CONTINUE
```

```
  904 IBORN=L-IBORN1
C----------THE LINEAR INTERPOLATION PROCEDURE IS USED HERE
C----------TO DETERMINE THE FOLD CHARACTERISTICS AT BIRTH PLACE-----
      FACTOR=(ARRAY(IBORN,6)-FVAL(I))/(ARRAY(IBORN,6)
     1 -ARRAY(IBORN+1,6)+TINY)
      HFOL=(1.-FACTOR)*ARRAY(IBORN,1)+FACTOR*
     1 ARRAY(IBORN+1,1)
      OMDIVF=(1.-FACTOR)*ARRAY(IBORN,2)+FACTOR*
     1 ARRAY(IBORN+1,2)
      FFRESH=(1.-FACTOR)*ARRAY(IBORN,3)+FACTOR*
     1 ARRAY(IBORN+1,3)
      FREENG=(1.-FACTOR)*ARRAY(IBORN,4)+FACTOR*
     1 ARRAY(IBORN+1,4)
      RSTR=(ARRAY(IBORN,5)+EMPC3*DUDYB(I))/2.
      ADIF=(1.-FACTOR)*ARRAY(IBORN,7)+FACTOR*
     1 ARRAY(IBORN+1,7)
      ADIF=ADIF/RSTR
      FFI=FVAL(I)
      UBORN=(1.-FACTOR)*ARRAY(IBORN,8)+FACTOR*ARRAY(IBORN+1,8)
C----------THE "PROFILE" METHOD IS EMPLOYED HERE TO CALCULATE
C----------THE DIFFUSION PROCESS INSIDE EACH FOLD.
C----------THE EVOLUTION OF THE SINUSOIDAL PROFILE IS
C----------DEVIDED INTO THREE SEPARATE STAGES.
C----------CALCULATION OF TIME SEPARATING THREE STAGES
      FBAR1=Ø.5*(FFRESH+FREENG)
      FAMP=Ø.5*ABS(FFRESH-FREENG)
      F1=AMAX1(FFRESH,FREENG)
      F2=AMIN1(FFRESH,FREENG)
      TERM=AMIN1(OMDIVF,1.-OMDIVF)**2
      RECAP=1./(ADIF*PI+1.E-3Ø)
      TIME1=(FBAR1-TWODPI*FAMP-F2)*TERM*RECAP/(FAMP+1.E-3Ø)
      TIME2=(.25-TERM)*RECAP+TIME1
      UFOLD=Ø.5*(UBORN+U(I))
      AGEDIM=AGEC(IA)*XD/UMIN
      ARGUM=AMIN1(2.*RSTR*AGEDIM,15Ø.)
      AGEND=EXP(ARGUM)-1.
      IF(TIME1.LT.AGEND) GO TO 2Ø
C----------THE DIFUSION IN FOLD STOPS DURING THE FIRST STAGE
      ISTAGE=1
      DELAJ2=ADIF*FAMP*PI*AGEND/(FBAR1-TWODPI*FAMP-F2+1.E-3Ø)
      DELAJ=SQRT(DELAJ2)
      OMLEFT=OMDIVF-DELAJ
      OMRIGT=OMDIVF+DELAJ
      DDELAJ=DELAJ*2./FLOAT(NDIFOM)
      IF(F1.GT.FSTOIC) GO TO 1Ø2
      FUL=Ø.
      OXL=OXD*(FSTOIC-F1)/FSTOIC
      PROL=1.-FUL-OXL-(1.-F1)*OXD1
      ENTHL=ENTHA*F1+ENTHD*(1.-F1)
      CPBORN=FUL*CFU(I)+OXL*COX(I)+(1.-F1)*OXD1*CN2(I)+
     1 (1.-FUL-OXL-(1.-F1)*OXD1)*CH2O(I)
```

```
      TEML=(ENTHL-FUL*HFU)/CPBORN
      GO TO 103
  102 FUL=FUA*(F1-FSTOIC)/FS1
      OXL=0.
      PROL=1.-FUL-OXL-(1.-F1)*OXD1
      ENTHL=ENTHA*F1+ENTHD*(1.-F1)
      CPBORN=FUL*CFU(I)+OXL*COX(I)+(1.-F1)*OXD1*CN2(I)+
     1 (1.-FUL-OXL-(1.-F1)*OXD1)*CH2O(I)
      TEML=(ENTHL-FUL*HFU)/CPBORN
  103 CONTINUE
      FUAV(I)=FUAV(I)+FUL*OMLEFT
      OXAV(I)=OXAV(I)+OXL*OMLEFT
      PRAV(I)=PRAV(I)+PROL*OMLEFT
      TEMAV(I)=TEMAV(I)+TEML*OMLEFT
      TEMAVS(I)=TEMAVS(I)+TEML*TEML*OMLEFT
      FUAVS(I)=FUAVS(I)+FUL*FUL*OMLEFT
      OXAVS(I)=OXAVS(I)+OXL*OXL*OMLEFT
      PRAVS(I)=PRAVS(I)+PROL*PROL*OMLEFT
      FFIAVS(I)=FFIAVS(I)+F1*F1*OMLEFT
      IF(F2.GT.FSTOIC) GO TO 106
      FUR=0.
      OXR=OXD*(FSTOIC-F2)/FSTOIC
      PROR=1.-FUR-OXR-(1.-F2)*OXD1
      ENTHR=ENTHA*F2+ENTHD*(1.-F2)
      CPBORN=FUR*CFU(I)+OXR*COX(I)+(1.-F2)*OXD1*CN2(I)+
     1 (1.-FUR-OXR-(1.-F2)*OXD1)*CH2O(I)
      TEMR=(ENTHR-FUR*HFU)/CPBORN
      GO TO 107
  106 FUR=FUA*(F2-FSTOIC)/FS1
      OXR=0.
      PROR=1.-FUR-OXR-(1.-F2)*OXD1
      ENTHR=ENTHA*F2+ENTHD*(1.-F2)
      CPBORN=FUR*CFU(I)+OXR*COX(I)+(1.-F2)*OXD1*CN2(I)+
     1 (1.-FUR-OXR-(1.-F2)*OXD1)*CH2O(I)
      TEMR=(ENTHR-FUR*HFU)/CPBORN
  107 CONTINUE
      OMR1=1.-OMRIGT
      FUAV(I)=FUAV(I)+FUR*OMR1
      OXAV(I)=OXAV(I)+OXR*OMR1
      PRAV(I)=PRAV(I)+PROR*OMR1
      TEMAV(I)=TEMAV(I)+TEMR*OMR1
      TEMAVS(I)=TEMAVS(I)+TEMR*TEMR*OMR1
      FUAVS(I)=FUAVS(I)+FUR*FUR*OMR1
      OXAVS(I)=OXAVS(I)+OXR*OXR*OMR1
      PRAVS(I)=PRAVS(I)+PROR*PROR*OMR1
      FFIAVS(I)=FFIAVS(I)+F2*F2*OMR1
      DENOM1=2.*DELAJ/PI
      DO 108 IO=1,NDIFOM
      OMA(IO)=DDELAJ*0.5*(FLOAT(IO-1)+FLOAT(IO))
      FSR(IO)=FBAR1+FAMP*SIN((DELAJ-OMA(IO))/(DENOM1+1.E-30))
      IF(FSR(IO).GT.FSTOIC) GO TO 104
```

```
      FUM(IO)=0.
      OXM(IO)=OXD*(FSTOIC-FSR(IO))/FSTOIC
      PROM(IO)=1.-FUM(IO)-OXM(IO)-(1.-FSR(IO))*OXD1
      ENTHFO(IO)=ENTHA*FSR(IO)+ENTHD*(1.-FSR(IO))
      CPBORN=FUM(IO)*CFU(I)+OXM(IO)*COX(I)+(1.-FSR(IO))*OXD1*CN2(I)+
     1 (1.-FUM(IO)-OXM(IO)-(1.-FSR(IO))*OXD1)*CH2O(I)
      TEMM(IO)=(ENTHFO(IO)-FUM(IO)*HFU)/CPBORN
      GO TO 105
  104 FUM(IO)=FUA*(FSR(IO)-FSTOIC)/FS1
      OXM(IO)=0.
      PROM(IO)=1.-FUM(IO)-OXM(IO)-(1.-FSR(IO))*OXD1
      ENTHFO(IO)=ENTHA*FSR(IO)+ENTHD*(1.-FSR(IO))
      CPBORN=FUM(IO)*CFU(I)+OXM(IO)*COX(I)+(1.-FSR(IO))*OXD1*CN2(I)+
     1 (1.-FUM(IO)-OXM(IO)-(1.-FSR(IO))*OXD1)*CH2O(I)
      TEMM(IO)=(ENTHFO(IO)-FUM(IO)*HFU)/CPBORN
  105 CONTINUE
      FUAV(I)=FUAV(I)+FUM(IO)*DDELAJ
      OXAV(I)=OXAV(I)+OXM(IO)*DDELAJ
      PRAV(I)=PRAV(I)+PROM(IO)*DDELAJ
      TEMAV(I)=TEMAV(I)+TEMM(IO)*DDELAJ
      TEMAVS(I)=TEMAVS(I)+TEMM(IO)*TEMM(IO)*DDELAJ
      FUAVS(I)=FUAVS(I)+FUM(IO)*FUM(IO)*DDELAJ
      OXAVS(I)=OXAVS(I)+OXM(IO)*OXM(IO)*DDELAJ
      PRAVS(I)=PRAVS(I)+PROM(IO)*PROM(IO)*DDELAJ
      FFIAVS(I)=FFIAVS(I)+FSR(IO)*FSR(IO)*DDELAJ
  108 CONTINUE
      GO TO 50
   20 IF(OMDIVF.EQ.0.5) GO TO 30
      IF(TIME2.LT.AGEND) GO TO 30
C----------THE DIFFUSION IN FOLD STOPS DURING THE SECOND STAGE
      DELAJ2=TERM+ADIF*PI*(AGEND-TIME1)
      DELAJ=SQRT(DELAJ2)
      FAMP=ABS(FFRESH-FREENG)*SQRT(TERM)/(2.*DELAJ+1.E-30)
      DDELAJ=2.*DELAJ/FLOAT(NDIFOM)
      DENOM2=2.*DELAJ/PI
      IF(OMDIVF.LT.0.5) GO TO 22
      ISTAGE=2
      OMLEFT=1.-2.*DELAJ
      IF(F1.GT.FSTOIC) GO TO 202
      FUL=0.
      OXL=OXD*(FSTOIC-F1)/FSTOIC
      PROL=1.-FUL-OXL-(1.-F1)*OXD1
      ENTHL=ENTHA*F1+ENTHD*(1.-F1)
      CPBORN=FUL*CFU(I)+OXL*COX(I)+(1.-F1)*OXD1*CN2(I)+
     1 (1.-FUL-OXL-(1.-F1)*OXD1)*CH2O(I)
      TEML=(ENTHL-FUL*HFU)/CPBORN
      GO TO 203
  202 FUL=FUA*(F1-FSTOIC)/FS1
      OXL=0.
      PROL=1.-FUL-OXL-(1.-F1)*OXD1
      ENTHL=ENTHA*F1+ENTHD*(1.-F1)
```

```
      CPBORN=FUL*CFU(I)+OXL*COX(I)+(1.-F1)*OXD1*CN2(I)+
     1 (1.-FUL-OXL-(1.-F1)*OXD1)*CH2O(I)
      TEML=(ENTHL-FUL*HFU)/CPBORN
  203 CONTINUE
      FUAV(I)=FUAV(I)+FUL*OMLEFT
      OXAV(I)=OXAV(I)+OXL*OMLEFT
      PRAV(I)=PRAV(I)+PROL*OMLEFT
      TEMAV(I)=TEMAV(I)+TEML*OMLEFT
      TEMAVS(I)=TEMAVS(I)+TEML*TEML*OMLEFT
      FUAVS(I)=FUAVS(I)+FUL*FUL*OMLEFT
      OXAVS(I)=OXAVS(I)+OXL*OXL*OMLEFT
      PRAVS(I)=PRAVS(I)+PROL*PROL*OMLEFT
      FFIAVS(I)=FFIAVS(I)+F1*F1*OMLEFT
      FBAR1=F1-FAMP
      DO 21 IO=1,NDIFOM
      OMA(IO)=DDELAJ*0.5*(FLOAT(IO-1)+FLOAT(IO))
      FSR(IO)=FBAR1+FAMP*SIN((DELAJ-OMA(IO))/(DENOM2+1.E-30))
      IF(FSR(IO).GT.FSTOIC) GO TO 204
      FUM(IO)=0.
      OXM(IO)=OXD*(FSTOIC-FSR(IO))/FSTOIC
      PROM(IO)=1.-FUM(IO)-OXM(IO)-(1.-FSR(IO))*OXD1
      ENTHFO(IO)=ENTHA*FSR(IO)+ENTHD*(1.-FSR(IO))
      CPBORN=FUM(IO)*CFU(I)+OXM(IO)*COX(I)+(1.-FSR(IO))*OXD1*CN2(I)+
     1 (1.-FUM(IO)-OXM(IO)-(1.-FSR(IO))*OXD1)*CH2O(I)
      TEMM(IO)=(ENTHFO(IO)-FUM(IO)*HFU)/CPBORN
      GO TO 205
  204 FUM(IO)=FUA*(FSR(IO)-FSTOIC)/FS1
      OXM(IO)=0.
      PROM(IO)=1.-FUM(IO)-OXM(IO)-(1.-FSR(IO))*OXD1
      ENTHFO(IO)=ENTHA*FSR(IO)+ENTHD*(1.-FSR(IO))
      CPBORN=FUM(IO)*CFU(I)+OXM(IO)*COX(I)+(1.-FSR(IO))*OXD1*CN2(I)+
     1 (1.-FUM(IO)-OXM(IO)-(1.-FSR(IO))*OXD1)*CH2O(I)
      TEMM(IO)=(ENTHFO(IO)-FUM(IO)*HFU)/CPBORN
  205 CONTINUE
      FUAV(I)=FUAV(I)+FUM(IO)*DDELAJ
      OXAV(I)=OXAV(I)+OXM(IO)*DDELAJ
      PRAV(I)=PRAV(I)+PROM(IO)*DDELAJ
      TEMAV(I)=TEMAV(I)+TEMM(IO)*DDELAJ
      TEMAVS(I)=TEMAVS(I)+TEMM(IO)*TEMM(IO)*DDELAJ
      FUAVS(I)=FUAVS(I)+FUM(IO)*FUM(IO)*DDELAJ
      OXAVS(I)=OXAVS(I)+OXM(IO)*OXM(IO)*DDELAJ
      PRAVS(I)=PRAVS(I)+PROM(IO)*PROM(IO)*DDELAJ
      FFIAVS(I)=FFIAVS(I)+FSR(IO)*FSR(IO)*DDELAJ
   21 CONTINUE
      GO TO 50
   22 OMRIGT=2.*DELAJ
      ISTAGE=3
      IF(F2.GT.FSTOIC) GO TO 206
      FUR=0.
      OXR=OXD*(FSTOIC-F2)/FSTOIC
      PROR=1.-FUR-OXR-(1.-F2)*OXD1
```

```
      ENTHR=ENTHA*F2+ENTHD*(1.-F2)
      CPBORN=FUR*CFU(I)+OXR*COX(I)+(1.-F2)*OXD1*CN2(I)+
     1 (1.-FUR-OXR-(1.-F2)*OXD1)*CH2O(I)
      TEMR=(ENTHR-FUR*HFU)/CPBORN
      GO TO 207
  206 FUR=FUA*(F2-FSTOIC)/FS1
      OXR=0.
      PROR=1.-FUR-OXR-(1.-F2)*OXD1
      ENTHR=ENTHA*F2+ENTHD*(1.-F2)
      CPBORN=FUR*CFU(I)+OXR*COX(I)+(1.-F2)*OXD1*CN2(I)+
     1 (1.-FUR-OXR-(1.-F2)*OXD1)*CH2O(I)
      TEMR=(ENTHR-FUR*HFU)/CPBORN
  207 CONTINUE
      OMR1=1.-OMRIGT
      FUAV(I)=FUAV(I)+FUR*OMR1
      OXAV(I)=OXAV(I)+OXR*OMR1
      PRAV(I)=PRAV(I)+PROR*OMR1
      TEMAV(I)=TEMAV(I)+TEMR*OMR1
      TEMAVS(I)=TEMAVS(I)+TEMR*TEMR*OMR1
      FUAVS(I)=FUAVS(I)+FUR*FUR*OMR1
      OXAVS(I)=OXAVS(I)+OXR*OXR*OMR1
      PRAVS(I)=PRAVS(I)+PROR*PROR*OMR1
      FFIAVS(I)=FFIAVS(I)+F2*F2*OMR1
      FBAR2=F2+FAMP
      DO 23 IO=1,NDIFOM
      OMA(IO)=DDELAJ*0.5*(FLOAT(IO-1)+FLOAT(IO))
      FSR(IO)=FBAR2+FAMP*SIN((DELAJ-OMA(IO))/(DENOM2+1.E-30))
      IF(FSR(IO).GT.FSTOIC) GO TO 231
      FUM(IO)=0.
      OXM(IO)=OXD*(FSTOIC-FSR(IO))/FSTOIC
      PROM(IO)=1.-FUM(IO)-OXM(IO)-(1.-FSR(IO))*OXD1
      ENTHFO(IO)=ENTHA*FSR(IO)+ENTHD*(1.-FSR(IO))
      CPBORN=FUM(IO)*CFU(I)+OXM(IO)*COX(I)+(1.-FSR(IO))*OXD1*CN2(I)+
     1 (1.-FUM(IO)-OXM(IO)-(1.-FSR(IO))*OXD1)*CH2O(I)
      TEMM(IO)=(ENTHFO(IO)-FUM(IO)*HFU)/CPBORN
      GO TO 232
  231 FUM(IO)=FUA*(FSR(IO)-FSTOIC)/FS1
      OXM(IO)=0.
      PROM(IO)=1.-FUM(IO)-OXM(IO)-(1.-FSR(IO))*OXD1
      ENTHFO(IO)=ENTHA*FSR(IO)+ENTHD*(1.-FSR(IO))
      CPBORN=FUM(IO)*CFU(I)+OXM(IO)*COX(I)+(1.-FSR(IO))*OXD1*CN2(I)+
     1 (1.-FUM(IO)-OXM(IO)-(1.-FSR(IO))*OXD1)*CH2O(I)
      TEMM(IO)=(ENTHFO(IO)-FUM(IO)*HFU)/CPBORN
  232 CONTINUE
      FUAV(I)=FUAV(I)+FUM(IO)*DDELAJ
      OXAV(I)=OXAV(I)+OXM(IO)*DDELAJ
      PRAV(I)=PRAV(I)+PROM(IO)*DDELAJ
      TEMAV(I)=TEMAV(I)+TEMM(IO)*DDELAJ
      TEMAVS(I)=TEMAVS(I)+TEMM(IO)*TEMM(IO)*DDELAJ
      FUAVS(I)=FUAVS(I)+FUM(IO)*FUM(IO)*DDELAJ
      OXAVS(I)=OXAVS(I)+OXM(IO)*OXM(IO)*DDELAJ
```

```
      PRAVS(I)=PRAVS(I)+PROM(IO)*PROM(IO)*DDELAJ
      FFIAVS(I)=FFIAVS(I)+FSR(IO)*FSR(IO)*DDELAJ
   23 CONTINUE
      GO TO 50
C----------THE DIFFUSION IN FOLD STOPS DURING THE THIRD STAGE
   30 DDELAJ=1./FLOAT(NDIFOM)
      ISTAGE=4
      DENOM3=1.
      AGEND=AGEND-TIME2
      ARGUM3=AMAX1(-ADIF*PI*PI*AGEND,-60.)
      FAMP=ABS(FFRESH-FREENG)*SQRT(TERM)*EXP(ARGUM3)/DENOM3
      DO 31 IO=1,NDIFOM
      OMA(IO)=DDELAJ*0.5*(FLOAT(IO-1)+FLOAT(IO))
      FSR(IO)=FFI+FAMP*SIN(PI*(0.5-OMA(IO)))
       IF(FSR(IO).GT.FSTOIC) GO TO 311
      FUM(IO)=0.
      OXM(IO)=OXD*(FSTOIC-FSR(IO))/FSTOIC
      PROM(IO)=1.-FUM(IO)-OXM(IO)-(1.-FSR(IO))*OXD1
      ENTHFO(IO)=ENTHA*FSR(IO)+ENTHD*(1.-FSR(IO))
      CPBORN=FUM(IO)*CFU(I)+OXM(IO)*COX(I)+(1.-FSR(IO))*OXD1*CN2(I)+
     1 (1.-FUM(IO)-OXM(IO)-(1.-FSR(IO))*OXD1)*CH2O(I)
      TEMM(IO)=(ENTHFO(IO)-FUM(IO)*HFU)/CPBORN
      GO TO 312
  311 FUM(IO)=FUA*(FSR(IO)-FSTOIC)/FS1
      OXM(IO)=0.
      PROM(IO)=1.-FUM(IO)-OXM(IO)-(1.-FSR(IO))*OXD1
      ENTHFO(IO)=ENTHA*FSR(IO)+ENTHD*(1.-FSR(IO))
      CPBORN=FUM(IO)*CFU(I)+OXM(IO)*COX(I)+(1.-FSR(IO))*OXD1*CN2(I)+
     1 (1.-FUM(IO)-OXM(IO)-(1.-FSR(IO))*OXD1)*CH2O(I)
      TEMM(IO)=(ENTHFO(IO)-FUM(IO)*HFU)/CPBORN
  312 CONTINUE
      FUAV(I)=FUAV(I)+FUM(IO)*DDELAJ
      OXAV(I)=OXAV(I)+OXM(IO)*DDELAJ
      PRAV(I)=PRAV(I)+PROM(IO)*DDELAJ
      TEMAV(I)=TEMAV(I)+TEMM(IO)*DDELAJ
      TEMAVS(I)=TEMAVS(I)+TEMM(IO)*TEMM(IO)*DDELAJ
      FUAVS(I)=FUAVS(I)+FUM(IO)*FUM(IO)*DDELAJ
      OXAVS(I)=OXAVS(I)+OXM(IO)*OXM(IO)*DDELAJ
      PRAVS(I)=PRAVS(I)+PROM(IO)*PROM(IO)*DDELAJ
      FFIAVS(I)=FFIAVS(I)+FSR(IO)*FSR(IO)*DDELAJ
   31 CONTINUE
   50 CONTINUE
C----------CALCULATION OF FOLD-AVERAGE QUANTITIES ENDS HERE
      IF(ISTEP.GT.1) GO TO 53
      CMIX(I)=F(I,JF)*CFU(1)+F(I,JOX)*COX(1)+(1.-F(I,JF)-F(I,JOX))
     1 *CPR(1)
      FUUNBT=T3*F(I,JP)+T4
      IF(FUAV(I).GT.FUUNBT) FUAV(I)=FUUNBT
   53 CONTINUE
      EXPO=EXP(-ARRCON/TEMAV(I))
      PHII=(-FFI*(PHID-PHIB))+0.232
```

```
      FUBRNT=0.5/STOICH*(ABS(PHII)-PHII)
      TERM=-EXPO*OXAV(I)
      RATEA1(I)=TERM*FUAV(I)/(FUAV(I)-FUBRNT+TINY)
      RATEA2(I)=-RATEA1(I)*FUBRNT
C----------CALCULATION OF POPULATION AVERAGE QUANTITIES
      FDAGE=F(I,IA+JA1-1)*DAGE(IA)
      AVRAT1(I)=AVRAT1(I)+RATEA1(I)*FDAGE
      AVRAT2(I)=AVRAT2(I)+RATEA2(I)*FDAGE
      AVFU(I)=AVFU(I)+FUAV(I)*FDAGE
      AVOX(I)=AVOX(I)+OXAV(I)*FDAGE
      AVPR(I)=AVPR(I)+PRAV(I)*FDAGE
      AVTEM(I)=AVTEM(I)+TEMAV(I)*FDAGE
      AVTEMS(I)=AVTEMS(I)+TEMAVS(I)*FDAGE
      AVFUS(I)=AVFUS(I)+FUAVS(I)*FDAGE
      AVOXS(I)=AVOXS(I)+OXAVS(I)*FDAGE
      AVPRS(I)=AVPRS(I)+PRAVS(I)*FDAGE
      AVFFIS(I)=AVFFIS(I)+FFIAVS(I)*FDAGE
      POPAGE(I)=POPAGE(I)+AGEC(IA)*FDAGE
C----------CALCULATION OF POPULATION-AVERAGE PDF QUANTITIES --------
C----------STARTS HERE.
      IF(IPDF.NE.1) GO TO 411
      IF(MOD(ISTEP1,NSTAT).NE.0.AND.XD.NE.XULAST) GO TO 411
      DO 390 II=1,NDIFOM
  390 PHI(II)=TEMM(II)
      PHIL=TEML
      PHIR=TEMR
      CALL PDF
      IF(EMIX.LT.0.999) GO TO 381
      DO 382 K=1,NPDFM1
  382 PDFIT(K)=1./FLOAT(NPDFM1)
      GO TO 383
  381 DO 380 K=1,NPDFM1
  380 PDFIT(K)=PDF1(K)*PHIDIF
      TOPDF=0.
      DO 385 K=1,NPDFM1
  385 TOPDF=TOPDF+PDFIT(K)
      IF(TOPDF.GT.0.95) GO TO 383
      DO 386 K=1,NPDFM1
  386 PDFIT(K)=1./FLOAT(NPDFM1)
  383 PHIMAA=2700.
      PHIMIA=300.
      FMAX(I)=PHIMAA
      PHIBVA(1)=PHIMIA
      PHIBVA(NPDF)=PHIMAA
      DPHI=(PHIMAA-PHIMIA)/FLOAT(NPDFM1)
      DO 330 K=2,NPDFM1
  330 PHIBVA(K)=DPHI*FLOAT(K-1)+PHIMIA
      DO 320 K=1,NPDFM1
  320 PDFITA(K)=0.
      NPDFM2=NPDF-2
      DO 360 K=1,NPDFM2
```

```
      IF((PHIBV(1)-PHIBVA(K))*(PHIBV(1)-PHIBVA(K+1)).GT.0.)
     1 GO TO 340
      IF((PHIBV(2)-PHIBVA(K))*(PHIBV(2)-PHIBVA(K+1)).LE.0.)
     1 GO TO 280
      FAC1=PHIBV(2)-PHIBV(1)
      FAC2=PHIBVA(K+1)-PHIBV(1)
      PDFITA(K)=PDFITA(K)+PDFIT(1)*ABS(FAC2/FAC1)
      IF(ABS(FAC2).GT.0.)PDFITA(K+1)=PDFITA(K+1)+PDFIT(1)*
     1 (1.-ABS(FAC2/FAC1))
      GO TO 340
  280 PDFITA(K)=PDFITA(K)+PDFIT(1)
  340 DO 360 II=2,NPDFM1
      IF((PHIBV(II)-PHIBVA(K))*(PHIBV(II)-PHIBVA(K+1)).GT.0.)
     1 GO TO 360
      IF((PHIBV(II+1)-PHIBVA(K))*(PHIBV(II+1)-PHIBVA(K+1)).LE.0.)
     1 GO TO 290
      FAC1=PHIBV(II+1)-PHIBV(II)
      FAC2=PHIBVA(K+1)-PHIBV(II)
      PDFITA(K)=PDFITA(K)+PDFIT(II)*ABS(FAC2/FAC1)
      IF(ABS(FAC2).GT.0.)PDFITA(K+1)=PDFITA(K+1)+PDFIT(II)*
     1 (1.-ABS(FAC2/FAC1))
      GO TO 360
  290 PDFITA(K)=PDFITA(K)+PDFIT(II)
  360 CONTINUE
      DO 370 II=1,NPDFM1
      IF((PHIBV(II)-PHIBVA(NPDFM1))*(PHIBV(II)-PHIBVA(NPDF)).LE.
     1 0.) PDFITA(NPDFM1)=PDFITA(NPDFM1)+PDFIT(II)
      IF(PHIBV(II).LT.PHIBVA(1)) PDFITA(1)=PDFITA(1)+
     1 PDFIT(II)
  370 CONTINUE
      DO 410 K=1,NPDFM1
      AVPFA(I,K)=AVPFA(I,K)+PDFITA(K)*F(I,IA+JA1-1)*DAGE(IA)
      SUMPDF(I)=SUMPDF(I)+PDFITA(K)*F(I,IA+JA1-1)*DAGE(IA)
  410 AVPDF(I,K)=AVPFA(I,K)/DPHI
  411 CONTINUE
  900 CONTINUE
 1000 CONTINUE
C----------CALCULATION OF RMS QUANTITIES HERE----------
      DO 1500 I=2,NM1
      TFLU(I)=AVTEMS(I)-AVTEM(I)**2
      TFLU(I)=SQRT(ABS(TFLU(I)))
      FUFLU(I)=AVFUS(I)-AVFU(I)**2
      FUFLU(I)=SQRT(ABS(FUFLU(I)))
      OXFLU(I)=AVOXS(I)-AVOX(I)**2
      PRFLU(I)=AVPRS(I)-AVPR(I)**2
      PRFLU(I)=SQRT(ABS(PRFLU(I)))
      OXFLU(I)=SQRT(ABS(OXFLU(I)))
      FRFLU(I)=AVFFIS(I)-FVAL(I)**2
      FRFLU(I)=SQRT(ABS(FRFLU(I)))
      FRFLU(I)=FRFLU(I)/FVAL(I)
 1500 CONTINUE
```

```
C-----------CALCULATION OF REACTION RATE
      DO 2000 I=2,NM1
      FUBRNT=T2*(ABS(F(I,JP))-F(I,JP))
      FUUNBT=T3*F(I,JP)+T4
C-----------MODIFY FOR ACCOUNT THE FU.LT.FUUNBT AS IT IS DONE IN GENMIX
C----------A PHYS.177
      IF(F(I,JF).LT.FUUNBT) GO TO 910
      SIP(I)=-BIG
      SI(I)=-SIP(I)*FUBRNT
      GO TO 930
  910 SIP(I)=AVRAT1(I)*DX*ADPEI(I)*PREEXP*PRESS**2
      SI(I)=AVRAT2(I)*DX*ADPEI(I)*PREEXP*PRESS**2
  930 IF(MOD(ISTEP,NSTAT).NE.0) GO TO 2000
 2000 CONTINUE
C------CALCULATION OF MOLAR FRACTION OF
C------VARIOUS SPECIES HERE
      DO 3000 I=2,NM1
      FH2O(I)=1.-AVFU(I)-AVOX(I)-FN2(I)
      FH2O(I)=AMAX1(0.,FH2O(I))
      TMIX=AVFU(I)/WFU+AVOX(I)/WOX+FN2(I)/WN2+FH2O(I)/WH2O
      FMFU(I)=(AVFU(I)/WFU)/TMIX
      FMOX(I)=(AVOX(I)/WOX)/TMIX
      FMN2(I)=(FN2(I)/WN2)/TMIX
      FMH2O(I)=(FH2O(I)/WH2O)/TMIX
      PRFLUM(I)=(PRFLU(I)/WH2O)/TMIX
 3000 CONTINUE
C------THE FOLLOWING BOUNDARY CONDITIONS ARE
C------VALID FOR AXISYMMETRIC FREE JET ONLY
      AVFU(1)=AVFU(2)
      AVFU(N)=F(N,JF)
      AVOX(1)=AVOX(2)
      AVOX(N)=F(N,JOX)
      AVTEM(1)=AVTEM(2)
      AVTEM(N)=TD
      SUMPDF(1)=SUMPDF(2)
      SUMPDF(N)=SUMPDF(NM1)
      TFLU(1)=TFLU(2)
      TFLU(N)=0.
      PRFLU(1)=PRFLU(2)
      PRFLU(N)=0.
      PRFLUM(1)=PRFLUM(2)
      PRFLUM(N)=0.
      FRFLU(1)=FRFLU(2)
      FRFLU(N)=0.
      FMAX(1)=FMAX(2)
      FMAX(N)=FMAX(NM1)
      POPAGE(1)=POPAGE(2)
      POPAGE(N)=POPAGE(NM1)
      FN2(1)=FN2(2)
      FN2(N)=1.-OXD
      FH2O(1)=FH2O(2)
```

```
FH2O(N)=FUD
FMFU(1)=FMFU(2)
FMFU(N)=FUD
FMOX(1)=FMOX(2)
FMOX(N)=Ø.2Ø97
FMN2(1)=FMN2(2)
FMN2(N)=Ø.7934
FMH2O(1)=FMH2O(2)
FMH2O(N)=FUD
FUFLU(1)=FUFLU(2)
FUFLU(N)=Ø.
OXFLU(1)=OXFLU(2)
OXFLU(N)=Ø.
RETURN
END
```

```
      SUBROUTINE PDF
$INCLUDE 9,COMA1.FTN
$INCLUDE 9,COMB.FTN
C
C----------THIS SUBROUTINE IS CALLED FROM SUBROUTINE BIOG,
C----------AFTER ENTRY BIOS.IT CALCULATES THE PROBABILITY
C----------DENSITY FUNCTION OF PROPERTY PHI IN A FOLD.
C----------FIND MAXIMUM AND MINIMUM OF PHI
      GO TO (1,2,3,4), ISTAGE
    1 PHIMIN=AMIN1(PHIL,PHIR)
      PHIMAX=AMAX1(PHIL,PHIR)
      GO TO 5
    2 PHIMIN=PHIL
      PHIMAX=PHIL
      GO TO 5
    3 PHIMIN=PHIR
      PHIMAX=PHIR
      GO TO 5
    4 PHIMIN=PHI(1)
      PHIMAX=PHI(1)
    5 DO 10 I=1,NDIFOM
      PHIMIN=AMIN1(PHIMIN,PHI(I))
   10 PHIMAX=AMAX1(PHIMAX,PHI(I))
C----------DETERMINE BOUNDARY VALUES OF PHI INTERVALS
      PHIDIF=(PHIMAX-PHIMIN)/FLOAT(NPDF-1)
      NPDFM1=NPDF-1
      DO 20 K=1,NPDFM1
   20 PHIBV(K)=PHIDIF*FLOAT(K-1)+PHIMIN
      PHIBV(NPDF)=PHIMAX
C
C----------DETERMINE MASS PROPORTION IN INTERVAL
C----------JUST ABOVE PHIBV(K) AND INSERT IN PDF1(K)
      DO 25 K=1,NPDFM1
   25 PDF1(K)=0.
C
      EMIX=PHIMIN/(PHIMAX+TINY)
      IF(EMIX.LT.0.999) GO TO 26
      DO 27 K=1,NPDFM1
   27 PDF1(K)=PDF1(K)+1./FLOAT(NPDFM1)
      GO TO 80
   26 DO 40 I=1,NDIFOM-1
      L1=0
      PHI1=PHI(I)
      PHI2=PHI(I+1)
      IF((PHI(I+1)-PHI(I)).LT.0.) PHI1=PHI(I+1)
      IF((PHI(I+1)-PHI(I)).LT.0.) PHI2=PHI(I)
      DO 30 K=1,NPDFM1
      IF((PHIBV(K)-PHI1)*(PHIBV(K+1)-PHI1).LE.0.) L1=K
      IF(L1.NE.0) GO TO 31
   30 CONTINUE
   31 DO 32 K=L1,NPDFM1
```

```
32 IF((PHIBV(K)-PHI2)*(PHIBV(K+1)-PHI2).LE.0.) L2=K+1
   L2M1=L2-1
   DO 35 K=L1,L2M1
35 PDF1(K)=PDF1(K)+DDELAJ/FLOAT(L2-L1)
40 CONTINUE
   GO TO (50,60,70,80), ISTAGE
50 DO 51 K=1,NPDFM1
   IF((PHIBV(K)-PHIL)*(PHIBV(K+1)-PHIL).LE.0.)
  1 PDF1(K)=PDF1(K)+OMLEFT
   IF((PHIBV(K)-PHIR)*(PHIBV(K+1)-PHIR).LE.0.)
  1 PDF1(K)=PDF1(K)+(1.-OMRIGT)
51 CONTINUE
   GO TO 80
60 DO 61 K=1,NPDFM1
   IF((PHIBV(K)-PHIL)*(PHIBV(K+1)-PHIL).LE.0.)
  1 PDF1(K)=PDF1(K)+OMLEFT
61 CONTINUE
   GO TO 80
70 DO 71 K=1,NPDFM1
   IF((PHIBV(K)-PHIR)*(PHIBV(K+1)-PHIR).LE.0.)
  1 PDF1(K)=PDF1(K)+(1.-OMRIGT)
71 CONTINUE
80 DO 81 K=1,NPDFM1
81 PDF1(K)=PDF1(K)/(PHIDIF+1.E-30)
   RETURN
   END
```

```
      SUBROUTINE PHYS
C----- GENMIX-T (TURBULENCE MODELS), HTS/77/4,
C       BASED ON GENMIX, HTS/77/9, FEB.1977, APPENDIX A.
C/ FEB.1978 --------- GENMIX --------- COPYRIGHT, D.B.SPALDING ---------
C
$INCLUDE 9,COMA1.FTN
$INCLUDE 9,COMB.FTN
C
      DIMENSION DUDY(60),YEDGE(6)
      DIMENSION ADPEDX(50)
C
C     ------------------------------------------------------------------
CHAPTER A ---------- PHYSU ---------- PHYSU ---------- PHYSU ----------
C     ------------------------------------------------------------------
      ENTRY PHYSU
      KUDIF=-1
C     ---------------------------------------- LAMINAR VISCOSITY
C     -- SQUARE-ROOT FORMULA, WITH WEIGHTING ACCORDING TO MASS FRACTION
      DO 110 I=1,N
  110 EMU(I)=(VISFU*F(I,JF)+VISOX*F(I,JOX)+VISPR*F(I,JPR))*
     1                                              SQRT(F(I,JTE))
      IF(MODEL.EQ.1) GO TO 209
C
C
C     ---------------------------------------- TURBULENT FLOW
C     ----- VELOCITY GRADIENTS
      DO 114 I=2,NM1
  114 DUDY(I)=ABS(U(I+1)-U(I-1))/(Y(I+1)-Y(I-1))
  666 CONTINUE
C
C     ----- CALCULATE LENGTHS ACCORDING TO CHOSEN TURBULENCE MODEL.
      IF(MODEL-4) 162,163,164
C
C
C     ----------------------------------- MODELS 2 AND 3
  162 GOTO(112,117,1200), LENGTH
C
C     -------------------- LENGTH=1, MIXING-LENGTH MODEL,
C     ---------- STANDARD GENMIX FORMULATION OF HTS/77/9, FEB.1977.
C
  112 IF(KUDIF.EQ.ISTEP) GO TO 102
C     ----- CALCULATE UDIF, IF NOT ALREADY DONE IN MAIN, CH.6.
      UMAX=U(1)
      UMIN=U(1)
      DO 101 I=2,N
      UMAX=AMAX1(UMAX,U(I))
  101 UMIN=AMIN1(UMIN,U(I))
      UDIF=UMAX-UMIN
C
  102 HUDIF=.5*UDIF
      DUDYMN=FR*UDIF/Y(N)
```

```
      K=1
      EX=DUDY(2)-DUDYMN
      IF(EX.LT.0.) GO TO 103
      YEDGE(K)=0.
      K=2
  103 DO 104 I=3,NM1
      EXL=EX
      EX=DUDY(I)-DUDYMN
      IF(EX*EXL.GE.0.) GO TO 104
      YEDGE(K)=.5*(Y(I)+Y(I-1))
      IF(K.EQ.6) GO TO 107
      K=K+1
  104 CONTINUE
      IF(EX.LT.0.) GO TO 108
      YEDGE(K)=Y(N)
      IF(K.EQ.6) GO TO 107
      K=K+1
  108 DO 106 KAY=K,6
  106 YEDGE(KAY)=Y(N)
  107 EL12=(YEDGE(2)-YEDGE(1))*ELCON
      EL34=(YEDGE(4)-YEDGE(3))*ELCON
      EL56=(YEDGE(6)-YEDGE(5))*ELCON
      EL23=.5*(EL12+EL34)
      EL45=.5*(EL34+EL56)
      ASSIGN 119 TO K
C
      DO 130 I=2,NM1
      YVALUE=Y(I)
      GO TO K, (119,121,123,125,127,129)
  119 IF(YVALUE.LT.YEDGE(1)) GO TO 120
      ASSIGN 121 TO K
  121 IF(YVALUE.LT.YEDGE(2)) GO TO 122
      ASSIGN 123 TO K
  123 IF(YVALUE.LT.YEDGE(3)) GO TO 124
      ASSIGN 125 TO K
  125 IF(YVALUE.LT.YEDGE(4)) GO TO 126
      ASSIGN 127 TO K
  127 IF(YVALUE.LT.YEDGE(5)) GO TO 128
      ASSIGN 129 TO K
      GO TO 129
  120 EL=0.
      GO TO 130
  122 EL=EL12
      GO TO 130
  124 EL=EL23
      GO TO 130
  126 EL=EL34
      GO TO 130
  128 EL=EL45
      GO TO 130
  129 EL=EL56
```

```
C     ------------------- UPPER LIMITS TO MIXING LENGTH
  130 F(I,JEL)=AMIN1(EL,HUDIF/(DUDY(I)+TINY))
C
      IF(KIN.NE.1) GO TO 141
      DO 142 I=2,NM1
  142 F(I,JEL)=AMIN1(F(I,JEL),AK*Y(I))
  141 IF(KEX.NE.1) GO TO 173
      DO 144 I=2,NM1
  144 F(I,JEL)=AMIN1(F(I,JEL),AK*(Y(N)-Y(I)))
      GO TO 138
C
C
C     ---------- LENGTH=2, NIKURADSE"S LENGTH SCALE, WALL AT E.
  117 FACTOR=ELCON/(.14*Y(N))
      DO 115 I=2,NM1
      YTILDE=1.-Y(I)*FACTOR
  115 F(I,JEL)=Y(N)*YTILDE*(.4-YTILDE*(.44-YTILDE*(.24-.06*YTILDE)))
      GO TO 138
C
C
C     ---------- LENGTH=3, UNIFORM LENGTH SCALE.
 1200 UDIF=U(N)-U(1)
      REUDIF=1./(UDIF+TINY)
C     ----- FIND REFERENCE LENGTHS, ACCORDING TO BOUNDARY CONDITIONS.
      IF(KIN.EQ.KINL.AND.KEX.EQ.KEXL) GO TO SEARCH, (1201,1202,1205)
      KINL=KIN
      KEXL=KEX
C     ----- DEFAULT VALUES APPLY FOR A WALL OR A SYMMETRY AXIS.
      YREF1=0.
      YREF2=Y(N)
C     PRINT,YREF1,YREF2
      IF(KIN.EQ.2.AND.KEX.EQ.2) GO TO 92
      IF(KIN.EQ.3.AND.KEX.EQ.2) GO TO 93
      IF(KIN.EQ.2.AND.KEX.EQ.3) GO TO 94
      IF(KIN.EQ.1.AND.KEX.EQ.2) GO TO 95
      IF(KIN.EQ.2.AND.KEX.EQ.1) GO TO 96
      ASSIGN 1205 TO SEARCH
      GO TO 1205
C     ----- INNER BOUNDARY IS FREE AND OUTER BOUNDARY IS FREE
   92 UREF1=0.1
      UREF2=0.9
C     PRINT,UREF1,UREF2
      ASSIGN 1202 TO NEXT
      ASSIGN 1201 TO SEARCH
      GO TO 1201
C     ---------- INNER IS A SYMMETRY AXIS AND OUTER IS FREE
   93 UREF2=0.5
      ASSIGN 1202 TO SEARCH
C     PRINT,UREF2
      GO TO 1202
C     ---------- INNER IS FREE AND OUTER IS A SYMMETRY AXIS
```

```
   94 UREF1=0.5
C     PRINT,UREF1
      ASSIGN 1205 TO NEXT
      ASSIGN 1201 TO SEARCH
      GO TO 1201
C     ---------- INNER IS A WALL AND OUTER IS FREE
   95 UREF2=0.99
      ASSIGN 1202 TO SEARCH
C     PRINT,UREF2
      GO TO 1202
C     ---------- INNER IS FREE AND OUTER IS A WALL
   96 UREF1=0.01
C     PRINT,UREF1
      ASSIGN 1205 TO NEXT
      ASSIGN 1201 TO SEARCH
C     ------------------------------ SEARCH FOR YREF1
 1201 UTILDL=0.
      DO 1203 I=2,N
      UTILD=(U(I)-U(1))*REUDIF
      IF(UTILD.LE.UREF1) GO TO 1203
      YREF1=Y(I-1)+(Y(I)-Y(I-1))*(UREF1-UTILDL)/(UTILD-UTILDL)
      GO TO NEXT, (1202,1205)
 1203 UTILDL=UTILD
C     ------------------------------ SEARCH FOR YREF2
 1202 UTILDL=1.
      DO 1206 IDASH=2,N
      I=N+1-IDASH
      UTILD=(U(I)-U(1))*REUDIF
      IF(UTILD.GE.UREF2) GO TO 1206
      YREF2=Y(I+1)+(Y(I)-Y(I+1))*(UREF2-UTILDL)/(UTILD-UTILDL)
      GO TO 1205
 1206 UTILDL=UTILD
C     ------------------------------ CALCULATION OF LENGTHS
 1205 EL=ELCON*(YREF2-YREF1)
      DO 1207 I=2,NM1
 1207 F(I,JEL)=EL
      GO TO 138
C
C
C     -------------------- MODELS 4 AND 5, CALCULATE LENGTHS.
C     THESE ARE USED ONLY IN OUTPUT AND MAY BE SKIPPED FOR ECONOMY.
C     NOTE THAT WE USE MODEL 2 INSTEAD OF MODELS 4 OR 5 AT THE START.
C     ------------------------ MODEL 4
  163 IF(ISTEP.LT.3) GO TO 162
      DO 165 I=2,NM1
  165 F(I,JEL)=CD*SQRT(F(I,JK))/(F(I,J2)+TINY)
      GO TO 138
C     ------------------------ MODEL 5
  164 IF(ISTEP.LT.3) GO TO 162
      DO 166 I=2,NM1
  166 F(I,JEL)=CD*F(I,JK)*SQRT(F(I,JK))/(F(I,J2)+TINY)
```

```
C
C
C     ------------------------------ LENGTH ADJUSTMENTS NEAR EDGES
  138 F(1,JEL)=F(2,JEL)
      F(N,JEL)=F(NM1,JEL)
      IF(ISTEP.GT.2) GO TO 173
C
C
C     -------------------------------- COMPUTE SOME STARTING VALUES.
C     ------------------------------ INITIAL MINIMUM LENGTH VALUE.
      ELMIN=.ØØØ1*Y(N)
      DO 172 I=1,N
  172 F(I,JEL)=AMAX1(F(I,JEL),ELMIN)
      IF(MODEL.EQ.2) GO TO 181
C
C     ---------- COMPUTE INITIAL PROFILES FOR MODELS 3, 4, 5
C     ---------------------------------- INITIAL PROFILE OF ENERGY
      FAC1=CMU/CD
      DO 145 I=2,NM1
      FIJK=FAC1*(DUDY(I)*F(I,JEL))**2
  145 F(I,JK)=AMAX1(FIJK,.ØØØ1*U(I)**2)
      F(1,JK)=F(2,JK)
      F(N,JK)=F(NM1,JK)
      IF(MODEL.EQ.3) GO TO 181
C     ------------------------- INITIAL PROFILE OF FREQUENCY
      FAC2=SQRT(CMUCD)
      DO 146 I=2,NM1
  146 F(I,J2)=FAC2*AMAX1(DUDY(I),TINY)
      F(1,J2)=F(2,J2)
      F(N,J2)=F(NM1,J2)
      IF(MODEL.EQ.4) GO TO 181
C     ----------------- INITIAL PROFILE OF DISSIPATION RATE
      DO 147 I=1,N
  147 F(I,J2)=F(I,J2)*F(I,JK)
      GO TO 181
C
C
C     ------------------------------------ EFFECTIVE VISCOSITIES
C     SIMPLE ADDITION OF TURBULENT AND LAMINAR CONTRIBUTIONS.
  173 GO TO (2Ø9,181,182,183,184), MODEL
C     -------------------- MIXING LENGTH, HIGH RE, MODEL=2
  181 DO 2Ø1 I=2,NM1
      DUDYL=DUDY(I)*F(I,JEL)
      UDMIN=UFAC*U(I)
      DUDYL=AMAX1(DUDYL,UDMIN)
      EMUT=RHO(I)*F(I,JEL)*DUDYL
      EMU(I)=EMU(I)+EMUT
  2Ø1 CONTINUE
      GO TO 2Ø9
C
C     -------------------- PRANDTL ENERGY, HIGH RE, MODEL=3
```

```
  182 DO 151 I=2,NM1
      EMUT=CMU*RHO(I)*SQRT(ABS(F(I,JK)))*F(I,JEL)
  151 EMU(I)=EMU(I)+EMUT
      GO TO 209
C
C     -------------------- KOLMOGOROV, HIGH RE, MODEL=4
  183 DO 152 I=2,NM1
      EMUT=CMUCD*RHO(I)*F(I,JK)/(F(I,J2)+TINY)
  152 EMU(I)=EMU(I)+EMUT
      GO TO 209
C
C     -------------------- HARLOW, HIGH RE, MODEL=5
  184 DO 153 I=2,NM1
      EMUT=CMUCD*RHO(I)*F(I,JK)**2/(F(I,J2)+TINY)
  153 EMU(I)=EMU(I)+EMUT
C
C
C     ------------------------------------------------ MOMENTUM SOURCE
  209 AGRVDX=AGRAV*DX
      RPRLST=1.
      IF(ABS(DP).GT.TINY) GO TO 204
      IF(ABS(AGRAV).GT.TINY) GO TO 204
      MOMSOU=0
      RETURN
  204 DO 210 I=2,NM1
  210 SI(I)=ADPEI(I)*(AGRVDX*(RHO(N)-RHO(I))-DP)
      MOMSOU=1
C
C      ------ WRITE TEST OUTPUT IF REQUIRED, THEN RETURN
      IF(ITEST.EQ.1) RETURN
      WRITE(6,9011) J,(F(I,JEL),I=1,N)
      IF(MODEL.GT.2) WRITE(6,9012) (F(I,JK),I=1,N)
      IF(MODEL.GT.3) WRITE(6,9013) (F(I,J2),I=1,N)
      GO TO 9001
C
C
C     ------------------------------------------------------------------
CHAPTER B ---------- PHYSF ---------- PHYSF ---------- PHYSF ----------
      ENTRY PHYSF
      IF(MODEL.NE.1) GO TO 312
      RECPR=RECPRL(J)
      GO TO 310
  312 RECPR=RECPRT(J)
  310 NEWPR=1
      IF(ABS(RECPR-RPRLST).LT.1.E-10) GO TO 314
      NEWPR=2
      DO 313 I=2,NM2
  313 DIF(I)=DIFU(I)*RECPR
      RPRLST=RECPR
C     ------------------------------------------ KINETIC HEATING SOURCE
  314 IF(J.NE.JH) GO TO 3000
```

```
      IF(ABS(RECPR-1.).LT.1.E-10) GO TO 320
      IF(NOVEL.NE.1) GO TO 321
  320 KSOURC=3
      RETURN
  321 DUSQP=0.
      USQP=U(2)**2
      DO 322 I=2,NM2
      USQ=U(I+1)**2
      DUSQ=(DIFU(I)-DIF(I))*(USQ-USQP)
      SI(I)=.5*(DUSQ-DUSQP)
      DUSQP=DUSQ
  322 USQP=USQ
      KSOURC=2
      SI(NM1)=-.5*DUSQP
      GO TO 9000
C
C     ------------------------------------------------ FUEL SOURCE
 3000 IF(J.NE.JF) GO TO 4000
      IF(INERT.EQ.2) GO TO 342
      KSOURC=3
      RETURN
  342 KSOURC=1
      IF(MODEL.NE.1) GO TO 352
      T1=DX*PREEXP*PRESS**2
      T2=.5/STOICH
      DO 344 I=2,NM1
      FUBRNT=T2*(ABS(F(I,JP))-F(I,JP))
      IF(F(I,JF).GT.FUBRNT) GO TO 346
      SIP(I)=0.
      GO TO 344
  346 EXPO=EXP(-ARRCON/F(I,JTE))
      F(I,JOX)=AMAX1(0.,F(I,JP)+F(I,JF)*STOICH)
      TERM=-T1*EXPO*ADPEI(I)*F(I,JOX)
      SIP(I)=TERM/(1.-FUBRNT/F(I,JF))
  344 SI(I)=-SIP(I)*FUBRNT
      GO TO 9000
  352 T2=.5/STOICH
      IF(IBIO.EQ.1) GO TO 354
      T3=1./(PHIB-PHID+TINY)
      T4=-PHID*T3
C     ----- RATE CONTROLLED BY EDDY BREAK-UP
      CEBUDX=CEBU*DX
      DO 353 I=2,NM1
      FUBRNT=T2*(ABS(F(I,JP))-F(I,JP))
      FUUNBT=T3*F(I,JP)+T4
      IF(F(I,JF).LT.FUUNBT) GO TO 356
      SIP(I)=0.
      GO TO 353
  356 SIP(I)=-ADPEI(I)*CEBUDX*DUDY(I)*RHO(I)*(FUUNBT-F(I,JF))/
     1                                        (FUUNBT-FUBRNT+TINY)
  353 SI(I)=-SIP(I)*FUBRNT
```

```
      GO TO 358
C     ----------------THE ENTRY BIOS IN SUBROUTINE----------
C     ------------BIOG IS CALLED HERE-----------------------
  354 CALL BIOS
  358 CONTINUE
      GO TO 9000
C
C     ------------------------------------------- JP (PHI)
 4000 IF(J.NE.JP) GO TO 5000
      KSOURC=3
      RETURN
C
C     ------------------------------------------- ENERGY SOURCE
 5000 IF(J.NE.JK) GO TO 6000
C     ---------------------------- GENERATION OF TURBULENCE ENERGY
      DO 3001 I=2,NM1
 3001 GENK(I)=DX*ADPEI(I)*EMU(I)*DUDY(I)**2
C     ------------------------- DISSIPATION OF TURBULENCE ENERGY
      IF(MODEL-4) 3003,3004,3005
C     ------------------------------------------------- MODEL 3
 3003 CDDX=CD*DX
      DO 3006 I=2,NM1
 3006 DISSK(I)=CDDX*ADPEI(I)*ABS(F(I,JK))**1.5/(F(I,JEL)+TINY)
      GO TO 3007
C     ------------------------------------------------- MODEL 4
 3004 DO 3008 I=2,NM1
 3008 DISSK(I)=DX*RHO(I)*ADPEI(I)*F(I,J2)*F(I,JK)
      GO TO 3007
C     ------------------------------------------------- MODEL 5
 3005 DO 3009 I=2,NM1
 3009 DISSK(I)=DX*RHO(I)*ADPEI(I)*F(I,J2)
 3007 CONTINUE
C     ------------------------------------------- SI AND SIP
      KSOURC=1
      CONST1=1.5
      CONST2=C2MOD5-1.
      CONST3=.5
      CONST4=C2MOD5
      DO 3010 I=2,NM1
      RECFJK=1./(F(I,JK)+TINY)
      SI(I)=CONST1*GENK(I)+CONST2*DISSK(I)
 3010 SIP(I)=-RECFJK*(CONST3*GENK(I)+CONST4*DISSK(I))
C     ------------------------------------- NEAR-WALL CELLS
      IF(KIN.NE.1) GO TO 3011
      TAU=TAUI+Y(2)*DPDX+RMI*U(2)/R(2)
      F2JK=TAU/(RHO(2)*TAUDK)
      SI(2)=F2JK*BIG
      SIP(2)=-BIG
 3011 IF(KEX.NE.1) GO TO 9000
      TAU=TAUE+(Y(N)-Y(NM1))*DPDX-RME*U(NM1)/R(NM1)
      FNM1JK=TAU/(RHO(NM1)*TAUDK)
```

```
      SI(NM1)=FNM1JK*BIG
      SIP(NM1)=-BIG
      GO TO 9000
C
C     ------------------------- SOURCE OF 2ND TURBULENCE QUANTITY
 6000 IF(J.NE.J2) GO TO 7000
      KSOURC=1
C     --------------------------- SOURCE OF FREQUENCY (MODEL=4)
C                                          OR DISSIPATION (MODEL=5)
      IF(MODEL.EQ.4) GO TO 4001
      CONST1=C1MOD5
      CONST2=C2MOD5-1.
      CONST3=0.
      CONST4=2.*C2MOD5-1.
      GO TO 4002
 4001 CONST1=3.*C1MOD4
      CONST2=C2MOD4-1.
      CONST3=2.*C1MOD4
      CONST4=2.*C2MOD4-1.
 4002 DO 4003 I=2,NM1
      RECFJK=1./(F(I,JK)+TINY)
      FJ2DJK=F(I,J2)*RECFJK
      SI(I)=FJ2DJK*(CONST1*GENK(I)+CONST2*DISSK(I))
 4003 SIP(I)=-RECFJK*(CONST3*GENK(I)+CONST4*DISSK(I))
C     ------------------------------------ NEAR-WALL CELLS
      IF(KIN.NE.1) GO TO 4004
      F2J2=WALCON*SQRT(F2JK)*RECYDF(1)
      IF(MODEL.EQ.5) F2J2=F2J2*F2JK
      SI(2)=F2J2*BIG
      SIP(2)=-BIG
 4004 IF(KEX.NE.1) GO TO 9000
      FNM1J2=WALCON*SQRT(FNM1JK)*RECYDF(NM1)
      IF(MODEL.EQ.5) FNM1J2=FNM1J2*FNM1JK
      SI(NM1)=FNM1J2*BIG
      SIP(NM1)=-BIG
C
C********** SOURCE TERMS FOR FOLD POPULATION DISTRIBUTION*****
C----------   SOURCE TERM FOR AGE(1)
 7000 IF(J.NE.JA1) GO TO 8000
      KSOURC=1
      TRANF=UMIN/XD
      DTRANF=-1./XD
      DO 540 I=2,NM1
      ADPEDX(I)=ADPEI(I)*DX
      AVELP=TRANF/U(I)+DTRANF*AGE(2)
      SIAP=AMIN1(0.,AVELP)*F(I,JA2)
      SIPAP=AMAX1(0.,AVELP)
      SI(I)=(PA0(I)*RECDA(1)-SIAP)*ADPEDX(I)
      SIP(I)=(-RHO(I)*U(I)*SIPAP*RECDA(1)-PA0(I))*ADPEDX(I)
  540 CONTINUE
      GO TO 9000
```

```
C
C----------  SOURCE TERMS FOR AGE(2)...AGE(NAGE)
 8000 KSOURC=1
      JM2=J-JA1M1
      DO 620 I=2,NM1
C------ PFLUX THROUGH THE WEST FACE
      AVELM=TRANF/U(I)+DTRANF*AGE(JM2)
      SIAM=AMAX1(0.,AVELM)*F(I,J-1)
      SIPAM=AMIN1(0.,AVELM)
C------ PFLUX THROUGH THE EAST FACE
      AVELP=TRANF/U(I)+DTRANF*AGE(JM2+1)
      FIJP1=F(I,J+1)
      IF(J.EQ.JAL) FIJP1=F(I,J)
      SIAP=AMIN1(0.,AVELP)*FIJP1
      SIPAP=AMAX1(0.,AVELP)
      SI(I)=RHO(I)*U(I)*(-SIAP+SIAM)*RECDA(JM2)*ADPEDX(I)
      SIP(I)=(RHO(I)*U(I)*(-SIPAP+SIPAM)*RECDA(JM2)-PA0(I))
     1 *ADPEDX(I)
  620 CONTINUE
C     ----- WRITE TEST OUTPUT,IF REQUIRED, THEN RETURN
 9000 IF(ITEST.EQ.1) RETURN
      WRITE(6,9021) J,(SIP(I),I=2,NM1)
 9001 WRITE(6,9022) (SI(I),I=2,NM1)
      RETURN
C
 9011 FORMAT(18H PHYS TESTS FOR J=,I3/10H F(I,JEL)=/(3X,1P6E11.3))
 9012 FORMAT(9H F(I,JK)=/(3X,1P6E11.3))
 9013 FORMAT(9H F(I,J2)=/(3X,1P6E11.3))
 9021 FORMAT(18H PHYS TESTS FOR J=,I3/8H SIP(I)=/(3X,1P6E11.3))
 9022 FORMAT(7H SI(I)=/(3X,1P6E11.3))
      END
```

```
      SUBROUTINE COMP
C/FEB.1977 ---------- G E N M I X ---------- COPYRIGHT, D.B.SPALDING ---
      DIMENSION A(60),B(60),C(60),CON(60),D(60),HCON(60),OMDIF(60)
$INCLUDE 9,COMA2.FTN
$INCLUDE 9,COMB.FTN
C
      EQUIVALENCE (A(1),DIF(1)),(C(1),SI(1)),(D(1),SIP(1))
C
CHAPTER A ------------------------------------------------------------
C     INIT ------------ INIT ------------ INIT ------------ INIT
      ENTRY INIT
C     ------------------------- INITIAL VALUES AND DEFAULT VALUES
      NM1=N-1
      NM2=N-2
      NM3=N-3
      ISTEP=0
      IF(KRAD.EQ.3) NOVEL=1
      JUSTIN=ISTEP
      JUSTEX=ISTEP
      IFIN=1
      DXLAST=BIG
      DX=BIG
      PSII=0.
      BPE=1.
      BPI=1.
      Y(1)=0.
      DP=0.
      DO 13 I=1,N
      EMU(I)=0.
      CON(I)=0.
   13 R(I)=1.
      IF(NOVEL.NE.1) RETURN
      DO 16 I=1,N
   16 U(I)=1.
      RETURN
CHAPTER B ------------------------------------------------------------
C     GRID ------------ GRID ------------ GRID ------------ GRID
      ENTRY GRID
      OMI=OM(2)
      OME=1.-OM(NM1)
      BOM(2)=.5*(OM(2)+OM(3))
      OMINT(1)=0.
      OMINT(2)=BOM(2)
      DO 202 I=3,NM2
      OMINT(I)=.5*(OM(I)+OM(I+1))
      BOM(I)=OMINT(I)-OMINT(I-1)
  202 OMDIF(I)=OM(I)-OM(I-1)
      HOMDFI=.5*OMDIF(3)
      BOM(NM1)=1.-OMINT(NM2)
      OMINT(NM1)=1.
      OMDIF(NM1)=OM(NM1)-OM(NM2)
```

```
      HOMDFE=.5*OMDIF(NM1)
      RETURN
CHAPTER C ------------------------------------------------------------
C     DISTAN ---------- DISTAN ---------- DISTAN ---------- DISTAN
      ENTRY DISTAN
      IF(NOVEL.NE.1) GO TO 220
      DO 224 I=1,N
  224 RECRU(I)=1./(RHO(I)+TINY)
      GO TO 222
  220 DO 221 I=1,N
      RECRU(I)=1./(RHO(I)*U(I)+TINY)
      IF(RECRU(I).GT.0.) GO TO 221
      IFIN=2
      WRITE(6,223) RECRU(I),I,ISTEP
  223 FORMAT(14H *** RECRU(I)=,1PE10.3,6H AT I=,I4,11H AND ISTEP=,I5,
     1 16H *** COMP DISTAN)
  221 CONTINUE
C     -------------------- CALCULATION OF Y"S AND R"S
  222 IF(KIN.EQ.1) GO TO 308
      RAT=RECRU(2)*RHO(1)*U(1)
      IF(KRAD.EQ.2) GO TO 307
      BPI=.33333+.66667*RAT
      GO TO 308
  307 BPI=(R(1)*(.83333*RAT+.16667)+.5*R(2)*(RAT+1.))/(R(1)+R(2))
  308 IF(KEX.EQ.1) GO TO 230
      RAT=RECRU(NM1)*RHO(N)*U(N)
      IF(KRAD.EQ.2) GO TO 327
      BPE=.33333+.66667*RAT
      GO TO 230
  327 BPE=(R(N)*(.833333*RAT+.16667)+.5*R(NM1)*(RAT+1.))/(R(N)+R(NM1))
C     -------------------- Y"S FOR PLANE FLOW
  230 STORE=OM(2)/BPI
      ADPEI(2)=(HOMDFI+STORE)*RECRU(2)
      Y(2)=PEI*RECRU(2)*STORE
      HPEI=.5*PEI
      DO 231 I=3,NM1
      ADPEI(I)=BOM(I)*RECRU(I)
  231 Y(I)=Y(I-1)+HPEI*OMDIF(I)*(RECRU(I)+RECRU(I-1))
      STORE=OME/BPE
      ADPEI(NM1)=(HOMDFE+STORE)*RECRU(NM1)
      Y(N)=Y(NM1)+PEI*RECRU(NM1)*STORE
C     ------------------------------------------------
      IF(KRAD-2) 270,240,280
C     ---------------- Y"S AND R"S FOR AXIAL SYMMETRY
  240 IF(CSALFA.LT.TINY) GO TO 260
C     ------------------------------ CSALFA NE 0.
      COSD2=.5*CSALFA
      TWDCOS=2./CSALFA
      IF(R(1).GT.TINY) GO TO 250
C     ------------------------------ R(1)=0.
      DO 242 I=2,N
```

```
      Y(I)=SQRT(ABS(Y(I)*TWDCOS))
  242 R(I)=Y(I)*CSALFA
      GO TO 270
C     ------------------------------ R(1) NE 0.
  250 R1D2=.5*R(1)
      R1D2SQ=R1D2*R1D2
      DO 251 I=2,N
      Y(I)=Y(I)/(R1D2+SQRT(ABS(R1D2SQ+COSD2*Y(I))))
  251 R(I)=R(1)+Y(I)*CSALFA
      GO TO 270
C     ------------------------------ CSALFA=0.
  260 RECR1=1./R(1)
      DO 261 I=2,N
      R(I)=R(1)
  261 Y(I)=Y(I)*RECR1
      GO TO 270
C     ------------------------------- POINT SYMMETRY, KRAD=3
  280 R1CUB=R(1)**3
      DO 281 I=2,N
      R(I)=(R1CUB+Y(I))**.3333333
  281 Y(I)=R(I)-R(1)
C     ------------------------------ GENERAL
  270 YI=Y(2)
      YE=Y(N)-Y(NM1)
      DO 273 I=1,NM1
  273 RECYDF(I)=1./(Y(I+1)-Y(I))
      IF(ITEST.EQ.1) RETURN
      WRITE(6,274) (RHO(I),I=1,N)
      WRITE(6,275) (RECRU(I),I=1,N)
      WRITE(6,276) (ADPEI(I),I=1,N)
      WRITE(6,277) (Y(I),I=1,N)
      WRITE(6,278) (R(I),I=1,N)
      WRITE(6,279) (RECYDF(I),I=1,N)
      RETURN
  274 FORMAT(18HØCOMP DISTAN TESTS/8H RHO(I)=/(3X,1P6E11.3))
  275 FORMAT(10H RECRU(I)=/(3X,1P6E11.3))
  276 FORMAT(10H ADPEI(I)=/(3X,1P6E11.3))
  277 FORMAT(6H Y(I)=/(3X,1P6E11.3))
  278 FORMAT(6H R(I)=/(3X,1P6E11.3))
  279 FORMAT(11H RECYDF(I)=/(3X,1P6E11.3))
CHAPTER D ------------------------------------------------------------
C     SOLVE ---------- SOLVE ---------- SOLVE ---------- SOLVE
      ENTRY SOLVE
C     ---------------------------------------- PRELIMINARIES
      DXDPEI=DX/PEI
      CONST1=.5*DXDPEI
      ENT=ABS(RMI)+ABS(RME)
      IF(ENT.LE.TINY) GO TO 310
      HCONI=RMI*CONST1
      HCONDF=(RME-RMI)*CONST1
      DO 412 I=2,NM1
```

```
      HCON(I)=HCONI+HCONDF*OMINT(I)
  412 CON(I)=HCON(I)+HCON(I)
C     ------------------------------------------ COEFFICIENTS FOR U
  310 IF(NOVEL.EQ.1) GO TO 442
      J=0
C     ----- CALL SUBROUTINE PHYS AT ENTRY PHYSU
      CALL PHYSU
      IF(KRAD-2) 410,415,411
  410 DO 413 I=2,NM2
  413 DIFU(I)=CONST1*(EMU(I)+EMU(I+1))*RECYDF(I)
      GO TO 414
  415 CONST2=.5*CONST1
      DO 416 I=2,NM2
  416 DIFU(I)=CONST2*(R(I+1)+R(I))*(EMU(I)+EMU(I+1))*RECYDF(I)
      GO TO 414
  411 CONST3=.25*CONST1
      DO 419 I=2,NM2
  419 DIFU(I)=CONST3*(R(I+1)+R(I))**2*(EMU(I)+EMU(I+1))*RECYDF(I)
C     ------------------------------------------ A"S AND B"S
  414 IF(ENT.LE.TINY) GO TO 312
      DO 417 I=2,NM2
      A(I)=AMAX1(0.,DIFU(I)-HCON(I),-CON(I))
  417 B(I+1)=A(I)+CON(I)
      GO TO 314
  312 DO 315 I=2,NM2
      A(I)=DIFU(I)
  315 B(I+1)=A(I)
  314 TI=0.
      TE=0.
      IF(KIN.EQ.1) CALL WALL(1,BPI,TI)
      IF(KEX.EQ.1) CALL WALL(N,BPE,TE)
      B(2)=AMAX1((TI+RMI)*DXDPEI,0.)
      A(NM1)=AMAX1((TE-RME)*DXDPEI,0.)
C     ------------------------------------------ C"S AND D"S
      IF(MOMSOU.EQ.0) GO TO 431
      DO 418 I=2,NM1
      C(I)=U(I)*BOM(I)+SI(I)
  418 D(I)=A(I)+B(I)+BOM(I)
      GO TO 432
  431 DO 433 I=2,NM1
      C(I)=U(I)*BOM(I)
  433 D(I)=A(I)+B(I)+BOM(I)
  432 CONTINUE
      IF(ITEST.EQ.1) GO TO 404
      WRITE(6,341) (DIFU(I),I=2,NM1)
      WRITE(6,342) (CON(I),I=2,NM1)
      WRITE(6,405) (A(I),I=2,NM1)
      WRITE(6,406) (B(I),I=2,NM1)
      WRITE(6,407) (C(I),I=2,NM1)
      WRITE(6,408) (D(I),I=2,NM1)
  341 FORMAT(23H0COMP SOLVE TESTS FOR U/9H DIFU(I)=/(3X,1P6E11.3))
```

```
  342 FORMAT(8H CON(I)=/(3X,1P6E11.3))
  405 FORMAT(6H A(I)=/(3X,1P6E11.3))
  406 FORMAT(6H B(I)=/(3X,1P6E11.3))
  407 FORMAT(6H C(I)=/(3X,1P6E11.3))
  408 FORMAT(6H D(I)=/(3X,1P6E11.3))
  404 CONTINUE
C  ------------------------------ ADJUST FREE-BOUNDARY VALUES ---------
      IF(KIN.EQ.2) U(1)=U(1)-DP*RECRU(1)
      IF(KEX.EQ.2) U(N)=U(N)-DP*RECRU(N)
C-----------------------------   SOLVE FOR DOWNSTREAM U "S  ------------
      C(2)=(B(2)*U(1)+C(2))/D(2)
      D(2)=A(2)/D(2)
      DO 421 I=3,NM1
      T=1./(D(I)-B(I)*D(I-1))
      D(I)=A(I)*T
  421 C(I)=(B(I)*C(I-1)+C(I))*T
      DO 422 IDASH=1,NM2
      I=N-IDASH
  422 U(I)=D(I)*U(I+1)+C(I)
      IF(KIN-2) 444,445,446
  444 TAUI=TI*U(2)/R(1)
      GO TO 445
  446 U(1)=U(2)
  445 IF(KEX-2) 447,440,448
  447 TAUE=TE*U(NM1)/R(N)
      GO TO 440
  448 U(N)=U(NM1)
  440 IF(ITEST.NE.1) WRITE(6,443) (U(I),I=1,N)
  443 FORMAT(6H U(I)=/(3X,1P6E11.3))
C     ------------------------------------------
C     ------------------------------------------- F-SECTION
  442 IF(NF.LT.1) GO TO 481
C----------RESTORAGE OF UPSTREAM VALUES----------
      DO 4802 J=1,NF
      IDJ=IDIMF*(J-1)
      DO 4802 I=1,N
      IJ=I+IDJ
      FP(IJ)=F(IJ)
 4802 CONTINUE
C----------ITERATION LOOP STARTS HERE------------
      DO 4801 ITER=1,4
      DO 480 J=1,NF
C----------ITERATION FOR P-A EQUATIONS ONLY-------
      IF(J.LT.JA1.AND.ITER.GT.1) GO TO 480
      IF(J.GT.JAL.AND.ITER.GT.1) GO TO 480
      IDJ=IDIMF*(J-1)
      I1J=1+IDJ
      I2J=2+IDJ
      INM1J=NM1+IDJ
      INJ=N+IDJ
C     ----- CALL SUBROUTINE PHYS AT ENTRY PHYSF
```

```
      CALL PHYSF
      TIF=Ø.
      FDIFI=Ø.
      TEF=Ø.
      FDIFE=Ø.
      IF(KIN.EQ.1) CALL WALL(1,FDIFI,TIF)
      IF(KEX.EQ.1) CALL WALL(N,FDIFE,TEF)
      IF(ITEST.EQ.1) GO TO 45Ø
      WRITE(6,451) J,(DIF(I),I=2,NM1)
  451 FORMAT(24H COMP SOLVE TESTS FOR J=,I3/8H DIF(I)=/(3X,1P6E11.3))
C     ---------------------------------- COEFFICIENTS FOR F"S
C     ------------------------------------------ A"S AND B"S
  45Ø IF(NEWPR.EQ.1) GO TO 337
      IF(ENT.LE.TINY) GO TO 335
      DO 484 I=2,NM2
      A(I)=AMAX1(Ø.,DIF(I)-HCON(I),-CON(I))
  484 B(I+1)=A(I)+CON(I)
      GO TO 337
  335 DO 338 I=2,NM2
      A(I)=DIF(I)
  338 B(I+1)=A(I)
  337 CONTINUE
      B(2)=AMAX1((TIF+RMI)*DXDPEI,Ø.)
      A(NM1)=AMAX1((TEF-RME)*DXDPEI,Ø.)
C     ------------------------------------------ C"S AND D"S
      GO TO (5Ø1,5Ø2,5Ø3), KSOURC
C     ------------------------------ KSOURC=1, GENERAL
  5Ø1 SI2=SI(2)
      SINM1=SI(NM1)
      DO 485 I=2,NM1
      IJ=I+IDJ
      D(I)=A(I)+B(I)+BOM(I)-SIP(I)
  485 C(I)=FP(IJ)*BOM(I)+SI(I)
      GO TO 5Ø4
C     ------------------------------ KSOURC=2, NO SIP
  5Ø2 SI2=SI(2)
      SINM1=SI(NM1)
      DO 5Ø5 I=2,NM1
      IJ=I+IDJ
      D(I)=A(I)+B(I)+BOM(I)
  5Ø5 C(I)=F(IJ)*BOM(I)+SI(I)
      GO TO 5Ø4
C     ------------------------------ KSOURC=3, NO SIP OR SI
  5Ø3 SI2=Ø.
      SINM1=Ø.
      DO 5Ø6 I=2,NM1
      IJ=I+IDJ
      D(I)=A(I)+B(I)+BOM(I)
  5Ø6 C(I)=F(IJ)*BOM(I)
C     ----------------------------
  5Ø4 C(2)=C(2)-TIF*FDIFI*DXDPEI
```

```
      C(NM1)=C(NM1)-TEF*FDIFE*DXDPEI
      IF(KIN.GT.1) GO TO 486
      IF(IBIN(J).EQ.1) GO TO 486
      B(2)=0.
      C(2)=F(I2J)*BOM(2)+SI2+RJTOTI(J)*DXDPEI
      D(2)=D(2)-TIF*DXDPEI
  486 IF(KEX.GT.1) GO TO 491
      IF(IBEX(J).EQ.1) GO TO 491
      A(NM1)=0.
      C(NM1)=F(INM1J)*BOM(NM1)+SINM1-RJTOTE(J)*DXDPEI
      D(NM1)=D(NM1)-TEF*DXDPEI
  491 CONTINUE
      DO 492 I=2,NM1
      A1(I)=A(I)
  492 B1(I)=B(I)
      IF(ITEST.EQ.1) GO TO 464
      WRITE(6,405) (A(I),I=2,NM1)
      WRITE(6,406) (B(I),I=2,NM1)
      WRITE(6,407) (C(I),I=2,NM1)
      WRITE(6,408) (D(I),I=2,NM1)
C     ------------------------------ SOLVE FOR DOWNSTREAM F "S
  464 C(2)=(B(2)*F(I1J)+C(2))/D(2)
      D(2)=A(2)/D(2)
      DO 465 I=3,NM1
      T=1./(D(I)-B(I)*D(I-1))
      D(I)=A(I)*T
  465 C(I)=(B(I)*C(I-1)+C(I))*T
      DO 466 IDASH=1,NM2
      I=N-IDASH
      IJ=I+IDJ
  466 F(IJ)=D(I)*F(IJ+1)+C(I)
C     ---------------------------- ADJUST F(1,J) AND F(N,J)
      IF(J.GE.JA1.AND.J.LE.JAL) GO TO 469
      IF(KIN-2) 467,460,469
  467 IF(IBIN(J).EQ.1) GO TO 468
      F(I1J)=FDIFI+F(I2J)+(RJTOTI(J)-F(I1J)*RMI)/TIF
      GO TO 460
  469 F(I1J)=F(I2J)
      IF(J.GE.JA1.AND.J.LE.JAL) GO TO 473
      GO TO 460
  468 RJTOTI(J)=TIF*(F(I1J)-F(I2J)-FDIFI)+RMI*F(I1J)
  460 IF(KEX-2) 471,470,473
  471 IF(IBEX(J).EQ.1) GO TO 472
      F(INJ)=FDIFE+F(INM1J)-(RJTOTE(J)-F(INJ)*RME)/TEF
      GO TO 470
  473 F(INJ)=F(INM1J)
      GO TO 470
  472 RJTOTE(J)=TEF*(F(INM1J)+FDIFE-F(INJ))+RME*F(INJ)
  470 IF(ITEST.EQ.1) GO TO 480
      WRITE(6,476) J,(F(I+IDJ),I=1,N)
  476 FORMAT(6H  F(I,,I2,1H)/(3X,1P6E11.3))
```

```
  480 CONTINUE
C----------THE ERROR CAN BE CHECKED HERE---------
 4801 CONTINUE
C     ----------------------------------------
  481 XU=XD
      PSII=PSII-RMI*DX
      PSIE=PSIE-RME*DX
      PEI=PSIE-PSII
      ISTEP=ISTEP+1
      RETURN
      END
```

```
      SUBROUTINE WALL
C/FEB.1977 ---------- G E N M I X ---------- COPYRIGHT, D.B.SPALDING ---
      DIMENSION S1(2),S2(2),S3(2),S4(2),S5(2),S6(2)
$INCLUDE 9,COMA1.FTN
$INCLUDE 9,COMB.FTN
C
C     EFFECTS OF PRESSURE GRADIENT AND MASS TRANSFER ARE INCLUDED
C     EFFECTS OF RADIUS VARIATION ARE NEGLECTED
C     FOR VELOCITY,  OUT1=BP,     OUT2=T
C     FOR F "S,      OUT1=FIDIF,  OUT2=T
C
CHAPTER A ------------------------------ PRELIMINARIES ---------------
      DATA SHALF/.04/, BPLAST/1./
      KWALL=2-1/I1
      I2=I1+3-2*KWALL
      I3=I1+6-4*KWALL
      IF(J.GT.0) GO TO 200
CHAPTER B ---------------------------------- VELOCITY ------------------
      UREF=U(I2)
      RHOREF=RHO(I2)
      RUREF=RHOREF*UREF
      RREF=R(I2)
      VREF=EMU(I1)
      YREF=YI+(YE-YI)*OM(I1)
      RE=RUREF*YREF/VREF
      RRUREF=RREF*RUREF
      AM=(RMI-(RME+RMI)*OM(I1))/RRUREF
      EF=YREF*DP/(DX*RUREF*UREF)
      IF(MODEL.EQ.1) GO TO 110
      IF(RE.LT.132.25) GO TO 110
C     ------------------------------ TURBULENT FLOW
C     ---------- EXTENDED LOG LAW
      ER=RE*EWALL
      ARGMIN=11.5*EWALL
      NIT=0
  101 SHALF1=SHALF
      S=SHALF**2
      SLOC=S+AM+EF
      IF(SLOC.GT.0.) GO TO 104
      SLOC=TINY
      SHALF=SQRT(ABS(AM+EF))
  104 BEE=SQRT(SLOC)/AK
      ARG=ER*(SHALF+(AM/(1.+BEE)+.5*EF)/SHALF)
      IF(ARG.LT.ARGMIN) GO TO 110
      SHALF=AK/ALOG(ARG)
      IF(ABS(SHALF-SHALF1).LT..0001) GO TO 102
      NIT=NIT+1
      IF(NIT.LT.11) GO TO 101
  102 S=SHALF**2
      SAV=.5*(S+SLOC)
      BP=1./(1.+BEE)
```

```
      GO TO 103
C     ------------------------------ LAMINAR FLOW
  110 AMRE=AM*RE
      FRE=EF*RE
      IF(ABS(AMRE).LT..01) GO TO 111
      AMRE=AMAX1(-60.,AMIN1(60.,AMRE))
      EXPMRE=EXP(AMRE)
      STORE=EXPMRE-1.-AMRE
      AMRESQ=AMRE*AMRE
      SRE=AMRE*(1.-STORE*FRE/AMRESQ)/(EXPMRE-1.)
      BP=SRE*STORE/AMRESQ+FRE*(STORE-.5*AMRESQ)/(AMRESQ*AMRE)
      GO TO 112
  111 SRE=(2.-FRE*(1.+AMRE*.33333))/(2.+AMRE)
      BP=SRE*(.5+AMRE*.16667)+FRE*(.16667+AMRE*.041667)
  112 IF(SRE.GT.TINY) GO TO 113
      SRE=TINY
      BP=.33333
  113 S=SRE/RE
      SAV=S
  103 T=S*RRUREF
C     -------------------- UNDER-RELAX BP
      BP=BPLAST+.5*(BP-BPLAST)
      BPLAST=BP
      OUT1=BP
      OUT2=T
      S1(KWALL)=SAV
      S2(KWALL)=RRUREF
      S3(KWALL)=UREF
      S4(KWALL)=AM
      S5(KWALL)=AMRE
      S6(KWALL)=RE
      GO TO 900
C-------------------------------------------------------------------------
CHAPTER C ------------------------ OTHER DEPENDENT VARIABLES -----------
  200 SAV=S1(KWALL)
      RRUREF=S2(KWALL)
      UREF=S3(KWALL)
      AM=S4(KWALL)
      AMRE=S5(KWALL)
      RE=S6(KWALL)
      IF(MODEL.EQ.1) GO TO 210
C     ------------------------------- TURBULENT FLOW
      PRRAT=PRL(J)*RECPRT(J)
C     ----- THE FOLLOWING P-FUNCTION IS NOT TO BE USED FOR PRRAT.LT.0.5
      PJAY=9.*(PRRAT-1.)/PRRAT**.25
      S=SAV*RECPRT(J)/(1.+AMAX1(-.99999,PJAY*SQRT(ABS(SAV))))
      OUT2=S*RRUREF
      IF(J.NE.JH) GO TO 221
      OUT1=(H-1.)*.5*UREF**2
      GO TO 900
  221 OUT1=0.
```

```
      GO TO 900
C     ------------------------------ LAMINAR FLOW
  210 IF(ABS(AMRE).LT..01) GO TO 211
      S=AM/(EXP(PRL(J)*AMRE)-1.)
      GO TO 212
  211 S=RECPRL(J)/(RE+.5*RE*PRL(J)*AMRE)
  212 OUT2=S*RRUREF
      IF(J.NE.JH) GO TO 214
      OUT1=(PRL(JH)-1.)*.5*UREF**2
      GO TO 900
  214 OUT1=0.
C-------------------------------------------------------------------------
C     ------------------------------ NULL OUTPUT FOR JK OR J2
  300 OUT1=TINY
      OUT2=TINY
  900 IF(ITEST.EQ.1) GO TO 901
      WRITE(6,9000)  J,I1,OUT1,OUT2
 9000 FORMAT(12H WALL TESTS,,3H J=,I3,4H I1=,I3,6H OUT1=,1PE10.3,
     1 6H OUT2=,E10.3)
  901 RETURN
      END
```

APPENDIX C

Sample Output of the Computer Program (H_2-Air Flame)

```
 GENMIX-T, SEPT.1977, TURBULENCE MODELS TEACHING PROGRAM,
 BASED ON APPENDIX A OF HTS REPORT NO. HTS/77/9, FEB.1977.
 COMBUSTION OF HYDROGEN AND AIR IN A JET, AXI-SYMMETRICAL FLOW
  KASE IRUN KIND KRAD CSALFA MODEL LENGTH MOD4C1 INERT NOVEL
    4    0    1    2  1.000     5      1      1     2     2

*****THE ESCIMO MODEL OF TURBULENT COMBUSTION*****
*****IS INCORPORATED IN THE PRESENT PROGRAM  *****
*****DEMOGRAPHIC CONSTANTS*****
 NAGE  JA1   JAL   FOLMO UMAX  MODFOR
   10   4    13    0.50151.00   3
  AGE1   AGE3    AGE5    AGE7     AGE9    AGE11
 0.00000 0.10000 0.20000 0.40000 0.65000 1.00000

*****BIOGRAPHIC CONSTANTS*****
 EMPC1      EMPC2      EMPC3
  0.200E+01 0.200E+01 0.500E+00
  OM(I), FOR OMPOW= 2.000
   0.000E+00  2.494E-03  9.975E-03  2.244E-02  3.990E-02  6.234E-02
   8.977E-02  1.222E-01  1.596E-01  2.020E-01  2.494E-01  3.017E-01
   3.989E-01  4.681E-01  5.429E-01  6.233E-01  7.091E-01  8.006E-01
   8.975E-01  1.000E+00
     HEXO       XHEXO       AHEX       BHEX       CHEX
   3.810E-03  0.000E+00  0.000E+00  0.000E+00  0.000E+00
     HINO       XHINO       AHIN       BHIN       CHIN
   0.000E+00  0.000E+00  0.000E+00  0.000E+00  0.000E+00
     UEXO       XUEXO       AUEX       BUEX       CUEX
   1.510E+01  0.000E+00  0.000E+00  0.000E+00  0.000E+00
     XEND       XOUT      XULAST       HDIV      AGRAV
   0.000E+00  0.000E+00  6.096E-01  2.000E-03  9.800E+00
     UA         UB         UC         UD         TA         TB         TC         TD
   151.000   151.000   151.000    15.100   300.000   300.000   300.000   300.000
    PRESS    PREEXP       REY     EQRAT     AMACH      ULIM    PEILIM
  1.00E+05 1.00E+00 2.70E+03 3.04E+10 8.31E-03 5.00E-02 1.00E-02
    AK          ELCON       TAUDK       ELEXP       SIGK        SIG2
  4.350E-01   1.985E-01   3.000E-01   2.380E+00   1.000E+00   1.314E+00
    CMU         CD          FJKA        FJ2A        FJKD        FJ2D
  5.477E-01   1.643E-01   6.840E+02   0.000E+00   1.000E-01   6.871E+00
    C1MOD5      C2MOD5
  0.144E+01   0.192E+01
```

*** XU= 3.035E-01 ISTEP= 312
JUSTIN= 0 JUSTEX= 0 DX= 1.918E-03 PRESSD= 0.000E+00

KIN= 3 KEX= 2 DXY= 3.066E-02 DPDX= 0.000E+00
PSII= 0.000E+00 PSIE= 1.940E-03 DXRE= 1.024E+02 PEI= 1.940E-03
RMI= 0.000E+00 RME=-1.002E-02 DXINC= 9.533E-03 YREF1= 0.000E+00
R(1)= 0.000E+00 R(N)= 3.252E-02 DXPSI= 1.918E-03 YREF2= 0.000E+00
ELCON= 1.985E-01
UFLUX= 1.254E-02
FLUX(J)= -7.234E-04 4.731E-02 1.228E+01 8.288E-03 7.142E-03
6.041E-03 4.956E-03 3.172E-03 1.763E-03 8.257E-04
2.407E-04 4.168E-05 2.066E-06 1.095E+04 4.682E-05
FACE= 2.052E-01 RATE= 9.956E-01
Y(N)= 3.25E-02

I	R/RO	UVEL	TEMP	FUEL	OXYG	H2M
1	0.00E+00	3.47E+01	1.31E+03	1.04E-01	0.00E+00	5.89E-01
2	4.31E-01	3.47E+01	1.31E+03	1.04E-01	0.00E+00	5.89E-01
3	8.65E-01	3.43E+01	1.33E+03	1.02E-01	9.44E-05	5.82E-01
4	1.30E+00	3.36E+01	1.34E+03	9.83E-02	2.08E-03	5.72E-01
5	1.74E+00	3.28E+01	1.35E+03	9.34E-02	4.44E-03	5.59E-01
6	2.18E+00	3.18E+01	1.37E+03	8.74E-02	6.99E-03	5.41E-01
7	2.62E+00	3.07E+01	1.40E+03	8.05E-02	9.79E-03	5.20E-01
8	3.07E+00	2.95E+01	1.43E+03	7.28E-02	1.27E-02	4.93E-01
9	3.53E+00	2.81E+01	1.46E+03	6.46E-02	1.58E-02	4.61E-01
10	3.99E+00	2.68E+01	1.50E+03	5.60E-02	1.89E-02	4.24E-01
11	4.45E+00	2.54E+01	1.55E+03	4.70E-02	2.18E-02	3.81E-01
12	4.93E+00	2.40E+01	1.61E+03	3.80E-02	2.55E-02	3.30E-01
13	5.72E+00	2.17E+01	1.69E+03	2.35E-02	3.35E-02	2.32E-01
14	6.23E+00	2.03E+01	1.76E+03	1.48E-02	3.94E-02	1.59E-01
15	6.75E+00	1.90E+01	1.80E+03	6.94E-03	4.85E-02	8.14E-02
16	7.24E+00	1.79E+01	1.66E+03	2.90E-03	7.87E-02	3.62E-02
17	7.69E+00	1.71E+01	1.48E+03	6.03E-04	1.10E-01	7.90E-03
18	8.09E+00	1.65E+01	1.24E+03	1.58E-04	1.40E-01	2.13E-03
19	8.42E+00	1.61E+01	9.99E+02	2.43E-04	1.68E-01	3.33E-03
20	8.54E+00	1.51E+01	3.00E+02	0.00E+00	2.32E-01	0.00E+00

I	O2M	H2OM	N2M	TEMF	FUFL	OXFL
1	0.00E+00	1.42E-01	2.69E-01	2.43E+02	3.12E-02	0.00E+00
2	0.00E+00	1.42E-01	2.69E-01	2.43E+02	3.12E-02	0.00E+00
3	3.37E-05	1.44E-01	2.73E-01	2.75E+02	3.26E-02	1.39E-03
4	7.56E-04	1.47E-01	2.80E-01	2.76E+02	3.39E-02	1.75E-02
5	1.66E-03	1.50E-01	2.90E-01	3.03E+02	3.48E-02	2.86E-02
6	2.71E-03	1.54E-01	3.02E-01	3.16E+02	3.53E-02	3.57E-02
7	3.95E-03	1.60E-01	3.17E-01	3.26E+02	3.51E-02	4.19E-02
8	5.39E-03	1.66E-01	3.35E-01	3.40E+02	3.42E-02	4.77E-02
9	7.05E-03	1.75E-01	3.57E-01	3.61E+02	3.26E-02	5.32E-02
10	8.94E-03	1.84E-01	3.82E-01	3.94E+02	3.05E-02	5.85E-02
11	1.10E-02	1.96E-01	4.12E-01	4.38E+02	2.79E-02	6.33E-02
12	1.38E-02	2.09E-01	4.47E-01	4.74E+02	2.48E-02	6.74E-02
13	2.06E-02	2.31E-01	5.16E-01	5.42E+02	1.90E-02	7.42E-02
14	2.65E-02	2.47E-01	5.67E-01	6.04E+02	1.48E-02	7.84E-02
15	3.55E-02	2.59E-01	6.24E-01	6.84E+02	1.07E-02	8.32E-02
16	6.15E-02	2.32E-01	6.71E-01	6.69E+02	5.71E-03	7.80E-02
17	8.98E-02	1.94E-01	7.08E-01	6.66E+02	1.62E-03	7.21E-02
18	1.18E-01	1.49E-01	7.30E-01	7.15E+02	7.45E-04	7.17E-02

19	1.44E-01	1.07E-01	7.46E-01	6.17E+02	1.35E-03	5.95E-02
20	2.10E-01	0.00E+00	7.93E-01	0.00E+00	0.00E+00	0.00E+00

*****POPULATION DISTRIBUTION OF FOLDS*****

I	FRAT	PA (1)	PA (2)	PA (3)	PA (4)	PA (5)
		PA (6)	PA (7)	PA (8)	PA (9)	PA (10)
2	4.693E+01	3.600E+00	4.231E+00	3.958E+00	3.207E+00	1.705E+00
		6.303E-01	1.357E-01	1.909E-02	1.553E-03	7.906E-05
3	1.179E+02	3.836E+00	4.215E+00	3.879E+00	3.129E+00	1.670E+00
		6.272E-01	1.410E-01	2.001E-02	1.649E-03	8.165E-05
4	1.641E+02	4.097E+00	4.204E+00	3.783E+00	3.034E+00	1.630E+00
		6.267E-01	1.499E-01	2.166E-02	1.819E-03	8.654E-05
5	2.053E+02	4.353E+00	4.193E+00	3.680E+00	2.931E+00	1.589E+00
		6.302E-01	1.627E-01	2.418E-02	2.081E-03	9.442E-05
6	2.395E+02	4.578E+00	4.178E+00	3.579E+00	2.832E+00	1.553E+00
		6.390E-01	1.795E-01	2.781E-02	2.458E-03	1.062E-04
7	2.660E+02	4.755E+00	4.156E+00	3.484E+00	2.741E+00	1.525E+00
		6.536E-01	2.000E-01	3.282E-02	2.985E-03	1.230E-04
8	2.845E+02	4.873E+00	4.125E+00	3.398E+00	2.663E+00	1.507E+00
		6.744E-01	2.241E-01	3.961E-02	3.709E-03	1.465E-04
9	2.958E+02	4.932E+00	4.083E+00	3.321E+00	2.600E+00	1.499E+00
		7.014E-01	2.515E-01	4.844E-02	4.692E-03	1.787E-04
10	3.005E+02	4.931E+00	4.027E+00	3.252E+00	2.552E+00	1.503E+00
		7.346E-01	2.823E-01	5.940E-02	6.024E-03	2.228E-04
11	2.997E+02	4.875E+00	3.957E+00	3.192E+00	2.518E+00	1.518E+00
		7.735E-01	3.165E-01	7.256E-02	7.832E-03	2.831E-04
12	2.911E+02	4.768E+00	3.873E+00	3.137E+00	2.498E+00	1.543E+00
		8.179E-01	3.538E-01	8.782E-02	1.029E-02	3.662E-04
13	2.789E+02	4.511E+00	3.707E+00	3.057E+00	2.486E+00	1.600E+00
		8.990E-01	4.204E-01	1.164E-01	1.617E-02	5.692E-04
14	2.569E+02	4.275E+00	3.595E+00	3.023E+00	2.498E+00	1.647E+00
		9.548E-01	4.647E-01	1.362E-01	2.127E-02	7.818E-04
15	2.350E+02	4.017E+00	3.490E+00	3.000E+00	2.519E+00	1.696E+00
		1.008E+00	5.070E-01	1.555E-01	2.693E-02	1.086E-03
16	2.055E+02	3.776E+00	3.418E+00	2.995E+00	2.542E+00	1.736E+00
		1.050E+00	5.405E-01	1.715E-01	3.204E-02	1.502E-03
17	1.728E+02	3.643E+00	3.402E+00	2.996E+00	2.548E+00	1.751E+00
		1.069E+00	5.577E-01	1.807E-01	3.542E-02	1.887E-03
18	1.402E+02	3.742E+00	3.429E+00	2.974E+00	2.516E+00	1.727E+00
		1.058E+00	5.545E-01	1.812E-01	3.642E-02	2.096E-03
19	3.049E+02	4.204E+00	3.421E+00	2.892E+00	2.430E+00	1.662E+00
		1.016E+00	5.317E-01	1.736E-01	3.506E-02	2.071E-03

*****PDF VALUES OF TEMPERATURE *****

I	PDF(1)	PDF(2)	PDF(3)	PDF(4)	PDF(5)
	PDF(6)	PDF(7)	PDF(8)	PDF(9)	PDF(10)
2	0.000E+00	0.000E+00	0.000E+00	1.565E-03	1.942E-03
	3.007E-04	2.022E-04	4.423E-05	5.276E-05	0.000E+00
3	0.000E+00	0.000E+00	0.000E+00	1.546E-03	1.932E-03
	2.226E-04	1.940E-04	6.289E-05	1.053E-04	5.728E-06
4	0.000E+00	0.000E+00	1.905E-05	1.586E-03	1.891E-03

```
     2.109E-04  2.196E-04  7.268E-05  9.608E-05  8.135E-07
  5  4.120E-05  8.057E-06  8.094E-06  1.441E-03  1.977E-03
     2.047E-04  2.024E-04  7.545E-05  1.349E-04  0.000E+00
  6  7.484E-05  8.430E-06  8.473E-06  1.229E-03  2.049E-03
     2.640E-04  2.438E-04  1.122E-04  1.013E-04  0.000E+00
  7  1.074E-04  8.633E-06  8.787E-06  1.051E-03  2.044E-03
     3.683E-04  2.923E-04  1.106E-04  9.719E-05  0.000E+00
  8  1.381E-04  8.654E-06  9.012E-06  8.241E-04  2.057E-03
     5.496E-04  2.548E-04  1.535E-04  9.181E-05  0.000E+00
  9  1.666E-04  8.499E-06  1.149E-05  7.427E-04  8.129E-04
     1.767E-03  2.875E-04  2.249E-04  7.221E-05  0.000E+00
 10  1.982E-04  3.895E-05  3.333E-05  5.444E-04  7.202E-04
     1.883E-03  3.299E-04  2.578E-04  1.145E-04  0.000E+00
 11  2.626E-04  4.311E-05  2.466E-05  1.378E-04  9.494E-04
     1.756E-03  5.303E-04  2.436E-04  1.726E-04  0.000E+00
 12  3.158E-04  3.117E-05  2.939E-05  2.926E-05  8.700E-04
     4.777E-04  1.853E-03  3.309E-04  1.847E-04  0.000E+00
 13  3.880E-04  4.563E-05  2.522E-05  3.216E-05  2.039E-04
     8.922E-04  5.010E-04  1.859E-03  1.769E-04  0.000E+00
 14  4.235E-04  4.782E-05  8.003E-05  1.312E-04  1.511E-04
     3.981E-04  7.333E-04  1.940E-03  2.211E-04  0.000E+00
 15  4.704E-04  1.199E-04  1.196E-04  1.331E-04  1.267E-04
     4.307E-04  6.977E-04  4.443E-04  1.586E-03  0.000E+00
 16  5.777E-04  8.804E-05  8.080E-05  1.754E-04  1.415E-04
     1.285E-04  1.506E-03  9.080E-04  4.657E-04  0.000E+00
 17  6.427E-04  1.032E-04  1.384E-04  1.965E-04  3.773E-04
     1.418E-03  3.376E-04  2.118E-04  6.716E-04  0.000E+00
 18  1.012E-03  1.464E-04  1.097E-04  1.014E-04  1.669E-03
     1.098E-04  1.180E-04  3.086E-04  4.201E-04  8.777E-05
 19  1.176E-03  9.642E-05  3.046E-04  1.781E-03  1.539E-04
     1.125E-04  1.537E-04  3.762E-05  1.049E-04  1.862E-04


*** XU= 6.096E-01  ISTEP=  420
 JUSTIN=          0 JUSTEX=          0     DX= 2.115E-03 PRESSD= 0.000E+00
    KIN=          3    KEX=          2    DXY= 4.704E-02   DPDX= 0.000E+00
   PSII= 0.000E+00   PSIE= 5.655E-03   DXRE= 2.489E+02    PEI= 5.655E-03
    RMI= 0.000E+00    RME=-1.367E-02 DXINC= 2.042E-02 YREF1= 0.000E+00
   R(1)= 0.000E+00   R(N)= 4.931E-02 DXPSI= 4.117E-03 YREF2= 0.000E+00
  ELCON= 1.985E-01
  UFLUX= 1.503E-02
FLUX(J)= -7.234E-04  2.754E-02  2.155E+00  1.809E-02  1.632E-02
 1.457E-02  1.287E-02  9.851E-03  7.046E-03  4.559E-03
 2.066E-03  6.252E-04  7.268E-05  1.095E+04  1.349E-05
 FACE= 1.712E-01 RATE= 9.996E-01
Y(N)=  4.93E-02
  I      R/RO      UVEL      TEMP      FUEL      OXYG      H2M
  1  0.00E+00  2.43E+01  1.84E+03  2.65E-02  5.65E-03  2.51E-01
  2  8.05E-01  2.43E+01  1.84E+03  2.65E-02  5.65E-03  2.51E-01
  3  1.61E+00  2.40E+01  1.84E+03  2.54E-02  7.93E-03  2.43E-01
```

4	2.41E+00	2.37E+01	1.84E+03	2.37E-02	1.11E-02	2.31E-01
5	3.21E+00	2.32E+01	1.84E+03	2.14E-02	1.46E-02	2.14E-01
6	4.01E+00	2.27E+01	1.84E+03	1.87E-02	1.90E-02	1.92E-01
7	4.81E+00	2.21E+01	1.85E+03	1.56E-02	2.36E-02	1.65E-01
8	5.61E+00	2.14E+01	1.86E+03	1.21E-02	2.87E-02	1.33E-01
9	6.40E+00	2.07E+01	1.87E+03	8.50E-03	3.46E-02	9.72E-02
10	7.20E+00	1.99E+01	1.86E+03	5.01E-03	4.32E-02	5.97E-02
11	7.97E+00	1.91E+01	1.77E+03	2.89E-03	6.26E-02	3.58E-02
12	8.71E+00	1.84E+01	1.66E+03	1.29E-03	8.38E-02	1.65E-02
13	9.83E+00	1.74E+01	1.41E+03	0.00E+00	1.22E-01	0.00E+00
14	1.05E+01	1.69E+01	1.22E+03	0.00E+00	1.46E-01	0.00E+00
15	1.10E+01	1.65E+01	1.05E+03	0.00E+00	1.65E-01	0.00E+00
16	1.15E+01	1.62E+01	9.02E+02	0.00E+00	1.80E-01	0.00E+00
17	1.20E+01	1.59E+01	7.87E+02	0.00E+00	1.91E-01	0.00E+00
18	1.24E+01	1.57E+01	6.84E+02	0.00E+00	2.00E-01	0.00E+00
19	1.27E+01	1.56E+01	5.92E+02	0.00E+00	2.08E-01	0.00E+00
20	1.29E+01	1.51E+01	3.00E+02	0.00E+00	2.32E-01	0.00E+00

I	O2M	H2OM	N2M	TEMF	FUFL	OXFL
1	3.35E-03	2.54E-01	4.92E-01	1.79E+02	1.29E-02	2.33E-02
2	3.35E-03	2.54E-01	4.92E-01	1.79E+02	1.29E-02	2.33E-02
3	4.75E-03	2.54E-01	4.98E-01	2.13E+02	1.27E-02	3.05E-02
4	6.74E-03	2.55E-01	5.08E-01	2.68E+02	1.26E-02	3.89E-02
5	9.10E-03	2.57E-01	5.20E-01	3.24E+02	1.22E-02	4.64E-02
6	1.21E-02	2.59E-01	5.37E-01	3.82E+02	1.18E-02	5.38E-02
7	1.56E-02	2.63E-01	5.57E-01	4.38E+02	1.11E-02	6.01E-02
8	1.97E-02	2.67E-01	5.80E-01	4.99E+02	1.01E-02	6.61E-02
9	2.47E-02	2.71E-01	6.07E-01	5.63E+02	8.94E-03	7.18E-02
10	3.22E-02	2.72E-01	6.36E-01	6.20E+02	7.37E-03	7.58E-02
11	4.84E-02	2.53E-01	6.62E-01	6.28E+02	4.95E-03	7.47E-02
12	6.69E-02	2.29E-01	6.87E-01	6.43E+02	2.53E-03	7.33E-02
13	1.01E-01	1.78E-01	7.20E-01	6.34E+02	0.00E+00	6.52E-02
14	1.23E-01	1.42E-01	7.35E-01	5.66E+02	0.00E+00	5.40E-02
15	1.41E-01	1.12E-01	7.47E-01	4.99E+02	0.00E+00	4.47E-02
16	1.56E-01	8.81E-02	7.56E-01	4.32E+02	0.00E+00	3.68E-02
17	1.67E-01	7.00E-02	7.63E-01	3.82E+02	0.00E+00	3.13E-02
18	1.76E-01	5.45E-02	7.69E-01	3.49E+02	0.00E+00	2.80E-02
19	1.84E-01	4.11E-02	7.75E-01	3.23E+02	0.00E+00	2.56E-02
20	2.10E-01	0.00E+00	7.93E-01	0.00E+00	0.00E+00	0.00E+00

*****POPULATION DISTRIBUTION OF FOLDS*****

I	FRAT	PA (1)	PA (2)	PA (3)	PA (4)	PA (5)
		PA (6)	PA (7)	PA (8)	PA (9)	PA (10)
2	1.580E+01	1.995E+00	2.593E+00	2.797E+00	2.749E+00	2.234E+00
		1.522E+00	8.166E-01	2.231E-01	1.708E-02	1.191E-03
3	3.964E+01	2.288E+00	2.671E+00	2.780E+00	2.687E+00	2.160E+00
		1.470E+00	7.940E-01	2.230E-01	1.843E-02	1.266E-03
4	5.507E+01	2.597E+00	2.774E+00	2.769E+00	2.618E+00	2.074E+00
		1.408E+00	7.687E-01	2.248E-01	2.079E-02	1.399E-03
5	6.894E+01	2.896E+00	2.885E+00	2.763E+00	2.548E+00	1.984E+00
		1.345E+00	7.442E-01	2.288E-01	2.444E-02	1.605E-03
6	8.072E+01	3.161E+00	2.987E+00	2.757E+00	2.483E+00	1.898E+00

		1.285E+00	7.235E-01	2.353E-01	2.972E-02	1.904E-03
7	9.034E+01	3.380E+00	3.070E+00	2.749E+00	2.423E+00	1.822E+00
		1.234E+00	7.086E-01	2.444E-01	3.668E-02	2.326E-03
8	9.800E+01	3.547E+00	3.128E+00	2.734E+00	2.369E+00	1.758E+00
		1.195E+00	7.009E-01	2.565E-01	4.535E-02	2.911E-03
9	1.039E+02	3.659E+00	3.155E+00	2.712E+00	2.321E+00	1.709E+00
		1.168E+00	7.013E-01	2.719E-01	5.581E-02	3.723E-03
10	1.076E+02	3.708E+00	3.150E+00	2.680E+00	2.281E+00	1.677E+00
		1.156E+00	7.108E-01	2.909E-01	6.809E-02	4.850E-03
11	1.080E+02	3.683E+00	3.111E+00	2.643E+00	2.251E+00	1.663E+00
		1.160E+00	7.296E-01	3.132E-01	8.174E-02	6.381E-03
12	1.044E+02	3.588E+00	3.044E+00	2.603E+00	2.233E+00	1.667E+00
		1.178E+00	7.562E-01	3.377E-01	9.584E-02	8.388E-03
13	9.818E+01	3.335E+00	2.892E+00	2.540E+00	2.227E+00	1.701E+00
		1.226E+00	8.083E-01	3.786E-01	1.182E-01	1.242E-02
14	8.597E+01	3.104E+00	2.802E+00	2.523E+00	2.245E+00	1.735E+00
		1.261E+00	8.410E-01	4.016E-01	1.302E-01	1.489E-02
15	7.618E+01	2.910E+00	2.741E+00	2.521E+00	2.264E+00	1.762E+00
		1.288E+00	8.647E-01	4.182E-01	1.391E-01	1.692E-02
16	6.717E+01	2.791E+00	2.723E+00	2.529E+00	2.276E+00	1.773E+00
		1.299E+00	8.761E-01	4.271E-01	1.445E-01	1.835E-02
17	5.912E+01	2.788E+00	2.751E+00	2.536E+00	2.270E+00	1.764E+00
		1.293E+00	8.735E-01	4.278E-01	1.462E-01	1.911E-02
18	5.176E+01	2.962E+00	2.808E+00	2.525E+00	2.236E+00	1.729E+00
		1.266E+00	8.561E-01	4.200E-01	1.442E-01	1.918E-02
19	1.189E+02	3.404E+00	2.834E+00	2.469E+00	2.166E+00	1.668E+00
		1.220E+00	8.246E-01	4.043E-01	1.389E-01	1.857E-02

*****PDF VALUES OF TEMPERATURE *****

I	PDF(1)	PDF(2)	PDF(3)	PDF(4)	PDF(5)
	PDF(6)	PDF(7)	PDF(8)	PDF(9)	PDF(10)
2	0.000E+00	0.000E+00	8.270E-06	2.425E-05	4.427E-05
	1.138E-03	2.136E-03	6.223E-04	9.420E-05	0.000E+00
3	3.898E-06	1.350E-05	2.980E-05	2.743E-05	4.728E-05
	6.673E-04	2.564E-03	6.406E-04	1.153E-04	0.000E+00
4	3.232E-05	3.186E-05	2.886E-05	2.624E-05	6.313E-05
	7.670E-04	2.386E-03	6.806E-04	8.902E-05	0.000E+00
5	8.006E-05	3.086E-05	2.940E-05	4.812E-05	5.867E-05
	5.685E-04	2.452E-03	7.444E-04	8.909E-05	0.000E+00
6	1.284E-04	3.039E-05	3.200E-05	7.730E-05	5.887E-05
	4.883E-04	1.300E-03	1.884E-03	9.831E-05	0.000E+00
7	1.798E-04	3.273E-05	6.121E-05	6.848E-05	5.239E-05
	4.634E-04	1.099E-03	2.048E-03	9.066E-05	0.000E+00
8	2.525E-04	4.137E-05	7.748E-05	4.190E-05	6.181E-05
	3.344E-04	1.042E-03	1.971E-03	2.701E-04	0.000E+00
9	3.017E-04	9.472E-05	6.093E-05	3.032E-05	1.506E-04
	1.841E-04	8.083E-04	1.058E-03	1.426E-03	0.000E+00
10	3.710E-04	8.670E-05	6.590E-05	1.153E-04	1.508E-04
	1.494E-04	5.402E-04	1.273E-03	1.362E-03	0.000E+00
11	4.375E-04	6.649E-05	9.574E-05	1.212E-04	1.051E-04
	1.051E-04	4.433E-04	2.202E-03	5.135E-04	0.000E+00

```
 12  4.964E-04  1.029E-04  1.416E-04  1.064E-04  9.658E-05
     3.321E-04  1.538E-03  4.939E-04  7.817E-04  0.000E+00
 13  5.968E-04  1.468E-04  1.491E-04  2.318E-04  1.650E-03
     4.139E-04  1.288E-04  3.372E-04  4.622E-04  0.000E+00
 14  6.873E-04  1.610E-04  3.014E-04  1.581E-03  3.669E-04
     2.897E-04  3.698E-04  3.658E-04  0.000E+00  0.000E+00
 15  8.266E-04  2.699E-04  3.354E-04  1.550E-03  3.366E-04
     4.172E-04  3.687E-04  0.000E+00  0.000E+00  0.000E+00
 16  9.949E-04  3.048E-04  1.533E-03  3.929E-04  4.536E-04
     4.294E-04  0.000E+00  0.000E+00  0.000E+00  0.000E+00
 17  1.210E-03  2.402E-04  1.512E-03  3.666E-04  7.483E-04
     0.000E+00  0.000E+00  0.000E+00  0.000E+00  0.000E+00
 18  1.358E-03  1.705E-03  3.675E-04  3.779E-04  2.449E-04
     6.329E-05  0.000E+00  0.000E+00  0.000E+00  0.000E+00
 19  1.553E-03  1.946E-03  2.421E-04  1.258E-04  1.046E-04
     1.406E-04  0.000E+00  0.000E+00  0.000E+00  0.000E+00
CROSS-STREAM PLOT, XU= 6.096E-01 ISTEP= 420
TERMINATED AT

ISTEP=  420 LASTEP= 1000 XU=  6.096E-01 XULAST=  6.096E-01 IFIN=  2
DOWN-STREAM PLOT, XU= 6.096E-01 ISTEP= 420
```